STUDY ON CALCIUM SILICATE/ POLY(ETHYLENE TEREPHTHALATE-*CO*-CAPROLACTONE) BIOMATERIALS

SUEBPONG SUEBWONGNAT

A THESIS SUBMITTED IN PARTIAL FULFILLMENT
OF THE REQUIREMENT FOR THE DEGREE OF
DOCTOR OF PHILOSOPHY IN APPLIED CHEMISTRY
FACULTY OF SCIENCE
KING MONGKUT'S INSTITUTE OF TECHNOLOGY LADKRABANG
2014

KMITL-2014-SC-D-010-043

STUDY ON CALCIUM SILICATE/ POLY(ETHYLENE TEREPHTHALATE-*CO*-CAPROLACTONE) BIOMATERIALS

SUEBPONG SUEBWONGNAT

A THESIS SUBMITTED IN PARTIAL FULFILLMENT

OF THE REQUIREMENT FOR THE DEGREE OF

DOCTOR OF PHILOSOPHY IN APPLIED CHEMISTRY

FACULTY OF SCIENCE

KING MONGKUT'S INSTITUTE OF TECHNOLOGY LADKRABANG

2014

KMITL-2014-SC-D-010-043

การศึกษาวัสดุชีวภาพจากแคลเซียมซิลิเกตและพอลิเมอร์ร่วมเอทิลีนเทอเรฟทาเลต-คาโปแลคโตน

STUDY ON CALCIUM SILICATE/ POLY(ETHYLENE TEREPHTHALATE-*CO*-CAPROLACTONE) BIOMATERIALS

สืบพงษ์ สืบวงษ์นาท

SUEBPONG SUEBWONGNAT

วิทยานิพนธ์นี้เป็นส่วนหนึ่งของการศึกษาตามหลักสูตรปรัชญาดุษฎีบัณฑิต

สาขาวิชา เคมีประยุกต์

คณะวิทยาศาสตร์

สถาบันเทคโนโลยีพระจอมเกล้าเจ้าคุณทหารลาดกระบัง

พ.ศ. 2557

KMITL-2014-SC-D-010-043

คณะวิทยาศาสตร์
สถาบันเทคโนโลยีพระจอมเกล้าเจ้าคุณทหารลาดกระบัง
ใบรับรองวิทยานิพนธ์

หัวข้อวิทยานิพนธ์	การศึกษาวัสดุชีวภาพจากแคลเซียมซิลิเกตและพอลิเมอร์ร่วมเอทิลีนเทอเรฟทาเลต-คาโปแลคโตน STUDY ON CALCIUM SILICATE/POLY(ETHYLENE TEREPHTHALATE-*CO*-CAPROLACTONE) BIOMATERIALS
นักศึกษา	นายสืบพงษ์ สืบวงษ์นาท
รหัสประจำตัว	51067101
ปริญญา	ปรัชญาดุษฎีบัณฑิต
สาขาวิชา	เคมีประยุกต์
อาจารย์ที่ปรึกษาวิทยานิพนธ์	ผศ.ดร.ปุณณมา ศิริพันธ์โนน
อาจารย์ที่ปรึกษาวิทยานิพนธ์ร่วม	ผศ.ดร.ภัทธาวุธ มนต์วิเศษ

คณะกรรมการสอบวิทยานิพนธ์		**ลายมือชื่อ**
รศ.ดร.อิทธิพล	แจ้งชัด	
ผศ.ดร.ชลลดา	ฤตวิรุฬห์	
ผศ.ดร.ดุจฤทัย	พงษ์เก่า คะชิมา	
ผศ.ดร.ภัทธาวุธ	มนต์วิเศษ	
ผศ.ดร.ปุณณมา	ศิริพันธ์โนน	

วัน / เดือน/ ปี ที่สอบ 5 สิงหาคม พ.ศ. 2557 เวลา 09.30 – 12.30 น.
สถานที่สอบ ณ ห้อง 316 ชั้น 3 อาคารปฏิบัติการใหม่

คณะวิทยาศาสตร์รับรองแล้ว

(รองศาสตราจารย์ ดร.ดุษณี ธนะบริพัฒน์)
คณบดีคณะวิทยาศาสตร์

วันที่ 27 **เดือน** ก.ค. **พ.ศ.** 57

หัวข้อวิทยานิพนธ์	การศึกษาวัสดุชีวภาพจากแคลเซียมซิลิเกตและพอลิเมอร์ร่วมเอทิลีนเทอเรฟทาเลต-คาโปแลคโตน
นักศึกษา	นายสืบพงษ์ สืบวงษ์นาท
รหัสประจำตัว	51067101
ปริญญา	ดุษฎีบัณฑิต
สาขาวิชา	เคมีประยุกต์
พ.ศ.	2557
อาจารย์ที่ปรึกษาวิทยานิพนธ์	ผศ.ดร.ปุณณมา ศิริพันธ์โนน
อาจารย์ที่ปรึกษาวิทยานิพนธ์ร่วม	ผศ.ดร.ภัทธาวุธ มนต์วิเศษ

บทคัดย่อ

งานวิจัยนี้มุ่งศึกษาการเตรียมวัสดุประกอบระหว่างแคลเซียมซิลิเกตกับพอลิเมอร์ร่วมเอทิลีนเทอเรฟทาเลต-คาโปแลคโตน (CS/PET-*co*-PCL) เพื่อนำไปประยุกต์ใช้ทางการแพทย์ โดยเริ่มจากการเตรียมสารตั้งต้นแคลเซียมซิลิเกต (CS) ด้วยวิธีตกตะกอนร่วมระหว่างแคลเซียม-ไนเตรทเตตระไฮเดรทกับเตตระเอทิลออโธซิลิเกต โดยมีโซเดียมไฮดรอกไซด์เป็นสารตกตะกอน และสังเคราะห์สารประกอบวงโอลิโกเอทิลีนเทอเรฟทาเลต (C-OET) จากปฏิกิริยาดีพอลิเมอไรเซชันแบบปิดวงของ PET จากนั้นสังเคราะห์พอลิเมอร์ร่วมเอทิลีนเทอเรฟทาเลต-คาโปแลคโตน (PET-*co*-PCL) จากสารผสมระหว่าง C-OET และแอปซีลอนคาโปแลคโตน (CL) โดยมีไดบิว-ทิลทินออกไซด์ (DBTO) เป็นตัวเร่งปฏิกิริยา ด้วยปฏิกิริยาพอลิเมอไรเซชันแบบเปิดวง ที่อุณหภูมิ 180, 200, 230, และ 250 ºC เป็นเวลา 8 และ 24 ชั่วโมง ในสภาวะสูญญากาศ ในขณะที่วัสดุประกอบ CS/PET-*co*-PCL เตรียมโดยผสมผง CS กับสารผสมระหว่าง C-OET CL และ DBTO แล้วนำไปขึ้นรูปโดยการกดอัดได้เป็นก้อน CS/C-OET-CL จากนั้นนำไปทำปฏิกิริยาพอลิเมอไรเซชันแบบเปิดวงที่อุณหภูมิ 180 และ 200 ºC เป็นเวลา 24 ชั่วโมง โดยมีการปรับเปลี่ยนอัตราส่วนโมลของ C-OET:CL ในสารประกอบวงผสมที่ใช้เป็น 50:50, 60:40, 70:30, 80:20, 90:10, และ 100:0 ในขณะที่มีการปรับเปลี่ยนอัตราส่วนร้อยละโดยน้ำหนักของผง CS:สารประกอบวงผสมเป็น 50:50 และ 60:40 หลังจากนั้นนำพอลิเมอร์ร่วม PET-*co*-PCL และวัสดุประกอบ CS/PET-*co*-PCL ที่ได้ไปตรวจพิสูจน์เอกลักษณ์ด้วยเทคนิค ^{1}H-NMR พบว่า โครงสร้างของพอลิเมอร์ร่วม PET-*co*-PCL ในวัสดุประกอบ CS/PET-*co*-PCL มีแนวโน้มการเปลี่ยนแปลงโครงสร้างจากพอลิเมอร์ร่วมแบบบล็อคไปเป็นแบบสลับเมื่อปริมาณของ CL เพิ่มขึ้น ซึ่งมีผลต่อสมบัติทางความร้อนและสมบัติเชิงกล ค่าอุณหภูมิการหลอมเหลวและค่าความแข็งแรงกดของวัสดุประกอบ CS/PET-*co*-PCL มีค่าลดลง เมื่อปริมาณของ CL ในวัสดุประกอบเพิ่มขึ้น ซึ่งสมบัติทั้งสองของวัสดุประกอบ CS/PET-*co*-

PCL มีค่ามากกว่าของ CS บริสุทธิ์และพอลิเมอร์ร่วม PET-*co*-PCL นอกจากนี้ค่าความแข็งแรงกดของวัสดุประกอบ CS/PET-*co*-PCL มีค่าสอดคล้องกับค่าความแข็งแรงกดของกระดูกหลายส่วนของร่างกาย ในการศึกษาโครงสร้างจุลภาคของวัสดุประกอบ CS/PET-*co*-PCL จาก SEM พบว่าพอลิเมอร์ร่วมมีลักษณะเป็นฟิล์มบางๆ ปกคลุมล้อมรอบเกรนของแคลเซียมซิลิเกต การทดสอบความสามารถในการขึ้นรูปใหม่ของวัสดุประกอบ CS/PET-*co*-PCL โดยให้ความร้อนที่อุณหภูมิ 150 °C เป็นเวลา 1 ชั่วโมง พบว่าผลึกของพอลิเมอร์ร่วม PET-*co*-PCL และ CS ในวัสดุประกอบ CS/PET-*co*-PCL และสมบัติทางความร้อนของวัสดุประกอบ CS/PET-*co*-PCL ไม่มีการเปลี่ยนแปลง แสดงถึงพฤติกรรมความเป็นเทอร์โมพลาสติก การทดสอบสมบัติความว่องไวทางชีวภาพของพอลิเมอร์ร่วม PET-*co*-PCL และวัสดุประกอบ CS/PET-*co*-PCL โดยนำไปแช่ในสารละลายจำลองคล้ายของเหลวในร่างกาย (Simulated Body Fluid, SBF) ที่อุณหภูมิ 37 ºC พบว่ามีการก่อผลึกของสารประกอบจำพวกฟอสเฟตบนพื้นผิวของวัสดุประกอบ CS/PET-*co*-PCL ภายในเวลา 7 วัน นอกจากนั้นการทดสอบความเป็นพิษกับเซลล์ของวัสดุประกอบ CS/PET-*co*-PCL โดยวิธี MTT assay ผลการทดสอบแสดงว่าวัสดุประกอบ CS/PET-*co*-PCL ไม่มีความเป็นพิษต่อเซลล์ ดังนั้นวัสดุประกอบ CS/PET-*co*-PCL ซึ่งสามารถสังเคราะห์จากปฏิกิริยาพอลิเมอไรเซชันแบบเปิดวงเป็นตัวเลือกหนึ่งในการประยุกต์ใช้งานทางด้านการแพทย์

คำสำคัญ : แคลเซียมซิลิเกต, พอลิเมอร์ร่วมเอทิลีนเทอเรฟทาเลต-คาโปแลคโตน, ปฏิกิริยาพอลิเมอ-ไรเซชันแบบเปิดวง, วัสดุชีวภาพ, พอลิเมอร์ร่วมพอลิเอสเทอร์

Thesis title	Study on calcium silicate/poly(ethylene terephthalate-*co*-caprolactone) biomaterials
Student	Mr. Suebpong Suebwongnat
Student ID	51067101
Degree	Doctor of Philosophy
Program	Applied Chemistry
Year	2014
Thesis advisor	Asst. Prof. Dr. Punnama Siriphannon
Thesis co-advisor	Asst. Prof. Dr. Pathavuth Monvisade

Abstract

This thesis aims to study the preparation of calcium silicate/poly(ethylene terephthalate-*co*-caprolactone) composites (CS/PET-*co*-PCL) for biomaterial applications. Firstly, the calcium silicate powder (CS) was synthesized by co-precipitation method of calcium nitrate tetrahydrate and tetraethyl orthosilicate using sodium hydroxide as a precipitating agent. Cyclic oligo(ethylene terephthalate) (C-OET) precursor was synthesized by cyclodepolymerization of PET. The neat PET-*co*-PCL copolyesters were obtained from the mixture of the C-OET precursor and ε-caprolactone (CL) cyclics in the presence of dibutyltinoxide (DBTO) catalyst by ring-opening polymerization at 180, 200, 230, and 250 ºC for 8 and 24 hr under vacuum. While the CS/PET-*co*-PCL was prepared by mixing the as-prepared CS powder in the mixture of the C-OET, CL and DBTO, shaping by uniaxial pressing and ring-opening polymerization at 180 and 200 ºC for 24 hr. The molar ratios of C-OET:CL in the cyclic mixtures were varied, i.e., 50:50, 60:40, 70:30, 80:20, 90:10, and 100:0. The weight percentages of CS:cyclics in the CS/C-OET-CL pre-composites were 50:50 and 60:40. The ^{1}H-NMR spectra revealed that the structures of ROP PET-*co*-PCL phases in the composites transformed from block to alternating copolymers when the CL content was increased, resulting in the change of thermal and mechanical properties of CS/PET-*co*-PCL composites. The melting temperature and compressive strength of the composites decreased with the increment of CL content, however, these properties were significantly increased comparing with both neat CS and PET-*co*-PCL copolymers. The compressive strengths of the CS/PET-*co*-PCL composites were compatible with those of various body parts. For morphological studies, the ring-opening polymerized PET-*co*-PCL film was obtained as the continuous film covering on the CS grains as examined by SEM. The CS/PET-

co-PCL composites were reshaped then annealed at 150 °C for 1 hr. The crystallinity and thermal properties of the reshaped and annealed composites were unchanged, indicating that the composites may have thermoplastic elastomer behaviors. The bioactivity tests performed by soaking in simulated body fluid solution (SBF) indicated that the CS/PET-*co*-PCL composites could induce the formation of phosphate-compounds on their surfaces within 7 days while the neat copolyesters could not. The cytotoxicity was studied by MTT assay, in which the test result revealed that the CS/PET-*co*-PCL composites were potentially non-toxic to cell. The CS/PET-*co*-PCL composites which successfully synthesized *via* ring-opening polymerization were potential candidates for medical applications.

Keywords : Calcium silicate, Poly(ethylene terephthalate-*co*-caprolactone), Ring-opening polymerization, Biomaterials, Copolyesters

ACKNOWLEDGEMENTS

The author would like to take this opportunity to express sincere thanks to his advisors and people who gave useful advice and full support in this thesis.

The author wishes to express deep gratitude to his advisors, Asst. Prof. Dr. Punnama Siriphannon, Asst. Prof. Dr. Pathavuth Monvisade and Prof. Brian Love, for his valuable guidance, attention and encouragement throughout this thesis. It goes without saying to the thesis committee, Assoc. Prof. Dr. Ittipol Jangchud, Asst. Prof. Dr. Chonlada Ritvirulh and Asst. Prof. Dr. Dujreutai Pongkao Kashima for reading and criticizing the manuscript.

The author greatly appreciates the entire professors who have invaluable knowledge while studying in the Department of Chemistry, Faculty of Science, King Mongkut's Institute of Technology Ladkrabang.

Special thanks go to Scientific Instruments Service Center at Faculty of Science at King Mongkut's Institute of Technology Ladkrabang, Scientific Equipment Center at Prince of Songkla University and Scientific and Technological Research Equipment Centre at Chulalongkorn University for helping in analysis with special instruments. In addition, thanks also go to Faculty of Science, King Mongkut's Institute of Technology Ladkrabang and Department of Materials Science and Engineering, University of Michigan for laboratory instruments and instrument analysis.

The author deeply appreciates the Thailand Research Fund (TRF) through the Royal Golden Jubilee Ph.D. Program for financial support (3.D.KL/50/B.1).

The author also would like to give the special thanks to all of his friends who have been helping and encouraging him while studying the Ph.D. program.

Last but not least, the author would like to express him the deepest appreciate his dearest family for love, care and encouragement that they have, which is the most important in his life forever.

MR. SUEBPONG SUEBWONGNAT

CONTENT

CONTENT (CONT.)

CONTENT (CONT.)

LIST OF TABLES

LIST OF FIGURES

LIST OF FIGURES (CONT.)

LIST OF FIGURES (CONT.)

SYMBOLS AND ABBREVIATION

CS	Calcium silicate
PET	Poly(ethylene terephthalate)
PCL	Poly(caprolactone)
C-OET	Cyclic oligomer ethylene terephthalate
CL	ε-caprolactone
PET-*co*-PCL	Poly(ethylene terephthalate-*co*-caprolactone)
CS/PET-*co*-PCL	Calcium silicate/poly(ethylene terephthalate-*co*-caprolactone)
DBTO	Dibutyltinoxide
SBF	Simulated body fluid
PBS	Phosphate buffer saline
CDP	Cyclodepolymerization
ROP	Ring-opening polymerization
XRF	X-ray fluorescence spectrometer
SEM	Scanning electron microscope
EDS	Energy dispersive spectroscopy
TGA	Thermogravimetric analyser
DSC	Differential scanning calorimeter
^{1}H-NMR	Proton nuclear magnetic resonance spectrometer
DMTA	Dynamic mechanical thermal analyser
XRD	X-ray diffractometry
δ	Chemical shift
T_g	Glass transition temperature
T_m	Melting temperature
T_c	Crystallization temperature
T_{cc}	Cold crystallization temperature
ΔH_m	Melting enthalpy
ΔH_c	Crystallization enthalpy
ΔH_{cc}	Cold crystallization enthalpy
χ_c	Degree of crystallinity

Chapter 1

Introduction

1.1 Introduction

Biomaterials are nonviable materials used to make parts/devices to replace any tissues, organs, and body functions. These materials are able to function as intimate contact with living tissue, with minimal harmful reaction or rejection by the body. The synthetic biomaterials have been being attracted widespread attention in medical uses because of their unlimited availability with uniform quality and reprocessibility. In addition, the synthetic biomaterials offer a wide range of biomaterials products in different application forms and with distinct biological properties. Among various kinds of the synthetic biomaterials including metals, ceramics, polymers and composites, hybrid composites between ceramics and polymers are the most attractive materials for implantation. They combine the advantages of different materials and mimic physiological system of hard and soft tissues. [1, 2]

Polyesters have been widely used in many biomaterial applications, especially aliphatic polyesters, such as poly(caprolactone) (PCL), polylactide (PLA) and polyglycolide (PGA) for drug delivery, resorbable sutures, stents and tissue regeneration scaffolds [3] because of their biodegradability and biocompatibility. On the other hand, aromatic polyesters were also applied as biomaterials such as poly(ethylene terephthalate) (PET) and poly(butylene terephthalate) (PBT) [4] due to their high mechanical properties and long-term performance. Since there are some different advantages from each type of polyester, the aromatic–aliphatic copolymers have attracted the attention in this work, because they possess high initial strength from the aromatic unit and partially biodegradability from the aliphatic unit. The attractive aromatic polyesters selected in this work was poly(ethylene terephthalate) (PET) because of its excellent mechanical properties. In addition, the PET has been widely used in medical applications such as implantable sutures, surgical mesh, vascular grafts, sewing cuffs for heart valves and components for percutaneous access devices. [5] However, the PET acts as bioinert material in physiological system, the surface treatment has been requested in order to biocompatible properties. From this point of view, this limitation of PET can be compensated by integrating the poly(caprolactone) (PCL) with the PET as the copolymers because the aliphatic PCL owns the excellent biocompatibility with cell, which has been approved by the United States Food and Drug

Administration (FDA). However, the usage of PCL for implantation might be limited because the PCL has low mechanical properties. In addition, its degradation and resorption kinetics are slower than other aliphatic polyesters due to its hydrophobic character and high crystallinity. These disadvantages could be also compensated when mixing with PET. From the previous discussion, this thesis aims to synthesis copolyesters, the poly(ethylene terephthalate-*co*-caprolactone) (PET-*co*-PCL), *via* ring-opening polymerization (ROP). These copolyesters are considered to be thermoplastic elastomers (TPEs), processing flexibility and reshapable, therefore they can be used in extensive medical applications.

Since the PET-*co*-PCL copolyesters have been considered to be partial bioinert-biodegrade materials in the physiological systems with good mechanical properties, the formation of fibrous encapsulation may occur after prolonged usages, resulting in implantation failure. To overcome this problem, the bioactive inorganic compounds, which are able to bond with living bone through the formation of apatite interface layer, have been incorporated with the PET-*co*-PCL copolyesters. These ceramic-polymer composites are biomimetic approach as natural bone consisting of inorganic hydroxyapatite and organic collagen phases. Among various bioactive ceramics such as glasses, glasses ceramics, hydroxyapatite, β-tricalcium phosphate [6], one which can attract our interest is calcium silicate ($CaSiO_3$, CS). Because the CS plays an important role as bioactive materials which can induce the fast formation of an hydroxyapatite layer after soaking in simulated body fluid (SBF), indicating the high ability to bond with living bond. Besides, the preparation of bioactive ceramic-polymer composites has been studied and improved by various research groups using conventional melt or solution mixing. [7, 8] The amount of bioactive ceramic added into the polymer melts/solutions was limited due to the apparent increase of ceramic-polymer viscosity, resulting in the confinement of ceramic bioactivity. The composites with low bioactive ceramic loading cannot create the continuous well-adhere layer of hydroxyapatite under *in vitro* system. [9, 10] Therefore, the composites between CS powder and PET-*co*-PCL copolyesters (CS/PET-*co*-PCL) have been prepared in this research work by well pre-mixing the high amount of CS powder with the mixture of cyclic oligo(ethylene terephthalate) (C-OET) and ε-caprolactone (CL) and then *in situ* ring-opening polymerization (ROP) to PET-*co*-PCL matrix, resulting in the composites with better CS dispersion. Nevertheless, another merit of the *in situ* ROP technique over the conventional free radical polymerization is non residual toxic monomers in the ROP products.

Before the synthesis of CS/PET-*co*-PCL composites, the neat PET-*co*-PCL copolymers were prepared by ROP technique using various reaction temperatures and times in order to determine the suitable conditions for further synthesis of the composites. The synthesis of the CS/PET-*co*-PCL composites was performed under the selected ROP conditions. The effects of ROP conditions on the characteristics and properties of the CS/PET-*co*-PCL composites were investigated by various techniques. The ROP CS/PET-*co*-PCL composites were reshaped then heated to investigate their reprocessibility. The preliminary cell biocompatibility of CS/PET-*co*-PCL composites was also tested.

1.2 Objectives

1. To synthesize the PET-*co*-PCL copolymers and the CS/PET-*co*-PCL composites with varying C-OET:CL molar ratios.

2. To investigate the effect of ROP conditions on characteristics and properties of PET-*co*-PCL copolymers and CS/PET-*co*-PCL composites.

3. To investigate the effect of CS powders on physical and mechanical properties and bioactivity of PET-*co*-PCL copolymers and CS/PET-*co*-PCL composites.

4. To investigate thermoplastic elastomer property and reprocessibility of ROP CS/PET-*co*-PCL composites.

1.3 Scope of study

1. Poly(ethylene terephthalate-*co*-caprolactone) copolymers were synthesized using various conditions as followed;

- Molar ratios of C-OET:CL, i.e., 10:0, 9:1, 8:2, 7:3, 6:4 and 5:5.

- Ring-opening polymerization temperatures, i.e., 180, 200, 230 and 250 °C.

- Ring-opening polymerization times, i.e. 8 and 24 hr.

2. Calcium silicate/poly(ethylene terephthalate-*co*-caprolactone) composites were synthesized using various conditions as followed;

- Weight ratios of calcium silicate:cyclics, i.e. 50:50 and 60:40.

- Molar ratios of C-OET:CL, i.e., 10:0, 9:1, 8:2, 7:3, 6:4 and 5:5.

- Ring-opening polymerization temperatures, i.e., 180 and 200 °C for 24 hr (selected from 1).

3. The ROP PET-*co*-PCL copolymers and CS/PET-*co*-PCL composites were characterized by ^{1}H-NMR, DSC, TGA, SEM, and XRD.

4. Physical, mechanical, bioactive, biodegradation properties of the ROP PET-*co*-PCL copolymers and CS/PET-*co*-PCL composites were tested.

5. The reprocessibility of ROP CS/PET-*co*-PCL composites was investigated with XRD and DSC.

1.4 Expected results

1. To obtain the suitable conditions for synthesis of the CS/PET-*co*-PCL composites.

2. To understand the relationship between ROP conditions and either characteristics or properties of the PET-*co*-PCL copolymers and the CS/PET-*co*-PCL composites.

3. To produce new bioactive materials from the CS/PET-*co*-PCL composites with varying mechanical properties and/or bioactivity in order to apply for different biomedical applications.

Chapter 2

Theory and Literature Review

2.1 Biomaterials

Biomaterials can be defined as any synthetic materials used to make devices to replace a part or a function of human body in a safe, reliable and physiologically acceptable manner. A variety of devices and materials is used in the treatment of disease or injury, such as, sutures, tooth fillings, bone plates, needles, catheters, etc. The Clemson University Advisory Board for Biomaterials has formally defined a biomaterial to be "a systemically and pharmacologically inert substance designed for implantation within or incorporation with living systems". [11] The National Institutes of Health Consensus Development Conference defined a biomaterial as ''any substance (other than a drug) or combination of substances, synthetic or natural in origin, which can be used for any period of time, as a whole or as a part of a system which treats, augments or replaces any tissue, organ or function of the body'' (Boretos and Eden, 1984). [12] Another definition of "biomaterial" endorsed by Williams (1987) is "A biomaterial is a nonviable material used in a medical device, intended to interact with biological systems". [2] These descriptions add to the many ways of looking at the same concept but expressing it in different ways. By contrast, a biological material is a material such as bone, skin, or artery produced by a biological system. [11]

Because the ultimate goal of using biomaterials is to improve human health by restoring the function of natural living tissues and organs in the body, it is essential to understand relationships among the structures, properties and functions of biological materials. Thus, three aspects of study on the subject of biomaterials can be envisioned: biological materials, implant materials, and interaction between the two in the body. [11]

The major difference between biological materials and biomaterials (implants) is *viability*. There are other equally important differences that distinguish living materials from artificial replacements. First, most biological materials are continuously bathed with body fluids. Exceptions are the specialized surface layers of skin, hair, nails, hooves, and the enamel of teeth. Second, most biological materials can be considered as *composites*. [11]

Structurally, biological tissues consist of a vast network of intertwining fibers with polysaccharide ground substances immersed in a pool of ionic fluid. Attached to the fibers are

cells that comprise the living tissues. Physically, ground substances function as a glue, lubricant and shock absorber in various tissues. [11]

Structures and properties of a given biological material are dependent upon the chemical and physical nature of the components present and their relative amounts. For example, neural tissues consist almost entirely of cells, while bone is composed of organic materials and calcium phosphate minerals with minute quantities of cells and ground substances as a glue. [11]

An understanding of the exact role played by a tissue and its interrelationship with the function of the entire living organism are essential if biomaterials are to be used intelligently. Thus, a person who wants to design an artificial blood vessel prosthesis has to understand not only the property–structure relationship of the blood vessel wall but also its systemic function. This is because the natural artery is not only a blood conduit, but a component of a larger system, including a pump (heart), an oxygenator (lung), as well as neural systems that control stress in its walls, and a complex feedback system that governs cellular remodeling of the vessel structure. [11]

Synthetic (manmade) materials based on the materials can be divided into four major classes: metals, polymers, ceramics and composites. Because the structures of these materials differ, they have different properties and, therefore, different uses in the body. [12] The list in Table 2.1 illustrates some of the advantages, disadvantages, and applications of four groups of synthetic materials used for implantation. Furthermore, reconstituted (natural) materials such as collagen have been used for replacements (e.g., arterial wall, heart valve, and skin). [11] Natural materials offer the advantage of being very similar, often identical, to macromolecular substances which the biological environment is prepared to recognize and to deal with metabolically. The problems of toxicity and stimulation of a chronic inflammatory reaction, as well as lack of recognition by cells, which are frequently provoked by many synthetic materials, may thereby be suppressed. Furthermore, the similarity to naturally occurring substances introduces the interesting capability of designing biomaterials that function biologically at the molecular, rather than the macroscopic, level. On the other hand, natural materials are frequently quite immunogenic. Furthermore, because they are structurally much more complex than most synthetic materials, their technological manipulation is quite a bit more elaborate. [2]

Table 2.1 Class of materials used in the body [12]

Materials	Advantages	Disadvantages	Applications
Polymers (nylon, silicone rubber, polytetrafuoroethylene, polyester, etc)	Resilient Easy to fabricate	Not strong Deforms with time May degrade	Sutures, blood vessels, other soft tissues, sutures, hip socket, ear, nose
Metals (Ti and its alloys, Co-Cr alloys, Au, Ag stainless steels, etc.)	Strong Tough Ductile	May corrode Dense Difficult to make	Joint replacements, dental root implants, pacer and suture wires, bone plates and screws
Ceramics (alumina zirconia, carbon, calcium phosphates including hydroxyapatite)	Very biocompatible	Brittle Not resilient Weak in tension	Dental and orthopedic implants
Composites (carbon-carbon, wire- or fiber-reinforced bone cement)	Strong Tailor-made	Difficult to make	Bone cement, Dental resin

In this thesis, the composites were selected to be synthesized as the biomaterials in order to integrate various advantages of each raw material, and hence, their weak points would be compensated. Therefore, copolyester matrix containing calcium silicate (CS) powders was used as the biomaterial. The copolymers composed of poly(ethylene terephthalate) (PET) and poly(caprolactone) (PCL) which were the aromatic and aliphatic polyesters, respectively.

2.2 Polyesters

Polyesters have in common the ester group ($-\overset{O}{\overset{\|}{C}}-O-$) in the main polymer chain, which is a polar group and brings inter- and intramolecular chain interactions that are reflected in some properties such as the mobility of the chains and melting characteristics. From the chemical point of view, the ester group increased sensibility to hydrolysis that can cause chain breakage. They contain widely different materials with a large spectrum of characteristics and applications which are produced by a variety of manufacturing techniques. [13]

Due to their large diversity, polyesters will be classified into two main categories, thermoplastic and thermosetting. In this thesis, the thermoplastic polyesters are presented because they may be softened and can be reshaped by heating. [14] Thermoplastic copolyesters of aromatic poly(ethylene terephthalate)-aliphatic poly(caprolactone) have attracted the attention in this research because of high mechanical properties of poly(ethylene terephthalate) and biocompatibility and biodegradability of poly(caprolactone).

2.2.1 Poly(ethylene terephthalate)

Poly(ethylene terephthalate) (PET) is linear thermoplastic polyester which has widespread commercially use as the major synthesis fiber as well as a film and molding material. The repeating unit of PET is the ester of terephthalic acid and ethylene glycol as shown in Scheme 2.1. [13]

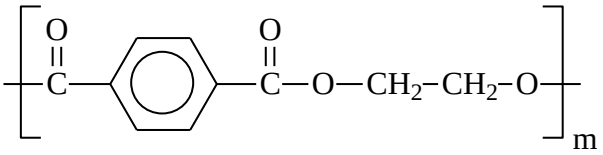

Scheme 2.1 Chemical structure of PET

PET was first synthesized in 1941 and the commercial production of textile fibers started in 1953. At the beginning, the polymer was considered unsuitable for molding as it crystallizes from the melt which makes it brittle. It was not until the late 1960s that the polymer was produced in the amorphous state that provided toughness and transparency and enabled PET to be extensively used for blow molded bottles for carbonated soft drinks. [13]

Today, PET is produced as homopolymers or as copolymers. The copolymers have lower glass transition (T_g) and melting temperature (T_m) and are amorphous and more flexible

materials. They are obtained by using either a mixture of acids (terephthalic and isophthalic) or a mixture of glycols (ethylene glycol and 1,4-cyclohexanedimethanol). [13]

PET has the ability to exist in either an amorphous or a crystalline state. The degree of crystallinity can range from 0 to 60 % and is determined by the history of the material. The T_m is 265 ºC and the T_g is rather high, being reported about 80 ºC. When the amorphous polymer is maintained at a temperature between T_g and T_m, it crystallizes spontaneously. The highest rate of crystallization occurs at 170-180 ºC. [13]

- **Synthesis**

The production of poly(ethylene terephthalate) is conducted in two steps. Dimethyl terephthalate is heated with ethylene glycol to give a mixture consisting of dihydroxyethyl terephthalate and higher oligomers. Further heating to 270 ºC under vacuum in the presence of a catalyst produces the final polymer as shown in Scheme 2.2. [15]

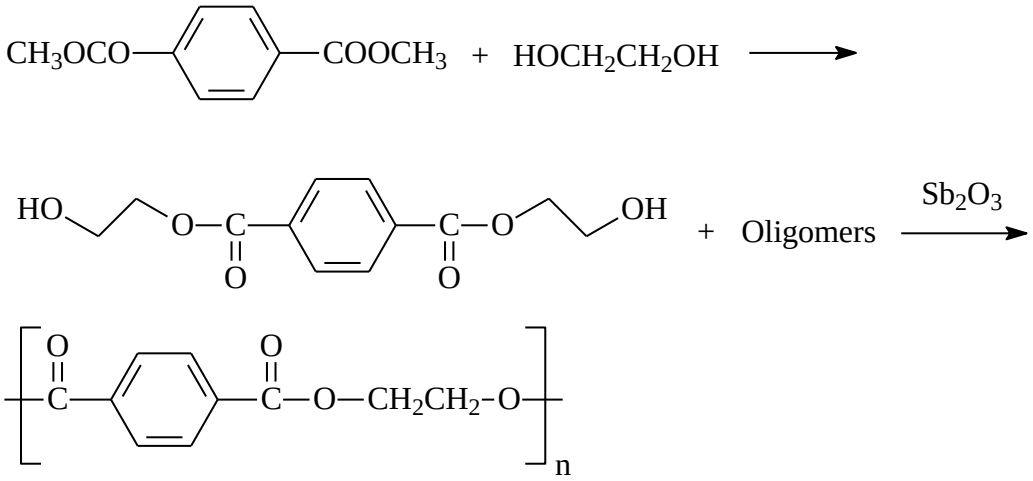

Scheme 2.2 Synthesis of PET

- **Applications**

- Commodity applications:

The strength of PET in its oriented form is outstanding. Biaxially oriented PET film is used as magnetic tape, X-ray and the other photographic film application, electrical insulation, and food packaging, including boil-in-bag food pouch. Production of PET bottles for carbonated beverages by blow molding has gained prominence because PET has low permeability to carbon dioxide, and it can be easily recycled. Other PET containers include bottles for toiletries,

cosmetics, and household products. Because of its excellent thermal stability, PET is also used as coating material for microwave and conventional ovens. [13]

- Medical applications:

Current medical applications of PET include implantable sutures, surgical mesh, vascular grafts and sewing cuffs for heart valves and components for percutaneous access devices. PET sutures were firstly introduced in the 1950s and are used for critical procedures where high strength and predictable long-term performance is emphasized. Mersilene® polyester fiber sutures were the first synthetic braided suture shown to last indefinitely in the body. Woven PET is commonly used as surgical meshes for abdominal wall repair and similar procedures where surgical "patching" is required. Synthetic vascular prostheses were constructed of both woven and knitted PET and have been used clinically since the 1960s. They have been used in the repair of the thoracic aorta, ruptured abdominal aortic aneurysms and to replace iliac, femoral and popliteal vessels. Heart valves have incorporated PET by using it as a sewing cuff around the circumference of the valve to promote tissue in-growth and to provide a surface to suture the valve to the surrounding tissue. Over one million heart valves have been implanted since their inception in the late 1970s. Percutaneous tunneled catheters incorporate a PET cuff to stabilize catheter location and minimize bacterial migration through the skin. In addition, braids and similar constructions made of multifilament PET yarns have shown promise for repairing tendons and ligaments and for fixation of intraocular lenses. [5] Moreover, PET was used in many field of medicine, for example; Y. Li *et* al. [16] synthesized nonwoven PET fibrous matrices as tissue scaffolds by thermal compression. It was found that the samples yielded a uniformly distributed pore size. The compressed matrices with two different pore sizes were structurally stable in cell culture media. The smaller pores in the matrix allowed cells to spread better and proliferate faster, while cells in the larger pores tended to form large aggregates and had lower proliferation rate. These results suggested that the thermal compression was the effective method that could be employed to modify the microstructure of nonwoven fibrous matrices.

Due to the bioinert of PET, the PET surfaces were modified for improving its biocompatibility. Z. Ma *et* al. [17] modified surface of PET nanofibers by grafting with gelatin for blood vessel engineering. The gelatin grafting method could obviously improve the spreading and proliferation of endothelial cells (ECs) on non woven PET nanofiber mats, and the gelatin-grafted PET nanofiber mats can preserve the EC's phenotype. N. Blanchemain *et* al. [18] synthesized vascular PET grafts were coated with cyclodextrin (CD) using a pad-dry-cure

method. CD-coating did not modify cell response compared to untreated PET. The CD which contains many hydrophilic hydroxide groups could improve the interaction between the PET and the human embryonic epithelial cells L132. For antibiotic release, a linear release of Vancomycin in physiological medium was depicted over a 50-day period. This study confirmed that CD coating was an efficient drug delivery system adapted to antibiotics.

The PET surfaces were also modified with laser irradiation followed as G. Mayer *et* al. [19] The surface of irradiated PET demonstrated the appearance of new chemical species favorable for cell attachment. Laser treatment was shown to enhance the human epithelial cells L132 behavior, in particular cell proliferation and cell adhesion, and to modify cell morphology. It proved the importance of the choice of PET-films for such an investigation and for further application as an implantable biomaterial.

Furthermore, R. Ng *et* al. [20] and A. Hadjizadeh *et* al. [21] concerned in surface modifications of nonwoven PET matrices by NaOH treatment for biomedical applications. The dynamic seeding study demonstrated that the cell adhesion on PET fibers could be enhanced by NaOH treatment, largely due to the increased surface roughness of the PET fibers. However, the decrease in fiber diameter caused an increase in surface curvature of the fibers and the decrease in available surface area for cell attachment, resulting in slower cell growth. The PET fibers with NaOH treatment duration of 1-2 hr showed tensile properties close to that of natural vessels. The NaOH treated PET matrices are biocompatible and can be used as scaffolds for cell culture and tissue engineering.

2.2.2 Poly(caprolactone)

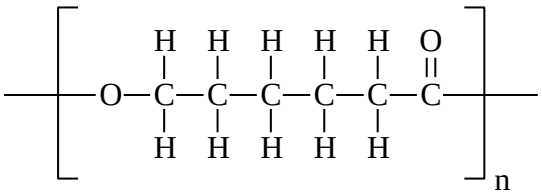

Scheme 2.3 Chemical structure of PCL

Polycaprolactone (PCL) is an important member of the aliphatic polyester family, which is a semicrystalline polyester. It is of great interest as it can be obtained by the ring-opening polymerization of a relatively cheap monomeric unit 'ε-caprolactone' as shown in Scheme 2.4. [22, 23]

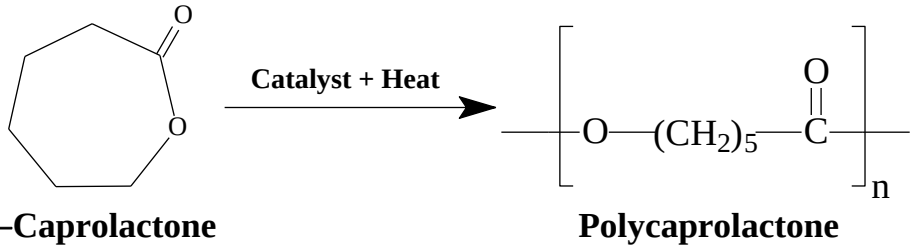

Scheme 2.4 Synthesis of PCL [24]

The PCL is highly processible as it is soluble in a wide range of organic solvents. PCL has a low melting point (55–60 ºC) and glass transition temperature (-60 ºC) while having the ability to form miscible blends with wide range of polymers. The polymer undergoes hydrolytic degradation due to the presence of hydrolytically labile aliphatic ester linkages; however, the rate of degradation is rather slow (2–3 years). Due to the slow degradation, high permeability to many drugs and non-toxicity, PCL was initially investigated as a long-term drug/vaccine delivery vehicle. PCL has low tensile strength (approximately 23 MPa) but an extremely high elongation at breakage (>700 %). [23] This polymer, produced commercially, can be fabricated by conventional thermoplastic processes and is utilized for making degradable containers for transplanting trees, etc. Thin foils, decomposing within a few days in moist soil, are useful for agricultural and packaging applications. [24] PCL has also been extensively investigated as scaffolds for tissue engineering due to its excellent biocompatibility [23] and the utilization of PCL in medical application are shown as followed;

H.Y. Kweon *et* al. [25] concerned in a novel degradable PCL networks for tissue engineering *via* photopolymerization. Degradation of PCL networks was faster than that of PCL

itself due to the lower crystallinity than PCL itself and incorporation of acrylate groups into PCL. Human osteoblast cell culture showed that the PCL networks were biocompatible and it can be expected to use as scaffold for tissue engineering.

J.M. Williams *et* al. [26] concerned in PCL scaffolds fabricated using selective laser sintering (SLS) to engineer bone tissue. The PCL scaffolds fabricated *via* SLS show great potential for replacement of skeletal tissues. These scaffolds possessed mechanical properties within the lower range of trabecular bone, suggesting they may have the ability to withstand early functional loading. *In vivo* results with bone morphogenetic protein-7 showed that SLS processed PCL scaffolds enhance tissue in-growth. The PCL scaffolds fabricated *via* SLS should prove advantageous for bone and cartilage tissue engineering in the future.

M. R. Williamson *et* al. [27] concerned in the synthesis of gravity spun PCL fibres for soft tissue engineering by wet spinning. Proliferation of Swiss 3T3 mouse fibroblasts and C2C12 mouse myoblasts on as-spun, 500% extension cold-drawn and gelatin-modified PCL fibres was consistently higher on gelatin-coated fibres relative to as-spun fibres at time points below 7 days. Fibroblast growth rates on cold-drawn PCL fibres exceeded those on as-spun fibres but myoblast proliferation was similar on both substrates. After 1 day in culture, both cell types had spread and coalesced on the fibres to form a cell layer, which conformed closely to the underlying topography. These properties recommended further investigation of gravity spun PCL fibres for 3D scaffold production in soft tissue engineering.

P.S. Tan and S.H. Teoh [28] concerned in effect of stiffness of PCL membrane synthesized by biaxial stretching on cell proliferation. The PCL membrane could be successfully manipulated by changing its thickness from 0.55±0.09 N/mm to 0.05±0.01 N/mm, its stiffness dropped from 0.55±0.09 N/mm to 0.05±0.01 N/mm. In addition, it is possible to induce better cell proliferation for 3T3 cells on PCL membranes of decreasing stiffness.

H. Zhang *et* al. [29] concerned in the interaction between bone marrow stromal cells (BMSC) and Arg-Gly-Asp (RGD) peptide-modified three-dimensional porous PCL scaffolds. The results demonstrated that the RGD modified PCL promoted BMSC attachment. The integrin-mediated signal transduction FAK–PI3K–Akt pathway was significantly up-regulated by

RGD modification and a subsequent increase in cell survival and growth was found in the modified scaffold. The modification of PCL with RGD peptide had advantage for its practical applications in tissue engineering.

S. Ozkan *et* al. [30] concerned in the fabrication with a twin screw extrusion/spiral winding process (TSESW) and *in vitro* assessment of protein-encapsulated PCL scaffolds for tissue engineering. The rate of proliferation of human fetal osteoblast (hFOB) cells and the rate of mineral deposition for wet extrusion method were found to be greater than for dry extruded scaffolds, presumably due to the important differences in surface topographies (smoother scaffold surfaces upon wet extrusion). Using hFOB cells, it was demonstrated that the scaffolds are non-cytotoxic with favorable cell adhesion, penetration and differentiation rates. The TSESW process offered significant advantages and flexibility in generating a wide variety of non-cytotoxic tissue engineering scaffolds.

Z. Shao *et* al. [31] concerned in the construction of MSC-homing peptide (E7) conjugated PCL electrospun meshes. After 7 days of implantation into a cartilage defect site of rat knee joints, the cells grown into the E7-conjugated PCL electrospun meshes yielded a high positive rate for specific MSC surface markers (CD44, CD90, and CD105), comparing with those in arginine-glycine-aspartic acid (RGD)-conjugated PCL electrospun meshes. Furthermore, the percentage of CD68 positive cells in the E7-conjugated PCL electrospun meshes was much lower than that in the RGD-conjugated PCL electrospun meshes. This result indicated that the E7-conjugated PCL electrospun meshes absorb much less inflammatory cells *in vivo* than the RGD-conjugated PCL electrospun meshes. The results of the present study suggested that the identified E7 peptide sequence had a high specific affinity to MSCs. Covalently conjugating this peptide on the synthetic PCL mesh significantly enhanced the MSC recruitment of PCL *in vivo*. This method provided a wide range of potential applications in tissue engineering.

M. Liu *et* al. [32] concerned in the preparation of liposome-loaded PCL microspheres (LPMs) as a drug delivery system for controlling the release of flurbiprofen. Liposomes were successfully encapsulated in LPMs using water/oil/water double emulsion solvent extraction/evaporation method. The higher concentration of PCL was conducive to gain slower cumulative release rate of LPMs. However, the larger amount of liposomes promoted the

aggregation between emulsion droplets and causes more pores on the surface of LPMs, which leads to lower drug encapsulation efficiency. In addition, the presence of poly(vinyl alcohol) (PVA) in the outer water phase stabilized the emulsion droplets against coalescence and resulted in an increased difficulty for flurbiprofen liposomes to diffuse out. The smaller LPMs with more porous surface had faster cumulative release rate.

From the literature reviews, PET which must be improved its surface for good biocompatibility had high mechanical properties; on the other hand, PCL was biodegradable and biocompatible polymers. Therefore, PET and PCL were selected for the preparation of calcium silicate/poly(ethylene terephthalate-*co*-caprolactone) composites (CS/PET-*co*-PCL). The composites prepared by *in situ* polymerization technique could gain better distribution of polymer into the structure of CS. Therefore, the CS/PET-*co*-PCL composites were synthesized *via in situ* ring-opening polymerization (ROP) of cyclic reagents in this thesis because ROP did not have the residual monomers which can cause toxicity problem and need the elimination step before applied. The cyclic reagents of CS/PET-*co*-PCL synthesize were cyclic oligo(ethylene terephthalate) (C-OET) and ε-caprolactone (CL). C-OET was synthesized from cyclodepolymerization (CDP) of commercial grade PET.

2.3 Synthesis of cyclic oligomers

The cyclic oligoesters can be prepared as the major products by using very high dilution conditions. Usually only small amount of cyclic oligomers are formed during the bulk condensation polymerization. However, much more cyclic oligomers can be produced under dilute conditions because the local concentrations of reactive chain ends belong to the same oligomer is much higher under dilute conditions. The syntheses can be conducted by using high-dilution methods, polymer-supported techniques, and cyclodepolymerizations (ring-chain reaction). [33]

a) Direct synthesis

Cyclic oligomers have been prepared by a classical high dilution technique. It is a simple reaction at a high dilution of: a) diol and diacid, b) diacid and diester, c) or diester only. [33]

b) Polymer-supported method

The cyclic oligomers can be prepared by using polymer-supported reagents. It was reported that cyclic polyester was prepared by the utilization of an intramolecular alkylation reaction of a ω-bromocarboxylic acid using an anion-exchange resin. [33]

c) Cyclodepolymerization (ring-chain reaction)

These cyclic oligomers can also be obtained by the cyclodepolymerization (CDP) of linear polyesters. This technique is useful for recycling of polyesters. A typical depolymerization is carried out by refluxing in dilute solution for many hours in the presence of metal catalysts such as organotin or titanate compound. Different solvents and catalysts were used for the

depolymerization at low concentrations. At the end of the reaction time, the solution is cooled down to a temperature until the polymer is precipitated. [33]

2.4 Ring-opening polymerization

Polymers may be prepared by routes involving ring-opening, which must be classed stoichiometrically as addition, since no small molecule is split off in the reaction. Ring-opening polymerization (ROP) is an important polymerization technique, along with other step and chain polymerization techniques, for production of polymers. Some typical examples are given in Table 2.2. The polymerization of these compounds has some aspects of both chain and step polymerization as far as kinetics and mechanism are concerned. It resembles chain polymerization in that it proceeds by the addition of monomer (but never of larger units) to growing chain molecules. However, the chain-initiating and subsequent addition steps may proceed at similar rates; if so, these are not chain reactions in the kinetic sense. As in stepwise polymerization, the polymer molecules continue to increase in molecular weight throughout the reaction. [34]

Table 2.2 Typical ring-scission polymers [34]

Type	Example
Lactone	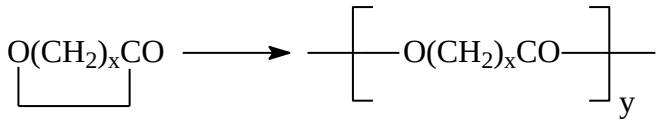
Lactam	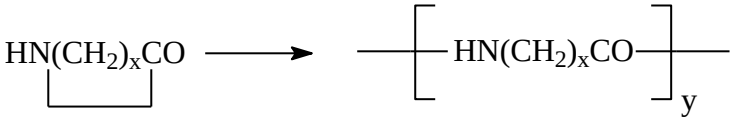
Cyclic ether	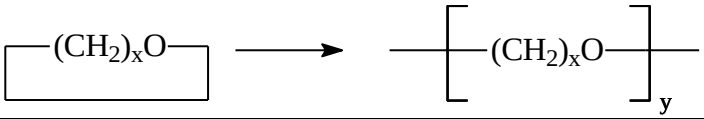
Cyclic anhydride	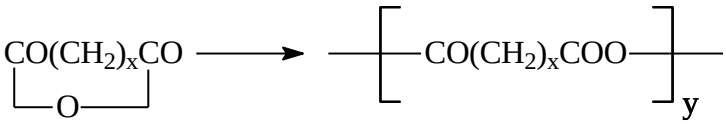
N-carboxyanhydride	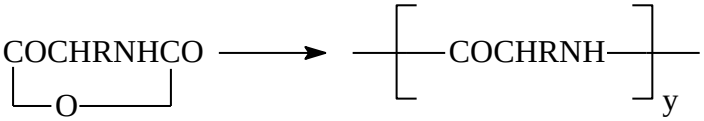

The inherent advantage of ROP is the transformation of low molecular weight cyclic precursors to high molecular weight polymers without formation of any by products. Molecular weights as high as 100,000-300,000 g/mol are reported for the ROP, while the highest molecular weights achieved by step polymerization are 40,000-60,000 g/mol. The low melt viscosity of the cyclic oligomers allows processing by various techniques, such as pultrusion, resin-transfer molding, melt filtration, or reaction injection molding either concurrent with or just prior to polymerization. Low viscosities are thought to be very useful for polyesters with high melting points and high melt viscosities such as poly(ethylene naphthalate) or poly(butylene naphthalate). High molecular weight polyesters have been prepared by ROP using simple procedures in the presence of various transesterification catalysts. The most effective catalysts are usually organotin and organotitanate compounds. The application of ROP technique in the preparation of engineering thermoplastics relies on the availability of corresponding aromatic cyclic monomers. Thus, the synthesis of the cyclic monomers has been the major subject in this field. [33, 35]

The literature reviews involved with cyclodepolymerization (CDP) and ring-opening polymerization (ROP) are shown as followed;

A.J. Hall *et* al. [36] concerned in the synthesis of a series of cyclic oligo(alkylidene isophthalate)s by CDP. With up to 15 ring atoms per repeat unit, the main products were the cyclic dimers with smaller amounts of the larger rings. When there were more than 16 ring atoms per repeat unit, the main products were the cyclic monomers with smaller amounts of the larger rings. Possible applications for such cyclic oligomers were discussed including their possible used as feedstocks for entropically driven ring-opening polymerizations (ED-ROP) and as building blocks for novel polymeric structures.

S.D. Kamau *et* al. [37, 38] concerned in the CDP of poly(propylene terephthalate) (PPT) , polyurethane (PU) and its ROP. Each polymer was heated under refluxing in 1,2-dichlorobenzene for CDP. The CDP of PPT or PU gave a mixture of cyclic oligomers in high yield. The major cyclic oligomer of PPT in the mixture product was cyclic dimer and of PU was approximately 20 ring atoms per repeat unit. For PPT, some ED-ROP of the cyclic oligomers and some copolymerizations with cyclic oligomers were successfully carried out. ^{13}C-NMR spectroscopic analysis showed that the copolymers were random structure. The molecular weights of PU which were obtained from the ED-ROPs using the pure cyclic monomers and tetrabutylammonium tetraphenylborate catalyst were higher than those of the starting polymers.

M. Alessi *et* al. [39] concerned in CDP of PET, poly(trimethylene terephthalate) (PTT) and poly(butylene terephthalate) (PBT) and *in situ* polymerization of cyclic oligomers. The CDP of the polymers was prepared by refluxing in 1,2-dichlorobenzene with di-*n*-butyltinoxide as a transesterification catalyst. At low concentration (1 %wt/v), GPC analysis indicated that the major products were cyclotrimer for PET, cyclodimer for PTT and a mixture cyclodimer-cyclotrimer for PBT. By increasing reaction concentration the residual insoluble fraction (POL) increased, while the macrocyclic oligomers (MCO) fractions decreased containing progressively higher amounts of large rings. An increasing the initial polymer concentration in CDP reaction resulted in the peaks broaden and shift towards lower temperatures in DSC profiles. Blends of the macrocyclic oligomers and the corresponding polymer showed greatly lowered melt viscosities due to the presence of the less viscous cyclic oligomers. Indeed, the required blends could be obtained easily in one step by carrying out polymer synthesis or CDP at the proper concentration in order to directly achieve a polymer/MCO mixture with the desired melt viscosity.

K.Y. Chang and Y.D. Lee [40] concerned in the ROP of ε-caprolactone (ε-CL). A novel 5′-deoxy-5-fluorouridine-poly(ε-caprolactone) (5′-DFUR-PCL) polymer was synthesized by the ROP of ε-CL using the 5′-DFUR as initiator and Sn(II) 2-ethylhexanoate ($Sn(Oct)_2$) as the catalyst. The results revealed that the molecular weights of the 5′-DFUR-PCL polymers were close to the theoretical values calculated from the ε-CL to 5′-DFUR molar ratios and their recovery yields were as high as 90 %. This study has provided an efficient method for the preparation of 5′-DFUR-PCL polymers. These novel 5′-DFUR-PCL polymers could be applied as drugs on carriers without the need for the coating or grafting processes associated with drugs in drug delivery and had great potential for cancer therapy.

2.5 Copolymers

Generally, copolymers are defined as polymeric materials containing two or more kinds of mers. The copolymers may be produced by step reaction or by chain reaction polymerization. It is important to note that if the reactant species are A and B, the composition of the copolymer is not a mixture or blend $[A]_n + [B]_n$. [14]

Most naturally occurring polymers are largely homopolymers, but both proteins and nucleic acids are copolymers. While many synthetic polymers are homopolymers, the most widely used synthetic rubber (SBR) is a copolymer of styrene (S) and butadiene (B). A widely used plastic (ABS) is a copolymer or blend of polymers of acrylonitrile, butadiene, and styrene. A special fiber called Spandex is a block copolymer of stiff polyurethane and flexible polyester. [14]

The copolymers may be alternating copolymers, in which there is a regular order of A and B in the chain.

—A—B—A—B—A—B—A—B—A—B—

; Alternating copolymers

; random copolymers, in which the sequences of A and B are arranged in a random fashion.

—A—B—B—B—A—B—A—B—A—A—

; Random copolymers

; block copolymers, in which there are long sequences of the same repeating unit in the chain.

—B—B—B—B—B—A—A—A—A—A—

; Block copolymers

; or graft copolymers, in which the chain extension of the second monomer is as branches.

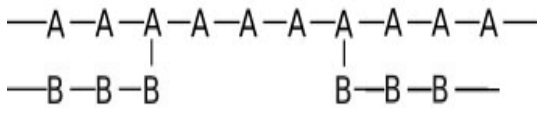

; Graft copolymers [14, 41]

There were the literature reviews about PET or PCL copolymers which were synthesized by ROP. Z.Y. Qian *et* al. [42] concerned in the synthesis of poly(ethylene terephthalate)/poly(ethylene glycol) (PET/PEG) multiblock copolymer by the macromolecular transesterification method and its *in vitro* degradation study. Water absorption decreased with

increase in concentration of PET segment, and it increased with molecular weight of PEG segment *via* microphase separation. The degradation rate increased with decrease in the PET concentration. During hydrolytic degradation, the amorphous region is attacked by the first, and then the crystalline region was also attacked.

A.R. Tripathy *et* al. [43] concerned in the synthesis of copolyesters using ROP of cyclic poly(butylenes terephthalate) oligomers (c-PBT) and ε-caprolactone monomer (CL) in the presence of stannoxane catalyst. The NMR results indicated that the c-PBT/CL copolymers were random structure and the reaction between c-PBT oligomers and the CL was a transesterification reaction. The synthesized copolymers exhibited a range of thermal properties from very low glass transition temperature (-30 °C) to high melting temperature dependent on c-PBT content. Furthermore, the mechanical properties could be adjusted by varying the CL amount in the copolymers. Therefore, the c-PBT/CL copolymers with various properties could be candidates to use in the various applications by adjusting the ratio of c-PBT:CL in the copolymer.

R. Saint-Loup and J.J. Robin [44] concerned in the synthesize of thermoplastic elastomers by direct copolyesterification of reactive oligomers of poly[(ethylene terephthalate)-*co*-(ε-caprolactone)] and poly(propylene oxide) (PPO) with the ROP of ε-caprolactone onto the hydroxyl end groups of the PET oligomers. The chemical structure of the poly(ester-ether) from ^{1}H-NMR spectroscopy showed that a polyesterification reaction occurred. The poly(ester-ether) was determined to show thermoplastic elastomer behavior with two glass transition temperatures and a melting point. The multiblock poly(ester-ether) was shown to be a segmented product made up of three different phases: an amorphous one constituting mainly PPO, an amorphous phase with amorphous PET-co-(ε-caprolactone) segments and a crystalline phase.

P. Monvisade and P. Loungvanidprapa [45] concerned in the synthesis of poly(ethylene adiapate-*co*-terephthalate) (ROP-PEA-*co*-PET) *via* ROP of cyclic oligo(ethylene adipate) (C-OEA) and cyclic oligo(ethylene terephthalate) (C-OET). Firstly, PEA was prepared by polycondensation between dimethyl adipate and ethylene glycol in the presence of tetraisopropyl orthotitanate (0.5 %wt of dimethyl adipate) under nitrogen gas. C-OEA and C-OET were synthesized *via* CDP by reflux of the mixture of PEA or PET in dichlorobenzene in the presence of di-*n*-butyltin oxide. ROP-PEA-*co*-PET was achieved *via* ROP of C-OEA and C-OET. T_g of

ROP-PEA-*co*-PET was at -8 °C with no melting temperature. There are two new ^{1}H-NMR signals with different chemical shifts of ethylene unit. This indicated the random tranesterification of C-OEA and C-OET.

P. Monvisade and P. Loungvanidprapa [46] concerned in the synthesis of poly(ethylene terephthalate-*co*-isophthalate) (PET-*co*-PEI) *via* ROP. The ROP-PET-*co*-PEI were prepared by equilibrating an equimolar amount of cyclic oligo(ethylene terephthalate) and cyclic oligo(ethylene isophthalate) using di-*n*-butyltinoxide catalyst under high concentration conditions at 270 and 290 ºC for 8 and 12 hr. The copolyesters were obtained in yields of 70-91 % with the inherent viscosity of 1.27-2.89 dl/g indicating the drastically high molecular weight compared with the conventional and ROP routes for the synthesize of PEI. The DSC data of ROP-PET-*co*-PEI showed the T_m above 400 ºC indicated the potential used in high temperature application.

N. Gonzalez-Vidal *et* al. [47] concerned in an influence of size of the cyclic oligoesters on the ROP reaction and on the structure and properties of the resulting polyesters. The copolyesters with oligomeric hexamethylene terephthalate (HT) and ε-caprolactone (CL) were prepared by ROP. The microstructure evolved from random to blocky as the content in CL increased. When comparing with the copolymerization of the 6–7 fractions of HT, the 2–5 fractions with ε-caprolactone produced copolyesters with almost undistinguished composition, microstructure and thermal properties but with significantly lower molecular weight. The polymerization rate evidenced a lower reactivity of $c(HT)_n$ with decreasing values of n.

This thesis involved with PET-*co*-PCL copolymers which there were the literature reviews as followed;

D. Ma *et* al. [48] concerned in synthesize and characterization of ET-ε-CL copolyesters (TCL) with different hard segment contents. The analysis from ^{1}H-NMR revealed that when the hard segment content in TCL was higher than 70 % or lower than 30 %, the molecular weight of the copolymers was greater than 400 and the ET segments or CL segments could crystallize even during quenching from melt. TCL copolyesters with about 50 % hard segment content had mechanical properties of elastomers, while TCL copolyesters with hard segment content higher than 60 % showed the properties of plastics as a result of the crystallization of ET segments.

Z.P. Zhang *et* al. [49] concerned in the transesterification of PET with PCL. The ^{1}H-NMR results showed that the transesterification took place in the melt blends. However, even in the blend that has been tranesterified for 8 hr; the random PET-PCL copolyester, PET-PCL copolyester with long PET or long PCL segments and the unreacted PET and PCL homopolymers may coexist. Due to the low mobility of PET and PCL chains and the high viscosity of the two macromolecules, the transesterification proceeded with difficulty and occurred at the interface or in the interfacial region between two phases, and finally the reaction could only reach a local equilibrium. These results indicated that in fact the transesterification in the melt blend between two incompatible homopolymers could not lead to the formation of completely random or typical block copolyesters.

K.Y. Lim *et* al. [50, 51] concerned in preparation and characterization of PET/PCL copolyesters. In the case of copolyesters containing CL units less than 26 %mol, the melting and crystallization temperatures decreased with increasing CL content. They exhibited diffraction patterns similar to PET. However, the variation of *d*-spacing on the diffraction pattern suggested that a small amount of CL could be into the crystal of ET. In the copolyesters containing CL components higher than 38 %mol, they acted as amorphous random copolymers. Furthermore, the copolyesters with CL contents higher than 38 %mol exhibited a viscosity behavior similar to Bingham fluid and the copolyesters with CL contents lower than 26 %mol exhibited a Newtonian flow behavior similar to PET. In addition, relationship between properties of PET/PCL copolymers and blending time was investigated. At a longer blending time, the PET/PCL copolymers tend to be random. With an increasing blending time, the melting and crystallization temperatures of PET/PCL copolymers decreased. Therefore, the biodegradability of PET/PCL copolyesters increased with an increase in the blending time. This suggested that these copolyesters with desired biodegradability behaviors were successfully prepared by the melt blending of polymers.

R. Saint-Loup *et* al. [52] concerned in the synthesis of multiblock poly(ethylene terephthalate)/poly(Ɛ-caprolactone) copolyesters by polyesterification of hydroxytelechelic poly(ethylene terephthalate) (PET) and carboxytelechelic poly(Ɛ-caprolactone) oligomers. For the synthesis of poly(ethylene terephthalate)/poly(Ɛ-caprolactone) copolyesters (PET/PCL), the

copolyesterification of hydroxytelechelic PET and the carboxytelechelic poly(ε-caprolactone) oligomers which was performed under nitrogen at 260 °C for 30 mins using dibutyltinoxide (DBTO) as catalyst was an optimum condition. The ^{1}H-NMR spectrum of products showed signals corresponding to PET and poly(ε-caprolactone) blocks and the chemical linkage between the different blocks. The DSC and DMA data indicated that there were three different phases in the copolyester. The main phase was composed of the ester-ester exchange reaction resulting in the random polyester. Other two phases were constituted by PCL and by PET.

2.6 Calcium silicate or wollastonite

2.6.1 General information

- **Chemical composition**

A calcium silicate with the following formula:

$$CaSiO_3$$

Theoretical calcium silicate is as follows: [53]

$$48.3\%\ CaO + 51.7\%\ SiO_2$$

- **Mineralogical structure**

Calcium silicate has a sorosilicate structure where two silicon tetrahedrons connect to form a pair sharing an oxygen ion (Fig. 2.1).

Usually of fibrous appearance (the crystals are needle-shaped or, sometimes, tabular), this mineral has a specific weight of 2.9, scores 4.5-5 on the Mohs hardness scale and is white in color.

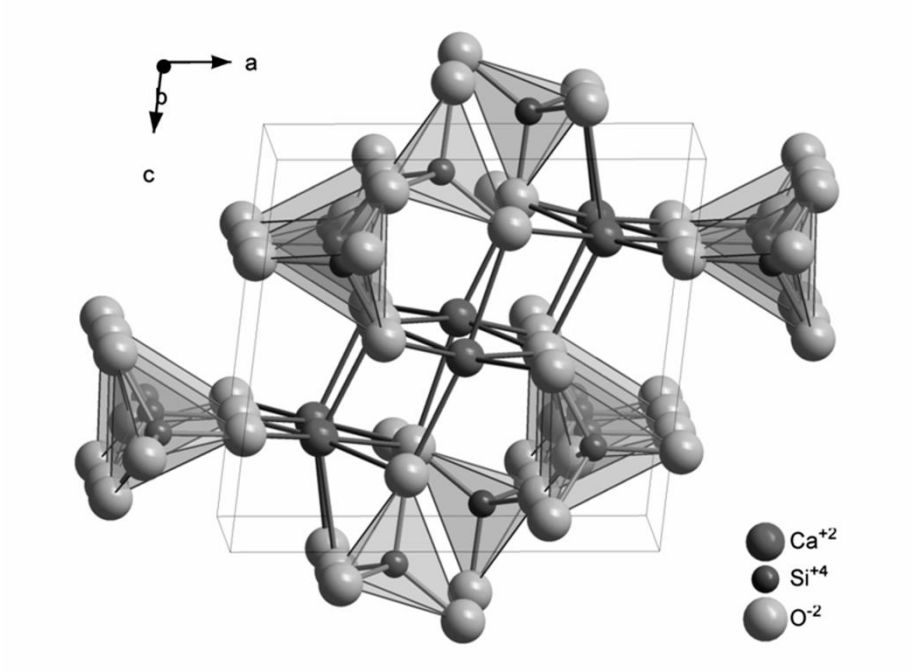

Figure 2.1 Unit cell of calcium silicate

The natural form, stable at ambient temperature, changes to allotropic pseudowollastonite at 1,125 °C. [53]

- **Physical Properties [54, 55, 56]**
  - Density : 2.87-3.09 g/cm^3

- Color: Although, pure calcium silicate is white in common, other color is occurred from impurity of other compound in its.
- Thermal expansion: Quite high thermal expansion and highly endure to thermal shock to be suitable high temperature application.
- Melting point: 1,540 °C
- Calcium silicate is a highly stable mineral that shows no material loss or allotropic transformation below 1,000 °C.

- **Chemical properties [54, 55, 56]**
  - Low solubility
  - pH of calcium silicate suspension in water is 8-10

In recent years, calcium silicates have been investigated as a new bioceramics for many applications in dental root, bone regeneration and biotechnology such as enzyme immobilization, and gene transfection because of their bioactivity. [53]

2.6.2 Synthesis of calcium silicate

- **Solid-state reaction**

Solid-state reaction is a simple process which most products are oxide groups. The effect to structure and properties of compound is atomic size, oxidation state and bonding between cation. [57, 58]

F.M.Z. Kaifi *et* al. [59] concerned in the synthesis of wollastonite from solid-state reaction between calcite ($CaCO_3$) and silica (SiO_2). The 26 g silica and varied amount of calcite (15-30 g) were heated at temperature range from 650-1000 °C. It was observed that synthetic CS from 26 g silica to 15 g calcite at 650 °C for 1 hr to be achieved maximum yield (98.72 %). For comparative study, CS was also prepared by reacting calcium chloride with sodium silicate in a hot solution of calcium chloride dehydrate sodium silicate. All synthetic CS had the chemical formula close to the natural CS. CS prepared from 1:1.5 ratio of calcium chloride and sodium silicate obtained the highest yield at 82.6 %. While this chemical procedure is not economically feasible as both reactants are expensive.

J. Podporska *et* al. [60] concerned in the wollastonite-containing bioceramics and determined its bioactivity. Poly(methylphenylsiloxane) resin, $Ca(OH)_2$ and SiO_2 pellets were heat-treated at 1,000 °C for 24 hr in an inert atmosphere and then sintered at 1,000, 1,100 or 1,200 °C. XRD analysis confirmed the presence of α-$CaSiO_3$ with mean grain size of about 52 nm. When the sintering temperature was increased, grain growth was visible and the mean grain size increased. For chemical composition, the samples sintered at 1,000 and 1,200 °C contained CS as the main phase. However, the samples sintered at 1,100 °C had an additional phase, consisting significantly lower quantities of calcium because CS could be partly dissolved, creating another silicate (metastabile phase). Finally, all the samples showed very good bioactivity, in which the surface was totally covered by the cauliflower shape crystalline layer of hydroxyapatite after soaking in SBF solution for 30 days at 37 °C.

T.V. Vakalova *et* al. [61] concerned in the solid phase synthesis of wollastonite from natural and technogenic raw materials. The synthesis of CS was reaction between lime (CaO) and natural silica (diatomite, opoka, marshallite) or technogenic (microsilica, and anhydrous silicic acid) silica. In case of the mixtures of 1:1 lime and silica composition were heated to 1,200 °C, the endothermic effects in the range 712–812 °C was connected with thermal dissociation of the carbonate component and an exothermic effect with a maximum at 877–896 °C was caused by polymorphism of different forms of silica. Less intense exothermic effects in the range 990–1,060 °C were connected with synthesis of wollastonite and its polymorphic transitions.

The wollastonite synthesis by a semidry method was accomplished in the range 1,000–1,200 °C with soaking at the maximum temperature for 1 hr. An increase in synthesized temperature from 1,000 to 1,200 °C showed the presence of formation of crystals of predominantly isometric shape with increasing of crystal size. The phase formation corresponded to β- and α-wollastonite. In addition, it had been revealed that the excess content of silica (lime:silica = 1:1.2) within the composition of wollastonite promoted more active occurrence of synthesis and provided preparation of highly porous ceramic materials with open porosity from 50 to 55 %, and with a sufficiently high ultimate strength in compression.

- **Sol-gel synthesis**

Sol-gel synthesis is prepared by dissolving metal alkoxide compounds such as tetramethoxy silane (TMOS), tetraethylorthosilicate (TEOS) in suitable solution. Next hydrolysis and condensation process are occurred in order to get gel. Finally, the gel was dried. [62]

W. Xia and J. Chang [63] concerned in the synthesis of well-ordered amorphous mesoporous CS (MCS) by sol-gel technique between TEOS and $Ca(NO_3)_2 \cdot 4H_2O$ using triblock copolymer as a template. The phase transformation to α-CS was observed at 800 °C which was lower than common CS at 1,125 ºC phase transformation temperature and α-CS was completely crystallized. Furthermore, the BET surface area of MCS decreased with the increase of the calcination temperature because of the growth of the α-CS. The SEM image revealed that the morphology of MCS was changed from smooth to rough surface after calcinations at 800 ºC, occurred from the collapse of mesopores and the aggregation of pore walls. The results suggested that phase transformation behavior of the CS not only provided a new idea for design and preparation of materials, but also gave an alternative way for preparation of high temperature ceramics at lower temperature.

A. Meiszterics and K. Sinko [64] concerned in the preparation of CS ceramics by a low energy-consuming sol-gel method between TEOS and $Ca(NO_3)_2 \cdot 4H_2O$ using various catalysts. The acetic acid proved to be the best catalyst for the preparation of a homogeneous system. The use of surplus water in the synthesis yielded porous final products. Above 500 ºC, the amorphous silica network decomposed, the bond system of CS started developing, a crystalline phase disappeared, and a new one formed. A loose open randomly branched CS network catalyzed with acetic acid altered into a compact aggregate structure above 500 ºC. Before the sintering, a treatment of the dried CS gels with TEOS resulted in the best material's properties.

- **Coprecipitation**

The recent ceramic literature is filled with many examples of ceramic powders produced by "coprecipitation" of a precursor salt then thermal decomposition to the oxide. The benefit of coprecipitation is "atomistic mixing" in the resulting ceramic powders. A solution of metal salts, often nitrates, is mixed with a precipitating agent common for all the metals. Oxalic, citric, or other organic acid or ammonium hydroxide are frequently used as the precipitating agent because

many metal oxalates or citrates or hydroxides have a low solubility. Basically there are two possibilities during coprecipitation process: (1) precipitation of a mixed metal precursor crystal (i.e., a double, or triple, salt) with a specific stoichiometric ratio of the metals, which will be called *true coprecipitation;* or (2) segregative precipitation of individual particles of the different metal oxalates, for example, that are colloidally unstable and hetero-coagulate together into a mixed aggregate particle, which will be called *simultaneous precipitation and coaggregation.* Which possibility takes place depends on the thermodynamics of the solution. [65]

Therefore, the coprecipitation is the process to precipitate the solutions which have required cation by mixing with precipitation agent such as ammonium hydroxide. The products are the precipitation of oxide compounds which were filtered and then dried. [66]

P. Siriphannon *et* al. [67] concerned in the preparation of fine $CaSiO_3$ powder by the coprecipitation method from $Ca(NO_3)_2 \cdot 4H_2O$ and $Si(OC_2H_5)_4$ (TEOS) using NaOH solution as a precipitant and its biocompatibility. From XRF, the amount of Na residue in nonwashed powders increased with increasing concentration of NaOH precipitant, while those of Ca and Si components decreased. The exothermic peaks at 600-800 °C corresponded to the crystallization of β-CS in the DTA curves. In addition, the Na residue could crystallize together with the Ca and Si components to form sodium calcium silicate phases as well as calcium silicate in the nonwashed powders fired at 900 °C. The amount of the Na residue decreased with the de-ionized water number of washing treatments. The exothermic peak of the washed powders was a higher temperature than those of the nonwashed powders and the XRD peak intensities of sodium calcium silicate phases apparently decreased in the washed powders.

And then, the amorphous CS was calcined at 900 °C for 2 hr to crystallize the CS phase. The green bodies were fired at 1,350, 1,400, and 1,450 °C for 2 hr with a heating rate of 2 °C/min. The highest bulk density of 2.59 g/cm^3 was obtained by firing of CS at 1400 °C, when the theoretical density of α-CS is 2.90 g/cm^3 because the transformation of β-CS to crystalline phase α-CS occurred at high temperature. In the microstructures, elongated large α-CS grains were observed with a very thick glassy phase in the grain boundaries. The grain sizes increased with increasing firing temperature. The formation of glassy phase and the reduction of grain sizes were also related to the presence of a small amount of Na residue in the starting powder.

X. Wan *et* al. [68] concerned in the preparation and *in vitro* bioactivities of calcium silicate nanophase materials. Nano-sized amorphous $CaSiO_3$ (A-CS) and β-wollastonite (β-CS) powder were produced by chemical precipitation method and subsequent heat treatment, using $Ca(NO_3)_2 \cdot 4H_2O$ and $Na_2SiO_3 \cdot 9H_2O$ as the starting materials, polyethylene glycol as the dispersant. Two forms of $CaSiO_3$ nanophase materials were prepared with different amorphous and crystalline phases using relevant nano-sized powders as precursors. A-CS compact was rough, porous and composed of elongated particles, while the β-CS crystallites were smooth, dense and spheric and some crystallites formed agglomerates. The results of *in vitro* test revealed that only uniformly sized HAp particles crystallized on β-CS surfaces. A-CS was however covered with $CaCO_3$, which crystallized from the amorphous $CaCO_3$ nuclei present in the starting powder. The A-CS showed a faster formation of HAp because of the high release rate of Ca. The results suggested that both A-CS and β-CS had good *in vitro* bioactivity and the bioactivity of A-CS was higher than that of β-CS.

The CS powders could be also synthesized from other methods such as hydrothermal method. K. Lin *et* al. [69] concerned in the CS preparation *via* hydrothermal microemulsion method using cetyltrimethyl ammonium biomide (CTAB) as surfactant and n-pentanol as cosurfactant. The $Ca(NO_3)_2$ and Na_2SiO_3 microemulsion solutions were used to obtain a suspension. The suspension of the microemulsion was heated at 200 °C for 18 hr.

The XRD pattern of the CS powders before calcinations showed numerous sharp peaks of the tobermorite as fairly well crystallize. On the other hand, some residual calcium oxide component existed as an amorphous state. The FETEM image indicated that the tobermorite powders had a smooth surface and a wire-like shape, 20-30 nm in diameter and up to tens of micrometers in length.

After calcination at 800 °C, the phase of the powders transformed from tobermorite to CS which had the Ca/Si molar ratio of 0.96. A mechanism of the CS formation from tobermorite was followed as:

$$Ca_5(Si_6O_{16})(OH)_2 \cdot 4H_2O + CaO \longrightarrow 6CaSiO_3 + 5H_2O$$

From the FETEM image, it can be seen that the crystal structure of CS similar to tobermorite structure. The electron diffraction pattern of the nanowires demonstrated the single crystal of CS nanowires, indicating the successful synthesis of CS single crystal by hydrothermal microemulsion method.

The CS was widely used in the medical applications as followed;

P. Siriphannon *et* al. [70] concerned in the effect of the structure of the $CaSiO_3$ powders on the formation behavior of HAp by soaking in a SBF solution. The CS powder was prepared by coprecipitation of $Ca(NO_3)_2 \cdot 4H_2O$ and TEOS with NaOH solution as a precipitant. The resultant CS was calcined at 500 ºC. The calcined powder (amorphous CS) was divided into three parts and subjected to different firing processes as follows; (1) fired at 1,000 °C for 2 hr to obtain the low temperature crystalline phase β-CS and (2) fired at 1,400 °C for 2 hr to obtain the high temperature phase α-CS. The results indicated that the increased firing temperature caused the powder particles to densify and a decrease in their specific surface area.

In the case of HAp forming, the $CaSiO_3$ powders were soaked in the SBF solution at 36.5 °C. The SBF soaked CS was observed the peaks composed of the HAp band and a crystalline peak of HAp. Anyway, co-existence of $CaCO_3$ in the only amorphous-CS was observed. At longer soaking times, the number of agglomerated HAp particles increased with the formation of tiny new ball-like HAp particles. Corresponding to the differences in growth behavior of these three samples, the HAp layers formed on the β-CS and α-CS surfaces appeared denser than those on the amorphous-CS surfaces. The size of the product HAp particles decreased in the order α-CS>β-CS>amorphous-CS. The higher release of Ca from the amorphous-CS caused a more rapid increase in the pH of the SBF solution, resulting in the faster precipitation of HAp as effect to decrease in the P concentration of the solution. After prolonged soaking, the Ca concentration was similar in the solutions from amorphous-CS and β-CS, but was higher in the α-CS solution due to the complete dissolution of α-CS. After that, the Ca, Si, and P concentrations became almost constant, indicating an apparent equilibrium state between the dissolution of the powder surfaces and the formation of HAp.

W. Xue *et* al. [71] concerned in the behaviour of the bone tissue around CS coatings by *in vivo* testing. After that, the CS coatings were deposited on titanium coated Ti–6Al–4V rods substrate as a bond layer using an atmospheric plasma spray system. The SEM morphologies of the polished cross-section of the CS coatings after implantation in the dog's dorsal muscle for 3 months can be seen that a Ca–P layer to form on the surface of the coating which was precursor phase with 1.43 Ca/P ratio similar to bone apatite. Furthermore, a silica-rich intermediate layer could be observed between apatite and the CS coating, which was the result of the surface reaction of CS with surrounding body fluids. The histological morphologies of the interface

between CS coatings and bone tissue after implantation for 1 month could be seen that a new bone formed and filled up the gap between the implant and bone tissue. There was a distinct border between the newly formed bone and pre-existing bone. Three months after implantation, the newly formed bone around the implant appeared to be progressively replaced by a mature bone which could not be discriminated from the pre-existing bone. The CS coating was shown to stimulate more bone formation on its surface than titanium coating after implantation for 1 month, enhancing the short-term osseointegration properties of implant. Bone tissue did not bond directly to the CS coating, but through a Ca/P layer; on the other hand, the fibrous tissue was clearly seen around the non coated surface. The formation of bone-like apatite layer was very important for bonding to bone tissue which showed high bone inductivity property. Therefore, the results suggested that a CS coating may be suitable for the repair or replacement of living bone.

S. Xu *et* al. [72] concerned in the osteogenic property and degradability of CS ceramic scaffolds to compare with β-$Ca_3(PO_4)_2$ (β-TCP) ceramic scaffolds. The CS powders were synthesized by the reaction of $Ca(NO_3)_2 \cdot 4H_2O$ with $Na_2SiO_3 \cdot 9H_2O$. Porosity and compressive strength of the CS was close to of the β-TCP ceramics. The process of new bone formation was observed in CS and bone tissue could grow into the porous structure of CS ceramics after implantation in rabbit calvarial defects. The CS possessed much faster resorption rate and better bone regenerative capacity *in vivo* comparing with β-TCP. The TRAP-positive multinucleated cells were observed on the surface of CS, which suggested that the cell-mediated process is involved in the degradation of CS *in vivo*. Moreover, SEM and EDS analysis revealed that bone did not bond to the CS directly, but through the bone-like apatite layer. These results in this study suggested that the porous CS ceramics may be used as the bioactive and biodegradable materials for hard tissue repair and tissue engineering applications.

W. Xue *et* al. [73] concerned in the synthesis of mesoporous CS and its possible application in protein/drug delivery. The CS was synthesized by wet chemical method and then acid modified with hydrochloric acid at pH 7, 4.5, and 0.5. The results showed that a hydrated silica gel with abundant Si–OH functional group formed on the surface of CS due to acid modification. This surface layer had mesoporous structure which average surface area increased when pH of acid modification was decreased. Protein adsorption studies indicated that

mesoporous CS had higher ability to adsorb bovine serum albumin and lysozyme compared to unmodified particles. The release kinetics showed that proteins on mesoporous CS released sequentially over one week, whereas the proteins on unmodified particle followed burst release kinetics within a few hours. Human osteoblast cell–material interaction study showed that these materials were biocompatible and promoted excellent bone cell proliferation. In summary, this work had demonstrated the potential to produce mesoporous CS as a carrier for protein/drug delivery for bone regeneration and other biomedical applications.

M.A. de la Casa-Lillo *et* al. [74] concerned in the effect of the composition and thermal treatment on the bioactivity of wollastonite which obtained by sol–gel method. The results showed that all CS had bioactive property because an apatite could grow on their surface. The bioactivity was influenced by various parameters, such as, the thermal treatment, the different phases (glass-phase, wollastonite and pseudowollastonite) and the porous size. However, the sintering process was the important effect on the bioactivity of samples. The bioactivity decreased with increasing of the sintering temperature which observed from the ionic changes in the SBF. The sintering process made to the dissolution process of wollastonite delayed and therefore the rate of apatite formation also decreased.

P.N. Jagadale *et* al. [75] concerned in the structural, compositional and antibiotics carrier properties of novel nano-sized CS bioceramics. This CS was synthesized from $Ca(NO_3)_2 \cdot 4H_2O$ and $Na_2SiO_3 \cdot 9H_2O$ solution by a simple wet chemical technique. The X-ray diffraction pattern of the powder sintered at 1,250 °C for 3 hr revealed formation of single phase, hexagonal structure with about 34 nm-crystalline size. Norfloxacins solution was used in antibiotic charging experiment by measuring norfloxacins amount adsorbed on CS pellets. Every sample reached the adsorption equilibrium within 10 mins. The CS showed much higher charging amount of norfloxacins than those of calcium phosphate. This facilitated their future application in biomedicines.

2.7 Composites

Composite materials are those that contain two or more distinct constituent materials or phases, on a microscopic or macroscopic size scale. The term "composite" is usually reserved for those materials in which the distinct phases are separated on a scale larger than the atomic, and in which properties such as the elastic modulus are significantly altered in comparison with those of a homogeneous material. Accordingly, fiberglass and other reinforced plastics as well as bone are viewed as composite materials, but alloys such as brass or metals such as steel with carbide particles are not. Such composites consist of one or more discontinuous phases embedded within a continuous phase. The discontinuous phase is usually harder and stronger than the continuous phase and is called the *reinforcement* or *reinforcing material*, whereas the continuous phase is termed the *matrix*. [2, 11]

Composite materials offer a variety of advantages in comparison with homogeneous materials. However, in the context of biomaterials, it is important that each constituent of the composite be biocompatible, and that the interface between constituents not be degraded by the body environment. Composites currently used in biomaterial applications include the following: dental filling composites; bone particle or carbon fiber reinforced methyl methacrylate bone cement and ultrahigh-molecular-weight polyethylene; and porous surface orthopedic implants. Moreover, rubber used in catheters, rubber gloves, etc. is usually filled with very fine particles of silica to make the rubber stronger and tougher. [2, 11]

The composites between polyesters or their copolyesters and bioceramics were widely synthesized as the biomaterials. The examples of these composites were the preparation of HAp/poly(ethylene adipate)-*co*-poly(ethylene terephthalate) composites (HAp/PEA-*co*-PET) for biomaterial application by S. Chanawong *et* al. [76] The HAp powder was synthesized by co-precipitation method of calcium hydroxide and phosphoric acid and then shaped to the porous blocks. Cyclic oligo(ethylene adipate)-*co*-oligo(ethylene terephthalate) (C-PEA/PET) was synthesized by CDP technique. After that, HAp/PEA-*co*-PET composites were prepared by soaking the porous HAp blocks into the C-PEA/PET solution, and then *in situ* ROP of C-PEA/PET within the HAp blocks. The results from the weight difference between pre-composites and composites and TGA indicated an approximate HAp:PEA-*co*-PET ratio of 4:1 by weight. The compressive strength of composites was higher than that of the porous HAp blocks. Bioactivity of HAp/PEA-*co*-PET composites was studied by SBF. It was seem that HAp at the surface of samples dissolved in the SBF solution resulting in an increasing of the pH of SBF

solution suitable for deposition of HAp crystals on the composites surface. This result indicated the bioactive of HAp/PEA-*co*-PET composites.

Y.H. Koh *et* al. [77] concerned in the fabrication of macrochanneled poly(ε-caprolactone) (PCL)/hydroxyapatite (HAp) scaffolds with a controlled structure using the rapid direct deposition method. A warm PCL-HAp/acetone slurry was extruded through a 520-μm orifice in an ethanol coagulation reservoir in a layer-by-layer building sequence, in which the rapid solidification of the filament occurred *via* solvent extraction. This method produced a ~330-μm filament, wherein the HAp particles were homogenously dispersed in the PCL matrix. The fabricated PCL/HAp scaffold showed a periodic pore structure, with good bonding between the PCL-HAp filaments being obtained by post heat-treatment at 60 °C for 30 min. In addition, the sample showed linear elasticity followed by densification with non-catastrophic failure.

The CS was selected and incorporated with the polyesters or their copolyesters which there were some literature reviews followed as;

M. Risbud *et* al. [78] concerned in the preparation of composites of poly(butylene terepthalate)/CS (PBT/CS) and evaluation of their properties and *in vitro* biocompatibility. Composites of PBT with CS were prepared in two different proportions, 70/30 (PW-30) and 50/50 (PW-50). The DSC studies indicated the marginal changes in the melting behavior and enhanced crystallization in PBT/CS composites. The mechanical properties of the composites showed remarkable improvement as a result of incorporation of CS. SEM studies of fractured surfaces of impact samples showed no evidence of bonding between PBT and CS. Direct cell contact test did not show deleterious effects on NIH3T3 fibroblast morphology and DNA integrity indicating its compatibility. Leach out products (LOP) of PW-30 was evaluated non-toxic as tested by MTT assay. LOP did not induce proliferation of mouse splenic lymphocytes suggesting its immuno-tolerance. PW-30 also exhibited preliminary blood compatibility. These physical properties and biocompatibility of PBT/CS composites showed their suitability as potential biomaterials.

V. Suteesuksataporn *et* al. [79] concerned in the preparation of HAp/PET and CS/PET composites. The HAp and CS were prepared by co-precipitation and C-OET was synthesized by CDP of PET. The composites were prepared by mixing of HAp or CS with C-OET in the present

of DBTO as a catalyst and then packing in cylindrical shape. The C-OET in the composites was then ring-opening polymerized at 250 ºC for 24 hr. The composites were formulated with HAp or CS to PET ratios of 60:40 and 50:50. It was found that the values of compressive strength of both composites were higher than those of virgin ceramics and CS/PET composite was higher than that of HAp/PET composite. In addition, the higher of PET ratio in the composite had higher of compressive strength. *In vitro* bioactivity of composites was studied by soaking in SBF at 36.5 ºC for 7-28 days. After prolonged soaking, the HAp nanocrystals precipitated from the SBF solution and formed as a cauliflower-like shape on the composite surface. In addition, HAp crystal film covered on CS/PET composite was thicker than that of HAp/PET composite.

H. Li and J. Chang [80, 81, 82] concerned in the fabrication of a bioactive porous composite scaffolds by incorporation of CS powders into polyhydroxybutyrate-polyhydroxyvalerate (PHBV) for potential tissue repair and tissue engineering applications. Composite scaffolds of PHBV with bioactive CS were fabricated by a compression moulding, thermal processing, and salt particulate leaching method. The addition of bioactive wollastonite to the PHBV matrix resulted in higher compressive strength than pure PHBV. In addition, the incorporation of CS into PHBV could improve the hydrophilicity of the composites. The bioactivity of the composites in SBF showed that the CS/PHBV composites could induce the formation of HAp on the surface of the composite scaffolds within 14 days. *In vitro* degradation behaviors of the composite scaffolds in PBS solution within 15 weeks, it could be concluded that the addition of CS into PHBV delayed the degradation of PHBV in the composite scaffolds. This delayed degradation in the composite scaffolds was caused probably by the dissolution of alkaline ions from the CS, resulting in a buffering effect to the acidification of the PBS due to the acid degradation products of PHBV. These results suggested that the addition of CS into polymer may be a useful method to adjust the degradation rate of the composite scaffolds. In addition, PHBV/CS composite was applied for drug delivery. The *in vitro* release of the gentamicin from the composites was performed in SBF and PBS at 37 ºC for 22 days. The results showed that gentamicin was controlled released from the PHBV/CS composite at a relatively lower release rate as compared to that for the pure PHBV microspheres. The analysis of the microspheres after soaking demonstrated that a microporous apatite layer was formed on the surfaces of the composite microspheres when the release experiments were performed in SBF and PBS. This microporous apatite layer strongly decreased the release rate of gentamicin from the PHBV/CS

composite microspheres and resulted in a controlled release behavior. All of these results suggested that the PHBV/CS composite microspheres might be used as a drug release system. All of these results suggested that the incorporation of CS was a useful approach to obtain composite scaffolds with improved properties.

The composites between CS and poly-(D, L-lactide acid) (PDLLA) were researched for the medical applications. The composite scaffolds of PDLLA with bioactive wollastonite which were fabricated by the conventional solvent casting-particulate leaching method were concerned by H. Li and J. Chang [83] and by L. Xu *et* al. [84] The mechanical property and hydrophilicity of the composites were improved with incorporation of CS into PDLLA. The HAp could form on the surface of composites after soaking in SBF for 7 days and the degradation of composites was slower than of pure PDLLA. The *in vitro* cell culture experiment proved that the composite scaffold had good biocompatibility for the growth of the osteoblast. L. Ye *et* al. [85] and M. Zhang *et* al. [10] synthesized the bioactive PDLLA and wollastonite composite films as CS surfaces were modified with dodecyl alcohol. Then, the obtained composite films were treated in boiled water to remove the dodecyl chains. SEM images showed the homogenous dispersion of β-CS particles in composites after hydrolysis and the strength of composite films both before and after hydrolysis was higher than that of pure PDLLA films while the modified composite before and after treatment could induce the formation of HAp on its surface after the immersion in SBF. In addition, cells cultured on composite films after hydrolysis presented the highest cell proliferation rate and differentiation level. All these results suggested that the CS/PDLLA composites may be biomaterials candidates for tissue engineering applications.

H. Li and J. Chang [86] investigated the degradation of poly(lactic acid-*co*-glycolic acid) (PLGA) in the composites between PLGA and bioactive inorganic fillers such as CS, bioglass 45S5 (BG) and HAp. The composite scaffolds which were immersed in PBS solution at 37 °C for 8 weeks indicated that the pH of the pure PLGA fell to 4.3 in 8 weeks while the pH of the composites with CS and BG was maintained approximately 7.4 throughout the soaking period. However, the pH of the composites containing HAp decreased from 7.4 to 5.6 during the whole soaking time. It indicated that the incorporation of CS and BG delayed the degradation of the PLGA in the composites while the incorporation of HAp accelerated the degradation. All of these results suggested that incorporations of both CS and BG into PLGA strongly affected the

degradation behavior of scaffolds. L. Zhao *et* al. [87] concerned in preparation and characterization of CS/PLGA composites. Hydrophilicity of the composites decreased which indicated an increase of the cell biocompatibility, confirmed by the attachment and proliferation of rabbit bone marrow stromal cells (rMSCs) on the surface of the composites. Furthermore, the apatite-forming ability of the PLGA-coated CS was maintained. This study suggested that the CS coating with PLGA may be candidate in the applications of bone tissue engineering.

P. Monvisade *et* al. [88] concerned in the preparation of hydroxyapatite/poly(methyl methacrylate) (HAp/PMMA) and calcium silicate/poly(methyl methacrylate) (CS/PMMA) composites by interpenetrating bulk polymerization of methyl methacrylate (MMA) monomer in porous structures of HAp and CS. The porous HAp and CS templates were prepared by mixing their calcined powders with poly(vinyl alcohol) (PVA) solution, shaping by uniaxial pressing and then firing at 1,100 °C for HAp and 900 °C for CS. The templates were soaked in the solution mixture of MMA monomer and 0.1 %mol of benzoyl peroxide (BPO) for 24 hr. The pre-composites were then bulk polymerized at 85 °C for 24 hr under nitrogen gas. The results showed the interpenetrating of PMMA into the porous HAp and CS structures. TGA indicated that the PMMA content in the HAp/PMMA and CS/PMMA composites were 13 and 26 %wt, respectively. Weight average molecular weights ($\overline{M}_w$) of PMMA were about 491,000 for HAp/PMMA composites and about 348,000 for CS/PMMA composites. Compressive strengths of these composites were about 90-131 MPa.

G. Chouzouri and M. Xanthos [89, 90] concerned in the effects of degradation in PBS on the properties of the composites between aliphatic polyesters (PCL and Poly(lactic acid); PLA) and bioactive fillers (Bioglass; BG and CS) and their bioactivity. The CS and BG fillers enhanced the degradation behavior for both PCL and PLA composites. Thermal data showed crystallinity increased with immersion time in all samples. BG appeared to affect the crystallinity of PCL more than the CS. In the case of PLA composite, BG decreased the T_g of the composite as immersion time was increased. Mechanical testing showed a significant decrease of elongation at break for PLA after a short 2-week immersion period. The bioactive glass composite initially showed fast growth of the precipitated minerals and partial surface coverage after 1-week SBF soaking, whereas in the CS composite, growth and surface coverage increased as a function of immersion time in the SBF solution until 4 weeks of soaking. XRD results showed appearance of

HAp for both types of composites within 1-week SBF soaking. Both fillers enhanced the hydrolytic degradation of the matrix in PBS.

J. Wei *et* al. [91, 92] concerned in the bioactive composite scaffold preparation from mesoporous wollastonite (m-WS) and PCL. The m-WS were synthesized with sol-gel method of tetraethyl orthosilicate and calcium nitrate tetrahydrate with surfactant and the conventional wollastonite (c-WS) was synthesized as same as m-WS without using surfactant. The c-WS/PCL (c-WPC) and m-WS/PCL (m-WPC) composites scaffolds were prepared by a solvent casting-particular leaching method. The TEM images and BET showed the lower surface area, pore volume and pore size of c-WS than of m-WS. The compressive strength of m-WPC scaffold decreased with increasing porosity in order to the m-WPC structure exhibited a macrostructure with completely interconnected open pores which were spherical in shape. In addition, the incorporation of WS into PCL could improve the hydrophilicity of the composites and m-WPC scaffold had more hydrophilicity than c-WPC scaffolds. The m-WPC had a much faster degradation than c-WPC because of its huge specific surface area and pore volume. The results of composites bioactivity in SBF showed that m-WPC scaffold could induce a dense and continuous layer of apatite compared with scattered and discrete apatite on c-WPC surfaces. *In vitro* testing with MG_{68} cells of composites indicated that higher attachment and proliferation on m-WPC scaffolds than on c-WPC which revealed that the m-WPC scaffolds had excellent biocompatibility because of lower contact angle but higher hydrophilic surface and specific surface area of m-WPC than of c-WPC scaffolds.

Furthermore, nano-sized CS/PCL (n-CPC) and micro-sized CS/PCL (m-CPC) composites were fabricated and investigated their properties. The results indicated that the n-CPC had significantly greater hydrophilicity, compressive strength and elastic modulus than those of m-CPC. Both n-CPC and m-CPC exhibited good *in vitro* bioactivity as the apatite layer on n-CPC was more homogeneous and compact than on m-CPC throughout the 14-day soaking period and n-CPC exhibited significantly greater weight loss than m-CPC during the first seven weeks, which might have been caused by crystallinity of micro-sized CS (m-CS) greater than nano-sized CS (n-CS). MTT results indicated that the attachment, growth and proliferation of MG63 cells were significantly better on n-CPC surfaces than on m-CPC surfaces. In summary, the n-CPC composite exhibited superior mechanical properties, hydrophilicity, *in vitro* bioactivity and cell response than its microscale counterpart which could be applied as a bone implant material.

I. Kotela *et* al. [93] concerned in the processing of nanocomposite made of PCL matrix and wollastonite particles for bone tissue engineering. CS nanopowder was obtained by thermal treatment of polymethyloxosilane resin mixed with silica and calcium hydroxide. The apatite formation on CS surface after immersion in SBF was observed. The presence of small amount of wollastonite nanoparticles (0.5-1.0 %wt) improved the Young's modulus, tensile strength and work-of-fracture of polymer matrix composite. Increased content of ceramic (> 2 %) in nanocomposites resulted in decrease of their mechanical characteristics. The PCL/nanowollastonite composite may constitute a suitable candidate material for bone tissue engineering.

The research involved with production and investigation the properties of composites of biodegradable poly(hydroxyalkanoates) (PHA) with CS and HAp by E.I. Shishatskaya *et* al. [94] Filling of HAp and CS into PHA improved the hydrophilicity of the composites but the melting and thermal degradation temperatures decreased due to the "loosening" effect of the ceramic materials (HAp and CS). The composite materials had high mechanical strength (30-40 MPa), especially the composites of polymers and CS. The extremely significant properties indicated the composites as candidate for bone-substitute implants.

L.M. Rodriguez-Lorenzo *et* al. [95] concerned in the synthesis and characterization of CS-poly(ethylmethacrylate-*co*-vinylpyrrolidone) (CS-poly(EMA-*co*-VP)) *via* free radical bulk polymerization. Greater compression and flexural strength, in comparison with the pure copolymers was obtained only when the ceramic load got up to 60 % of the total weight. The maximum swelling with soaking in NaCl solution was reached after 2–3 hr of immersion and it was significantly greater for lower ceramic loads. After soaking in SBF, the formation of an apatite-like layer on the composites surfaces could be observed. Biocompatibility *in vitro* studies showed the absence of cytotoxicity of all composites. The cells were able to adhere on the composites containing 60 %wt CS forming a monolayer. The results suggested that CS-poly(EMA-*co*-VP) composites provided with new bioactive materials that are able to develop nanoporous structures in physiological conditions and their mechanical properties were suitable for bone substitution.

L.M. Rodriguez-Lorenzo *et* al. [96] synthesized the composites between cryopolymers made of 2-hydroxyethyl methacrylate and acrylic acid with CS for bone tissue engineering. The elastic modulus of the specimens which was in the range of cancellous bone rose with increasing CS content in the composites. The biocompatibility of the samples was tested using human mesenchymal stem cells isolated from bone marrow and adipose tissues. Both types of cells attached and grew on the composites and colonized their inner regions. These results indicated that the composites between cryopolymers and CS with appropriate properties and structure may favor for bone regeneration.

2.8 Testing biomaterials

- ***In vitro* assessment of tissue compatibility**

In vitro tests involve exposing cultured cells to the agent in question. Their usefulness is predicated on the fact that carcinogenicity is correlated with mutagenicity. Following *in vitro* testing, the cells are examined for gene mutations, chromosomal aberrations, and/or deoxyribonucleic acid (DNA) damage and repair. *In vitro* tests have the advantages of being quick and relatively inexpensive, but they are not sensitive to all carcinogenic agents (e.g., asbestos), and they do not reflect the complexities of uptake, organ specificity, distribution, and excretion found in whole animals and in humans. [2]

The term "cytotoxicity" means to cause toxic effects (death, alterations in cellular membrane permeability, enzymatic inhibition, etc.) at the cellular level. It is distinctly different from physical factors that affect cellular adhesion (surface charge of a material, hydrophobicity, hydrophilicity, etc.). [2]

- ***In vivo* assessment of tissue compatibility**

The goal of *in vivo* assessment of tissue compatibility of a biomaterial, prosthesis, or medical device is to determine the biocompatibility or safety of the biomaterial, prosthesis, or medical device in a biological environment. Biocompatibility has been defined as the ability of a medical device to perform with an appropriate host response in a specific application, and biocompatibility assessment is considered to be a measurement of the magnitude and duration of the adverse alterations in homeostatic mechanisms that determine the host response. *In vivo* testing is often employed over *in vitro* because it is better suited for observing the overall effects of an experiment on a living subject. [2]

- ***In silico* assessment of tissue compatibility**

In silico is an expression used to mean "performed on computer or *via* computer simulation". The expression *in silico* was first used in public in 1989 in the workshop "Cellular Automata: Theory and Applications" in Los Alamos, New Mexico. Pedro Miramontes, a mathematician from National Autonomous University of Mexico (UNAM), presented the report "DNA and RNA Physicochemical Constraints, Cellular Automata and Molecular Evolution". In

his talk, Miramontes used the term "*in silico*" to characterize biological experiments carried out entirely in a computer. [97]

Although *in silico* studies represent a relatively new avenue of inquiry, it has begun to be used widely in studies which predict how drugs interact with the body and with pathogens. For example, a 2009 study used software emulations to predict how certain drugs already on the market could treat multiple-drug-resistant and extensively drug-resistant strains of tuberculosis. [97]

Chapter 3

Experimental

3.1 Materials

- Calcium nitrate tetrahydrate ($Ca(NO_3)_2 \cdot 4H_2O$), CARLO ERBA, Analytical grade
- Tetraethylorthosilicate (TEOS), Fluka Chemika, Analytical grade
- Ethanol (CH_3OH), CARLO ERBA, Analytical grade
- Sodium hydroxide (NaOH), CARLO ERBA, Analytical grade
- Fresh water poly(ethylene terephthalate) (PET) bottles, Singha Corporation Co., Ltd.
- Ɛ-caprolactone (CL), Sigma Aldrich, Analytical grade
- *o*-dichlorobenzene ($C_6H_4Cl_2$), CARLO ERBA, Analytical grade
- Dibutyltinoxide ($C_8H_{18}OSn$), Fluka Chemika, Analytical grade
- Dichloromethane (CH_2Cl_2), CARLO ERBA, Analytical grade
- Sodium chloride (NaCl), CARLO ERBA, Analytical grade
- Sodium hydrogen carbonate ($NaHCO_3$), CARLO ERBA, Analytical grade
- Potassium chloride (KCl), Univar, Analytical grade
- Dipotassium hydrogen phosphate trihydrate ($K_2HPO_4 \cdot 3H_2O$), CARLO ERBA, Analytical grade
- Magnesium chloride hexahydrate ($MgCl_2 \cdot 6H_2O$), CARLO ERBA, Analytical grade
- Hydrochloric acid (HCl), Sigma Aldrich, Analytical grade
- Calcium chloride dihydrate ($CaCl_2 \cdot 2H_2O$), CARLO ERBA, Analytical grade
- Sodium sulphate (Na_2SO_4), CARLO ERBA, Analytical grade
- Tris(hydroxymethyl)aminomethane ($(CH_2OH)_3CNH_2$), CARLO ERBA, Analytical grade
- Phosphate buffer saline (PBS), Sigma Aldrich, Analytical grade
- Hydrogen peroxide (H_2O_2), Fisher chemical, Analytical grade

3.2 Apparatus

- Mastersizer-X, Malvern, MSX
- X-ray fluorescence spectrometer (XRF), Bruker AG, SRS 3400
- Milling machines for XRF sample, Rock Lab, Benchmill Model 1A

- Proton nuclear magnetic resonance spectrometer (^{1}H-NMR), Bruker AG, NMR 300 Ultra Shield
- Scanning electron microscope and energy dispersive spectroscopy (SEM-EDS), JEOL, JSM-5410
- Differential scanning calorimeter (DSC), Perkin Elmer, Pyris Diamond DSC
- Thermogravimetric analyser (TGA), Perkin Elmer, Pyris 1 TGA
- X-ray diffractometry (XRD), Rigaku, Miniflex600
- Dynamic mechanical thermal analyser (DMTA), Rheometric Scientific DMTA V, USA
- Rotary evaporator, BUCHI, Rotavapor R-114
- Water bath, Fisher scientific, Isotemp
- Suction filter, Buchi, B-169
- pH-meter, Denver Instrument, 225
- Balance, Denver Instrument, TC-254
- Hot plate, Fisher Scientific
- Heating mantle
- Pellet milling machine
- Universal testing machine (Lloyd Instument, LR5K, UK)
- Vacuum pump
- Thermostat, Euro-ST B, Ika Laboratory Staufen Ltd.
- Oven
- Furnace
- Mortar and pestle
- Porcelain crucible
- Glassware
- ROP set (Fig. 3.1)

Figure 3.1 Ring-opening polymerization set

3.3 Studied Factors

In this thesis, the experiment could be divided into 2 main sections as follows;

1. Preparation of calcium silicate/poly(ethylene terephthalate-*co*-caprolactone) composites (CS/PET-*co*-PCL composites)

Various preparation conditions were carried out, i.e.

1.1 Ring-opening polymerization time: 8 and 24 hr

1.2 Ring-opening polymerization temperature: 180, 200, 230 and 250 °C

1.3 CS content in the CS/PET-*co*-PCL composites: 50 and 60 %wt

1.4 Molar ratio of C-OET:CL: 10:0, 9:1, 8:2, 7:3, 6:4 and 5:5

2. Characteristic and properties of CS/PET-*co*-PCL composites

The effects of ring-opening polymerization conditions on characteristics and properties of CS/PET-*co*-PCL composites were investigated, i.e.

2.1 Structure of PET-*co*-PCL copolymers in CS/PET-*co*-PCL composites by ^{1}H-NMR

2.2 Thermal properties by TGA and DSC

2.3 Morphology by SEM-EDS

2.4 Crystalline phases by XRD

2.5 Mechanical properties by Universal testing machine and DMTA

2.6 Reprocessibility by XRD and DSC

2.7 Bioactivity by simulated body fluid

2.8 Biodegradablility by phosphate buffer saline and H_2O_2 and cytotoxicity

3.4 Experiment

3.4.1 Preparation of calcium silicate (CS)

Calcium nitrate tetrahydrate; $Ca(NO_3)_2 \cdot 4H_2O$ (47.56 g) and tetraethylorthosilicate; TEOS (41.68 g) were dissolved in 1000 ml of ethanol and stirred for 2 hr. Meanwhile, 0.33 M sodium hydroxide (NaOH) solution was prepared by dissolving 7.88 g of NaOH in 600 ml of distilled water. The pH value of both solutions was measured. Next, the NaOH solution was added into the mixture of $Ca(NO_3) \cdot 4H_2O$ and TEOS and stirred for 30 mins to obtain white precipitate. The precipitate was filtered, washed with distilled water and dried at 100 ºC for 24 hr. The calcium silicate (CS) precipitate was grinded and then calcined at 500 °C for 2 hr and 900 ºC for 2 hr. The calcined CS was grinded by milling machines. Finally, the calcined CS was characterized by X-ray fluorescence spectrometer (XRF, Bruker AG, SRS3400, USA) for measuring the chemical composition of CS powder, X-ray diffractometry (XRD, Rigaku, Miniflex600) for characterizing the crystallinity of the CS and measured the particle size by Mastersizer-X.

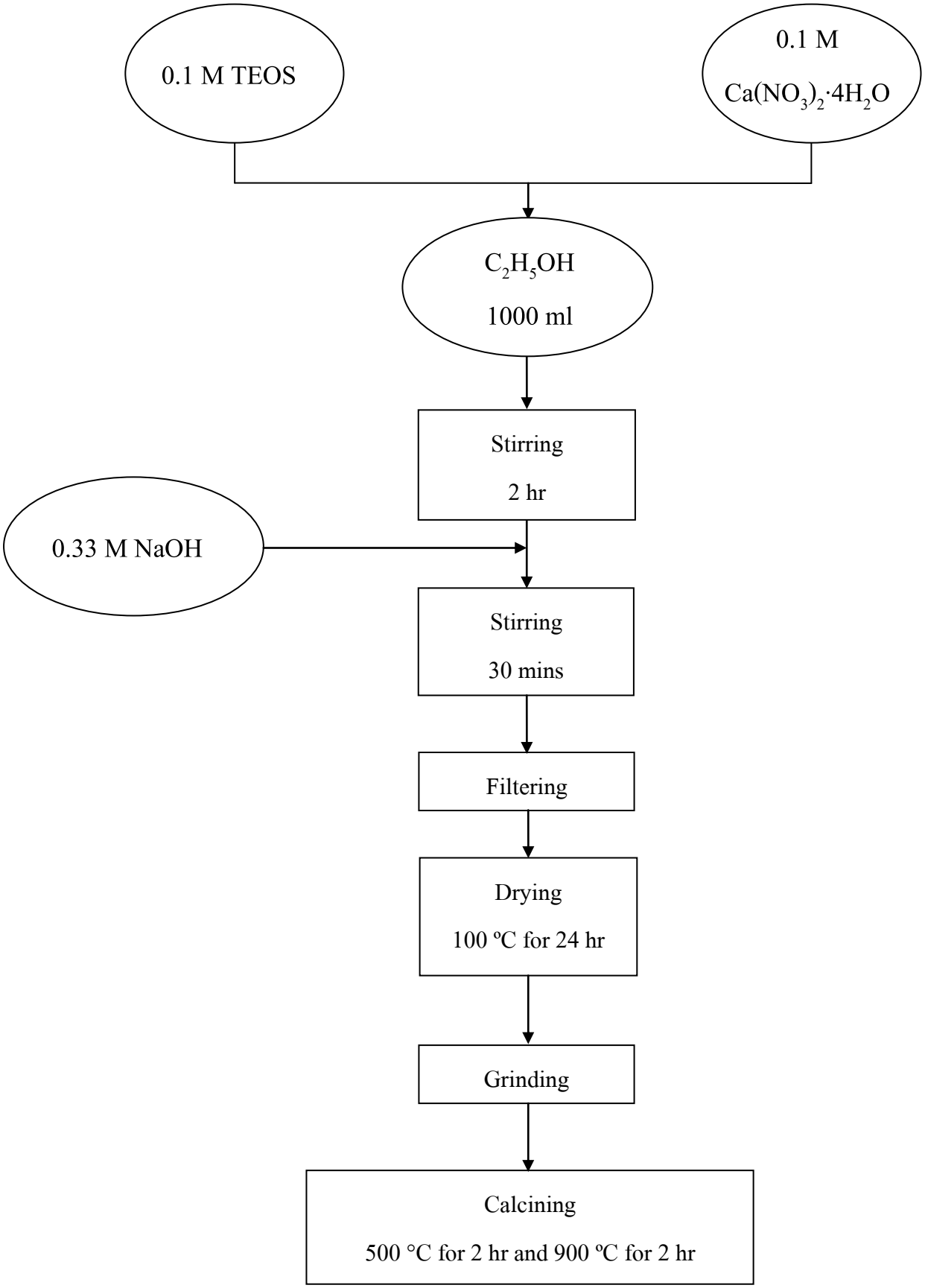

Figure 3.2 Preparation of calcium silicate

3.4.2 Preparation of cyclic oligo(ethylene terephthalate) (C-OET)

The commercial PET flakes (5 g) and dibutyltinoxide catalyst (DBTO) (3 %mol of polymer repeating unit) were dissolved in *o*-dichlorobenzene. The ratio of polymer to solvent was 1:40 g/ml. The mixture was refluxed for 4 days. The mixture was filtered and then the liquor was evaporated to receive C-OET precipitate. The precipitate was dried at 80 ºC for 24 hr. The C-OET product was characterized by ^{1}H-NMR (Bruker AG, NMR 300 ULTRA SHIELD, USA) and differential scanning calorimeter (DSC, NETZSCH, DSC204F1, UK).

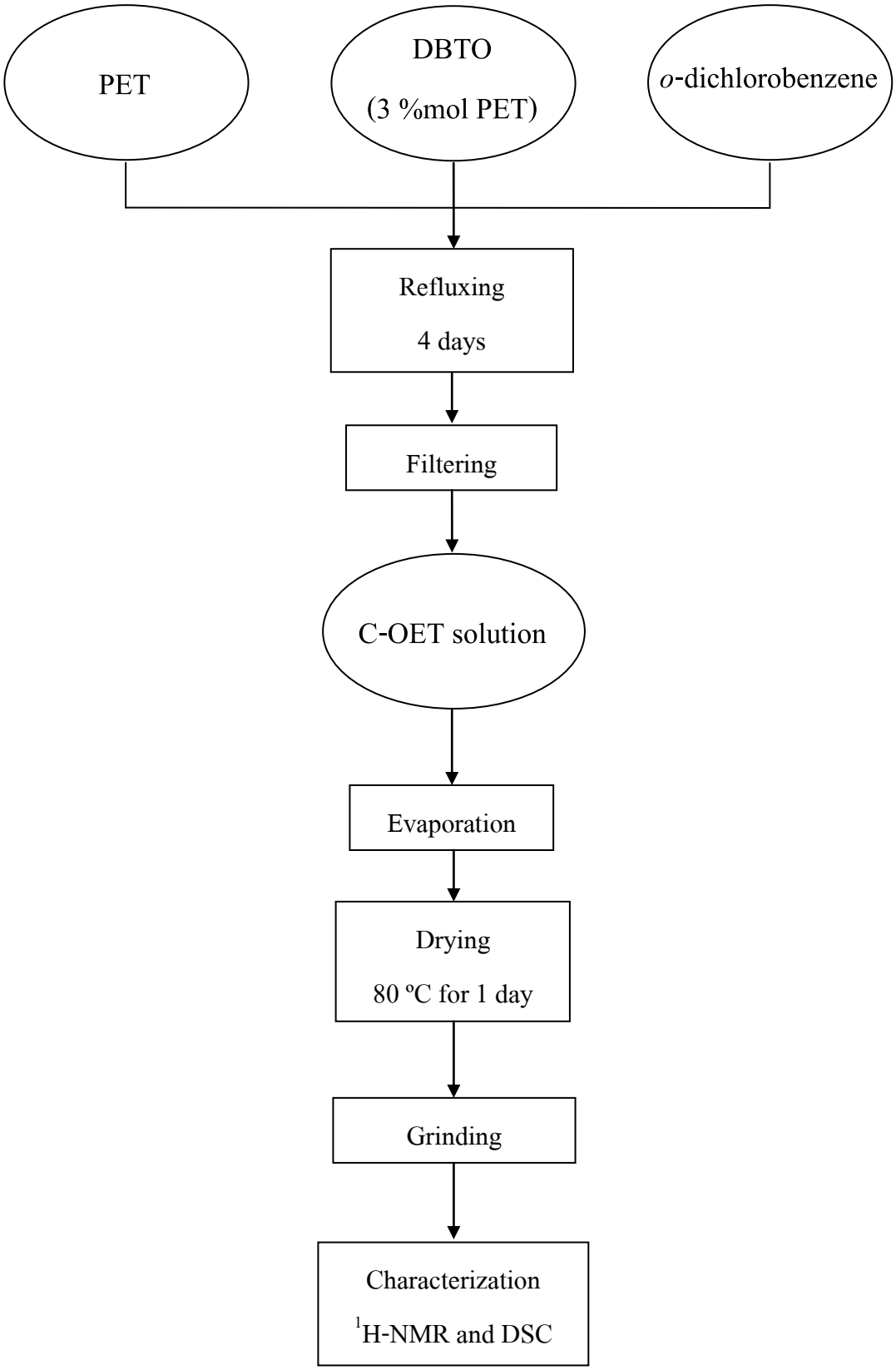

Figure 3.3 Preparation of cyclic oligo(ethylene terephthalate) (C-OET)

3.4.3 Preparation of poly(ethylene terephthalate-*co*-caprolactone) copolymers (PET-*co*-PCL) by ring-opening polymerization

C-OET, Ɛ-caprolactone (CL) and DBTO (3 %mol of polymer repeating unit) were mixed with dichloromethane. The molar ratio of C-OET/CL was varied as shown in Table 3.1. The mixtures pastes were shaped in teflon mold to cubic shape. The cubic samples were vacuum in glass vessel (Fig. 3.4) for 30 mins and then purged nitrogen gas for 15 mins in which these processes were repeated 3 times. The as-prepared cubic samples were ring-opening polymerized at various temperatures (i.e. 180, 200, 230 and 250 °C) for 8 and 24 hr. Finally, the ROP products were characterized and tested as follows;

a. ^{1}H-NMR spectroscope to characterize the structure of copolymers,

b. DSC to measure the transition temperatures of copolymers,

c. Universal testing machine (Lloyd Instument, LR5K, UK) to measure the compressive strength and compressive modulus of copolymers,

d. Dynamic mechanical thermal analyser (DMTA, Rheometric Scientific DMTA V, USA) to measure the dynamic mechanical property of copolymers.

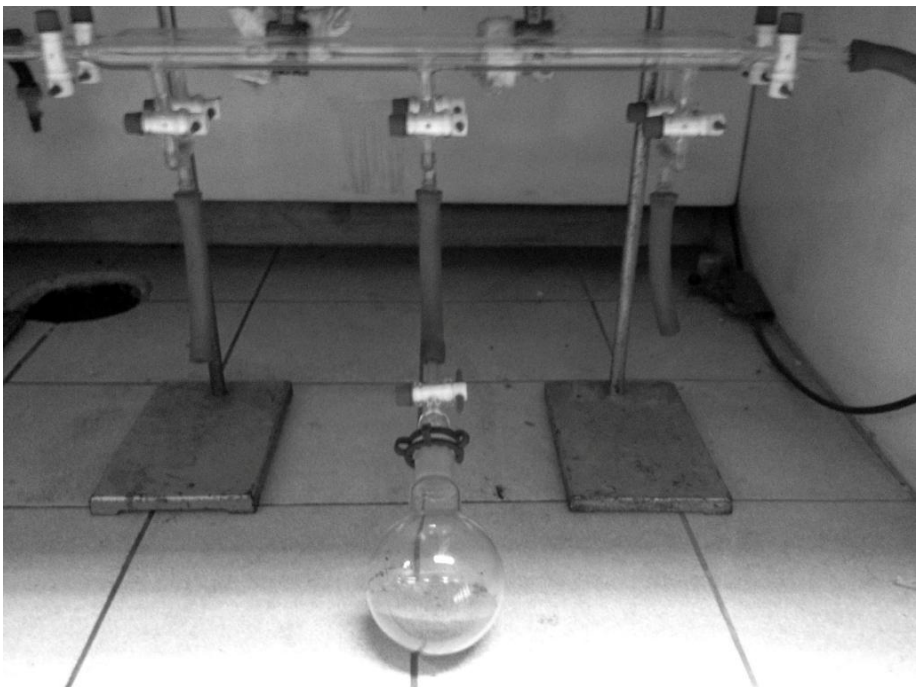

Figure 3.4 Vacuum and nitrogen gas purging line

Table 3.1 Molar ratio of C-OET:CL for synthesis of poly(ethylene terephthalate-*co*-caprolactone) copolymers (PET-*co*-PCL)

Sample	Molar ratio of cyclic content		Condition	
	C-OET	CL	Temperature	Time
E10C0-180-8	10	0	180 °C	8 hr
E9C1-180-8	9	1		
E8C2-180-8	8	2		
E7C3-180-8	7	3		
E6C4-180-8	6	4		
E5C5-180-8	5	5		
E10C0-200-8	10	0	200 °C	
E9C1-200-8	9	1		
E8C2-200-8	8	2		
E7C3-200-8	7	3		
E6C4-200-8	6	4		
E5C5-200-8	5	5		
E10C0-230-8	10	0	230 °C	
E9C1-230-8	9	1		
E8C2-230-8	8	2		
E7C3-230-8	7	3		
E6C4-230-8	6	4		

Table 3.1 (cont.)

Sample	Molar ratio of cyclic content		Condition	
	C-OET	CL	Temperature	Time
E10C0-180-24	10	0	180 °C	24 hr
E9C1-180-24	9	1		
E8C2-180-24	8	2		
E7C3-180-24	7	3		
E6C4-180-24	6	4		
E5C5-180-24	5	5		
E10C0-200-24	10	0	200 °C	
E9C1-200-24	9	1		
E8C2-200-24	8	2		
E7C3-200-24	7	3		
E6C4-200-24	6	4		
E5C5-200-24	5	5		
E10C0-230-24	10	0	230 °C	
E9C1-230-24	9	1		
E8C2-230-24	8	2		
E7C3-230-24	7	3		
E6C4-230-24	6	4		
E10C0-250-24	10	0	250 °C	
E9C1-250-24	9	1		
E8C2-250-24	8	2		
E7C3-250-24	7	3		
E6C4-250-24	6	4		

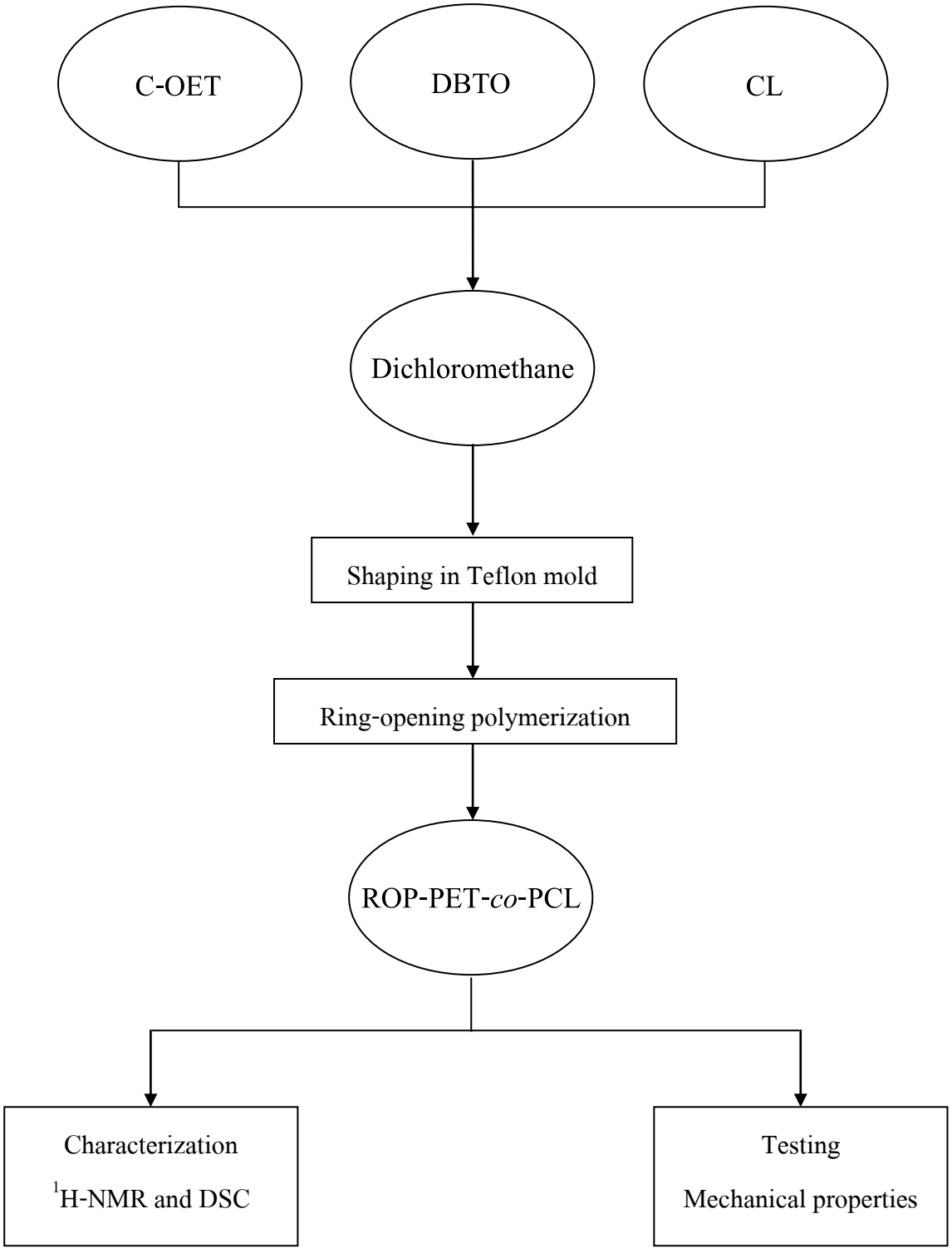

Figure 3.5 Preparation of poly(ethylene terephthalate-*co*-caprolactone) copolymers (PET-*co*-PCL) by ring-opening polymerization

3.4.4 Preparation of calcium silicate/poly(ethylene terephthalate-*co*-caprolactone) composites (CS/PET-*co*-PCL) by ring-opening polymerization

The C-OET and CL with the molar ratios as shown in Table 3.2 were mixed with DBTO catalyst (3 %mol of polymer repeating unit) and dichloromethane to form sticky pastes. The CS powders were added into the pastes, mixed well and shaped by unixial pressing to cylindrical pre-composite pellets. The weight percentage of CS:C-OET-CL in the pre-composites was varied to be 60:40 and 50:50. The cylindical pre-composites were vacuum in glass vessel (Figure 3.4) for 30 mins and then purged nitrogen gas for 15 mins in which these processes were repeated 3 times. The pre-composites were ring-opening polymerized at various temperatures (i.e. 180 and 200 °C) for 24 hr. Finally, the ROP composites products were characterized as follow;

a. ^{1}H-NMR spectroscope to characterize the structure of copolymers in composites,

b. DSC to measure the transition temperatures of composites,

c. Thermogravimetric analyser (TGA, Perkin Elmer, Pyris 1 TGA, USA) to calculate the quantity of polymer in composites,

d. Scanning electron microscope (SEM, LEO, LEO1455VP, USA) to characterize the microstructure of composites and the distribution of CS in copolymers,

e. X-ray diffractometry (XRD, Rigaku, Miniflex600) to characterize the crystalline phases of composites.

Table 3.2 Chemical ingredients for synthesis of calcium silicate/poly(ethylene terephthalate-*co*-caprolactone) composites (CS/PET-*co*-PCL)

Sample	Weight ratio of CS:C-OET-CL (%wt)	Molar ratio of cyclic content		Condition	
		C-OET	CL	Temperature	Time
S50-E10C0-180-24	50:50	10	0	180 °C	24 hr
S50-E9C1-180-24		9	1		
S50-E8C2-180-24		8	2		
S50-E7C3-180-24		7	3		
S50-E6C4-180-24		6	4		
S50-E5C5-180-24		5	5		
S50-E10C0-200-24	50:50	10	0	200 °C	
S50-E9C1-200-24		9	1		
S50-E8C2-200-24		8	2		
S50-E7C3-200-24		7	3		
S50-E6C4-200-24		6	4		
S50-E5C5-200-24		5	5		
S60-E10C0-180-24	60:40	10	0	180 °C	
S60-E9C1-180-24		9	1		
S60-E8C2-180-24		8	2		
S60-E7C3-180-24		7	3		
S60-E6C4-180-24		6	4		
S60-E5C5-180-24		5	5		
S60-E10C0-200-24	60:40	10	0	200 °C	
S60-E9C1-200-24		9	1		
S60-E8C2-200-24		8	2		
S60-E7C3-200-24		7	3		
S60-E6C4-200-24		6	4		
S60-E5C5-200-24		5	5		

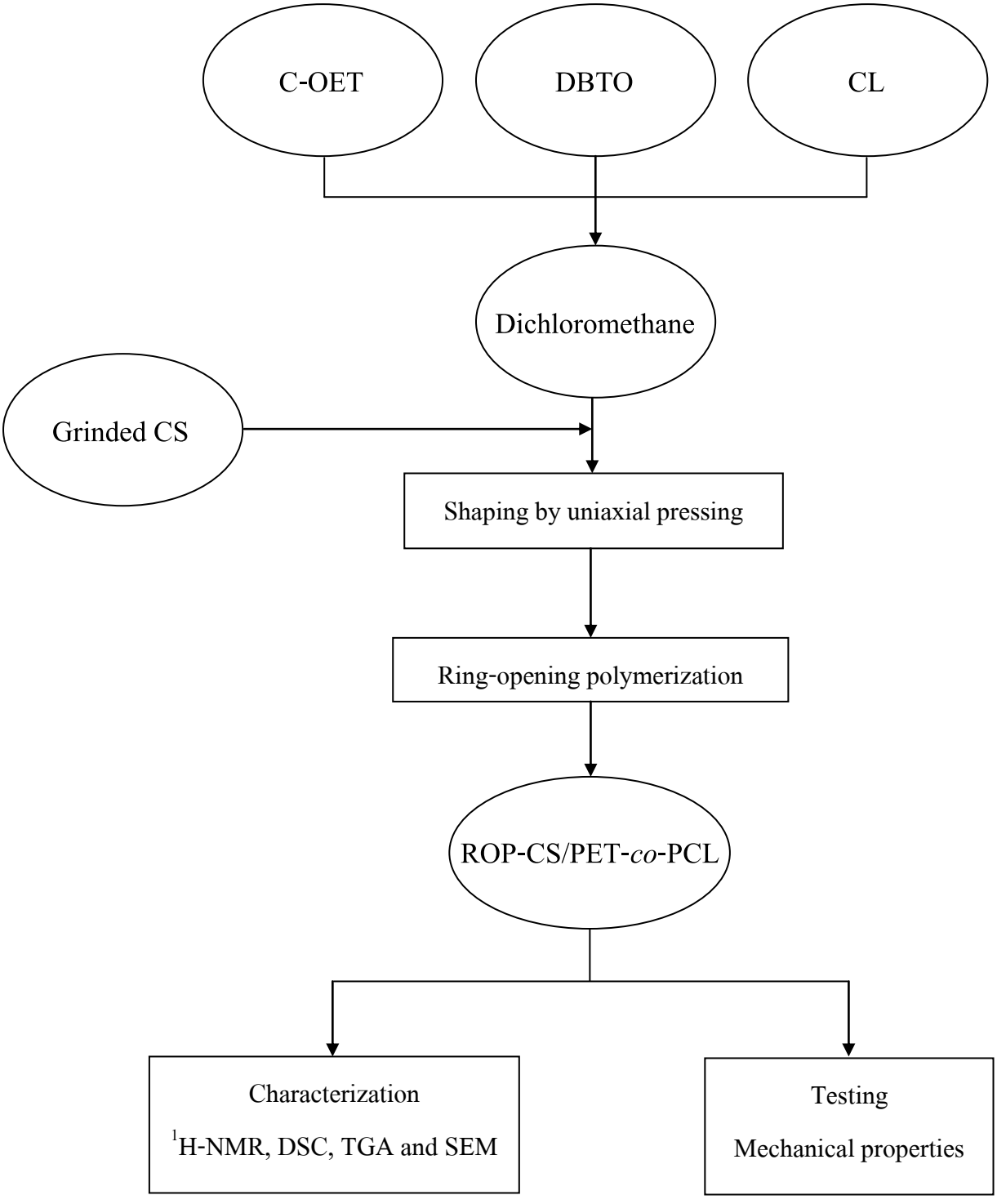

Figure 3.6 Preparation of calcium silicate/poly(ethylene terephthalate-*co*-caprolactone) composites (CS/PET-*co*-PCL) by ring-opening polymerization

3.4.5 Testing and characterization of CS/PET-*co*-PCL composites

- **Structure of PET-*co*-PCL copolymers in CS/PET-*co*-PCL composites**

The ROP PET-*co*-PCL products were extracted from the composites by immersing in chloroform for 24 hr. The structures of extracted copolymers were characterized by ^{1}H-NMR using tetramethylsilane (TMS) as standard.

- **Mechanical properties**

Synthesized composite surfaces were scrubbed and then the volume of each composite was measured. Compressive strength and compressive modulus of the composites were measured by Universal testing machines with 5 kN load cell and cross-head speed of 1 mm/min. In addition, dynamic mechanical property of the composites was measured by dynamic mechanical thermal analyser (DMTA) in the compression mode at frequency of 1.0 Hz over a temperature range of -50 to 200 ºC and at heating rate 5 ºC/min. The strain control remained at 0.05 %.

- **Thermal properties**

The thermal property of composites was characterized by DSC in a temperature range of -50 to 300 ºC under nitrogen atmosphere with a heating rate of 10 °C/min and a cooling rate of 10 °C/min and by TGA in a range of temperature of 50 to 900 °C at a heating rate of 10 °C/min.

- **Morphology**

The surface morphology of composites was characterized by SEM. Before observing in SEM microscope, the surface of the sample was coated with gold.

- **Crystalline phases**

The XRD scans were performed from 2θ = 10° to 40° at a rate of 3°/min with Cu x-ray tube.

3.4.6 Reprocessibility of CS/PET-*co*-PCL composites

The ROP CS/PET-*co*-PCL composites were ground and reshaped using compression molding in order to obtain the composite plates with thickness of about 1.4 to 1.7 mm. Then, the composite plates were annealed at 150 °C for 1 hr under vacuum. The CS/PET-*co*-PCL composites after annealing were analyzed crystalline structures and thermal behaviors by XRD and DSC, respectively. The XRD scans and DSC were performed in the same manner of the composites before annealing.

3.4.7 Bioactivity and biodegradation testing

- **Preparation of simulated body fluid**

Table 3.3 Chemicals in the preparation of simulated body fluid (SBF)

Chemicals	Quantity
NaCl	15.992 g
$NaHCO_3$	0.7 g
KCl	0.448 g
K_2HPO_4	0.348 g
$MgCl_2 \cdot 2H_2O$	0.612 g
1 M HCl	80 ml
$CaCl_2 \cdot 2H_2O$	0.556 g
Na_2SO_4	0.144 g
$(CH_2OH)_3CNH_2$	12.116 g

The preparation was performed according to Kokubo *et al* [98] in a plastic beaker containing 1,400 ml of distilled water. The chemicals no.1-8 were respectively added into distilled water with stirring in order to obtain clear solution. Finally, the pH of solution was adjusted to 7.4 by adding chemical no.9. The solution volume was adjusted to 2,000 ml with distilled water in volumetric flask. The ion concentrations of SBF solution were shown in Table 3.4. The SBF solution was kept in refrigerator at 5 ºC.

Table 3.4 Concentration of inorganic ions in SBF solution and blood plasma [98]

Ion	Simulated Body Fluid (mM)	Human plasma (mM)
Na^+	142.0	142.0
Cl^-	147.8	103.0
HCO_3^-	4.2	27.0
K^+	5.0	5.0
Mg^{2+}	1.5	1.5
Ca^{2+}	2.5	2.5
HPO_4^{2-}	1.0	1.0
SO_4^{2-}	0.5	0.5

- **Bioactivity**

Each PET-*co*-PCL copolymers or CS/PET-*co*-PCL composites was immersed in the SBF solution at 37 ºC (human body temperature) for 7, 14, 21 and 28 days. After pre-determined soaking time, the copolymers and composites were separated from the SBF solution, washed by distilled water and then dried at room temperature. The soaked copolymers and composites were characterized by SEM-EDS and XRD.

- **Biodegradation testing**

Biodegradation of the copolymers and composites was evaluated using the changes in dry weight after incubation for a predetermined time period. The specimens were immersed in phosphate buffer saline (PBS) or 5 %v/v hydrogen peroxide (H_2O_2) at 37 °C for 28 days. After immersion, the specimens were removed, gently rinsed with distilled water and dried at room temperature. The morphology of soaked composites were characterized by SEM. The percentage of weight loss (%w) was determined using the following equation:

$$\%w = \frac{(w_0 - w_t)}{w_0} \times 100$$

; where W_0 is the starting dry weight

W_t is the dry weight at 28-day soaking

3.4.8 Cytotoxicity testing

Cytotoxicity of the CS/PET-*co*-PCL composites was assessed by African green monkey kidney fibroblast (Vero) using MTT assay. The samples were exposed in DMEM (Dulbecco's Modified Eagle Medium) to vary the concentration at 125, 250, 500 and 1000 µg/ml. Vero culture was cultured in a medium containing DMEM supplemented with 15 % FBS (Fetal Bovine Serum) at a density of $5x10^4$ cells/ml and seeded in a 96-well plate at 100 µl/well, and then incubated at 37 °C for 24 hr. The 100 µl of composite solutions with various concentrations were added to each plate and incubated at 37 °C for 24 hr. Then, 10 µl of MTT solution (5 mg/ml) was added in each well and incubated at 37 °C. After 4 hr incubation, the 9:1 of DMSO:10 % SDS was added in each well plate at 150 µl/well to dissolve the formazan crystals. The optical density of the solution was measured at a wavelength of 570 nm using a microplate reader. The half maximal inhibitory concentration or IC_{50} was calculated and expressed as mean±SD of IC_{50}.

Chapter 4

Results and Discussion

4.1 Raw materials

4.1.1 Calcium silicate (CS)

CS powder was synthesized by co-precipitation method. The synthesized CS powder characterized by XRF was composed of 44.8 %wt of CaO and 46.8 %wt of SiO_2. The Ca/Si molar ratio of the calcined CS was 1.02, which was equal to the theoretical value of CS. The XRD pattern of CS powder is shown in Fig. 4.1. The crystalline peaks of the CS powder were observed at 2θ =11.5, 17.9, 23.1, 25.3, 26.8, 28.8, 29.9, 35.0, 36.2, 38.5 and 39.0°, corresponded to the triclinic structure of wollastonite. [99] In addition, the average particle size of CS powder measured by Mastersizer-X was approximately 7.09±0.80 μm.

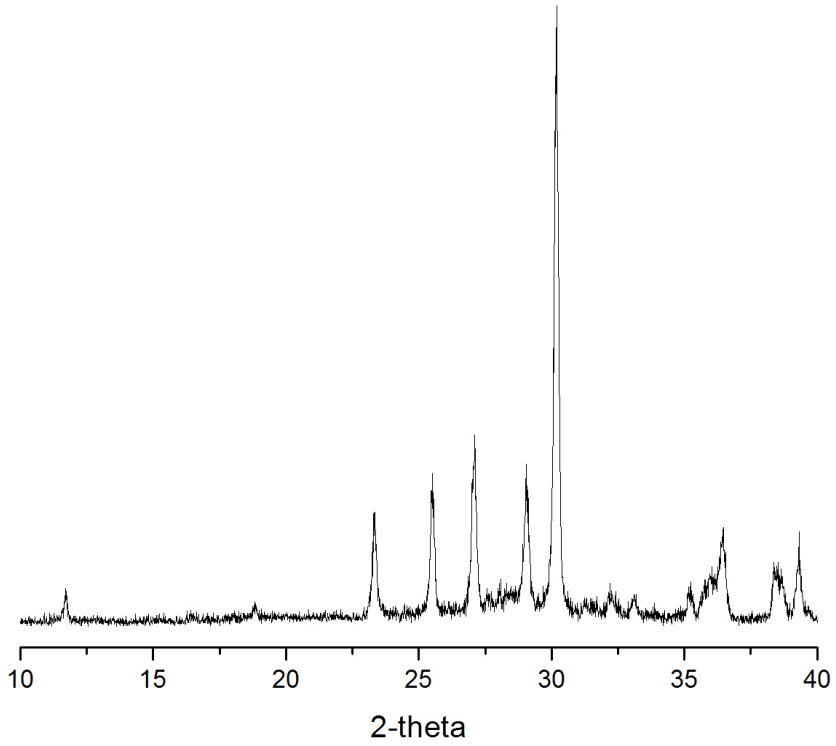

Figure 4.1 XRD pattern of CS powder

4.1.2 Cyclic oligomers

- **Cyclic oligo(ethylene terephthalate) (C-OET)**

The synthesis of C-OET could be achieved by cyclodepolymerization (CDP) of PET in dichlorobenzene at high dilution condition as shown in Scheme 4.1. The ^{1}H-NMR spectrum of C-OET is shown in Fig. 4.2 (a). The chemical shift of C-OET was observed at δ 4.8 ppm and δ 8.1 ppm for -OC***H*****$_2$**C***H*****$_2$**O- (a_1) and aromatic protons (a_2), respectively, in equimolar ratio. No signal of the PET end group was observed. These results indicated the transformation of PET to C-OET *via* CDP reaction. The melting temperature (T_m) of C-OET was observed at 273 °C by using DSC.

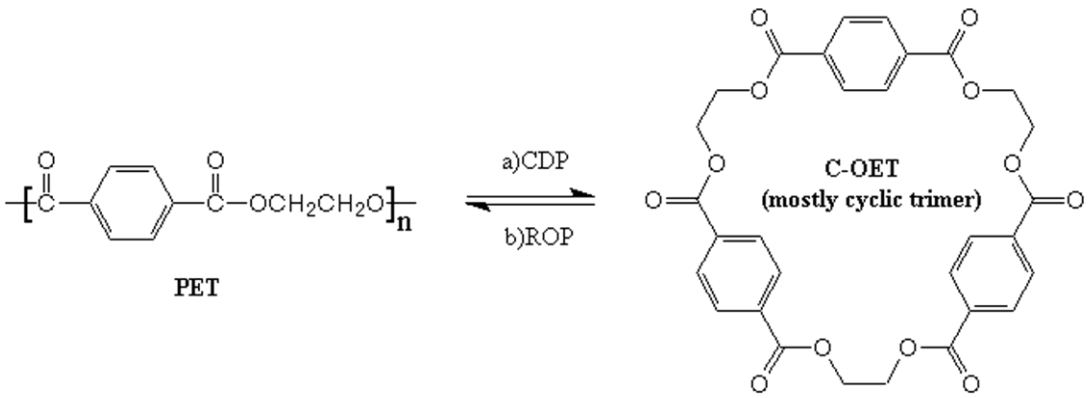

Scheme 4.1 Preparation of C-OET *via* cyclodepolymerization (CDP)

- **Ɛ-caprolactone (CL)**

The ^{1}H-NMR spectrum of CL is shown in Fig. 4.2 (b). The chemical shifts of the CL occurred at δ 1.4-1.7 ppm for protons adjacent to three middle methylene unit (b_1), δ 2.7 ppm for –CH$_2$C***H*****$_2$**COO- (b_2), and δ 4.2 ppm for –CH$_2$C***H*****$_2$**OOC- (b_3). Furthermore, no end group signal was observed in the spectrum.

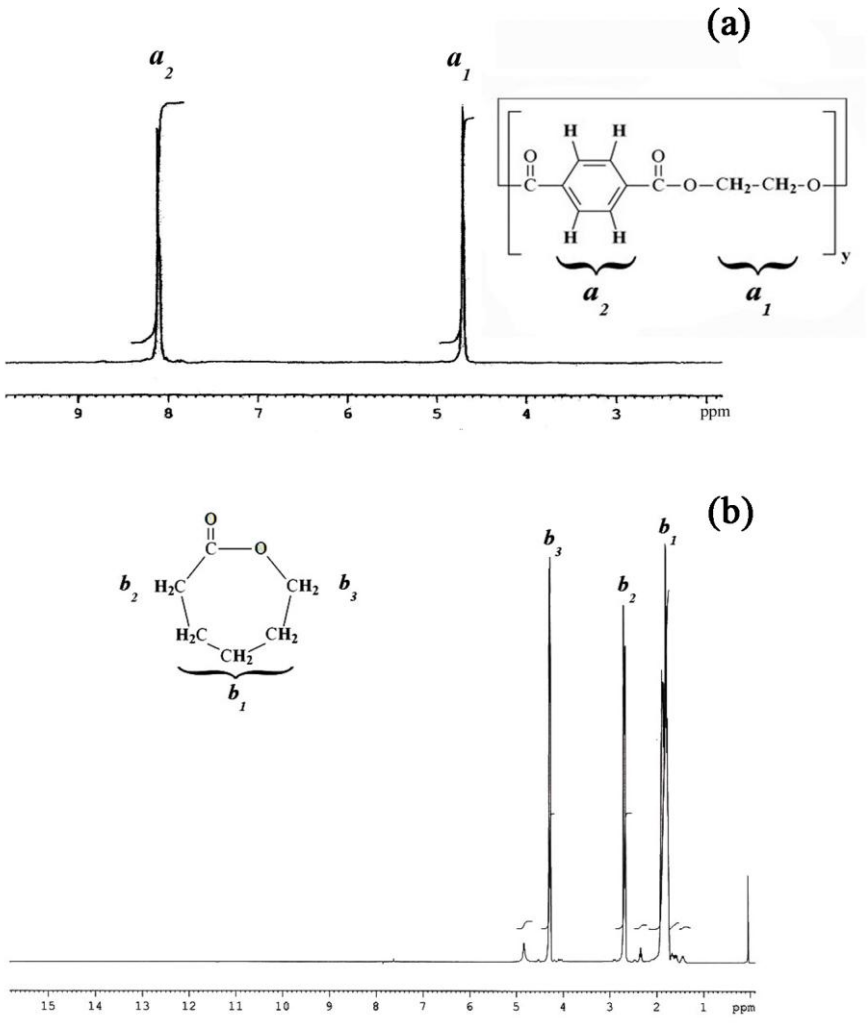

Figure 4.2 ^{1}H-NMR spectra of C-OET (a) and CL (b)

4.2 Poly(ethylene terephthalate-*co*-caprolactone) copolymers (PET-*co*-PCL)

4.2.1 Chemical Structure

The structure of neat PCL ring-opening polymerized at 100 ºC for 1 hr was investigated by ^{1}H-NMR as shown in Fig. 4.3 (a) and summarized in Table 4.1. There were the aliphatic protons in PCL at δ 1.4 (HO-CL1; C_1) and 1.7 ppm (HO-CL2; C_2). The protons connecting to carbonyl group (HO-CL3; C_3) and ether group (HO-CL4; C_4) were observed at δ 2.5 ppm and δ 4.2 ppm, respectively. In addition, the small signal at δ 3.8 ppm related to the PCL end group was also identified.

The ^{1}H-NMR spectrum of pure PET polymers synthesized from the ROP of C-OET at 180 ºC for 24 hr is shown in Fig. 4.3 (b) and the chemical shift-to-structure correlations are concluded in Table 4.1. The chemical shift at δ 4.8 ppm and δ 8.1 ppm corresponded to -OC***H***$_2$C***H***$_2$O- (HO-ET1; E_1) and aromatic protons (HO-ET2; E_2), respectively. In addition, the end group signal of the ROP-PET was observed at 4.0 ppm. These phenomena occurred in all ROP-PET homopolymers ring-opening polymerized at 180, 200, 230 or 250 °C for 8 or 24 hr, in which their ^{1}H-NMR spectra were in Appendix C. This result indicated that the C-OET could be successfully ring-opening polymerized at all conditions.

The PET-*co*-PCL copolymers were prepared by ROP of C-OET and CL. Figure 4.4 shows the spectrum of the ROP copolymer namely E5C5-180-24. Appendix C shows the spectra of the other neat copolymers with varying cocyclics molar ratios, ROP temperatures and times. There were two main proton signals, i.e. homolinkages of ET-ET (HO-ET) and CL-CL units (HO-CL) and heterolinkage of ET-CL unit (CO-ETCL). The chemical shift of homolinkage proton in PET occurred at δ 4.8 and 8.1 ppm corresponding to the ethylene protons (HO-ET1; E_1) and the aromatic protons (HO-ET2; E_2), respectively. In case of the CL homolinkage, there were four main chemical shift signals which located at δ 1.4, 1.7, 2.5, and 4.2 ppm. The signals at δ 1.4 and 1.7 ppm were the aliphatic protons corresponding to HO-CL1 (C_1) and HO-CL2 (C_2) structures, respectively. The chemical shift at δ 2.5 ppm was the methylene protons adjacent to carbonyl group of ester (HO-CL3; C_3) and another signal at δ 4.2 ppm was the methylene protons adjacent to ether group of ester (HO-CL4; C_4). In case of heterolinkage signals, the methylene protons of CL unit connected to ET unit were observed at the chemical shift δ 4.4 (CO-ETCL1; EC_1) and the ethylene protons of ET unit connected to CL unit were observed as 2 peaks of the protons nearby the CL unit at δ 4.55 ppm and aromatic unit at δ 4.65 ppm, as indicated CO-

ETCL2; EC_2. The correlations of chemical shift-to-structure were concluded in Table 4.1. In the ^{1}H-NMR spectra, varying in the ratios of C-OET:CL did not affect to peak positions but influenced to the peak intensities, depending on the C-OET and CL contents in the copolymers. This phenomenon could be observed in all conditions. Furthermore, the end group signal of ROP-copolymer was observed at δ 4.0 ppm corresponding to the methylene proton connected to hydroxyl group (-CH_2-C***H***$_2$-OH) in PET. In the case of PCL, the methylene proton end group signal which connected to hydroxyl group (-$(CH_2)_4$-C***H***$_2$-OH) was observed at δ 3.8 ppm. This result insisted that the successful ring-opening polymerization of PET-*co*-PCL copolymers.

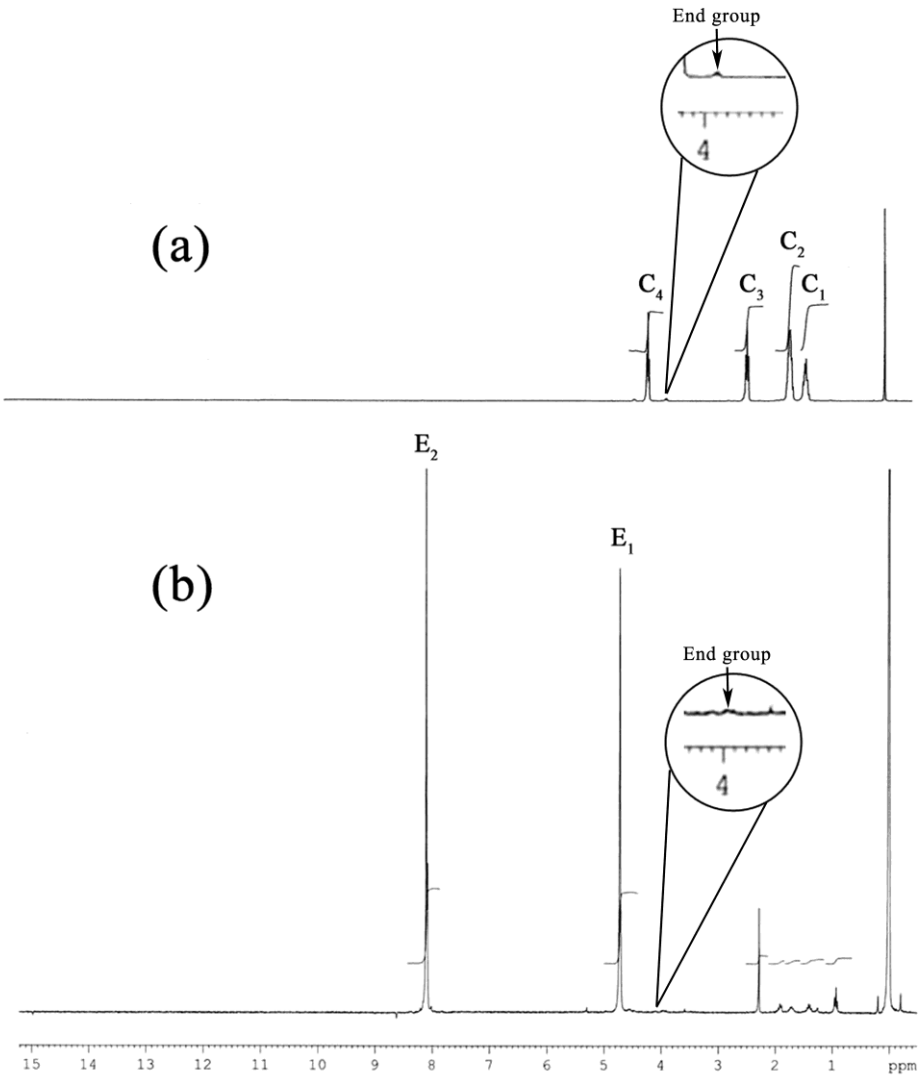

Figure 4.3 ^{1}H-NMR spectra of PCL homopolymer ring-opening polymerized at 100 ºC for 1 hr (a) and PET homopolymer ring-opening polymerized at 180 °C for 24 hr (b)

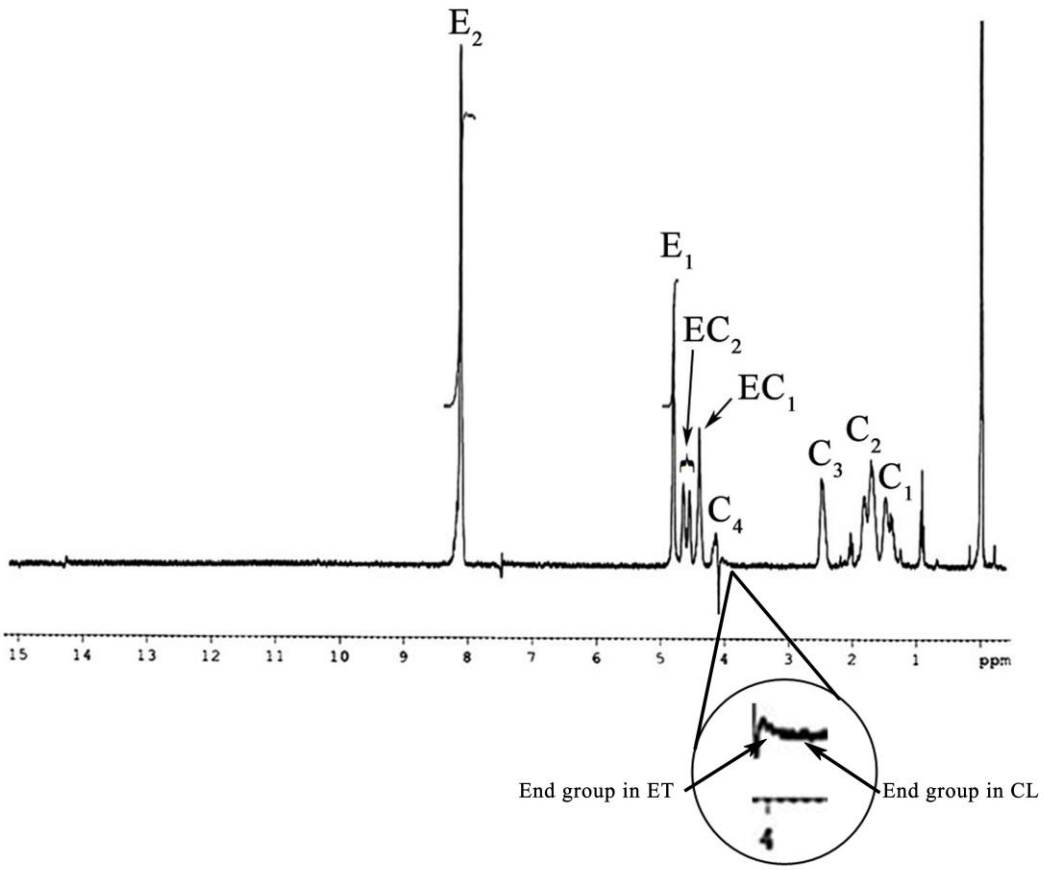

Figure 4.4 ^{1}H-NMR spectrum of copolymer with 50 %mol ET content ring-opening polymerized at 180 °C for 24 hr

Table 4.1 ^{1}H-NMR chemical shift-to-structure correlations

	Structure	Chemical Shift
HO-CL1; C_1	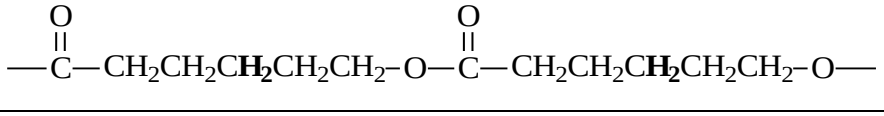	1.4
HO-CL2; C_2	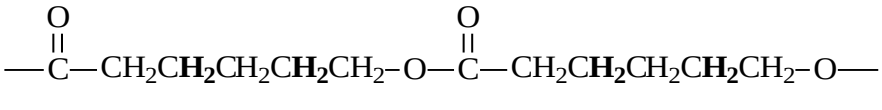	1.7
HO-CL3; C_3	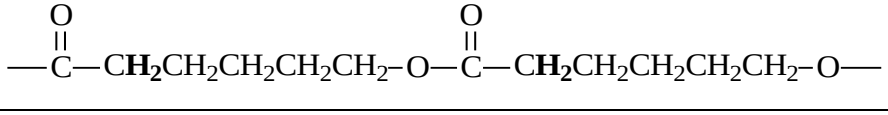	2.5
HO-CL4; C_4	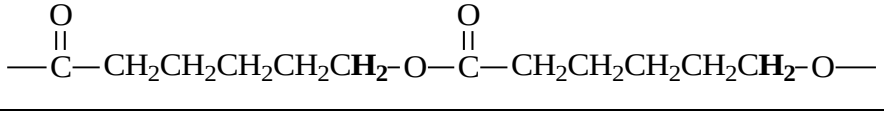	4.2
HO-ET1; E_1	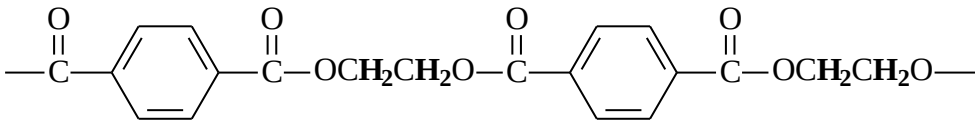	4.8
HO-ET2; E_2	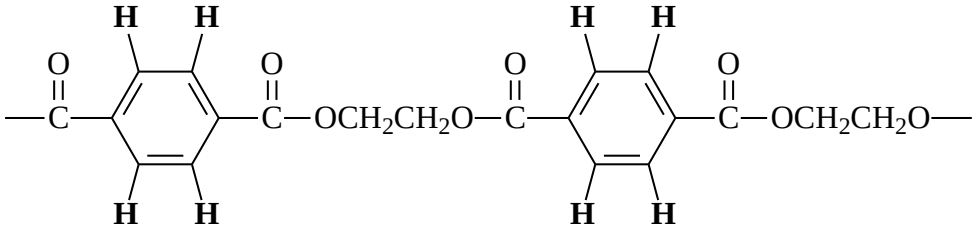	8.1
CO-ETCL1; EC_1	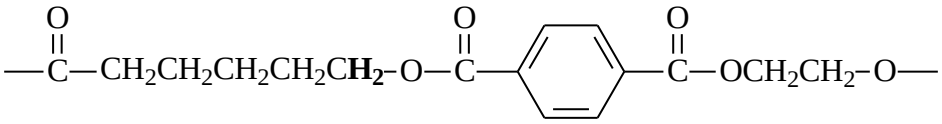	4.4
CO-ETCL2; EC_2	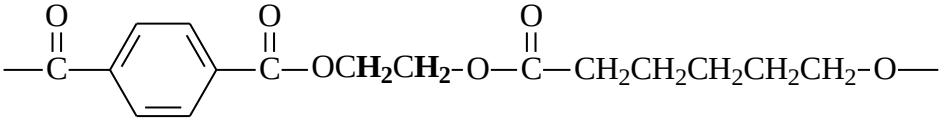	4.6

The integration of ^{1}H-NMR peaks in the copolymers of HO-ET1, CO-ETCL1, CO-ETCL2 and HO-CL4 were investigated as shown in Table 4.2. Not only the integration of CO-ETCL1 and HO-CL4 increased, but also the integration of CO-ETCL2 increased when the PCL content was increased, indicating higher tendency of copolymerization reaction between C-OET and CL. On the other hand, the HO-ET1 decreased with the increasing of PCL content. These results represented the probability of reaction between C-OET and CL increased with the increase of PCL content, resulting in the formation of PET-*co*-PCL copolymers.

The intensities of ^{1}H-NMR peaks could be used for calculation of the molar percentage of PET (MP_T) and PCL (MP_C) segments in the copolymers by the following equation: [48, 100]

$$MP_T = \frac{I_{8.1}}{I_{8.1} + 2I_{2.5}} \times 100 \qquad \text{eq.(4.1)}$$

$$MP_C = \frac{2I_{2.5}}{I_{8.1} + 2I_{2.5}} \times 100 \qquad \text{eq.(4.2)}$$

where $I_{8.1}$: integrated intensity of the corresponding peak at δ 8.1 ppm

$I_{2.5}$: integrated intensity of the corresponding peak at δ 2.5 ppm

If neglecting the end group, the molar fraction of PET and PCL dyads (MP_{TC}) can be calculated by the intensity of ^{1}H-NMR as followed: [48, 100]

$$MP_{TC} = \frac{I_{4.6} + 2I_{4.4}}{I_{8.1} + 2I_{2.5}} \times 100 \qquad \text{eq.(4.3)}$$

where $I_{4.6}$: integrated intensity of the corresponding peak at δ 4.6 ppm

$I_{4.4}$: integrated intensity of the corresponding peak at δ 4.4 ppm

Sequence structure is one of the important factor for further determining the chemical structures of copolymers. The sequence structure of the copolymers can be characterized from the degree of randomness; however, this method was not suitable for PET-*co*-PCL copolyesters because the PET-*co*-PCL structures are unsymmetrical structures from two different functional groups. In this thesis, the sequence structures of the copolyesters were determined by another

method, i.e., run number (R). The run number is the average number of sequence runs occurring in a copolymer chain per 100 monomer units. [48]

The number-average lengths, molecular weights of polymer units and reaction probabilities between terephthalate and caprolactone groups in the copolymers could also determine from the ^{1}H-NMR intensities. The number-average lengths of PET (L_T) and PCL (L_C) units are given by eq.(4.4) and (4.5). [48, 100]

$$L_T = \frac{2I_{8.1}}{I_{4.6}+2I_{4.4}} = \frac{2MP_T}{MP_{TC}} \qquad \text{eq.(4.4)}$$

$$L_C = \frac{4I_{2.5}}{I_{4.6}+2I_{4.4}} = \frac{2MP_C}{MP_{TC}} \qquad \text{eq.(4.5)}$$

For example, the same C-OET and CL contents in the E5C5-180-8 copolymer resulted in the same L_T and L_C values.

The molecular weights of aromatic (M_T) and aliphatic (M_C) polyester segments are: [48, 100]

$$M_T = 192 \times L_T \qquad \text{eq.(4.6)}$$

$$M_C = 114 \times L_C \qquad \text{eq.(4.7)}$$

The probability of a PET unit next to a PCL unit is: [48, 100]

$$P_{TC} = \frac{1}{L_T} = \frac{I_{4.6}+2I_{4.4}}{2I_{8.1}} \qquad \text{eq.(4.8)}$$

Similarly, the PCL unit was along with a PET unit with a probability of:

$$P_{CT} = \frac{1}{L_C} = \frac{I_{4.6}+2I_{4.4}}{4I_{2.5}} \qquad \text{eq.(4.9)}$$

thus,

$$P_{TT} = 1 - P_{TC} \qquad \text{eq.(4.10)}$$

$$P_{CC} = 1 - P_{CT} \qquad \text{eq.(4.11)}$$

where P_{TT} : probability of a PET unit having a PET unit on its right

P_{CC} : probability of a PCL unit having a PCL unit on its right

The run number (R) which corresponded with copolymers structures could be written as: [41, 101]

$$R = \frac{200}{L_T + L_C} \qquad \text{eq.(4.12)}$$

The R value can be interpreted as follows:

$0 < R < 50$: more block character

$50 < R < 100$: more alternating tendency of the copolymer than expected from the random distribution

$R = 0$: a completely block copolymer or the system is a mixture of two homo polymers

$R = 50$: the copolymer is random

$R = 100$: a copolymer exhibits completely alternating statistics

For example, the E5C5-180-8 copolymer, the L_T and L_C values were quite similar and closed to 1; therefore, the R was in the range of 50 to 100 which indicated that the copolymer structure tended to be more alternating structure.

The MP_T, MP_C and MP_{TC} values of all neat PET-*co*-PCL copolymers are showed in Table 4.2 and the number-average lengths, molecular weights of polymer units, probabilities and randomness values are shown in Table 4.3. The calculated MP_T and MP_C values of all copolymers closed to the feed compositions of terephthalate and caprolactone precursors.

The effect of PET or PCL molar content in the copolyesters was considered. The MP_{TC} of the copolymers increased when the PCL content was increased due to the increase of reaction probability between C-OET and CL as discussed previously. The stable main structure of starting C-OET obtained from the CDP of PET was trimer [39, 45], while the structure of CL was monomer. Therefore, the C-OET ring-opening polymerized to PET which has 3 times longer

chain length than PCL. It investigated that the L_T gradually decreased but the L_C which valued approximately 1 did not change when the PET content was decreased in the copolymers. Therefore, the ratios of L_T to L_C and M_T in the neat copolymers also declined with a constant M_C as the increase of the PCL segment. Furthermore, P_{TT} and P_{CT} decreased but P_{TC} and P_{CC} increased with the decreasing of the PET content or increasing of the PCL content as related with the MP_T:MP_C ratios. The R value increased from approximately 10 to 60, indicating that the structures in the neat PET-*co*-PCL copolymers gradually changed from block to alternating copolymers when the molar ratio of C-OET:CL was decreased because of more ROP probability between C-OET and CL.

For the effects of ROP temperatures and times on the structure of copolymers, increases of ROP temperatures and times promoted the flowing ability of cyclics, resulting in the enhancement of ROP reaction between C-OET and CL in the copolymers. Therefore, the structure of copolymers was more close to random or alternating than block copolymer when the ROP temperatures and times were increased. However, varying in the ROP temperature and time did not affect on the ^{1}H-NMR pattern of copolymers pattern at the same feed molar ratio. In this thesis, the ROP reaction at 180, 200, 230 and 250 °C for 8 and 24 hr were considered to reach equilibrium for ROP of C-OET and CL to PET-*co*-PCL copolymers. Therefore, the number-average lengths, molecular weights, probabilities and randomness values of copolymers did not changed when the ROP temperatures and times were varied. Furthermore, the tendency of copolymer structure at the same PET content still be similar when ROP temperatures and times was varied.

Table 4.2 Chemical shift integration and calculated molar percentage of PET and PCL segments in poly(ethylene terephthalate-*co*-caprolactone) copolymers (PET-*co*-PCL)

Sample	Input molar ratio of C-OET:CL	Chemical shift integration (%)				MP_T:MP_C ratio	MP_{TC} (%mol)
		HO-ET1 δ 4.8 ppm	CO-ETCL2 δ 4.6 ppm	CO-ETCL1 δ 4.4 ppm	HO-CL4 δ 4.2 ppm		
E9C1-180-8	90:10	77.1	9.2	10.8	3.0	91.8:8.2	19.6
E8C2-180-8	80:20	77.3	7.6	11.8	3.3	79.8:20.2	16.6
E7C3-180-8	70:30	49.1	15.1	26.4	9.4	72.3:27.7	40.6
E6C4-180-8	60:40	31.6	21.1	36.2	11.1	60.0:40.0	52.8
E5C5-180-8	50:50	22.2	19.2	40.5	18.1	51.3:48.7	56.8
E9C1-200-8	90:10	61.2	13.8	15.2	9.8	83.8:16.2	29.8
E8C2-200-8	80:20	55.1	16.6	18.0	10.3	83.3:16.7	35.9
E7C3-200-8	70:30	45.4	18.2	25.3	11.2	73.5:26.5	47.0
E6C4-200-8	60:40	27.8	11.7	35.7	24.9	51.1:48.9	45.5
E5C5-200-8	50:50	23.4	19.1	39.8	17.7	56.4:43.6	57.8

Table 4.2 (cont.)

Sample	Input molar ratio of C-OET:CL	Chemical shift integration (%)				MP_T:MP_C ratio	MP_{TC} (%mol)
		HO-ET1 δ 4.8 ppm	CO-ETCL2 δ 4.6 ppm	CO-ETCL1 δ 4.4 ppm	HO-CL4 δ 4.2 ppm		
E9C1-230-8	90:10	74.3	8.1	11.0	6.6	84.9:15.1	16.8
E8C2-230-8	80:20	49.2	14.9	22.9	13.0	76.5:23.5	38.8
E7C3-230-8	70:30	37.7	17.9	32.8	11.6	67.2:32.8	50.0
E6C4-230-8	60:40	26.0	22.1	38.0	13.9	59.9:40.1	65.1
E9C1-180-24	90:10	63.3	15.3	17.0	4.4	84.7:15.3	33.2
E8C2-180-24	80:20	60.1	15.6	21.1	3.2	83.5:16.5	34.0
E7C3-180-24	70:30	45.3	12.4	30.7	11.7	72.8:27.2	43.1
E6C4-180-24	60:40	34.2	19.7	34.8	11.3	65.3:34.7	57.0
E5C5-180-24	50:50	29.4	22.5	40.5	7.7	59.0:41.0	55.5

Table 4.2 (cont.)

Sample	Input molar ratio of C-OET:CL	Chemical shift integration (%)				MP_T:MP_C ratio	MP_{TC} (%mol)
		HO-ET1 δ 4.8 ppm	CO-ETCL2 δ 4.6 ppm	CO-ETCL1 δ 4.4 ppm	HO-CL4 δ 4.2 ppm		
E9C1-200-24	90:10	80.7	8.8	3.3	7.2	89.7:10.3	11.9
E8C2-200-24	80:20	52.0	18.8	22.7	6.6	77.5:22.5	41.9
E7C3-200-24	70:30	43.1	21.9	28.3	6.7	72.4:27.6	51.7
E6C4-200-24	60:40	28.4	21.6	34.7	15.3	58.6:41.4	57.2
E5C5-200-24	50:50	28.9	19.2	41.1	10.9	61.2:38.8	58.9
E9C1-230-24	90:10	66.5	13.2	12.6	7.7	85.7:14.3	26.9
E8C2-230-24	80:20	55.6	18.3	18.3	7.7	78.8:21.2	35.6
E7C3-230-24	70:30	47.9	18.4	26.5	7.3	74.2:25.8	45.9
E6C4-230-24	60:40	28.6	14.1	35.9	21.4	53.1:46.9	53.7

Table 4.2 (cont.)

Sample	Input molar ratio of C-OET:CL	Chemical shift integration (%)				MP_T:MP_C ratio	MP_{TC} (%mol)
		HO-ET1 δ 4.8 ppm	CO-ETCL2 δ 4.6 ppm	CO-ETCL1 δ 4.4 ppm	HO-CL4 δ 4.2 ppm		
E9C1-250-24	90:10	76.2	7.0	7.3	9.5	90.1:9.9	15.8
E8C2-250-24	80:20	58.3	15.7	17.7	8.4	84.3:15.7	36.0
E7C3-250-24	70:30	54.6	18.8	19.1	7.5	80.1:19.9	39.4
E6C4-250-24	60:40	34.9	20.5	32.5	12.1	64.8:35.2	54.7

Table 4.3 Calculated ^{1}H-NMR data of poly(ethylene terephthalate-*co*-caprolactone) copolymers (PET-*co*-PCL)

Sample	Probabilities of all dyad sequences				L_T	L_C	M_T	M_C	R
	P_{TT}	P_{TC}	P_{CC}	P_{CT}					
E9C1-180-8	0.89	0.11	0.00	1.00	9.4	0.8	1798.6	95.4	19.6
E8C2-180-8	0.90	0.10	0.59	0.41	9.6	2.4	1846.7	277.8	16.6
E7C3-180-8	0.72	0.28	0.27	0.73	3.6	1.4	684.4	155.9	40.6
E6C4-180-8	0.56	0.44	0.34	0.66	2.3	1.5	436.2	172.7	52.8
E5C5-180-8	0.45	0.55	0.42	0.58	1.8	1.7	346.6	195.7	56.8
E9C1-200-8	0.82	0.18	0.08	0.92	5.6	1.1	1080.2	123.6	29.8
E8C2-200-8	0.78	0.22	0.00	1.00	4.6	0.9	891.1	105.8	35.9
E7C3-200-8	0.68	0.32	0.11	0.89	3.1	1.1	600.6	128.6	47.0
E6C4-200-8	0.55	0.45	0.53	0.47	2.3	2.1	431.2	244.8	45.5
E5C5-200-8	0.49	0.51	0.34	0.66	2.0	1.5	374.7	172.2	57.8

Table 4.3 (cont.)

Sample	Probabilities of all dyad sequences				L_T	L_C	M_T	M_C	R
	P_{TT}	P_{TC}	P_{CC}	P_{CT}					
E9C1-230-8	0.90	0.10	0.44	0.56	10.1	1.8	1937.7	204.4	16.8
E8C2-230-8	0.75	0.25	0.18	0.83	3.9	1.2	756.4	138.2	38.8
E7C3-230-8	0.63	0.37	0.24	0.76	2.7	1.3	516.4	149.4	50.0
E6C4-230-8	0.46	0.54	0.19	0.81	1.8	1.2	353.3	140.5	65.1
E9C1-180-24	0.80	0.20	0.00	1.00	5.1	0.9	979.7	105.1	33.2
E8C2-180-24	0.80	0.20	0.00	1.00	4.9	1.0	943.8	111.1	34.0
E7C3-180-24	0.70	0.30	0.21	0.79	3.4	1.3	648.0	144.1	43.1
E6C4-180-24	0.56	0.44	0.18	0.82	2.3	1.2	440.1	138.6	57.0
E5C5-180-24	0.53	0.47	0.32	0.68	2.1	1.5	408.2	168.4	55.5

Table 4.3 (cont.)

Sample	Probabilities of all dyad sequences				L_T	L_C	M_T	M_C	R
	P_{TT}	P_{TC}	P_{CC}	P_{CT}					
E9C1-200-24	0.93	0.07	0.42	0.58	15.1	1.7	2906.0	197.2	11.9
E8C2-200-24	0.73	0.27	0.07	0.93	3.7	1.1	711.4	122.4	41.9
E7C3-200-24	0.64	0.36	0.06	0.94	2.8	1.1	537.6	121.6	51.7
E6C4-200-24	0.51	0.49	0.31	0.69	2.1	1.5	393.6	165.1	57.2
E5C5-200-24	0.52	0.48	0.24	0.76	2.1	1.3	399.2	150.3	58.9
E9C1-230-24	0.84	0.16	0.06	0.94	6.4	1.1	1221.5	121.3	26.9
E8C2-230-24	0.77	0.23	0.16	0.84	4.4	1.2	849.2	135.9	35.6
E7C3-230-24	0.69	0.31	0.11	0.89	3.2	1.1	621.7	128.1	45.9
E6C4-230-24	0.50	0.50	0.43	0.57	2.0	1.8	380.2	199.2	53.7

Table 4.3 (cont.)

Sample	Probabilities of all dyad sequences				L_T	L_C	M_T	M_C	R
	P_{TT}	P_{TC}	P_{CC}	P_{CT}					
E9C1-250-24	0.91	0.09	0.20	0.80	11.4	1.3	2191.1	143.1	15.8
E8C2-250-24	0.79	0.21	0.00	1.00	4.7	0.9	898.4	99.7	36.0
E7C3-250-24	0.75	0.25	0.01	0.99	4.1	1.0	781.8	115.0	39.4
E6C4-250-24	0.58	0.42	0.22	0.78	2.4	1.3	454.3	146.7	54.7

4.2.2 Thermal Property

The glass transition temperature (T_g), melting temperature (T_m), crystallization temperature (T_c), cold crystallization temperature (T_{cc}) and their enthalpies (ΔH_m, ΔH_c, ΔH_{cc}) of the PET-*co*-PCL copolymers are showed in Table 4.4.

When the molar ratio of C-OET:CL in the copolymers decreased from 10:0 to 5:5, it was found that the chemical structure of the copolymers changed from block or random to alternating. Therefore, various copolyester structures with varying cyclics molar ratio could affect to the thermal properties of copolymers. The T_g decreased when the CL content was increased because the aliphatic chain structure of CL in the neat PCL has lower T_g (-60 °C) than the aromatic structure of ET unit (T_g = 80 °C) in the neat PET. Not only the T_g decreased but the T_m and ΔH_m also decreased when the C-OET:CL ratios were decreased because the CL units inserted between the ET chains could obstruct the crystallization of ET units. The T_m and ΔH_m were suppressed when the PCL content was ≥ 40 %mol, resulting in thermoplastic elastomer property. At high PET content, the block copolymer with long aromatic chains had high thermal properties. The structure changed to the short aromatic chains alternating structure with low thermal properties when PCL content was increased. This phenomenon was confimed with the L_T value analyzed by ^{1}H-NMR. For example, the PET-*co*-PCL copolymers ROP at 200 °C for 8 hr showed the disappearance of T_m and ΔH_m when the CL content was ≥ 40 %mol, in which the polymeric structure in the copolymers changed from block to alternating copolymers.

When crystallized polymers were rapidly cooled, the polymers were completely amorphous glassy state. After that, the amorphous polymers were heated through the glassy region, molecular mobility increased and the substance crystallized. This behavior is referred to as cold crystallization which it occurs at temperature far below the melting point. [102] The cold crystallization is the exothermic peak in DSC thermogram as shown in Fig. 4.5 and Appendix D. From Table 4.4, the T_{cc} was approximately 120 °C, in which it did not significantly change when the ratio of C-OET:CL was varied. The DSC thermograms in Fig. 4.5 (c) and 4.5 (d) shows the exothermic cold crystallization peak at 120 °C, followed by the endothermic melting peak with an enthalpy equal to the ΔH_{cc} indicated that PET as the isotropic non-crystalline polymer. [103] The isotropic non-crystalline PET does not have the crystalline peak in the cooling run. Therefore, the melting and cold crystallization

affected to the appearance of crystalline peak and could use to calculate the degree of crystallinity of PET unit ($\chi_{c,\,PET}$) as [104];

$$\chi_{c,PET} = \frac{\Delta H_m - \Delta H_{cc}}{\propto_T \Delta H_f} \times 100 \qquad \text{eq.(4.13)}$$

;where α_T : the PET weight fraction as calculate from MP_T in ^{1}H-NMR

ΔH_f : the PET theoretical heat of fusion of 100 % of crystallinity (120 J/g) [105]

The $\chi_{c,PET}$ in the copolymers is showed in Table 4.4. When the PET content was reduced, the $\chi_{c,PET}$ would decrease indicating the reduction of crystallinity content in the copolymers.

The calculated $\chi_{c,PET}$ corresponded to the crystallization peak appeared in the DSC thermograms, in which the T_c and ΔH_c values were concluded in Table 4.4. The T_c and ΔH_c decreased with the decreasing of C-OET content because the CL units obstructed the crystallization of ET units.

The ROP temperature and time which were respectively varied from 180 to 250 °C and 8 to 24 hr did not clearly affect to the thermal properties of copolymers due to unchange in the copolymers structure as discussed previously. However, the peak area of cold crystallization peak decreased when the ROP temperature and time were increased. It indicated that the crystallization of copolymers increased with the increasing of ROP temperature and time.

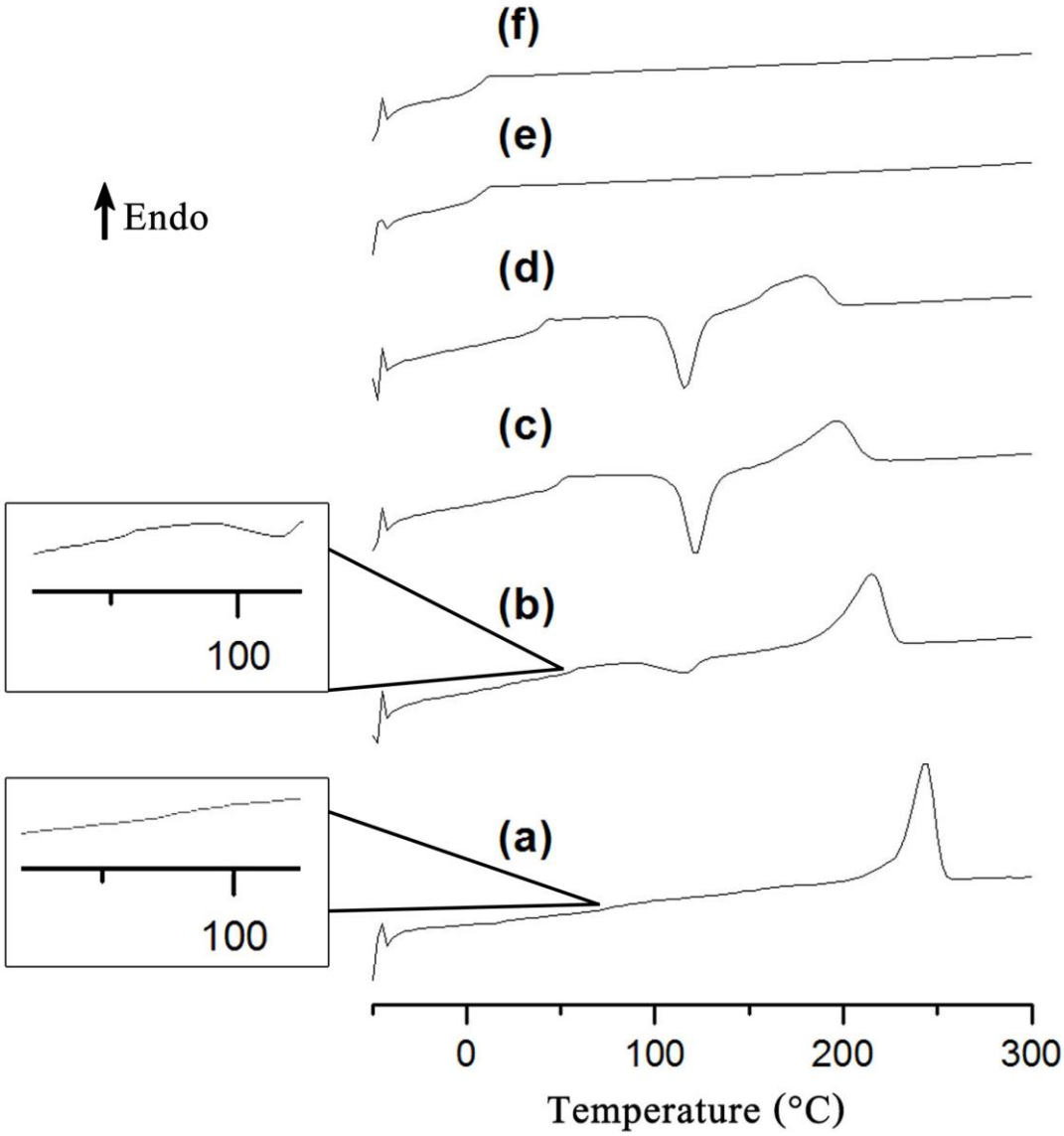

Figure 4.5 DSC thermograms (2nd heating) of PET-*co*-PCL copolymers; i.e. E10C0-200-24 (a), E9C1-200-24 (b), E8C2-200-24 (c), E7C3-200-24 (d), E6C4-200-24 (e) and E5C5-200-24 (f)

Table 4.4 Thermal properties of PET-*co*-PCL copolymers

Sample	T_g (°C)	T_m (°C)	ΔH_m (J/g)	T_c (°C)	ΔH_c (J/g)	T_{cc} (°C)	ΔH_{cc} (J/g)	$\chi_{c,\ PET}$ (%)
E10C0-180-8	92.6	242.2	34.5	192.6	37.4	n/a	n/a	28.8
E9C1-180-8	65.2	217.2	27.8	163.0	30.3	n/a	n/a	24.4
E8C2-180-8	53.2	198.4	23.8	144.8	23.0	n/a	n/a	22.8
E7C3-180-8	40.8	171.4	13.8	112.3	4.7	123.3	8.9	5.0
E6C4-180-8	26.3	159.5	1.0	n/a	n/a	n/a	n/a	1.2
E5C5-180-8	8.6	n/a	n/a	n/a	n/a	n/a	n/a	n/a
E10C0-200-8	72.5	240.2	36.7	167.4	34.9	n/a	n/a	30.6
E9C1-200-8	54.5	206.1	26.2	121.4	4.1	120.5	19.9	5.9
E8C2-200-8	57.4	198.6	16.6	n/a	n/a	135.4	17.1	n/a
E7C3-200-8	35.7	165.2	11.7	n/a	n/a	119.7	15.1	n/a
E6C4-200-8	9.8	n/a	n/a	n/a	n/a	n/a	n/a	n/a
E5C5-200-8	11.4	n/a	n/a	n/a	n/a	n/a	n/a	n/a
E10C0-230-8	76.3	240.0	35.0	164.1	31.0	n/a	n/a	29.2
E9C1-230-8	62.2	230.3	40.0	153.1	36.9	n/a	n/a	36.8
E8C2-230-8	46.3	194.0	24.6	n/a	n/a	119.4	21.8	2.8
E7C3-230-8	29.6	159.3	5.6	n/a	n/a	123.3	5.0	0.6
E6C4-230-8	18.0	n/a	n/a	n/a	n/a	n/a	n/a	n/a
E10C0-180-24	84.1	244.2	39.9	188.0	42.3	n/a	n/a	33.3
E9C1-180-24	53.5	205.5	26.2	137.7	26.4	n/a	n/a	24.2
E8C2-180-24	52.7	196.0	15.3	122.1	7.9	124.6	13.4	1.8
E7C3-180-24	40.3	168.5	6.4	n/a	n/a	127.7	5.2	1.2
E6C4-180-24	30.8	159.4	1.6	n/a	n/a	130.8	1.1	0.5
E5C5-180-24	23.6	n/a	n/a	n/a	n/a	n/a	n/a	n/a

Table 4.4 (cont.)

Sample	T_g (°C)	T_m (°C)	ΔH_m (J/g)	T_c (°C)	ΔH_c (J/g)	T_{cc} (°C)	ΔH_{cc} (J/g)	$\chi_{c\ PET}$ (%)
E10C0-200-24	79.0	243.8	42.8	174.1	39.7	n/a	n/a	35.7
E9C1-200-24	57.8	215.3	35.4	136.4	27.3	115.4	5.1	27.0
E8C2-200-24	48.9	196.1	22.3	n/a	n/a	121.3	21.7	0.6
E7C3-200-24	40.3	181.4	17.8	n/a	n/a	115.5	20.2	n/a
E6C4-200-24	7.5	n/a	n/a	n/a	n/a	n/a	n/a	n/a
E5C5-200-24	22.2	n/a	n/a	n/a	n/a	n/a	n/a	n/a
E10C0-230-24	77.6	240.9	45.5	168.6	40.8	n/a	n/a	37.9
E9C1-230-24	64.8	231.3	40.1	152.3	37.0	n/a	n/a	36.7
E8C2-230-24	47.1	189.0	19.0	n/a	n/a	121.1	18.7	0.3
E7C3-230-24	36.1	167.8	13.8	n/a	n/a	116.6	17.4	n/a
E6C4-230-24	16.6	n/a	n/a	n/a	n/a	n/a	n/a	n/a
E10C0-250-24	77.5	244.5	43.0	190.6	42.2	n/a	n/a	35.8
E9C1-250-24	60.4	219.8	32.4	158.6	20.8	n/a	n/a	28.8
E8C2-250-24	47.2	207.9	25.8	147.4	12.1	n/a	n/a	23.9
E7C3-250-24	32.6	164.5	12.4	n/a	n/a	117.6	12.0	0.4
E6C4-250-24	27.8	161.2	7.8	n/a	n/a	117.6	9.4	n/a

4.2.3 Physical appearances

Physical appearances of the ROP PET-*co*-PCL copolyesters were investigated.

- When the C-OET content in the copolymers ROP at 230 °C for 8 hr, 230 °C for 24 hr and 250 °C for 24 hr was more than 70 %mol, it was found that the ROP copolymers could maintain their shape, except the E8C2-250-24 copolymer. In addition, the E8C2-250-24 copolymer burned after ROP. However, the copolymers with ET content lower than 80 %mol could not maintain their shape and burn when ROP at 230 and 250 °C for 8 and 24 hr. Therefore, the copolymers with relatively low ET content ROP at high temperature could not maintain their shape.
- When ROP temperature was decreased to 200 °C for 24 hr, it was investigated that the surfaces of copolymers were brown color in all C-OET:CL molar ratios. In addition, the ROP copolymers with CL content less than 40 %mol could maintain their shape. When the ROP time was decreased to 8 hr at 200 °C, the ROP copolyesters could maintain their shape and their surfaces were brown color surfaces in all cyclics molar ratios. Therefore, at 200 °C, the copolymers with relatively high CL content ROP for long time could not maintain their shape.
- The copolymers were ring-opening polymerized at 180°C for 24 hr and 180°C for 8 hr, the ROP copolymers could maintain their shape and have brown surfaces. However, these copolymers should be characterized to confirm the appropriateness of ROP temperature at 180 °C.

The previous characterization data of PET-*co*-PCL copolymers were used as the preliminary decision for selection of the ROP condition for the preparation of CS/PET-*co*-PCL composites.

- From the physical appearances of the neat copolymers, it was found that the ROP temperatures at 180 and 200 °C and time at 8 and 24 hr were appropriate to prepare the ROP copolymers. However, the ROP of composites was performed for 24 hr because the cold crystallization peak decreased and the crystallization of copolymers increased when using longer ROP time. Therefore, the ROP temperatures at 180 and 200 °C for 24 hr were used for the ROP of composites.
- The composites with CS more than 60 %wt had worse properties than the composites with 50 and 60 %wt CS content as investigated in a previous literature review. [79] Furthermore, the composites with CS lower than 50 %wt could not be shaped for the preparation of composites. Therefore, the selected CS to cyclics weight ratios were 50:50 and 60:40.

The CS to cyclics weight ratios at 50:50 and 60:40 with varying in the molar ratios of C-OET to CL in the composites from 50:50 to 100:0 at 180 and 200 °C ROP temperature for 24 hr were used to perform in the preparation of composites.

4.3 Chemical structure of PET-*co*-PCL copolymers in CS/PET-*co*-PCL composites

Appendix C shows all ^{1}H-NMR spectra of PET-*co*-PCL copolymers in the CS/PET-*co*-PCL composites. The spectrum of the ROP copolymer in the S50-E5C5-180-24 composite was used as a representative of the characteristic of PET-*co*-PCL copolymers in the composites as shown in Fig. 4.6. The ^{1}H-NMR spectra of the copolymers in all composites were similar to those of the neat PET-*co*-PCL copolymers although the composites were prepared using various conditions, i.e., C-OET to CPL molar ratios, CS to cyclics weight ratios and ROP temperatures. Two main groups of chemical signals were observed, i.e., homolinkages of ET-ET and CL-CL units and heterolinkage of ET-CL units. The homolinkage chemical shifts were at δ 1.4 (C_1), 1.7 (C_2), 2.5 (C_3), 4.2 (C_4), 4.8 (E_1) and 8.1 (E_2) ppm. On the other hand, the heterolinkage signals were observed at the chemical shift δ 4.4 ppm (EC_1) and δ 4.55 and 4.65 ppm of EC_2 peaks. The end group signal of ROP-copolymer in composites was also observed at δ 4.0 and 3.8 ppm. These results indicated that the C-OET and CL could be successfully ring-opening polymerized to form PET-*co*-PCL in all CS/PET-*co*-PCL composites.

The chemical shift integrations of ^{1}H-NMR peaks of copolymers in the composites (HO-ET1, CO-ETCL1, CO-ETCL2, and HO-CL4) are shown in Appendix C. The integration results of ROP PET-*co*-PCL copolymers in composites are quite similar to those of the neat copolymers, in which the integration value of CO-ETCL1, CO-ETCL2 and HO-CL4 increased, but that of HO-ET1 decreased when the CL content in copolymers was increased.

In addition, the molar percentage of ET-ET (MP_T), CL-CL (MP_C) and ET-CL (MP_{TC}) of copolymers in the composites could be calculated from the ^{1}H-NMR peak intensities using eq.(4.1), (4.2) and (4.3), respectively. The MP_T, MP_C and MP_{TC} values of ROP polymers in the composites are showed in Table 4.5. In the CS/PET-*co*-PCL composites, the calculated MP_T:MP_C ratios were quite less than the feed values. These results were considered to be because the chloroform extracted product from the composites might be mainly composed of short chains copolymers. However, the MP_{TC} of the composites showed the same trend as the MP_{TC} of the neat copolymers, which was the MP_{TC} increased with the increase of the CL content.

The L_T, L_C, M_T, M_C of polymer units and P_{TC}, P_{CT}, P_{TT}, P_{CC} in the composites calculated using eq.(4.4)-(4.11) which are showed in Appendix C. The L_T and L_C trends in the composites were similar to those of the neat copolymers. While the L_T of the composites decreased, the L_C was still unchanged at approximately 1 when the PET content was decreased. It resulted to the decrease of L_T to L_C ratios and M_T of the composites. In addition, the P_{TT} and P_{CT} decreased when the amount of PET segment decreased, while the P_{TC} and P_{CC} increased when the amount of PCL segment was increased.

The run number of copolymers in the composites could be calculated with the same equation as used for the neat copolymers (eq.4.12). The run numbers of ROP copolymers in the composites are showed in Table 4.5. It can be seen that the ROP polymer structures in the composites changed from block to alternating copolyesters when the PCL content was increased.

However, the increment of ceramic in the composites from 50 to 60 %wt and the variation of the ROP condition did not clearly affect on the changes of trends in the molar percentages of PET, PCL segments and PET-PCL dyads, sequence lengths, molecular weights, probabilities and ROP copolymer chemical structures because the 24 hr-ROP reaction of C-OET and CL to PET-*co*-PCL copolymers in the composites could reach equilibrium.

The main product in the chloroform extracted copolymers from the composites was the short chains PET-*co*-PCL copolymers as indicated with the excess MP_T values and the random structure of copolymers in the composites. Therefore, the ^{1}H-NMR spectra and their calculated data were not real representative for all copolymers in the composites. However, the trend of all values from ^{1}H-NMR in the composites was quite similar to the trend in the pure copolymers.

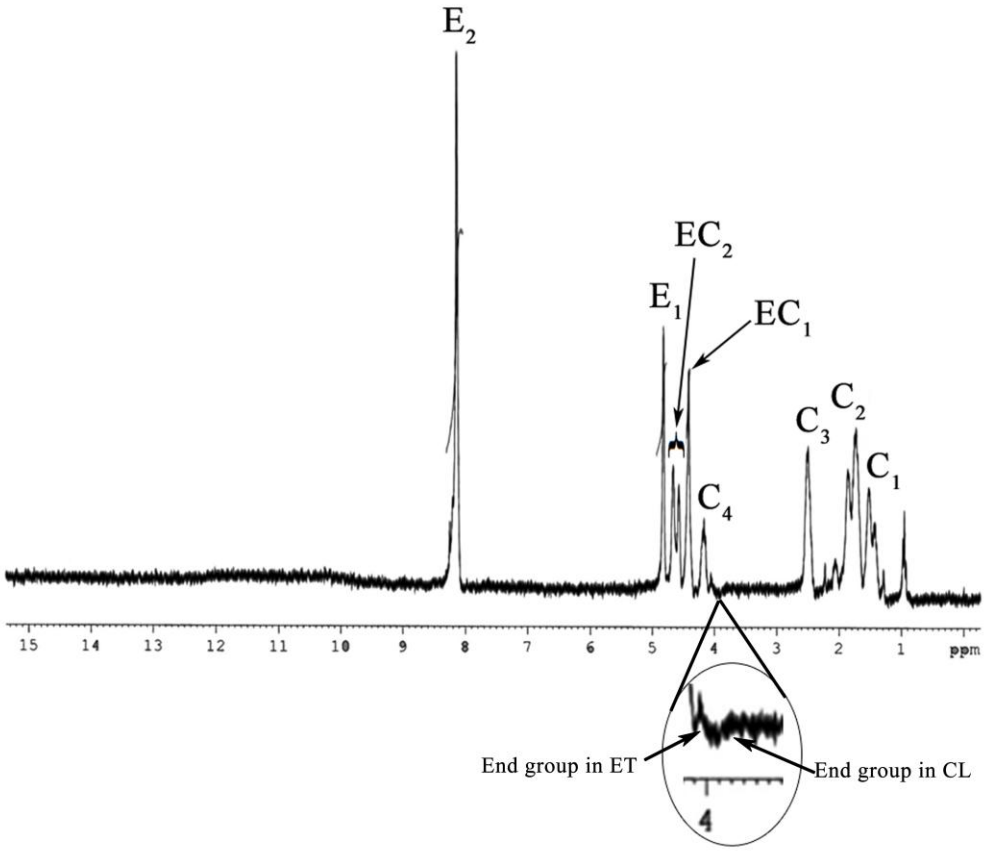

Figure 4.6 ^{1}H-NMR spectrum of PET-*co*-PCL copolymers with 50 %mol ET content in composite with 50 %wt CS which ring-opening polymerized at 180 °C for 24 hr

Table 4.5 Composition and randomness of copolymers in calcium silicate/poly(ethylene terephthalate-*co*-caprolactone) composites (CS/PET-*co*-PCL)

Sample	Input %mol ratio of C-OET:CL	MP_T:MP_C (%mol)	MP_{TC} (%mol)	R
S50-E9C1-180-24	90:10	74.4:25.6	10.3	10.3
S50-E8C2-180-24	80:20	74.0:26.0	47.5	47.5
S50-E7C3-180-24	70:30	92.0:8.0	19.2	19.2
S50-E6C4-180-24	60:40	53.6:46.4	69.0	69.0
S50-E5C5-180-24	50:50	44.0:56.0	79.1	79.1
S50-E9C1-200-24	90:10	81.0:19.0	38.1	38.1
S50-E8C2-200-24	80:20	77.1:22.9	58.1	58.1
S50-E7C3-200-24	70:30	67.8:32.2	56.1	56.1
S50-E6C4-200-24	60:40	61.0:39.0	57.2	57.2
S50-E5C5-200-24	50:50	44.5:55.5	76.4	76.4
S60-E9C1-180-24	90:10	96.1:3.9	56.4	56.4
S60-E8C2-180-24	80:20	78.0:22.0	30.4	30.4
S60-E7C3-180-24	70:30	78.1:21.9	29.2	29.2
S60-E6C4-180-24	60:40	62.5:37.5	43.8	43.8
S60-E5C5-180-24	50:50	47.4:52.6	68.4	68.4
S60-E9C1-200-24	90:10	74.4:25.6	12.1	12.1
S60-E8C2-200-24	80:20	69.8:30.2	36.8	36.8
S60-E7C3-200-24	70:30	79.0:21.0	30.5	30.5
S60-E6C4-200-24	60:40	53.9:46.1	74.0	74.0
S60-E5C5-200-24	50:50	58.6:41.4	61.4	61.4

4.4 Thermal properties of CS/PET-*co*-PCL composites

4.4.1 Differential scanning calorimeter (DSC)

Table 4.6 summarized the thermal properties of CS/PET-*co*-PCL composites. The effect of cyclics molar ratios in the composites to the thermal properties of composites was investigated. The T_g of copolymer was lowered by increasing amounts of aliphatic ester in PET-*co*-PCL copolymers. The T_g varied from ~80 °C for the E10C0 composites to ~20 °C at E5C5 composites for all conditions. Furthermore, the T_m and ΔH_m of PET-co-PCL copolymers in the composites decreased with increasing CL amount in the copolymer. However, the ΔH_m values of the composites with 60 and 70 %mol PET content were quite low, indicating that they consisted primarily of amorphous structure. Both T_m and ΔH_m were suppressed when the copolymer containing > 30 %mol CL. These results indicated that the PET partially crystallized when the ET content in the copolymers was more than 60 %mol. When the PET content in the CS/PET-*co*-PCL composites was diluted, the T_c and ΔH_c of ET phase would decrease. These results were because the driving force for crystallization decreased with increasing PCL content. The T_c peak would vanish when the PET content in the copolymers was lower than 70 %mol due to the complete amorphous structure in these composites. Furthermore, the $\chi_{m,\,PET}$ of copolymer in the composites could be determined by eq.(4.13) as same as in the neat copolymers. However, the cold crystallization peak in the composites disappeared in all conditions due to the complete ring-opening polymerization, so that, the ΔH_{cc} in eq.(4.13) was removed. Table 4.6 shows the $\chi_{m,\,PET}$ values in which it decreased with increasing of CL unit but suppressed with ET content less than 70 %mol as relate with the melting temperature.

Although, the ROP temperatures and CS:cyclics weight ratios were varied, the trend of thermal properties in all composites was similar in all conditions. However, the T_g values of the composites were higher than those of the neat copolymers as shown in Table 4.6 which the crystallization temperatures and its enthalpies of the neat copolymers and the composites were compared. These results were considered to be the effect of high CS content which interfered the polymer dynamics in the composites. Not only T_g, but also T_m, ΔH_m, T_c, ΔH_c and $\chi_{m,\,PET}$ of the neat copolymers were lower than those of the PET-*co*-PCL in the composites. This result indicated that the composites had more PET crystallization than the copolymers due to the CS nucleating agent in the composites.

Table 4.6 Thermal properties of CS/PET-*co*-PCL composites

Composites							Neat Copolymers		
Sample	**T_g (°C)**	**T_m (°C)**	**ΔH_m (J/g)**	**T_c (°C)**	**ΔH_c (J/g)**	**$\chi_{c,\,PET}$ (%)**	**Sample**	**T_c (°C)**	**ΔH_c (J/g)**
S50-E10C0-180-24	82.4	242.3	39.3	190.6	50.4	32.8	E10C0-180-24	188.0	42.3
S50-E9C1-180-24	78.5	231.9	25.0	180.5	30.3	25.1	E9C1-180-24	137.7	26.4
S50-E8C2-180-24	63.8	206.9	23.9	147.8	18.1	24.1	E8C2-180-24	122.1	7.9
S50-E7C3-180-24	56.0	206.1	6.0	132.0	5.8	5.3	E7C3-180-24	n/a	n/a
S50-E6C4-180-24	41.2	192.0	1.5	141.4	4.7	1.9	E6C4-180-24	n/a	n/a
S50-E5C5-180-24	37.7	n/a	n/a	n/a	n/a	n/a	E5C5-180-24	n/a	n/a
S50-E10C0-200-24	82.6	244.7	36.0	194.4	47.8	30.0	E10C0-200-24	174.1	39.7
S50-E9C1-200-24	73.3	228.1	23.4	172.2	28.3	22.2	E9C1-200-24	136.4	27.3
S50-E8C2-200-24	67.6	206.1	10.2	153.3	14.4	10.0	E8C2-200-24	n/a	n/a
S50-E7C3-200-24	56.6	203.1	2.6	134.7	9.5	2.8	E7C3-200-24	n/a	n/a
S50-E6C4-200-24	52.2	n/a	n/a	n/a	n/a	n/a	E6C4-200-24	n/a	n/a
S50-E5C5-200-24	19.5	n/a	n/a	n/a	n/a	n/a	E5C5-200-24	n/a	n/a

Table 4.6 (cont.)

Composites							Neat Copolymers		
Sample	**T_g (°C)**	**T_m (°C)**	**ΔH_m (J/g)**	**T_c (°C)**	**ΔH_c (J/g)**	**$\chi_{c,\,PET}$ (%)**	**Sample**	**T_c (°C)**	**ΔH_c (J/g)**
S60-E10C0-180-24	83.4	241.3	26.7	187.1	38.4	22.3	E10C0-180-24	188.0	42.3
S60-E9C1-180-24	70.2	232.9	21.6	174.9	28.2	18.4	E9C1-180-24	137.7	26.4
S60-E8C2-180-24	68.1	223.3	10.5	152.3	18.3	10.2	E8C2-180-24	122.1	7.9
S60-E7C3-180-24	60.2	206.9	4.7	124.8	5.8	4.6	E7C3-180-24	n/a	n/a
S60-E6C4-180-24	47.8	n/a	n/a	n/a	n/a	n/a	E6C4-180-24	n/a	n/a
S60-E5C5-180-24	38.4	n/a	n/a	n/a	n/a	n/a	E5C5-180-24	n/a	n/a
S60-E10C0-200-24	81.5	242.7	18.7	197.1	32.2	15.6	E10C0-200-24	174.1	39.7
S60-E9C1-200-24	73.3	228.7	18.5	182.9	25.3	18.6	E9C1-200-24	136.4	27.3
S60-E8C2-200-24	71.1	221.3	11.7	170.2	22.4	12.3	E8C2-200-24	n/a	n/a
S60-E7C3-200-24	65.8	202.5	9.1	142.7	8.4	8.8	E7C3-200-24	n/a	n/a
S60-E6C4-200-24	60.8	n/a	n/a	n/a	n/a	n/a	E6C4-200-24	n/a	n/a
S60-E5C5-200-24	38.5	n/a	n/a	n/a	n/a	n/a	E5C5-200-24	n/a	n/a

4.4.2 Thermogravimetric analyzer (TGA)

Table 4.7 shows thermal degradation temperatures of the composites from the TGA thermograms. The TGA thermograms of the composites showed 2 steps of degradation respectively at 350-430 and 430-610 ºC, corresponded to the aliphatic chain and the aromatic chain in the copolymers. The copolymer composition could be calculated from the summation of these two degradation data. The calculated copolymers content in the composites were about 33–40 and 34–49 %wt for the composites with 40 and 50 %wt copolymers, respectively, as summarized in Table 4.7. It showed that the calculated compositions were close to the feed compositions. In addition, the ROP-temperature, CS content and the molar ratio of C-OET:CL in composites did not clearly affect to the thermal degradation temperatures.

Table 4.7 Thermal degradation temperatures and copolymer composition of CS/PET-*co*-PCL composites

Sample	1st step temperature (°C)	2nd step temperature (°C)	ROP-PET-*co*-PCL content in composites (%wt)*
S50-E10C0-180-24	409	581	47.7
S50-E9C1-180-24	428	463	43.7
S50-E8C2-180-24	426	608	45.7
S50-E7C3-180-24	372	432	45.6
S50-E6C4-180-24	369	440	45.0
S50-E5C5-180-24	392	510	44.0
S50-E10C0-200-24	410	575	46.0
S50-E9C1-200-24	428	461	42.1
S50-E8C2-200-24	423	606	48.7
S50-E7C3-200-24	347	484	33.7
S50-E6C4-200-24	371	516	43.3
S50-E5C5-200-24	370	581	46.2
S60-E10C0-180-24	412	553	37.1
S60-E9C1-180-24	428	471	33.4
S60-E8C2-180-24	430	475	38.2
S60-E7C3-180-24	423	474	34.0
S60-E6C4-180-24	409	474	35.5
S60-E5C5-180-24	386	465	40.0
S60-E10C0-200-24	416	545	38.6
S60-E9C1-200-24	429	471	34.9
S60-E8C2-200-24	393	482	37.9
S60-E7C3-200-24	428	503	34.5
S60-E6C4-200-24	352	556	33.6
S60-E5C5-200-24	406	478	35.8

*Calculated from %weight loss in TGA thermograms

4.5 Morphology of CS/PET-*co*-PCL composites

The morphologies of all neat PET-*co*-PCL copolymers and CS/PET-*co*-PCL composites are shown in Appendix E. The surface of the agglomerate CS particles in the composites which had ≤ 80 %mol ET (E8, E7, E6 and E5) in both S50 and S60 composites was fully coated with a continuous phase of copolymer matrix obtained from the ROP of C-OET and CL at 180 and 200 °C as respectively observed in Fig. 4.7 (a) and 4.7 (b) for S50-E8C2-180-24 and S60-E8C2-180-24 composites. On the other hand, the neat E8C2-180-24 copolymer was observed as smooth and continuous surface as shown in Fig. 4.7 (c).

In the case of CS/PET-*co*-PCL composites with 90 %mol ET obtained at 180 °C ROP temperature, the layer of PET-*co*-PCL copolymer could not totally conceal the CS particles as shown in Fig. 4.7 (d) and 4.7 (e) for the S50-E9C1-180-24 and S60-E9C1-180-24 composites, respectively. When the ROP temperature was increased from 180 to 200 °C, the copolyester products would be observed as thin layer coating on the surfaces of CS particles for S50-E9C1-200-24 (Fig. 4.7 (f)) and S60-E9C1-200-24 (Fig. 4.7 (g)) composites. These results were because the 200 °C ROP temperature could promote the flowing ability of the ET segment of cyclics in the composites. This phenomenon also occurred in the neat copolyesters with the same ET content as shown in Fig. 4.7 (h) and 4.7 (i). The E9C1-180-24 copolymer showed the rough and porous surface, while the rough and continuous surface was obtained in the neat E9C1-200-24 copolymer. However, the neat copolyesters with ET content ≤ 80 %mol showed smoother surfaces even using lower ROP temperature as describe previously. At 180 °C ROP temperature, the amount of main trimer C-OET in both copolymers and composites which melted to homogenous phase was less than the ROP at 200 °C because the 200 °C ROP temperature was closed to T_m of C-OET. Therefore, the probability which C-OET will react with catalyst at 200 °C was higher than at 180 °C.

The microstructure of S60-E10C0-200-24 composite was showed in Fig. 4.7 (j). The composites with 100 %mol PET showed the non-continuous surface because there was the mixture between high melting temperature aromatic hard segment and low heat transfer CS. However, the S50-E10C0-200-24 composite possessed the continuous ET phase covering the CS particles as shown in Appendix E.

The SEM results showed full covering of copolymers phase on CS particles. It was the CS could act as nucleating agent in the composites; therefore, the crystallization of composites was higher than the crystallization of neat copolymers as shown in the DSC results.

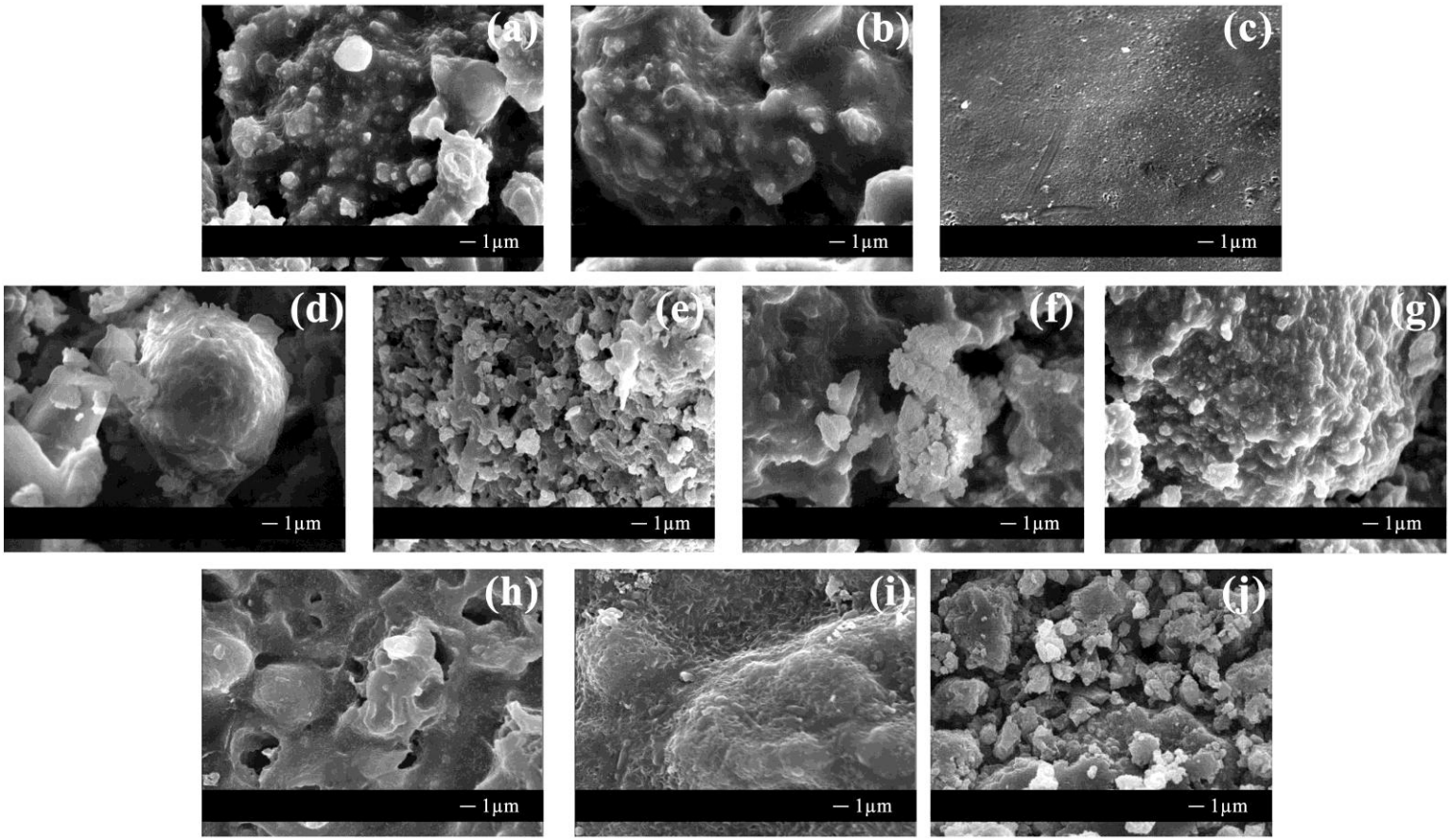

Figure 4.7 SEM micrographs of (a) S50-E8C2-180-24, (b) S60-E8C2-180-24 composites, (c) E8C2-180-24 copolymer, (d) S50-E9C1-180-24, (e) S60-E9C1-180-24, (f) S50-E9C1-200-24, (g) S60-E9C1-200-24 composites, (h) E9C1-180-24, (i) E9C1-200-24 copolymers and (j) S60-E10C0-200-24 composite

4.6 Crystallinity of CS/PET-*co*-PCL composites

Figure 4.8 and Appendix G shows the XRD patterns of the CS/PET-*co*-PCL composites. The CS/PET-*co*-PCL composites exhibited not only the diffraction peaks of CS particles but also the peaks at 2θ = 17.0, 22.0 and 25.5° which corresponded to (100), ($\bar{1}$10) and (010) planes of triclinic ET crystal structure. [106] The peaks assigned to CL unit were not observed in all composites. When the ET content in the copolymeric matrices was diluted, the peak intensity of the crystalline ET unit in the composites would gradually decrease especially the diffraction peak of (010) plane at 2θ = 25.5°. However, the crystalline peaks of ET unit suppressed in both S50 and S60 CS/PET-*co*-PCL composites when their ET contents were lower than 80 %mol at both 180 and 200 °C ROP temperatures. These results were considered to be because the CL units acted as defects in the ET crystalline sections, therefore, the copolyesters could crystallize when they composed of low CL content. [50] The ET segment could partially crystallize in the composites; however, the increase of amorphous CL segment could impede the ET crystallization as previously shown in the DSC results which T_m disappeared. It can be conclude that the driving force for crystallization of ET phase increased with decreasing of CL defect density in the PET-*co*-PCL copolyesters.

Furthermore, trace of broad peak at range of 2θ = 15-30° corresponding to the amorphous halo was observed in all composites, indicating the ROP PET-*co*-PCL in these composites were semicrystalline. However, the content of both CS and copolymers in the composites did not affect to the crystalline peaks patterns.

From XRD patterns, the apparent crystallite sizes (ACS) of CS and ET in the composites were calculated from the Scherrer equation;

$$\mathrm{ACS} = \frac{0.9\lambda}{\beta\cos\theta} \qquad \text{eq.(4.14)}$$

;where λ : X-ray wavelength (0.154 nm)

β : full-width at half maximum of the peak at 2θ (radians)

θ : scattering angle (degree)

The crystalline peaks at 2θ = 25.5 and 29.9° were used to determine the crystallite size of ET and CS, respectively. Table 4.8 shows the ACS of CS and ET in the composites. The ACS values of CS in the composites were ranged from 34 to 39 nm, in which they were approximately equal to that

of the starting CS powders (47.3±0.2 nm). These results indicated that copolymers and the heat treatment during ROP did not affect the crystallite size of CS.

The crystallite sizes of ET in the CS/PET-*co*-PCL composites containing 80, 90 and 100 %mol of PET were in the range of 27 to 38 nm, in which they unchanged when the conditions were varied. Some composites could not calculate the ACS of ET such as S60-E9C1-200-24, S60-E8C2-200-24, S60-E8C2-180-24, S50-E9C1-200-24 and S50-E8C2-200-24, even the small XRD peak of crystalline PET was observed at $2\theta = 25.5°$ as shown in Appendix G, the peak width (β value) could not be clearly resolved for calculation of PET crystallite size. However, these results indicated that the PET could crystallize in these composites. Due to the PET crystalline peak was not observed when the PET content in the copolyesters was decreased to 50, 60 and 70 %mol, the ACS of ET could be indeterminant. These results suggested that the crystallization of PET segment was interfered by increasing the PCL content in the CS/PET-*co*-PCL composites.

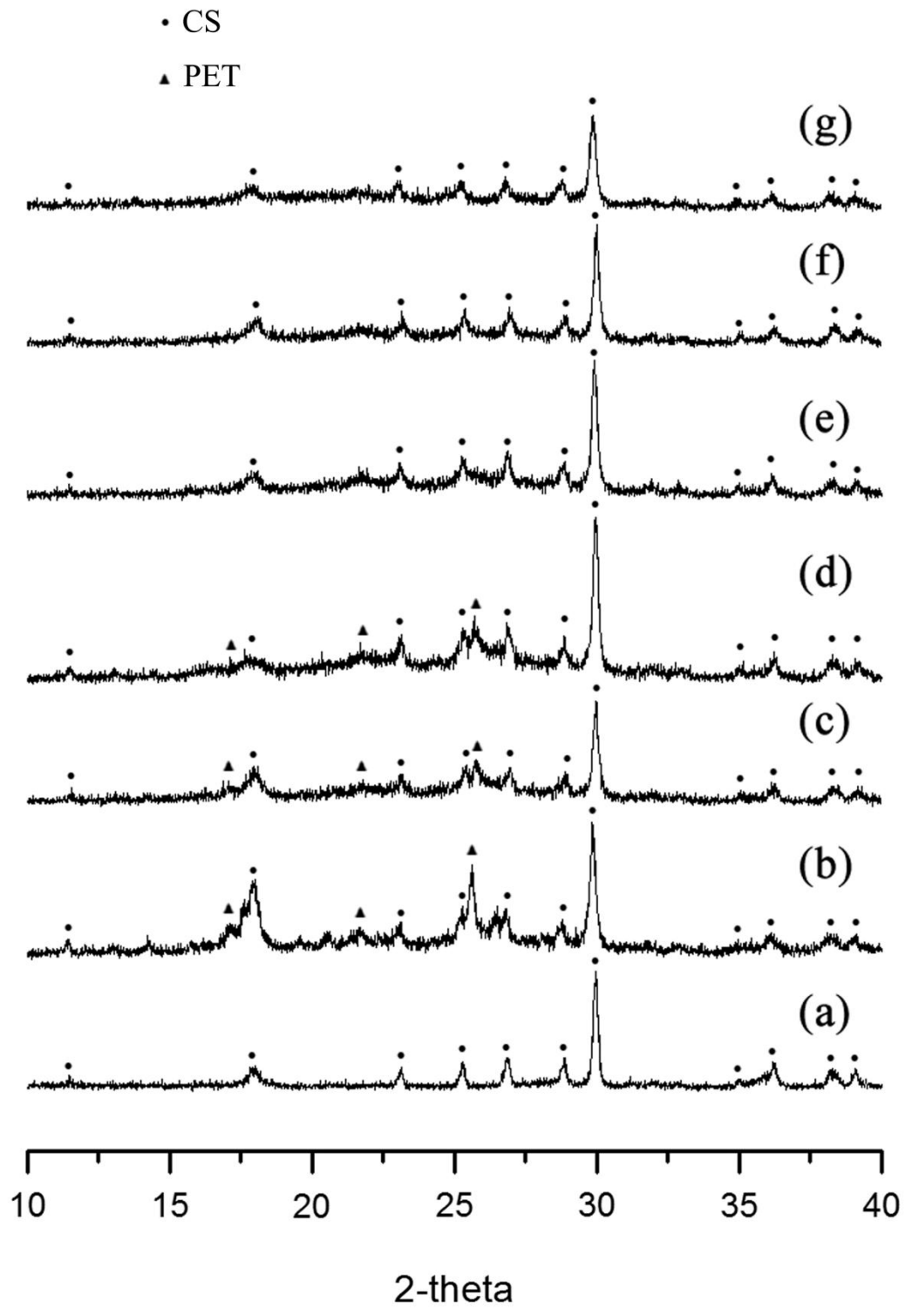

Figure 4.8 XRD patterns of (a) CS, (b) S50-E10C0-180-24, (c) S50-E9C1-180-24, (d) S50-E8C2-180-24, (e) S50-E7C3-180-24, (f) S50-E6C4-180-24 and (g) S50-E5C5-180-24 composites

Table 4.8 Crystalline sizes of CS and PET respectively calculated from crystalline peaks of composites at 2θ = 29.9 and 25.5°

Sample	ACS of CS (nm)	ACS of PET (nm)
S50-E10C0-180-24	35.37±0.11	32.12±3.20
S50-E9C1-180-24	36.89±0.71	38.51±4.33
S50-E8C2-180-24	35.37±0.33	38.54±0.91
S50-E7C3-180-24	37.56±0.49	n/a
S50-E6C4-180-24	36.80±0.35	n/a
S50-E5C5-180-24	33.91±0.30	n/a
S50-E10C0-200-24	34.50±1.31	34.14±2.72
S50-E9C1-200-24	38.54±1.15	n/a
S50-E8C2-200-24	34.68±3.61	n/a
S50-E7C3-200-24	37.90±0.49	n/a
S50-E6C4-200-24	39.54±0.01	n/a
S50-E5C5-200-24	34.63±0.32	n/a
S60-E10C0-180-24	35.18±1.49	27.40±0.85
S60-E9C1-180-24	36.39±0.23	32.29±0.99
S60-E8C2-180-24	35.78±1.10	n/a
S60-E7C3-180-24	37.39±0.23	n/a
S60-E6C4-180-24	35.22±2.13	n/a
S60-E5C5-180-24	36.02±1.22	n/a
S60-E10C0-200-24	33.99±0.40	27.63±0.66
S60-E9C1-200-24	36.72±0.45	n/a
S60-E8C2-200-24	35.77±0.23	n/a
S60-E7C3-200-24	37.99±0.12	n/a
S60-E6C4-200-24	34.49±0.31	n/a
S60-E5C5-200-24	36.97±0.60	n/a

4.7 Mechanical properties of PET-*co*-PCL copolymers and CS/PET-*co*-PCL composites

4.7.1 Universal testing machine

The compressive strengths of the CS/PET-*co*-PCL composites which were showed in Fig. 4.9 significantly increased up to 24 MPa, in which they were higher than 4.8 MPa of the CS pellet and 6.6 MPa of the highest value of the neat PET-*co*-PCL copolymer (E9C1-180-24). The drastic increase of the compressive strength of the CS/PET-*co*-PCL composites was attributed to the presence of ROP-PET-*co*-PCL as the continuous phase in the composites. The PET-*co*-PCL functioned as binder and load absorber among the CS grains; therefore, the tough and flexible PET-*co*-PCL copolymer could transfer the external load in the composites, resulting in the retardation of severe crack initiation and propagation in the composites. Furthermore, the dispersed CS particles in the composites acted as the reinforced material which terminated the cracking. However, the compressive strengths of the composites with $\geq$ 40 %mol PCL were lower than that of the neat CS sample due to the high quantity of aliphatic CL in the copolymer matrix.

The effect of the C-OET:CL molar ratios varying on the compressive strengths of composites were investigated. The compressive strengths of the composites with 100 %mol ET were lower than those of the composites with 90 %mol ET because the ROP temperatures were not high enough to completely ROP of C-OET to PET matrix in the E10 composites. Therefore, the E10 composites were not continuous phase as shown in the SEM micrograph (Fig. 4.7 (j) and Appendix E). However, the compressive strength gradually decreased when the ET content in the ROP-CS/PET-co-PCL composites decreased from 90 %mol to 50 %mol (concurrented with the increase of CL content) because the polymeric structure in the composites changed from the long ET unit block copolymer to the short ET unit alternating copolymer as confirmed in the ^{1}H-NMR (Table 4.6). Especially in the composites with the ET content $\geq$ 60 %mol, the strength drastically decreased due to the disappearance of crystallinity in the copolymer matrices as previously discussed in the DSC and XRD results. Therefore, the highest value was obtained in the composites which composed of 90 %mol ET in all conditions.

Consequently, the ROP temperature varying which affected on the compressive strengths of the composites was studied. When the ROP temperature was increased, the compressive strength

would increase in the composites with ≥ 90 %mol ET since the rising of ROP temperature resulted in the formation of continuous film ROP-PET-*co*-PCL covering on the CS grains in the composites as observed in the SEM (Fig. 4.7 (d), 4.7 (e), 4.7 (f) and 4.7 (g)). On the other hand, the strength of composites with CL content > 20 %mol decreased when the ROP temperature was increased because the copolymers polymerized at 200 ºC was higher flowing ability than 180 °C. It assumed that the copolymers flowed and unevenly distributed in the composites. This phenomenon occurred in both S50 and S60 composites; however, this effect decreased in the S60 composites because the higher CS content in the composites would impede the flowing of copolymers' matrices. The compressive strengths of neat copolymers showed the similar trend to those of the composites, such as the comparison between the E8C2-180-24 and E8C2-200-24 copolymers as shown in Fig. 4.11 (a).

Varying in CS weight content in the composites affected to the compressive strengths' composites was one of study parameter. The CS content in the composites had less effect to the compressive strength of the composites. The compressive strengths of composites with 50 %wt CS were slightly lower than those of composites with 60 %wt CS because the main phase of loading was the copolymers matrix which they had same morphologies for the composites preparing from the same ROP temperature and copolymer ratio.

The compressive moduli of composites were dramatically higher than of the CS and the neat PET-*co*-PCL copolymers as shown in Fig. 4.10 and 4.11 (b). The compressive moduli of the CS/PET-co-PCL composites had the same trend as the compressive strength, in which they decreased with increasing CL content in the composites and the highest value was the composites with 90 %mol ET. However, the compressive moduli of composites with high ET content were almost same.

Figure 4.12 shows the stress-strain curve of CS/PET-*co*-PCL composites with 60 %wt of CS with varying molar ratios of C-OET:CL ROP at 180 °C for 24 h and Appendix F shows the stress-strain curves of other composites. The stress-strain curves of the composites showed the combination behaviors of hard but brittle pattern CS and viscoelastic pattern PET-*co*-PCL matrices as shown in Fig. 4.13. From stress-strain curve and mechanical testing data, although both compressive strength and modulus values of the composites with high ET content were high, the strain at yield of the composites was low. When adding more CL content in copolymers, the strain at yield would increase, however, both mechanical values would significantly decrease. These results showed that

the composites had more elastic behavior when increasing the CL content because the structure of copolyester in the composites changed from block to alternating polymeric structures as confirmed by ^{1}H-NMR results. In addition, the strain at yield of the neat copolymers increased with the increase of CL content in the neat copolymers.

The compressive strengths of E9C1, E8C2 and E7C3 composites were in the range of compressive strength of the cartilage bone, i.e. 14-59 MPa [107], while, those of E10C0, E6C4 and E5C5 composites related to those of the cancellous bone or sponge bone, i.e. 0.2-13 MPa [108, 109]. These results suggested that these CS/PET-*co*-PCL composites might be used for implantation in various parts.

Table 4.9 concluded the densities of the CS/PET-*co*-PCL composites, the neat PET-*co*-PCL copolymers and the neat CS. The densities of composites were in the range of 0.96-1.63 g/cm^3 which were higher than those of neat copolymers (0.83-1.14 g/cm^3), but the highest density was 1.89 g/cm^3 of pure CS.

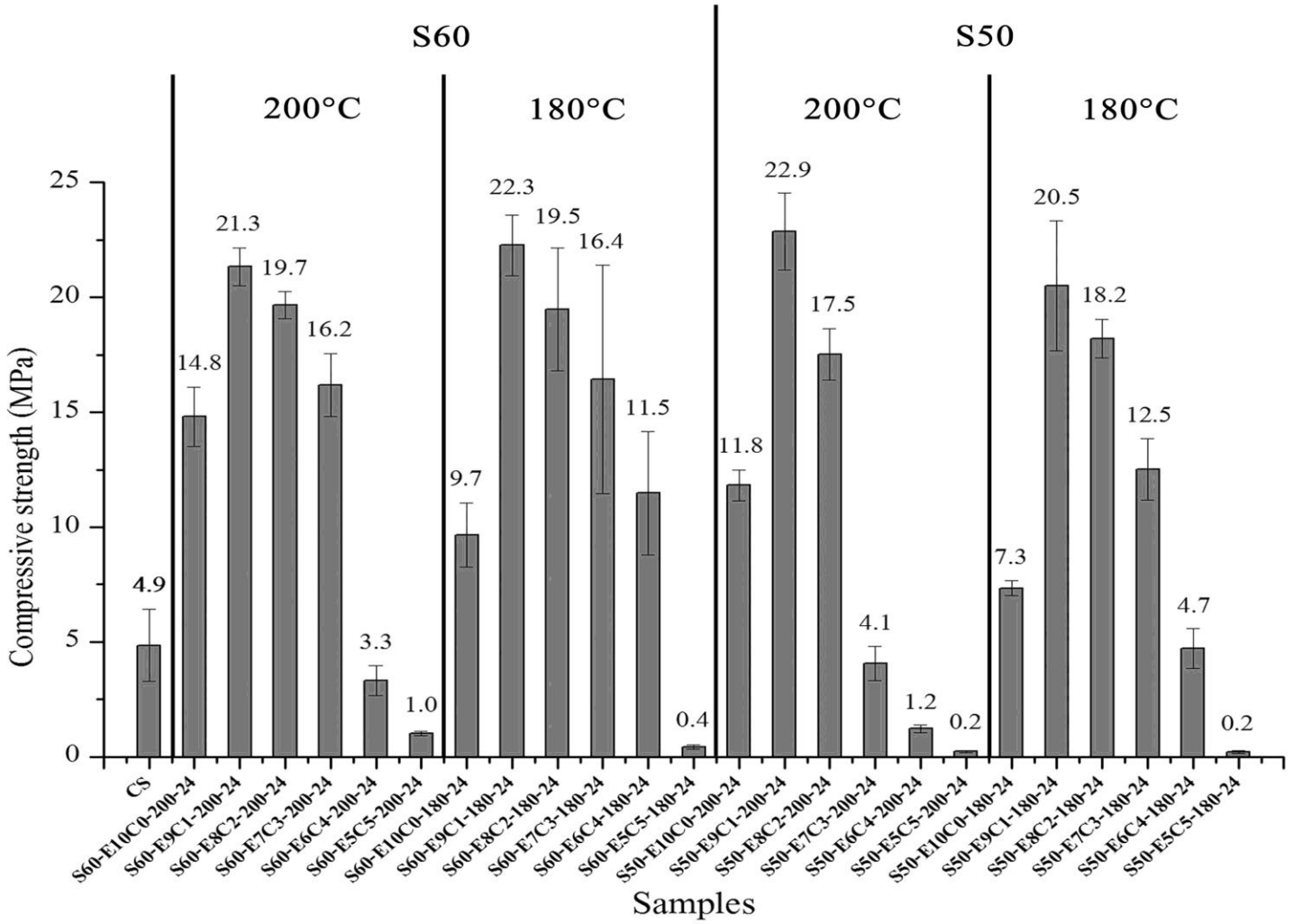

Figure 4.9 Compressive strengths of CS/PET-*co*-PCL composites

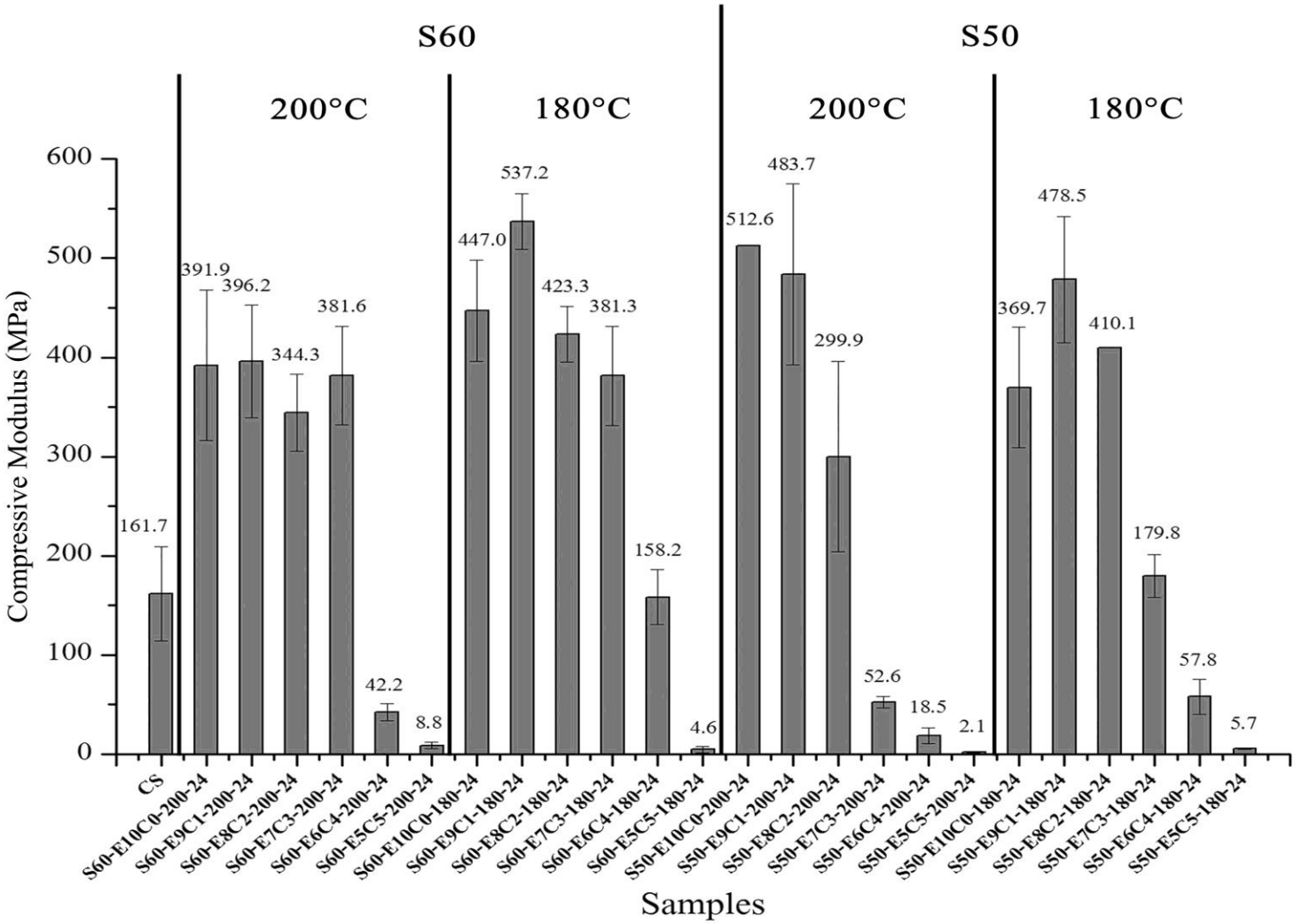

Figure 4.10 Compressive moduli of CS/PET-*co*-PCL composites

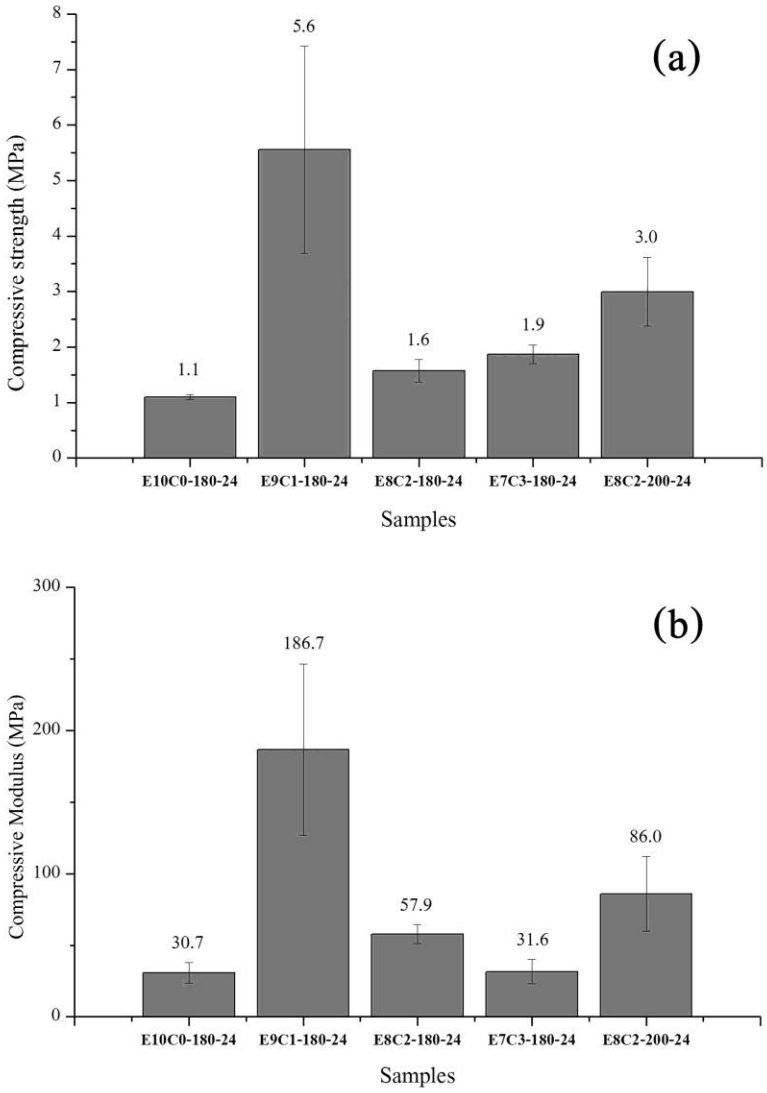

Figure 4.11 Compressive strengths (a) and compressive moduli (b) of virgin PET-*co*-PCL copolymers

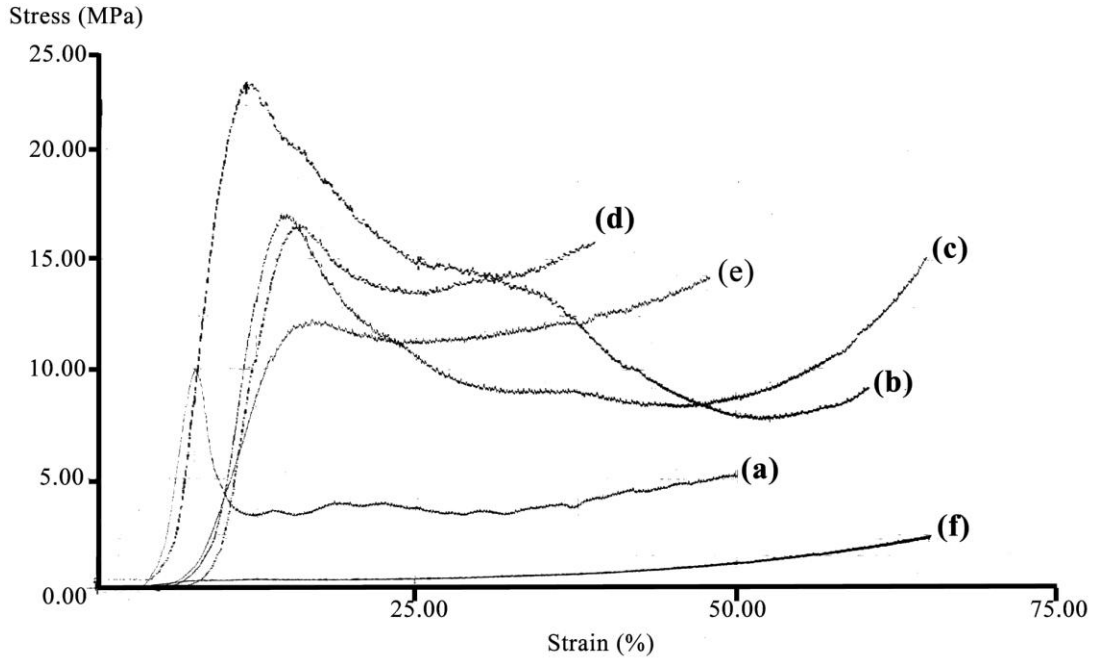

Figure 4.12 Stress-strain curves of CS/PET-*co*-PCL composites with 60 %wt CS containing 100:0 (a), 90:10 (b), 80:20 (c), 70:30 (d), 60:40 (e), 50:50 (f) of C-OET:CL molar ratios at 180 °C ROP temperature for 24 hr

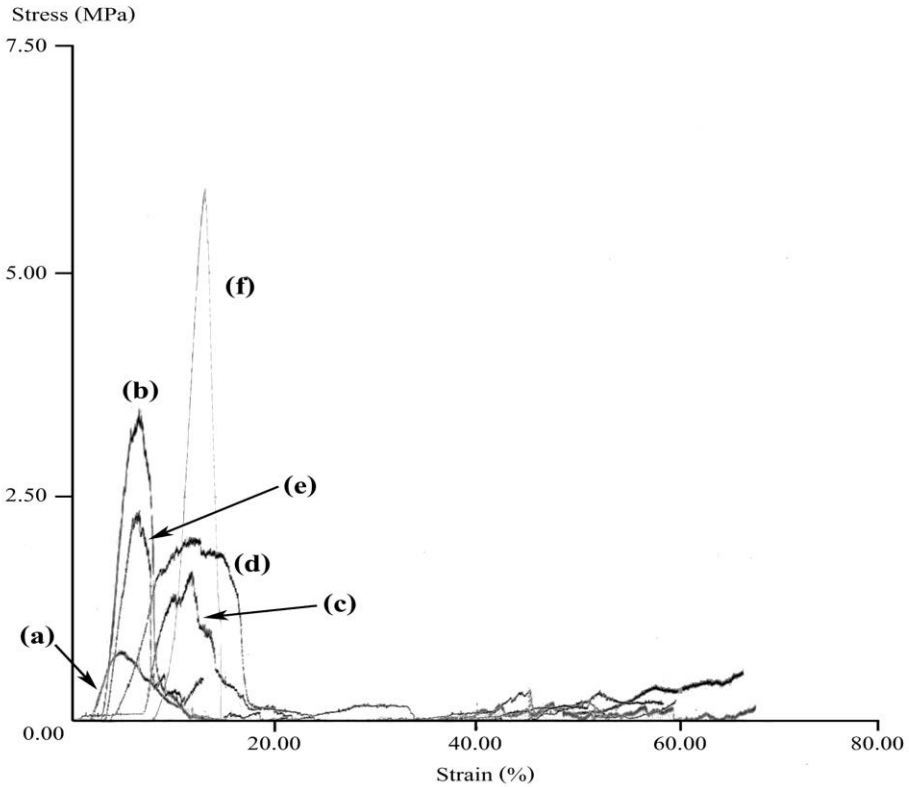

Figure 4.13 Stress-strain curves of E10C0-180-24 (a), E9C1-180-24 (b), E8C2-180-24 (c), E7C3-180-24 (d), E8C2-200-24 (e) copolymers and CS (f)

Table 4.9 Density of CS/PET-*co*-PCL composites, neat PET-*co*-PCL copolymers and CS

Sample	Density (g/cm^3)
S50-E10C0-180-24	1.28
S50-E9C1-180-24	1.41
S50-E8C2-180-24	1.48
S50-E7C3-180-24	1.58
S50-E6C4-180-24	1.50
S50-E5C5-180-24	1.10
S50-E10C0-200-24	1.25
S50-E9C1-200-24	1.58
S50-E8C2-200-24	1.57
S50-E7C3-200-24	1.39
S50-E6C4-200-24	1.23
S50-E5C5-200-24	0.96
S60-E10C0-180-24	1.40
S60-E9C1-180-24	1.53
S60-E8C2-180-24	1.54
S60-E7C3-180-24	1.58
S60-E6C4-180-24	1.68
S60-E5C5-180-24	1.17
S60-E10C0-200-24	1.47
S60-E9C1-200-24	1.56
S60-E8C2-200-24	1.60
S60-E7C3-200-24	1.63
S60-E6C4-200-24	1.31
S60-E5C5-200-24	1.25

Table 4.9 (cont.)

Sample	Density (g/cm^3)
E10C0-180-24	0.83
E9C1-180-24	1.14
E8C2-180-24	0.97
E7C3-180-24	0.90
E8C2-200-24	0.92
CS pure	1.89

4.7.2 Dynamic mechanical thermal analyser (DMTA)

Viscoelastic behaviors of ROP-PET-co-PCL in the neat copolymers and composites were determined from the DMTA data as shown in Fig. 4.14 and 4.15, respectively. The dynamic storage modulus (E') was used to predict the load bearing capability of the PET-*co*-PCL copolymers and CS/PET-*co*-PCL composites. The DMTA was performed on the neat copolymers containing 70-100 %mol of ET prepared at ROP temperature of 180 and 200 °C for 24 hr because the other could not be appropriately shaped for DMTA test. The E' of all copolymers steeply decreased when passing through the relaxation temperature due to the phase transition of amorphous region in the copolymers. The glass transition temperature (T_g) of copolymers was determined from the half-height of the reduction of E' as concluded in Table 4.10. The T_g values of copolymers were in the range of 45-99 °C, in which they were in agreement with the DSC results. The T_g values decreased with the presence of CL content which is the low T_g part in the copolymers chains. However, the increases of CL content and ROP temperature have less or no effect on the T_g values.

Comparing with the neat copolymers, the incorporation of CS particles in the ROP-PET-*co*-PCL copolymers enhanced stiffness and heat-transfer resistance of the composites as shown in Fig. 4.15 and Appendix F. The storage modulus was almost constant throughout the whole range of measuring temperatures for the S50 and S60 composites especially when the ET content was $\geq$ 70 %mol. In case of the composites with 50 and 60 %mol of ET, the E' value sharply decreased at the T_g due to the more co-polymerization between C-OET and CL to PET-*co*-PCL copolymers in the composites. In addition, the polymeric structures in the composites changed from the block or random copolymer structures to the alternating structure as previously discussed in ^{1}H-NMR. The ET segment containing the aromatic ring in the main chain increased the rigidity and thermal stability of the ROP-PET-co-PCL matrix. Therefore, the stiffness of the composites with 50 and 60 %mol ET was lower than that of the higher ET content composites at the same amount of CS particles. In addition, the E' value of the composites with 50 %wt CS dropped more than of the composites with 60 %wt CS. These results indicated the high stiffness of the CS/PET-co-PCL composites, in which they were considered to be due to the presence of higher CS content in the composites. The CS particles were high strength and stiffness part; therefore, the mobility and deformability of the ROP-PET-co-PCL matrix in the composites would be reduced. In addition, the mobility of polymer chains

was also confined due to the interfacial bonding between ROP-PET-co-PCL matrix and CS particles. The effect of ROP temperature did not clearly effect on the stiffness of the CS/PET-*co*-PCL composites.

The storage moduli of the composites with 50 and 60 %mol of ET at low temperature were higher than of the composites with PET content higher than 60 %mol because the porous defects in the composites with 50 and 60 %mol of ET formed during shaping.

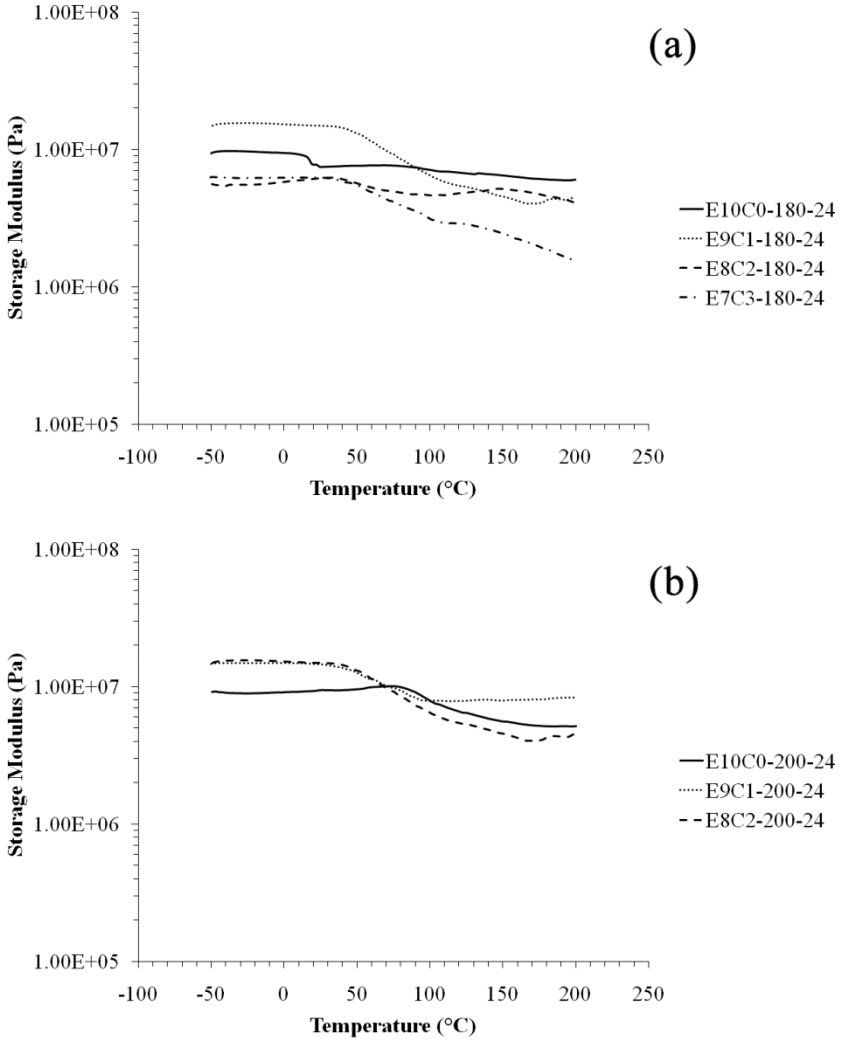

Figure 4.14 Storage moduli (E′)of neat PET-*co*-PCL copolymers prepared at ROP temperature of 180 °C (a) and 200 °C (b) for 24 hr

Table 4.10 T_g of neat copolymers determined from loss modulus peak

Sample	T_g (°C) at loss modulus peak
E10C0-180-24	95.0
E9C1-180-24	59.1
E8C2-180-24	44.6
E7C3-180-24	57.4
E10C0-200-24	99.0
E9C1-200-24	55.6
E8C2-200-24	59.1

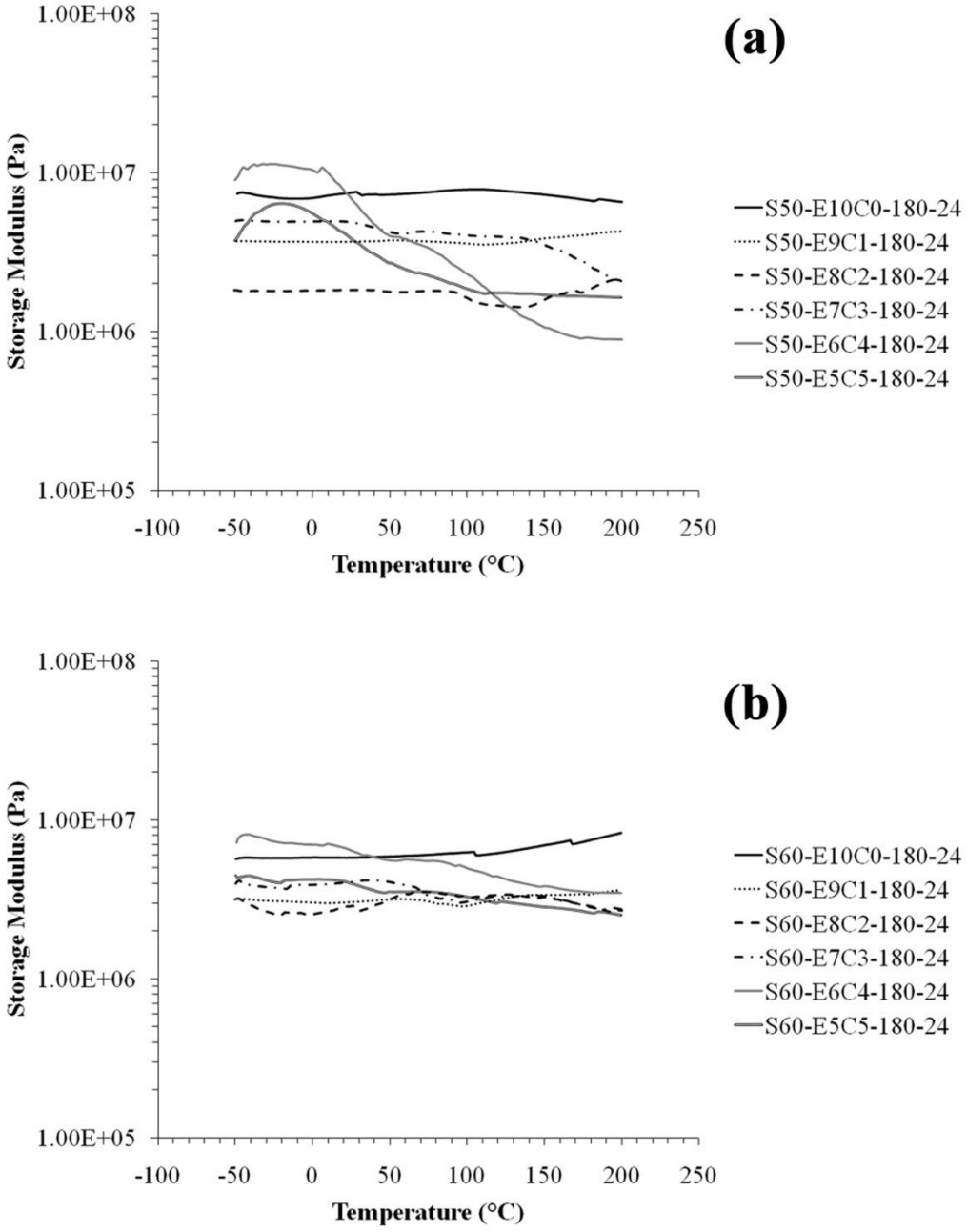

Figure 4.15 Storage moduli (E') of CS/PET-*co*-PCL composites containing 50 %wt copolymers (a) and 40 %wt copolymers (b) (ROP temperature as 180 °C for 24 hr)

4.8 Reprocessibility of CS/PET-*co*-PCL composites

The CS/PET-*co*-PCL composites were reshaped and annealed at 150 °C for 1 hr. The crystalline phase and thermal properties of the annealed composites were investigated in order to determine the reprocessibility of the CS composites.

Figure 4.16 and Appendix G show the XRD patterns of the CS/PET-*co*-PCL composites before and after annealing at 150 °C for 1 hr. It can be seen that the annealed composites mainly composed of the CS and ET diffraction peaks as same as the composites before annealing, including trace of broad halo peak of amorphous part in the copolymer matrices. In the same manner as the composites before annealing, the ACS of ET and CS in the annealed composites were calculated using eq.(4.14) with the crystalline peaks at 2θ = 25.5° and 29.9°, respectively. The ACS of CS and ET in the composites after annealing were quite similar to those in the composites before annealing. The ACS of CS and ET ranged from 32-41 and 28-46 nm, respectively, as shown in Appendix G. These results indicated that the composites could be reprocessed without significant change in the crystallite size of both CS and ET phases. After annealing, the crystallite size of the ET in some composites such as S60-E9C1-200-24, S60-E8C2-180-24 and S50-E9C1-200-24 could be calculated. In addition, when the ET content in the composites after annealing was 70 %mol, the small XRD peak of crystalline PET was also observed as shown in Fig. 4.16 (f) and Appendix G. However, the peak width (β value) could not be clearly resolved for calculation of PET crystallite size. These results were considered that the crystallinity of ET part increased after annealing. Furthermore, the composites with the molar ratio of 50:50 and 60:40, the crystallinity of ET would absolutely disappear after annealing.

Table 4.11 shows the thermal properties of CS/PET-*co*-PCL composites with 60 %wt CS ROP at 200 °C ROP temperature for 24 hr before and after annealing and of the other composites were showed in Appendix D. The T_g of the ROP-PET-*co*-PCL in the CS/PET-*co*-PCL composites before and after annealing varied in the range of 20-88 °C. The T_g of the after-annealed composites exhibited the trend as same as this of before-annealed composites which was the T_g values decreased when the ET content in the composites decreased. It indicated that annealing treatment did not affect to T_g values.

Figure 4.17 and Appendix D show the first heating DSC thermograms of the as-prepared CS/PET-*co*-PCL composites before annealing. The melting peaks (T_m) at around 100 ºC were observed in the E5C5, E6C4 and E7C3 composites before annealing, corresponding to the fusion of CL crystallites in the composites. [110] It was noted that the CL phase was immiscible with the ET phase in the ROP-PET-*co*-PCL copolyesters. The T_m and its peak area increased with increasing the CL contents in the composites. However, the T_m peak was not observed in the composites after annealing. These results were considered to be because the CS filler in the composites could act as nucleating agent, promoting the ring-opening copolymerization between the residual C-OET and CL to form PET-*co*-PCL in the annealed composites. After annealing at 150 ºC for 1 hr, there were two T_m and ΔH_m in the the E7C3, E8C2 and E9C1 composites as shown in the DSC thermograms of the 1st heating in Fig. 4.18 and Appendix D. The peak at lower temperature pertained to the fusion of crystallites formed during annealing process and the second one might be the fusion of recrystallized crystals during DSC scan. [110] These results suggested that the PET-*co*-PCL copolyesters in the composites could further crystallize at the annealing temperature. The values of lower T_m and its peak area decreased when increasing the PCL content in the composites. These two T_m peaks merged to a single peak in the 2nd DSC heating as shown in Table 4.11 and Appendix D. Besides, the T_m of the annealed composites with 50 and 60 %mol PET disappeared because the high amount of amorphous PCL in these composites could impede the crystallization during annealing process. Furthermore, the E10C0 composites showed only a single T_m peak in both composites before and after annealing.

The T_c of ET phase in the composites after annealing had the similar values and trend to the composites before annealing. Nevertheless, the ΔH_c of the CS/PET-*co*-PCL composites increased when the composites were annealed, indicating that the increase of crystalline ET in the annealed CS/PET-*co*-PCL composites because the CS filler could act as nucleating agent for ET crystallization.

In addition, the transition temperature and the enthalpy of melting of ROP-PET-*co*-PCL in the CS/PET-*co*-PCL composites did not change after annealing at 150 °C and the glass transition temperatures approached the room temperature (25 °C) with increase of PCL content, suggesting the thermoplastic elastomer behavior of ROP-PET-*co*-PCL in the CS/PET-*co*-PCL composites which could be reprocessible at 150 °C.

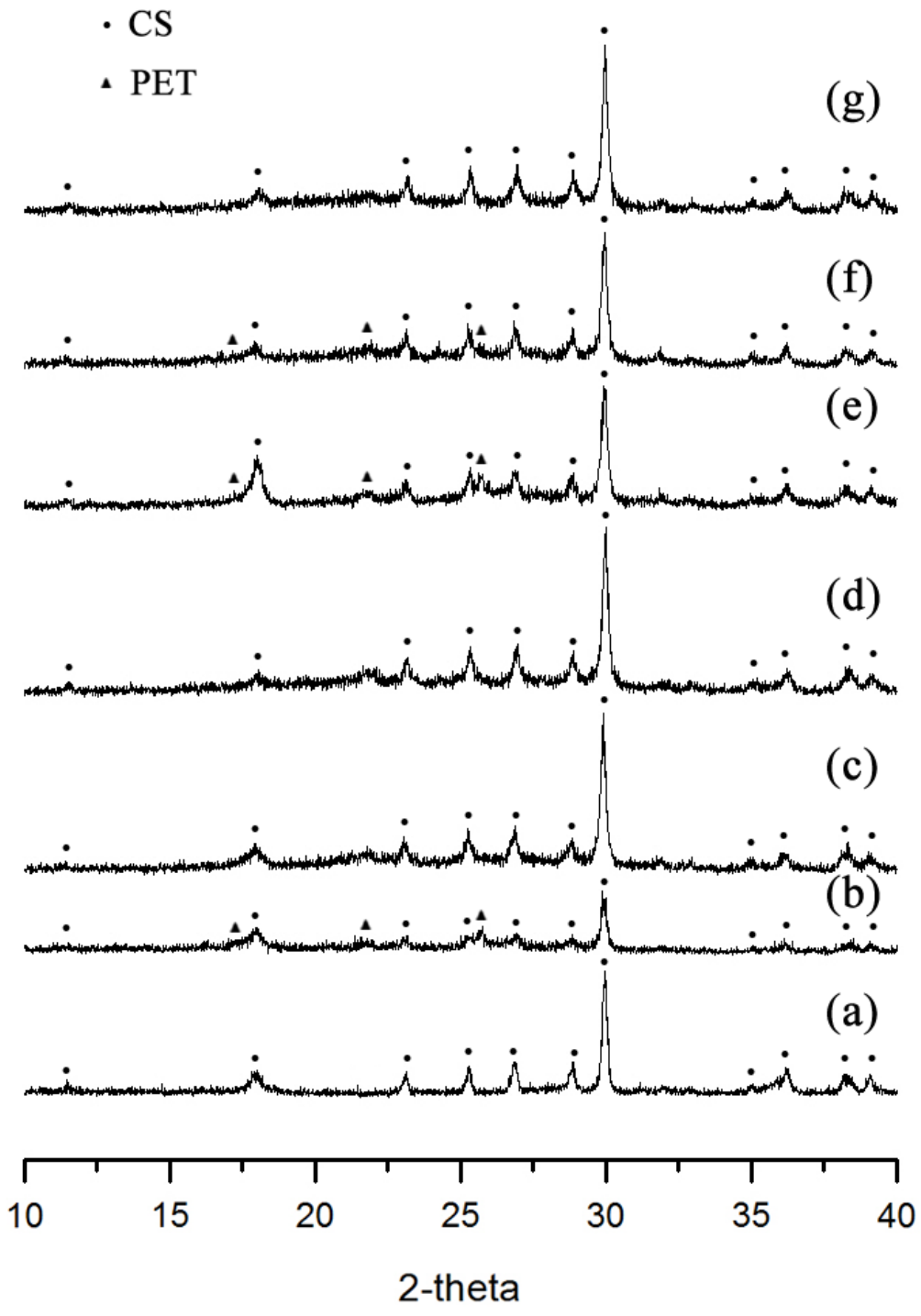

Figure 4.16 XRD patterns of (a) CS, composites before annealing with (b) S60-E10C0-200-24, (c) S60-E7C3-200-24, (d) S50-E5C5-200-24 and after annealing with (e) S60-E10C0-200-24, (f) S60-E7C3-200-24, (g) S60-E5C5-200-24

Table 4.11 Thermal properties of CS/PET-*co*-PCL composites before and after annealing

Sample	Before annealing							After annealing						
	T_g (°C)	First heating		Second heating		T_c (°C)	ΔH_c (J/g)	T_g (°C)	First heating		Second heating		T_c (°C)	ΔH_c (J/g)
		T_m (°C)	ΔH_m (J/g)	T_m (°C)	ΔH_m (J/g)				T_m (°C)	ΔH_m (J/g)	T_m (°C)	ΔH_m (J/g)		
S60-E10C0-200-24	81.5	240.7	31.9	242.7	18.7	197.1	32.2	82.1	248.6	37.7	245.2	30.0	188.7	46.0
S60-E9C1-200-24	73.3	241.6	21.5	228.7	18.5	183.0	25.3	71.1	176.4 249.8	3.1 30.9	230.5	21.2	188.5	39.9
S60-E8C2-200-24	71.1	190.7 236.0	4.7 4.7	221.3	11.7	170.2	22.4	67.7	174.3 238.6	12.1 3.6	219.3	17.9	157.9	19.3
S60-E7C3-200-24	65.8	182.9	3.2	202.5	9.1	142.7	8.4	64.8	174.3	13.5	217.2	13.0	143.3	18.4
S60-E6C4-200-24	60.8	n/a	n/a	n/a	n/a	n/a	n/a	56.1	166.4	2.4	n/a	n/a	n/a	n/a
S60-E5C5-200-24	38.5	n/a	n/a	n/a	n/a	n/a	n/a	41.7	n/a	n/a	n/a	n/a	n/a	n/a

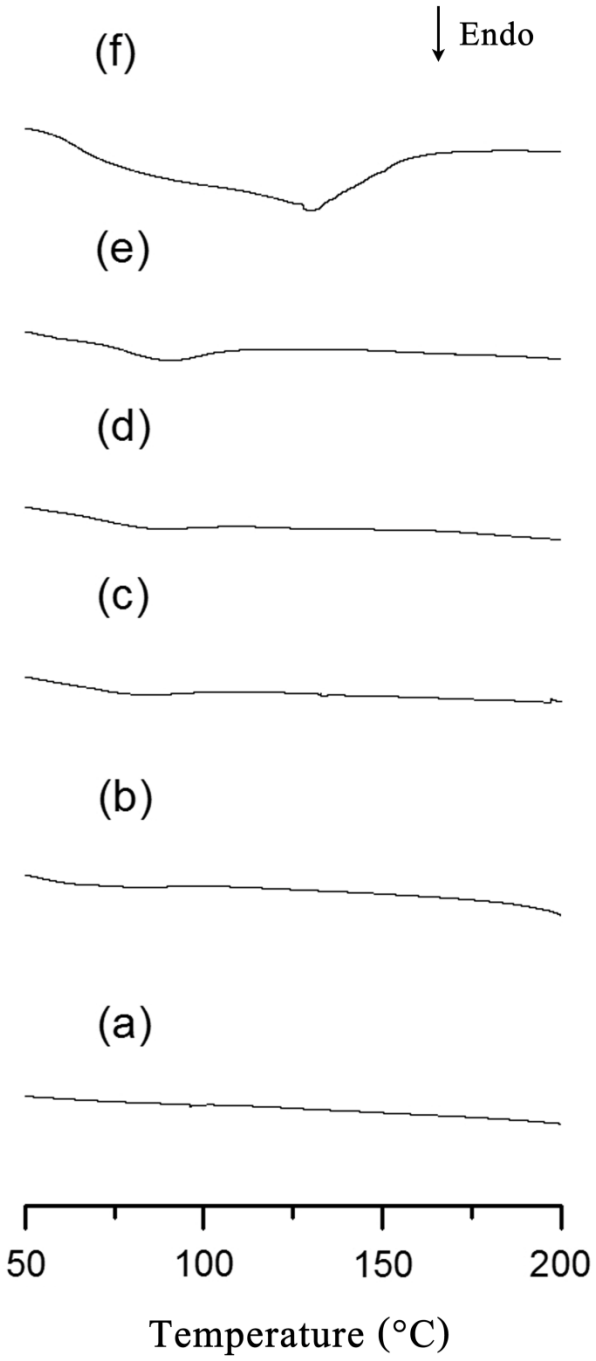

Figure 4.17 DSC thermograms of S50-E10C0-180-24 (a), S50-E9C1-180-24 (b), S50-E8C2-180-24 (c), S50-E7C3-180-24 (d), S50-E6C4-180-24 (e) and S50-E5C5-180-24 (f) composites before annealing (1st heating)

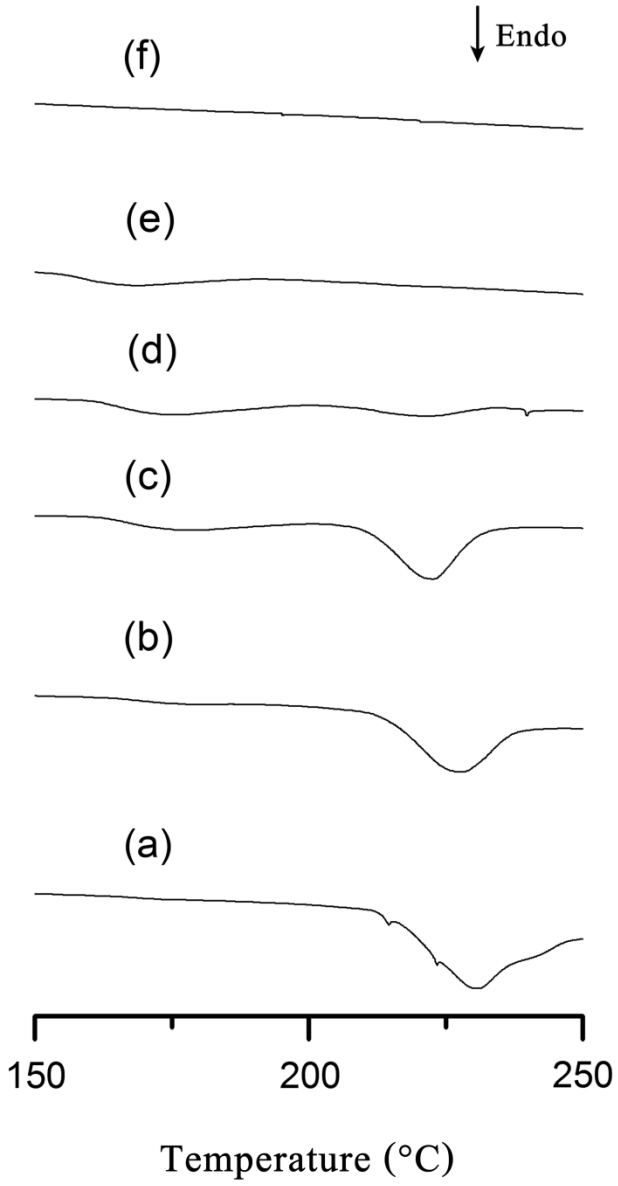

Figure 4.18 DSC thermograms of S50-E10C0-180-24 (a), S50-E9C1-180-24 (b), S50-E8C2-180-24 (c), S50-E7C3-180-24 (d), S50-E6C4-180-24 (e) and S50-E5C5-180-24 (f) composites after annealing (1st heating)

4.9 Bioactive and biodegradable properties of PET-*co*-PCL copolymers and CS/PET-*co*-PCL composites

4.9.1 Bioactivity

After soaking in the SBF for 7-28 days, the surfaces of CS/PET-*co*-PCL composites were completely covered with the newly formed layer of needle-like nanocrystals when the ET content of PET-*co*-PCL copolymers in the composites was 60, 70, 80, 90 and 100 %mol ROP at both 180 and 200 °C as shown in Fig. 4.19 and Appendix E. As the CS content changed from 50 to 60 %wt, it did not clearly showed the different nanocrystals formation. This might be because the CS content in both compositions was adequately high to induce the nanocrystals formation in the same behavior. The formed nanocrystals completely covered on the CS/PET-*co*-PCL composites' surfaces since the first 7 days of SBF soaking. It suggested that the nanocrystals formation might involve with the CS particles in the CS/PET-co-PCL composites.

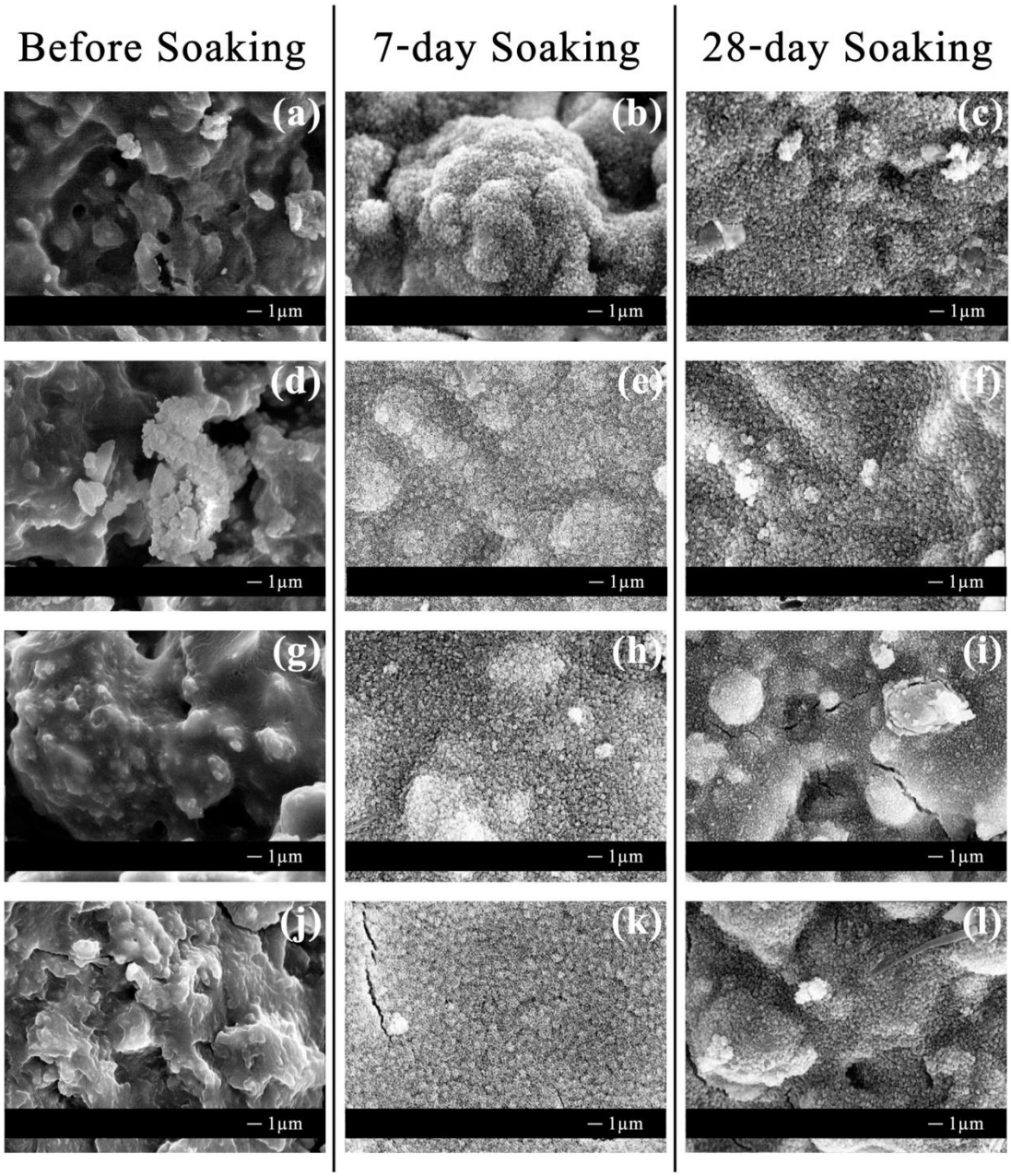

Figure 4.19 SEM micrographs of composites before and after soaking for 7 and 28 days;

(a), (b), (c) S50-E10C0-200-24 composite

(d), (e), (f) S50-E9C1-200-24 composite

(g), (h), (i) S50-E8C2-200-24 composite

(j), (k), (l) S50-E7C3-200-24 composite

Since the high quantities of bioinert copolymers (50 %wt) loaded in the S50-E5C5-180-24, S50-E5C5-200-24 and S50-E6C4-200-24 composites, the nanocrystals was not observed on the composites' surface even after prolonged soaking time period as shown in Fig. 4.20 (a)-(c) and Appendix E. It was because the PET-*co*-PCL copolymer layer totally concealed the composites' surface as confirmed with the SEM; therefore, the nanocrystals formation was obstructed. However, it was observed that the composites' surface became porous surfaces after prolonged soaking due to the dissolution and/or degradation of the PET-*co*-PCL matrices in the SBF solution, indicating that the E5C5 and E6C4 copolymers could be easily hydrolyzed in SBF solution.

Figure 4.20 (e) shows the porous surface on the S60-E5C5-200-24 composites, indicating the degradation of copolymers matrices. The S60-E5C5-180-24 and S60-E5C5-200-24 composites required soaking shorter time for the nanocrystals formation as it can be observed the continuous nanocrystals layer on the surface of the 14-day SBF soaked samples (Fig. 4.20 (f)). These results can be concluded that the higher CS content in the composites, the faster nanocrystals formation on the surface was obtained.

It was noted that the change in ROP temperature was not clearly affected to the nanocrystals formation on all composites as shown in Appendix E.

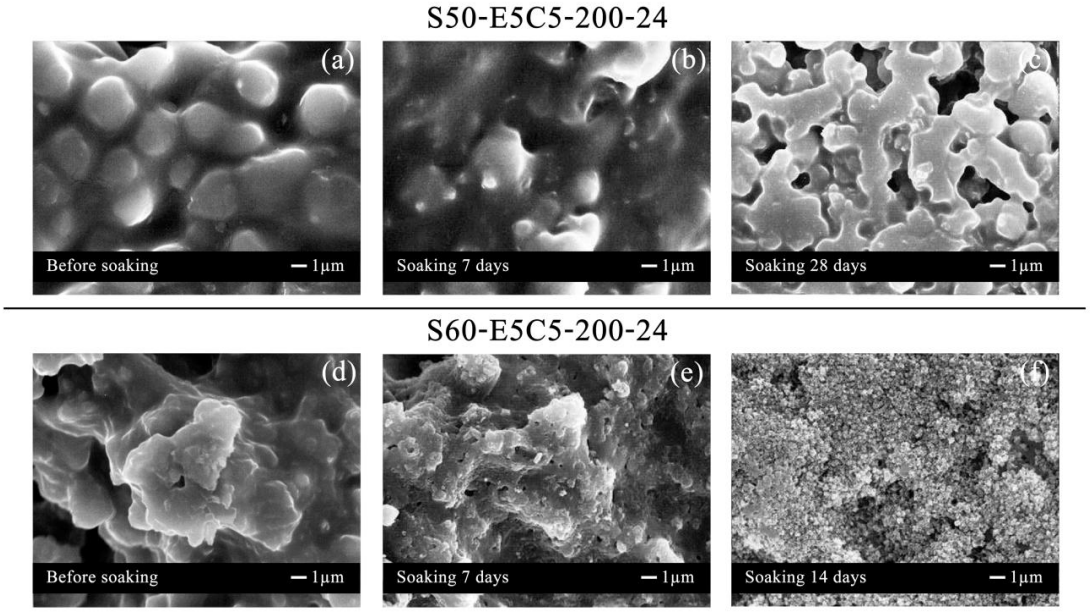

Figure 4.20 SEM micrographs of S50-E5C5-200-24 composite before (a) and after soaking in SBF for 7 days (b), 28 days (c) and of S60-E5C5-200-24 composite before (d) and after soaking in SBF for 7 days (e), 14 days (f)

To confirm the ability of CS to induce the nanocrystals formation on the surfaces of composites, the bioactivity of neat PET-*co*-PCL copolymers was tested in the same manner with the composites. The result showed that the neat copolymers were observed as the flat surface without the formation of nanocrystals particles even after soaking in SBF for 28 days as shown in Fig. 4.21 and Appendix E. This result indicated that the neat copolymers were bioinert materials; therefore, they could not induce the formation of nanocrystals particle in SBF solution. However, the porous surfaces were also observed in all neat copolymers, indicating that the degradation of copolymers in SBF.

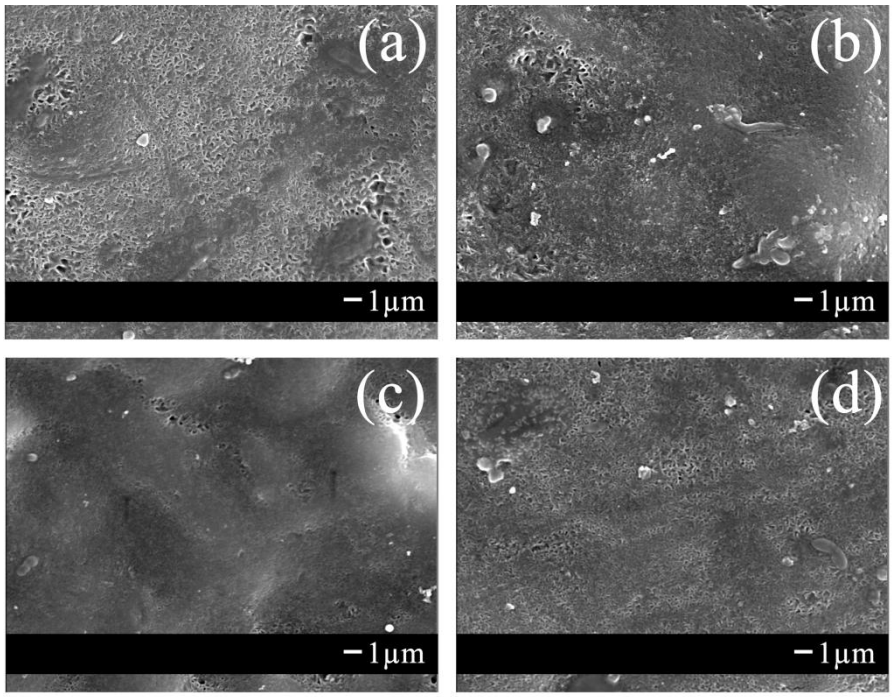

Figure 4.21 SEM micrographs of neat (a) E9C1-180-24, (b) E8C2-180-24, (c) E7C3-180-24 and (d) E9C1-200-24 copolymers after 28-day SBF soaking

EDS spectrum of the S50-E8C2-200-24 composites after soaking in SBF solution for 28 days is showed in Fig. 4.22. When considering the EDS spectrum, it can be seen the strong peaks of Ca, Si and P. The Ca signal was considered to be the signal from 2 main sources, i.e. the CS particles in the composite substrate and the nanocrystals newly formed layer which may be phosphate-compounds. It was, however, the Si signal from the CS particle was still observed together with the P signal from the phosphate-compounds layer. This result could insist the formation of phosphate-compounds layer on the CS/PET-*co*-PCL composites. The mechanism of phosphate-compounds formation mainly involved with the reaction between CS particles on the surfaces of CS/PET-*co*-PCL composites and inorganic ions in the SBF solution. Since the starting pH of SBF was 7.4, it could therefore induce the dissolution of CS particles embedded on the surfaces of CS/PET-*co*-PCL composites. The releasing of calcium and silicon ions resulted in the increase of pH of SBF solution to ~8, promoting the precipitation of phosphate-compounds through the consumption of Ca^{2+}, PO_4^{3-} and OH^- ions from the SBF solution.

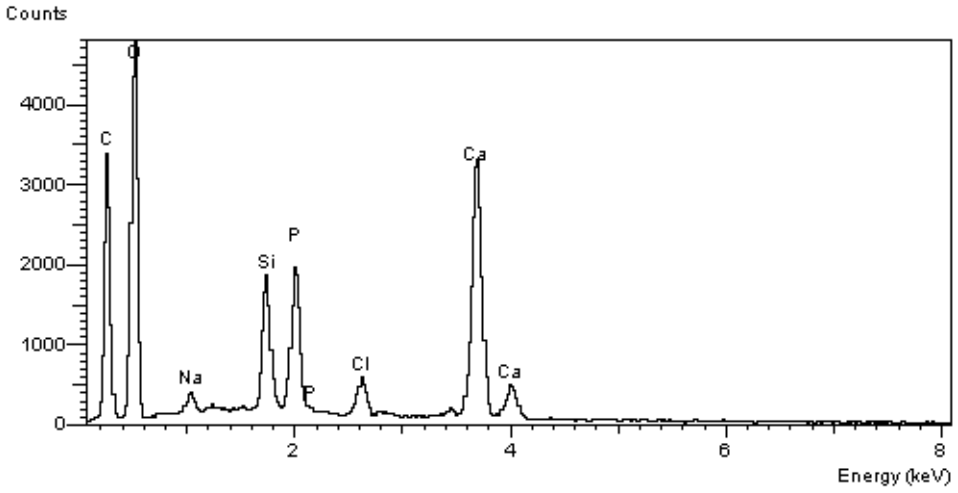

Figure 4.22 EDS spectrum of S50-E8C2-200-24 after 28-day SBF soaking

Figure 4.23 and Appendix G show the XRD patterns of the neat CS and composites before and after soaking in SBF. Both composites before and after soaking mainly consisted with the CS diffraction peaks. However, the CS peaks of composite after SBF soaking were broadened in comparison with the peaks of composite before soaking, indicating the change of well-crystalled CS after SBF soaking. However, the crystalline peaks of phosphate-compounds nanocrystals were not observed in the XRD patterns of composite after SBF soaking. These results were considered to be due to the trace amount of phosphate-compounds layer was obtained; therefore, it cannot conceal the CS signal from the composites substrates. It could not exactly conclude the type of phosphate-compound and other characterization should be used for finding the type of phosphate-compound.

The results of SEM, EDS and XRD characterizations indicated the bioactivity of CS/PET-*co*-PCL composites and the bioinert of the neat PET-*co*-PCL copolymers.

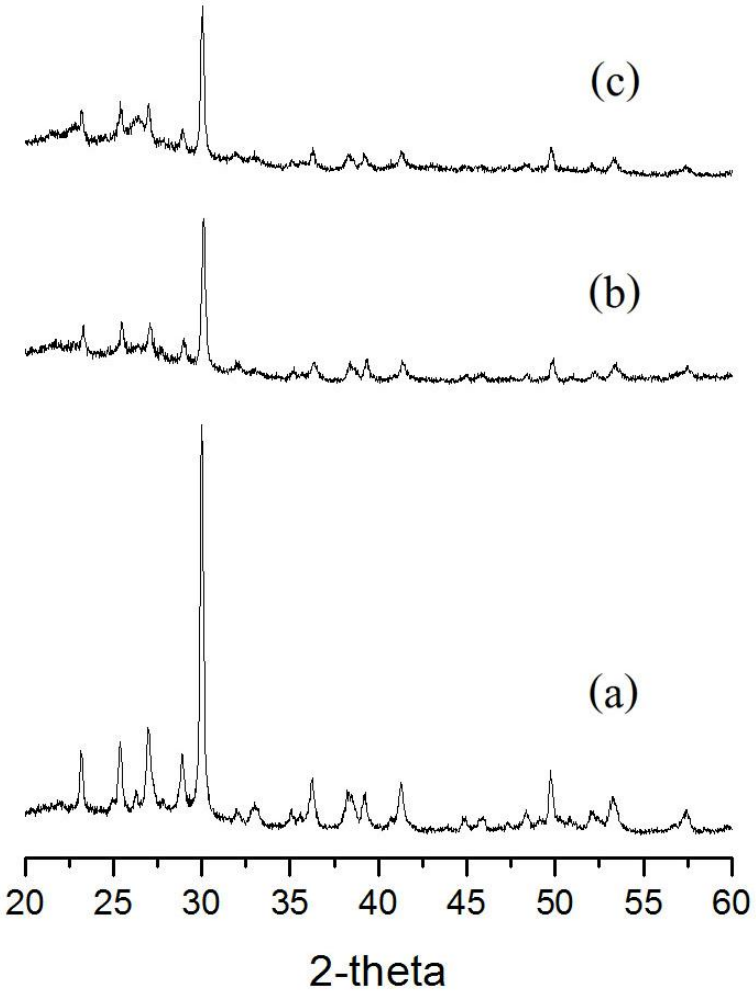

Figure 4.23 XRD patterns of CS (a), S50-E8C2-200-24 before (b) and after (c) 28-day SBF soaking

4.9.2 Biodegradability

Figure 4.24 (a) shows the %weight loss of the neat PET-*co*-PCL copolymers and CS/PET-*co*-PCL composites after soaking in 5 %v/v H_2O_2 solution for 28 days. The %weight losses in the H_2O_2 solution of the neat copolyesters and the composites ring-opening polymerized at 180 °C were quite constant with varying the C-OET:CL molar ratios. The %weight loss values were lower than 5 % for 28-day H_2O_2 soaking, indicating the copolymers in both neat copolymers and composites slightly degraded in the H_2O_2 solution. Furthermore, the CS particles in the composites also degraded in this solution due to the acidity of solution. The SEM micrographs of E9C1-180-24 copolymer and S50-E5C5-180-24 composite before and after soaking in H_2O_2 solution for 28 days could confirm the degradation of copolymers and CS in this solution as shown in Fig. 4.25 (a)-4.25 (d). The SEM micrographs of the other neat copolymers and composites are shown in Appendix E. The surfaces of the copolymers and composites after H_2O_2-soaking were smoother than before soaking, while the composites also showed more porous surface after soaking in H_2O_2 solution. In the case of ROP at 200 °C, all samples showed similar trend of degradation in H_2O_2 solution as the 180 °C-ROP neat copolymers and composites. These results suggested that the varying in the ROP temperatures, C-OET:CL molar ratio and CS quantity did not clearly affect to the degradation of both copolymers and composites in the H_2O_2 solution.

The biodegradations of the neat PET-*co*-PCL copolymers and CS/PET-*co*-PCL composites ROP at 180 and 200 °C in PBS solution after soaking for 28 days were investigated as shown in Fig. 4.24 (b). It was found that the %weight loss of the neat copolymers in PBS was similar to those in H_2O_2. The change of the PET content in the PET-*co*-PCL copolymers unaffected to the %weight loss of copolymers in the PBS solution, in which the %weight losses were lower than 5 % after 28-day soaking. The SEM micrographs of the neat copolymers before and after soaking in PBS are showed in Fig. 4.25 (e), 4.25 (f) and Appendix E. The surface of PBS-soaked copolymer was observed as porous morphology. On the other hand, the CS/PET-*co*-PCL composites showed the increase of composites' weight after soaking in the PBS solution, indicating that the formation of new compounds on the surfaces of composites. The SEM micrographs of the composites before and after soaking in PBS are showed in Fig. 4.25 (g)-4.25 (j) and Appendix E. The newly formed particles were observed on the composites' surfaces, corresponding with the increase of weight. The newly

formed particles were considered to be the phosphate-compounds such as hydroxyapatite (HAp) because the phosphate ion in the PBS solution could react with the CS particles in the composites as similar to the nanocrystals formation in SBF soaking.

However, the short soaking time in both H_2O_2 and PBS solutions was not enough to induce the biodegradation of PET-*co*-PCL copolymers in the neat copolymers and the composites because the copolyesters contained the bioinert PET together with the biodegrade PCL, then they took longer time than other biodegraded polyesters such as PLLA. [5, 19]

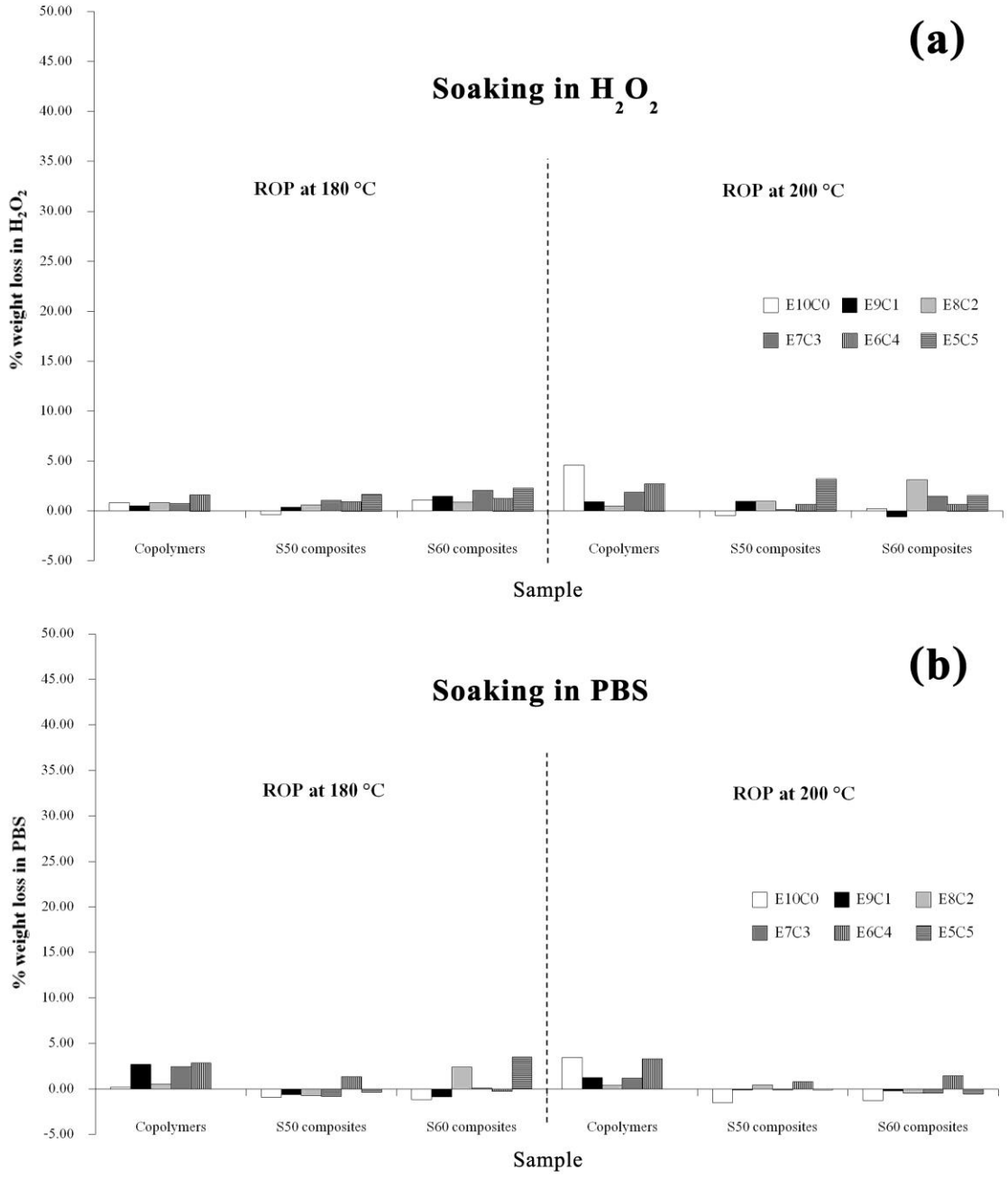

Figure 4.24 Weight loss percentage of neat PET-*co*-PCL copolymers and CS/PET-*co*-PCL composites ROP at 180 and 200 °C after soaking in H_2O_2 (a) and PBS (b) for 28 days

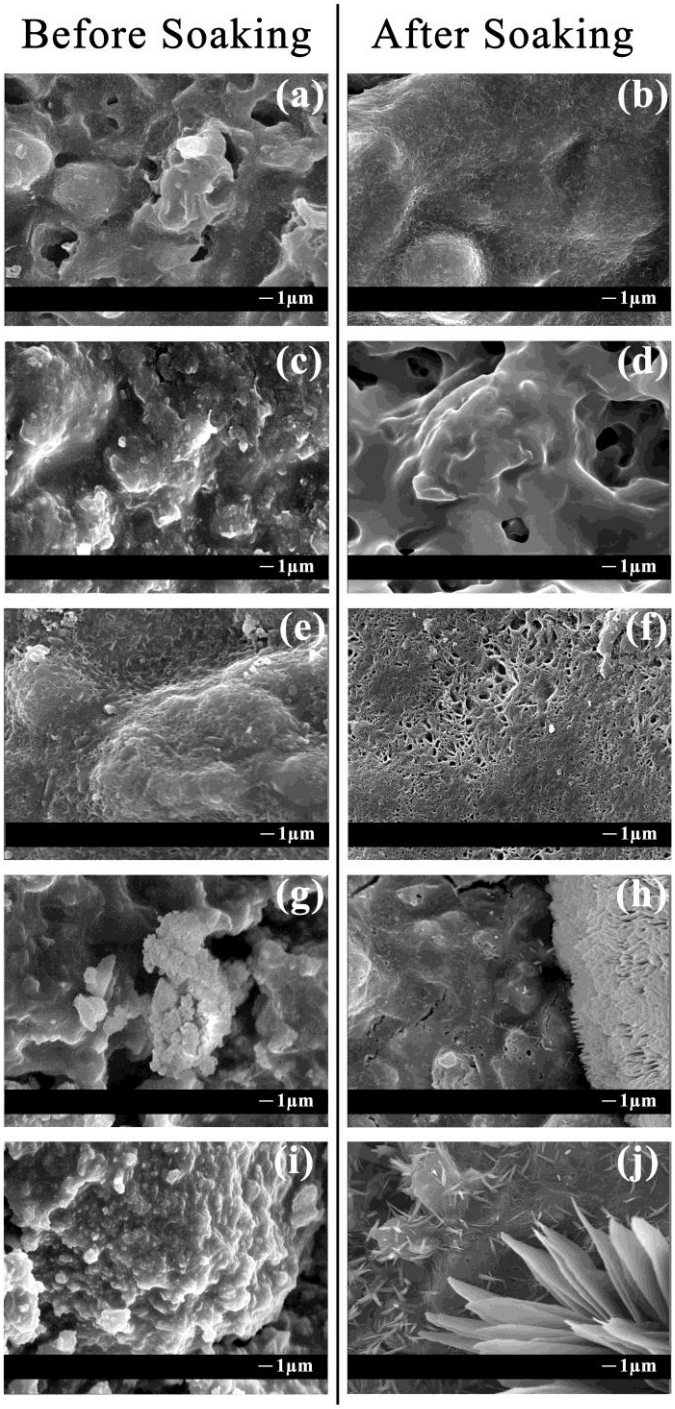

Figure 4.25 SEM micrographs of E9C1-180-24 copolymer ((a) and (b)), S50-E5C5-180-24 composite ((c) and (d)) before and after soaking in 5 %v/v H_2O_2 solution for 28 days, E9C1-200-24 copolymers ((e) and (f)), S50-E9C1-200-24 ((g) and (h)) and S60-E9C1-200-24 ((i) and (j)) before and after soaking in PBS for 28 days

4.10 Cytotoxicity of CS/PET-*co*-PCL composites

The cytotoxic assay of the CS/PET-*co*-PCL composites to the African green monkey kidney fibroblast with the aid of MTT assay as determined by the IC_{50} was tested. The chosen composites for cytotoxic test were S60-E5C5-180-24, S50-E7C3-180-24, S50-E7C3-200-24, S60-E7C3-180-24, S60-E7C3-200-24 and S60-E9C1-180-24 composites. It was found that the IC_{50} values of the composites were greater than 1000 μg/ml, indicating that the half cells content would be inhibited when the concentration of the compounds released from the CS/PET-*co*-PCL composites was higher than 1000 μg/ml. These results suggested that the CS/PET-*co*-PCL composites had the potentially non-toxic to cell.

Chapter 5

Conclusion and Recommendation

5.1 Conclusion

The neat poly(ethylene terephthalate-*co*-caprolactone) (PET-*co*-PCL) copolymers and the calcium silicate/poly(ethylene terephthalate-*co*-caprolactone) (CS/PET-*co*-PCL) composites were successfully synthesized *via in situ* ring-opening polymerization of cyclic oligo(ethylene terephthalate) (C-OET) and ε-caprolactone (CL) at 180, 200, 230 and 250 °C for 8 and 24 hr. The C-OET:CL molar ratio played the most important role in the polymeric structural arrangement and mechanical behaviors of the copolymers and composites. The structure of PET-*co*-PCL in the neat copolymers and composites changed from block to alternating copolymers when the ET content in the neat copolymers and composites was decreased. The compressive strength of the CS/PET-*co*-PCL composites was dramatically higher than of both CS and neat PET-*co*-PCL copolymers. These values decreased when the aliphatic CL units in the composites were increased. Varying of the C-OET:CL ratio in the composites possessed various compressive strength values, in which they might be applied in various human body parts. The composites with relatively high ET content were suitably applied for loading tissue part and the composites with relatively high CL segment were the soft tissue or unloading body part. In addition, the ROP conditions and CS powders partially affected to the morphology of the copolymers and composites. More ring-opening copolymerization between C-OET and CL in the copolymers and composites were investigated when the increment of ROP temperature especially the composites with high CS content.

Furthermore, the composites could be reprocessed at 150 °C for 1 hr with unchanging in the properties but increased the crystallization of PET-*co*-PCL copolymers in the composites suggesting that the composites may be the thermoplastic elastomer.

The CS/PET-*co*-PCL composites showed *in vitro* bioactivity, in which the composites could induce the formation of phosphate-compounds i.e., hydroxyapatite (HAp), etc. on their surface after soaking in SBF solution within 7 days. On the other hand, the neat copolymers could not induce the particles formation even after 28-day soaking in SBF solution, indicating the bioinertness of these copolymers. In addition, the composites were potentially non-toxic materials for cells as their IC_{50} values were greater than 1000 μg/ml. It could be concluded that

the CS/PET-*co*-PCL composites possessed the reasonable physical and mechanical properties and excellent bioactivity, indicating the possibility of these composites as the attractive candidates for medical applications.

5.2 Recommendation

1. The shaping process of CS/PET-*co*-PCL composites into exact size, shape and smooth surface should be improved and scaled up.

2. Other physical and mechanical properties of the CS/PET-*co*-PCL composites such as contact angle, tensile strength and impact strength should be studied in order to predict their tentative medical applications.

3. The bioactivity of the CS/PET-*co*-PCL composites should be tested in the SBF solution for longer soaking period and in flowing SBF system as the simulation of human body.

4. The relationship between biodegradation rate of the CS/PET-*co*-PCL composites and bone-formation rate in the simulated body system should be studied.

5. Other *in vitro* and *in vivo* biological testing of the CS/PET-*co*-PCL composites should be studied, for example, cell biocompatibility, attachment, proliferation, growth, morphology and bone formation.

References

1. D.F. Williams, 1987, **Definitions in Biomaterials. Proceedings of a Consensus Conference of the European Society For Biomaterials**, Elsevier, New York, USA.
2. J. Park and R.S. Lakes, 2007, **Biomaterials An Introduction**, Springer Science and Business Media, New York, USA.
3. V.M. Correlo, L.F. Boesel, M. Bhattacharya, J.F. Mano, N.M. Neves and R.L. Reis, 2005, Properties of melt processed chitosan and aliphatic polyester blends, **Materials Science and Engineering A**, 403, 57–68.
4. D.W. Van Klevelen, 1997, **Properties of polymers**, Elsevier, New York, USA.
5. A. Metzger, 2003, **Polyethylene terephthalate and the Pillar™ Palatal Implant: Its Historical Usage and Durability in Medical Applications**, Restore Medical Incorporated, Minnesota, USA.
6. W. Cao and L.L. Hench, 1996, Bioactive materials, **Ceramics International**, 22, 493-507.
7. W. Bonfield, M.D. Grynpas, A.E. Tully, J. Bowman and J. Abram, 1981, Hydroxyapatite reinforced polyethylene-A mechanically compatible implant material for bone replacement, **Biomaterials**, 2, 185–186.
8. K.H. Rao, K.S.E. Forssberg and W. Forsling, 1998, Interfacial interactions and mechanical properties of mineral filled polymer composites: wollastonite in PMMA polymer matrix, **Colloids Surf A: Physicochem Eng Asp**, 133, 107–117.
9. K. Okada, M. Tanuma, Y. Kameshima, A. Nakajima, S. Asai and M. Sumita, 2009, Bioactivity and mechanical properties of $CaSiO_3$/high-density polyethylene (HDPE) composites prepared by a new surface loading method of $CaSiO_3$ powder, **Materials Research Bulletin**, 44, 298–305.
10. M. Zhang, L. Ye, Y. Gao, X. Lv and J. Chang, 2009, Effects of hydrolysis on dodecyl alcohol modified β-$CaSiO_3$ particles and PDLLA/modified β-$CaSiO_3$ composite films, **Composites Science and Technology**, 69, 2547-2553.
11. R. Bizios, K.C. Dee and D.A. Puleo, 2003, **An introduction to tissue-biomaterial interactions**, John Wiley&Sons, Inc., New Jersey, USA.

12. B.D. Ratner, A.S. Hoffman, F.J. Schoen and J.E. Lemons, 2004, **Biomaterials science: an introduction to materials in medicine**, Elsevier Inc., California, USA.
13. D. Felfman and A. Barbalata, 1996, **Synthetic Polymer**, Chapman and Hall, London, UK.
14. C.E. Carraher, Jr., 2003, **Polymer Chemistry**, Marcel Dekker, Inc., New York, USA.
15. H. Ulrich, 1993, **Introduction to Industrial Polymer**, Hanser Publishers, New York, USA.
16. Y. Li, T. Ma, S.T. Yang and D.A. Kniss, 2001, Thermal compression and characterization of three-dimensional nonwoven PET matrices as tissue engineering scaffolds, **Biomaterials**, 22, 609-618.
17. Z. Ma, M. Kotaki, T. Yong, W. He and S. Ramakrishna, 2005, Surface engineering of electrospun polyethylene terephthalate (PET) nanofibers towards development of a new material for blood vessel engineering, **Biomaterials**, 26, 2527-2536.
18. N. Blanchemain, S. Haulon, B. Martel, M. Traisnel, M. Morcellet and H.F. Hildebrand, 2005, Vascular PET Prostheses Surface Modification with Cyclodextrin Coating: Development of a New Drug Delivery System, **Eur J Vasc Endovasc Surg**, 29, 628-632.
19. G. Mayer, N. Blanchemain, C. Dupas-Bruzek, V. Miri, M. Traisnel, L. Gengembre, D. Derozier and H.F. Hildebrand, 2006, Physico-chemical and biological evaluation of excimer laser irradiated polyethylene terephthalate (pet) surfaces, **Biomaterials**, 27, 553-566.
20. R. Ng, X. Zhang, N. Liu and S.T. Yang, 2009, Modifications of nonwoven polyethylene terephthalate fibrous matrices via NaOH hydrolysis: Effects on pore size, fiber diameter, cell seeding and proliferation, **Process Biochemistry**, 44, 992-998.
21. A. Hadjizadeh, A. Ajji and M.N. Bureau, 2010, Preparation and characterization of NaOH treated micro-fibrous polyethylene terephthalate nonwovens for biomedical application, **Journal of the mechanical behavior of biomedical materials**, 3, 574-583.
22. G. Scott and D. Gilead, 1995, **Degradable Polymers: Principles and applications**, Chapman and Hall, London, UK.
23. L.S. Nair and C.T. Laurencin, 2007, Biodegradable Polymers as Biomaterials, **Process in Polymer Science**, 32, 762-798.

24. W. Schnabel, 1981, **Polymer Degradation: Principles and Practical Applications**, Hanser, Munchen, Germany.
25. H.Y. Kweon, M.K. Yoo, I.K. Park, T.H. Kim, H.C. Lee, H.S. Lee, J.S. Oh, T. Akaike and C.S. Cho, 2003, A novel degradable polycaprolactone networks for tissue engineering, **Biomaterials**, 24, 801-808.
26. J.M. Williams, A. Adewunmi, R.M. Schek, C.L. Flanagan, P.H. Krebsbach, S.E. Feinberg, S.J. Hollister, S. Das, 2005, Bone tissue engineering using polycaprolactone scaffolds fabricated *via* selective laser sintering, **Biomaterials**, 26, 4817-4827.
27. M.R. Williamson, E.F. Adams and A.G.A. Coombes, 2006, Gravity spun polycaprolactone fibres for soft tissue engineering: Interaction with fibroblasts and myoblasts in cell culture, **Biomaterials**, 27, 1019-1026.
28. P.S. Tan and S.H. Teoh, 2007, Effect of stiffness of polycaprolactone (PCL) membrane on cell proliferation, **Materials Science and Engineering C**, 27, 304-308.
29. H. Zhang, C.Y. Lin and S.J. Hollister, 2009, The interaction between bone marrow stromal cells and RGD-modified three-dimensional porous polycaprolactone scaffolds, **Biomaterials**, 30, 4063-4069.
30. S. Ozkan, D.M. Kalyon, X. Yu, C.A. McKelvey and M. Lowinger, 2009, Multifunctional protein-encapsulated polycaprolactone scaffolds: Fabrication and *in vitro* assessment for tissue engineering, **Biomaterials**, 30, 4336-4347.
31. Z. Shao, X. Zhang, Y. Pi, X. Wang, Z. Jia, J. Zhu, L. Dai, W. Chen, L. Yin, H. Chen, C. Zhou and Y. Ao, 2012, Polycaprolactone electrospun mesh conjugated with an MSC affinity peptide for MSC homing *in vivo*, **Biomaterials**, 33, 3375-3387.
32. M. Liu, L. Chen, Y. Zhao, L, Gan, D. Zhu, W. Xiong, Y. Lv, Z. Xu, Z. Hao and L. Chen, 2012, Preparation, characterization and properties of liposome-loaded polycaprolactone microspheres as a drug delivery system, **Colloids and Surfaces A: Physicochem. Eng. Aspects**, 395, 131-136.
33. K. Pang, 2004, **Novel manufacturing, spinning, and characterization of polyesters based on 1,2-ethanediol and 1,3-propanediol**, Graduate Faculty of North Carolina State University, Raleigh, USA.
34. F.W. Billmeyer, JR., 1984, **Textbook of polymer science**, John Wiley and Son, Inc., Canada.

35. D. Xie, 1997, **Synthesis and ring opening polymerization of macrocyclic monomers for production of engineering thermoplastics**, Faculty of the Virginia Polytechnic Institute and State University, Virginia, USA.
36. A.J. Hall, P. Hodge, C.S. McGrail and J. Rickerby, 2000, Synthesis of a series of cyclic oligo(alkylidene isophthalate)s by cyclo-depolymerisation, **Polymer**, 41, 1239-1249.
37. S.D. Kamau, P. Hodge and M. Helliwell, 2003, Cyclo-depolymerization of poly(propylene terephthalate): Some ring-opening polymerizations of the cyclic oligomers produced, **Polym. Adv. Technol.**, 14, 492-501.
38. S.D. Kamau and P. Hodge, 2004, Cyclo-depolymerisations of polyurethanes to give macrocyclic oligomers: entropically driven ring-opening polymerisations of the macrocyclic oligomers produced, **Reactive & Functional Polymers**, 60, 55–64.
39. M. Alessi, P. Stagnaro, L. Conzatti, S. Tagliatatela Scafati, and P. Hodge, 2008, On the cyclo-depolymerization of alkyl aromatic polyesters and the *in* situ polymerization of the cyclic oligomers produced, **AIP Conf. Proc.**, 1042, 334-336.
40. K.Y. Chang and Y.D. Lee, 2009, Ring-opening polymerization of Ɛ-caprolactone initiated by the antitumor agent doxifluridine, **Acta Biomaterialia**, 5, 1075-1081.
41. H. J. Harwood and W. M. Ritchey, 1964, The characterization of sequence distribution in copolymers, **Polym Lett**, 2, 601-607.
42. Z.Y. Qian, S. Li, Y. He and X.B. Liu, 2004, Synthesis and in vitro degradation study of poly(ethylene terephthalate)/poly(ethylene glycol) (PET/PEG) multiblock copolymer, **Polymer Degradation and Stability**, 83, 93–100.
43. A.R. Tripathy, W.J. MacKnight and S.N. Kukureka, 2004, *In-situ* copolymerization of cyclic poly(butylene terephthalate) oligomers and Ɛ-caprolactone, **Macromolecules**, 37, 6793-6800.
44. R. Saint-Loup and J.J. Robin, 2005, Synthesis of poly[(ethylene terephthalate)-co-(Ɛ-caprolactone)]-poly(propylene oxide) block copolyester by direct polyesterification of reactive oligomers, **Macromol Chem Phys**, 206, 1190-1198.
45. P. Monvisade and P. Loungvanidprapa, 2007, Synthesis of poly(ethylene adipate) and poly(ethylene adipate-*co*-terephthalate) *via* ring-opening polymerization, **European Polymer Journal**, 43, 3408-3414.

46. P. Monvisade and P. Loungvanidprapa, 2008, Synthesis of poly(ethylene terephthalate-*co*-isophthalate) *via* ring-opening polymerization of their cyclic oligomers, **J Polym Res**, 15, 381-387.
47. N. Gonzalez-Vidal, A.M. Ilarduya and S. Munoz-Guerra, 2010, Poly(hexamethylene terephthalate-co-caprolactone) copolymers: Influence of cycle size on ring-opening polymerization, **European Polymer Journal**, 46, 792–803.
48. D. Ma, G. Zhang, Z. Huang and X. Luo, 1998, Synthesis and chain structure of ethylene terephthalate-Ɛ-caprolactone copolyesters, **J Polym Sci Part A: Polym Chem**, 36, 2961–2969.
49. Z.P. Zhang, X.L. Luo, Y.C. Lu and D.Z. Ma, 2000, Tranesterification of poly(ethylene terephthalate) with poly(Ɛ-caprolactone), **Chinese Journal of Polymer Science**, 18, 405-412.
50. K.Y. Lim, B.C. Kim and K.J. Yoon, 2002, Effect of structural characteristic on physical properties of copolyesters from poly(ethylene terephthalate) oligomer and polycaprolactone, **J Polym Sci Part B: Polym Phys**, 40, 2552–2560.
51. K.Y. Lim, B.C. Kim and K.J. Yoon, 2003, Structural and physical properties of biodegradable copolyesters from poly(ethylene terephthalate) and polycaprolactone blends, **J Appl Polym Sci**, 88, 131–138.
52. R. Saint-Loup, T. Jeanmaire, J.J. Robin and B. Boutevin, 2003, Synthesis of (polyethylene terephthalate/polyƐ-caprolactone) copolyesters, **Polymer**, 44, 3437-3449.
53. L. Mandragora s.r.l., 2005, **Applied Ceramic Technology Volume I**, SACMI IMOLA, Imola, Italy.
54. P.B. John, 1979, **Biomaterials An Introduction**, Plenum Press, New York, USA.
55. R.Z. LeGeros and J.P. LeGeros, 1993, **An introduction to bioceramics**, World Scientific Publishing Co., Singapore.
56. H. Aoki, 1994, **Medical Application of Hydroxyapatite**, Ishiyaky Euro, Tokyo, Japan.
57. A. Ulrioh, 1993, **Introduction to Industrial Polymer 2nd**, Hanser Publisher, Germany.
58. S.P. Parker, 1993, **Encyclopedia of Chemistry Vol.3**, McGraw-Hill Inc., USA.
59. F.M.Z. Kaifi, M. Aurangzeb, B. Ahmed and M. Khan, 2004, Manufacture of synthetic wollastonite, **Jour. Chem. Soc. Pak.**, 26, 1-4.

60. J. Podporska, M. Blazewicz, B. Trybalska and L. Zych, 2008, A novel ceramic material with medical application, **Processing and Application of Ceramics**, 2, 19–22.
61. T.V. Vakalova, N.P. Karionova, V.M. Pogrebenkov, V.I. Vereshchagin and V.V. Gorbatenko, 2010, Features of solid phase synthesis of wollastonite from natural and technogenic raw material, **Refractories and Industrial Ceramics**, 51, 295-301.
62. M.B. Smith, 1994, **Organic Synthesis, International edition**, McGraw-Hill, Germany.
63. W. Xia and J. Chang, 2008, Preparation and the phase transformation behavior of amorphous mesoporous calcium silicate, **Microporous and Mesoporous Materials**, 108, 345–351.
64. A. Meiszterics and K. Sinko, 2008, Sol–gel derived calcium silicate ceramics, **Colloids and Surfaces A: Physicochem. Eng. Aspects**, 319, 143–148.
65. T.A. Ring, 1995, **Fundamentals of ceramic powder processing and synthesis**, Academic Press, Inc., California, USA.
66. B. Dietoich, P. Viout and J.M. Lehn, 1993, **In Macrocyclic Chemistry**, VCM, Weinheim, Germany.
67. P. Siriphannon, S. Hayashi, A. Yasumori and K. Okada, 1999, Preparation and sintering of $CaSiO_3$ from coprecipitated powder using NaOH as precipitant and its apatite formation in simulated body fluid solution, **J. Mater. Res.**, 14, 529-536.
68. X. Wan, C. Chang, D. Mao, L. Jiang and M. Li, 2005, Preparation and in vitro bioactivities of calcium silicate nanophase materials, **Materials Science and Engineering C**, 25, 455–461.
69. K. Lin, J. Chang and J. Lu, 2006, Synthesis of wollastonite nanowires via hydrothermal microemulsion methods, **Materials Letters**, 60, 3007–3010.
70. P. Siriphannon, Y. Kameshima, A. Yasumori, K. Okada and S. Hayashi, 2002, Formation of hydroxyapatite on $CaSiO_3$ powders in simulated body fluid, **Journal of the European Ceramic Society**, 22, 511–520.
71. W. Xue, X. Liu, X.B. Zheng and C. Ding, 2005, *In vivo* evaluation of plasma-sprayed wollastonite coating, **Biomaterials**, 26, 3455–3460.
72. S. Xu, K. Lin, Z. Wang, J. Chang, L. Wang, J. Lu and C. Ning, 2008, Reconstruction of calvarial defect of rabbits using porous calcium silicate bioactive ceramics, **Biomaterials**, 29, 2588-2596.

73. W. Xue, A. Bandyopadhyay and S. Bose, 2009, Mesoporous calcium silicate for controlled release of bovine serum albumin protein, **Acta Biomaterialia**, 5, 1686–1696.
74. M.A. de la Casa-Lillo, P. Vela´squez and P.N.D. Aza, 2011, Influence of thermal treatment on the *"in vitro"* bioactivity of wollastonite materials, **J Mater Sci: Mater Med**, 22, 907–915.
75. P.N. Jagadale, V.V. Dhapte and S.R. Bamane, 2012, Nanoporous calcium silicate: Potentially an efficient biomaterial for antibiotics carrier, **Journal of Pharmacy Research**, 5, 360-362.
76. S. Chanawong, P. Siriphannon and P. Monvisade, 2004, **Preparation of composite from hydroxyapatite with poly(ethylene adipate)-*co*-poly(ethylene terephthalate)**, Thailand.
77. Y.H. Koh, I.K. Jun and H.E. Kim, 2006, Fabrication of poly(Ɛ-caprolactone)/hydroxyapatite scaffold using rapid direct deposition, **Materials Letters**, 60, 1184-1187.
78. M. Risbud, D.N. Saheb, J. Jog and R. Bhonde, 2001, Preparation, characterization and *in vitro* biocompatibility evaluation of poly(butylene terephthalate)/wollastonite composites, **Biomaterials**, 22, 1591-1597.
79. V. Suteesuksataporn, A. Jianprasert, O. Chaowakul, P. Siriphannon and P. Monvisade, 2003, **Hydroxyapatite/poly(ethylene terephthalate) (HAp/PET) and calcium silicate/poly(ethylene terephthalate) composites (CS/PET): Preparation, compressive strength and bioactivity**, Faculty of Science, King Mongkut's Institute of Technology Ladkrabang, Thailand.
80. H. Li and J. Chang, 2004, Fabrication and characterization of bioactive wollastonite/PHBV composite scaffolds, **Biomaterials**, 25, 5473-5480.
81. H. Li and J. Chang, 2005, *In vitro* degradation of porous degradable and bioactive PHBV/wollastonite composite scaffolds, **Polymer Degradation and Stability**, 87, 301-307.
82. H. Li and J. Chang, 2005, Preparation, characterization and *in vitro* release of gentamicin from PHBV/wollastonite composite microspheres, **Journal of Controlled Release**, 107, 463-473.

83. H. Li and J. Chang, 2004, Preparation and characterization of bioactive and biodegradable wollatonite/poly(D, L-lactide acid) composite scaffolds, **J Mat Sci: Mat in Med**, 15, 1089-1095.

84. L. Xu, Z.C. Xiong, D. Yang, L.F. Zhang, J. Chang and C.D. Xiong, 2009, Preparation and *in vitro* degradation of novel bioactive polylactide/wollastonite scaffolds, **J Appl Polym Sci**, 114, 3396–3406.

85. L. Ye, J. Chang, C. Ning and K. Lin, 2008, Fabrication of poly-(D,L-lactic acid)-wollastonite composite films with surface modified β-$CaSiO_3$ particles, **J Biomater Appl**, 22, 465-480.

86. H. Li and J. Chang, 2005, pH-compensation effect of bioactive inorganic fillers on the degradation of PLGA, **Composites Science and Technology**, 65, 2226-2232.

87. L. Zhao, K. Lin, M. Zhang, C. Xiong, Y. Bao, X. Pang and J. Chang, 2011, The influences of poly(lactic-co-glycolic acid) (PLGA) coating on the biodegradability, bioactivity, and biocompatibility of calcium silicate bioceramics, **J Mater Sci**, 46, 4986-4993.

88. P. Monvisade, P. Siriphannon, R. Jermsungnern and S. Rattanabodee, 2007, Preparation of hydroxyapatite/poly(methyl methacrylate) and calcium silicate/poly(methyl methacrylate) interpenetrating hybrid composites, **J Mater Sci: Mater Med**, 18, 1955-1959.

89. G. Chouzouri and M. Xanthos, 2007, Degradation of aliphatic polyesters in the presence of inorganic fillers, **J Plastic Film and Sheeting**, 23, 19-36.

90. G. Chouzouri and M. Xanthos, 2007, *In vitro* bioactivity and degradation of polycaprolactone composites containing silicate fillers, **Acta Biomaterialia**, 3, 745-756.

91. J. wei, S.J. Heo, D.H. Kim, S.E. Kim, Y.T. Hyun and J.W. Shin, 2008, Comparison of physical, chemical and cellular responses to nano- and micro-sized calcium silicate/poly(ε-caprolactone) bioactive composites, **J. R. Soc. Interface,** 5, 617–630.

92. J. Wei, F. Chen, J.W. Shin, H. Hong, C. Dai, J. Su, C. Liu, 2009, Preparation and characterization of bioactive mesoporous wollastonite-Polycaprolactone composite scaffold, **Biomaterials**, 30, 1080–1088.

93. I. Kotela, J. Podporska, E. Soltysiak, K.J. Konsztowicz and M. Blazewicz, 2009, Polymer nanocomposites for bone tissue substitutes, **Ceramics International**, 35, 2475-2480.

94. E.I. Shishatskaya, P.S. Mironov and T.G. Volova, Properties of composites of resorbable polyester “Bioplastotan” with wollastonite and hydroxyapatite, **Plasticheskie Massy**, 12, 51-54.
95. L.M. Rodriguez-Lorenzo, R. Garcia-Carrodeguas, M.A. Rodriguez, S.D. Aza, J. Jimenez, A. Lopez-Bravo, M. Fernandez and J.S. Roman, 2009, Synthesis, characterization, bioactivity and biocompatibility of nanostructured materials based on the wollastonite-poly(ethylmethacrylate-co-vinylpyrrolidone) system, **J. Biomed. Mater. Res.**, 88A, 53-64.
96. L.M. Rodriguez-Lorenzo, L Saldana, L. Benito-Garzon, R. Garcia-Carrodeguas, S. de Aza, N. Vilaboa and J.S. Roman, 2012, Feasibility of ceramic–polymer composite cryogels as scaffolds for bone tissue engineering, **J. Tissue Eng. Regen. Med**., 6, 421–433.
97. Autoimmunity Research Foundation, **Differences between *in vitro*, *in vivo*, and *in silico* studies**, [Online]. Available: http://mpkb.org/home/patients/assessing_literature/in_vitro_studies.
98. T. Kokubo, 1990, Surface chemistry of bioactive glass-ceramics, **Journal of Non-crystalline Solids**, 120, 138-151.
99. B.D. Cullity, 1978, **Elements of X-ray Diffraction**, Addison-Wesley, Reading, MA.
100. X. Cheng, X. Luo, Z. Li and D. MA, 1999, Proton NMR characterization of chain structure in butylene terephthalate-Ɛ-caprolactone copolyesters, **J Polym Sci A: Polym Chem**, 37, 3770–3777.
101. A.S. Brar and Sunita, 1992, Determination of microstructure and glass-transition temperature of acrylonitrile-methyl acrylate copolymers by ^{13}C-NMR spectroscopy, **J Polym Sci: Part A Polym Chemi**, 30, 2549-2557.
102. N.P. Cheremisinoff, 1989, **Handbook of polymer science and technology**, Marcel Dekker INC., USA.
103. S. Fakirov, 2002, **Handbook of Thermoplastic Polymers: Homopolymers, Copolymers, Blends, and Composites**, Wiley-VCH Verlag GmbH, Weinheim.
104. M. Kattan, E. Dargent and J. Grenet, 2002, Three phase model in drawn thermoplastic polyesters: comparison of differential scanning calorimetry and thermally stimulated depolarization current experiments, **Polymer**, 43, 1399-1405.

105. J.C. Viana, N.M. Alves and J.F. Mano, 2004, Morphology and mechanical properties of injection molded poly(ethylene terephthalate), **Polym. Engi. and Sci.**, 44, 2174-2184.
106. F.H. Chung and R.W. Scott, 1973, A new approach to the determination of crystallinity of polymers by X-ray diffraction, **J. Appl. Crystallogr.**, 6, 225-230.
107. A.J. Kerin, M.R. Wisnom and M.A. Adams, 1998, The compressive strength of articular cartilage, **Proc. Inst. Mech. Eng. H**, 212, 273-280.
108. L.L. Hench and J. Wilson, 1993, **An introduction to bioceramics**, World Scientific, Singapore.
109. S.I. Roohani-ESfahani, S. Nouri-Khorasani, R. Appleyard and H. Zreiqat, 2010, The influence hydroxyapatite nanoparticle shape and size on the properties of biphasic calcium phosphate scaffolds coated with hydroxyapatite-PCL composites, **Biomaterials**, 31, 5498-5509.
110. R. Zhang, X. Luo, and D. Ma, 1995, Multiple melting endotherms from ethylene terephthalate-caprolactone copolyesters, **Polymer**, 36, 4361-4364.

APPENDIX A

CALCULATION

Calculation of Ca:Si molar ratio in calcium silicate (CS)

- Ca which was analyzed with XRF was CaO compound; therefore, the molecular weight of CaO is 56.077 g/mol.
- Si which was analysed with XRF was SiO_2 compound; therefore, the molecular weight of SiO_2 is 60.084 g/mol.

The weight percentages of CaO and SiO_2 from XRF were used for Ca:Si molar ratio calculation.

CaO	56.077	g	has Ca	1	mol
If CaO	a	g	has Ca	$\frac{1\times a}{56.077}$ = A	mol
SiO_2	60.084	g	has Si	1	mol
If SiO_2	b	g	has Si	$\frac{1\times b}{60.084}$ = B	mol

Therefore, Ca/Si molar ratio = A/B

For example,

The weight percentages of CaO and SiO_2 in CS sample which characterized with XRF were 44.783 and 46.843 %, respectively.

CaO	56.077	g	has Ca	1	mol
If CaO	44.783	g	has Ca	$\frac{1\times 44.783}{56.077}$ = 0.799	mol
SiO_2	60.084	g	has Si	1	mol
If SiO_2	46.843	g	has Si	$\frac{1\times 46.843}{60.084}$ = 0.780	mol

Therefore, Ca/Si molar ratio = 0.799/0.780 = 1.024

APPENDIX B

JOINT COMMITTEE POWDER DIFFRACTION STANDARD

Phase Info - Wollastonite-1A 04-011-2265

Wollastonite-1A

$CaSiO_3$

Powder Pattern (QM: Star, Calculated)

Radiation: CuKα1 λ: 1.5406 Å Filter:

Calibration: 2θ: 65.015° Lines: 198 RIR: 0.91

Reference: Calculated from LPF using POWD-12++

Unit Cell Data (Single Crystal)

Crystal System: Triclinic S.G: P-1 (2) Z: 6 P.S: aP30

Lattice Constants: 7.9258, 7.3202, 7.0653 (Å) <90.055°, 95.217°, 103.426°>

Volume: 397.0 Density: 2.916 Mwt: 116.16 F(30): 116.6 (0.0057,45/0)

Reference: Ohashi, Y., Phys. Chem. Miner., v10 p217,229 (1984)

ANX: ABX3. LPF Collection Code: 1253098. Sample Source or Locality: Willsboro, New York, USA.

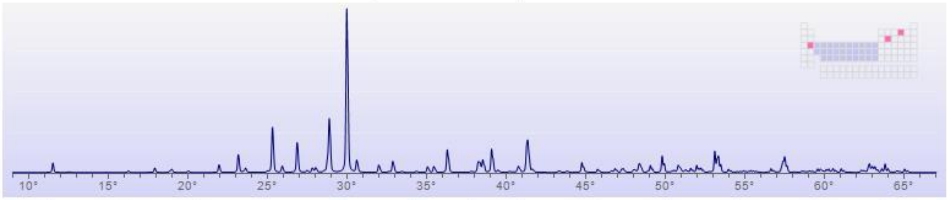

#	Angle	d(Å)	I%(f)	(h k l)	2π/d	#	Angle	d(Å)	I%(f)	(h k l)	2π/d
1	11.520	7.6753	9.3	(1 0 0)	0.8186	27	28.752	3.1025	11.5	(-1 1 2)	2.0252
2	12.425	7.1183	0.1	(0 1 0)	0.8827	28	28.874	3.0896	31.1	(2 1 0)	2.0336
3	12.574	7.0342	0.5	(0 0 1)	0.8932	29	28.874	3.0896	31.1	(1 0 2)	2.0336
4	14.857	5.9578	0.1	(-1 1 0)	1.0546	30	29.972	2.9789	100.0	(-2 2 0)	2.1092
5	16.262	5.4462	1.6	(-1 0 1)	1.1537	31	29.972	2.9789	100.0	(1 2 0)	2.1092
6	17.508	5.0614	0.1	(0-1 1)	1.2414	32	30.597	2.9195	7.3	(-2-1 1)	2.1522
7	17.915	4.9474	2.3	(1 0 1)	1.2700	33	30.597	2.9195	7.3	(-1-1 2)	2.1522
8	17.915	4.9474	2.3	(0 1 1)	1.2700	34	31.983	2.7961	4.6	(-1-2 1)	2.2472
9	18.862	4.7011	1.5	(1 1 0)	1.3365	35	31.983	2.7961	4.6	(-2 2 1)	2.2472
10	18.982	4.6716	3.3	(-1 1 1)	1.3450	36	32.602	2.7444	1.0	(2 1 1)	2.2895
11	20.025	4.4305	1.7	(1-1 1)	1.4182	37	32.863	2.7231	7.0	(1 1 2)	2.3073
12	21.949	4.0463	8.4	(-1-1 1)	1.5528	38	32.863	2.7231	7.0	(-2 0 2)	2.3073
13	23.158	3.8376	20.0	(2 0 0)	1.6373	39	33.421	2.6790	1.3	(-2 1 2)	2.3454
14	23.491	3.7840	1.1	(1 1 1)	1.6605	40	34.343	2.6091	1.5	(-3 1 0)	2.4082
15	23.614	3.7646	4.6	(-2 1 0)	1.6690	41	35.045	2.5584	7.2	(3 0 0)	2.4559
16	24.998	3.5592	0.6	(0 2 0)	1.7654	42	35.442	2.5307	3.8	(-1 2 2)	2.4828
17	24.998	3.5592	0.6	(-1 2 0)	1.7654	43	35.442	2.5307	3.8	(0-2 2)	2.4828
18	25.302	3.5171	26.1	(0 0 2)	1.7865	44	36.287	2.4737	14.6	(1-2 2)	2.5400
19	25.302	3.5171	26.1	(-2 0 1)	1.7865	45	36.287	2.4737	14.6	(0 2 2)	2.5400
20	25.915	3.4353	7.2	(-2 1 1)	1.8290	46	37.018	2.4265	0.1	(-2-1 2)	2.5895
21	26.854	3.3173	35.3	(-1 0 2)	1.8941	47	37.776	2.3795	1.5	(3-1 1)	2.6405
22	27.477	3.2435	2.2	(2 0 1)	1.9372	48	38.204	2.3538	7.8	(-3 2 0)	2.6693
23	27.810	3.2053	2.5	(-1 2 1)	1.9602	49	38.260	2.3505	7.9	(2 2 0)	2.6731
24	27.810	3.2053	2.5	(0-2 1)	1.9602	50	38.358	2.3447	5.4	(0 0 3)	2.6797
25	28.017	3.1821	5.5	(0-1 2)	1.9745	51	38.523	2.3351	7.6	(3 0 1)	2.6908
26	28.540	3.1251	1.2	(0 1 2)	2.0106	52	38.523	2.3351	7.6	(-2 2 2)	2.6908

Thursday, May 09, 2013, 1:16 PM • University of Michigan

Phase Info - Polyethylene terephthalate 00-060-0989

Polyethylene terephthalate

$(C_{10}H_8O_4)_n$

Powder Pattern (QM: Blank, Diffractometer)

Radiation: CuKα λ: 1.54184 Å Filter: Graph CAS#: 25038-59-9

Calibration: 2θ: 52.934° Lines: 15 RIR:

Reference: Blanton, T., Murthy, S., Eastman Kodak Company, Rochester, New York, USA., Private Communication (2009)

Unit Cell Data ( )

Crystal System: Triclinic S.G: P-1 (2) Z: 1 P.S: aP22

Lattice Constants: 4.5610, 5.9700, 10.8400 (Å) <98.300°, 118.500°, 112.450°>

Volume: 219.5 Density: 1.454 Mwt: 192.17 F(12): 1.1 (0.115,93/0)

Reference: Ibid.

Additional Patterns: See PDF 00-050-2275, 00-058-1447 and 02-072-2446. General Comments: The initial lattice parameters were taken from PDF 02-072-2446 and refined using the program unit cell.

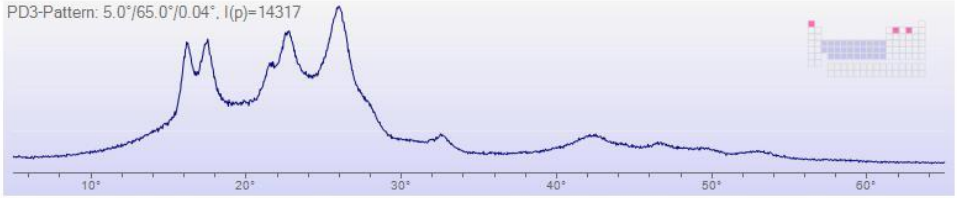

#	Angle	d(Å)	I%(f)	(h k l)	2π/d	#	Angle	d(Å)	I%(f)	(h k l)	2π/d
1	16.147	5.4848	77.0	(0-1 1)	1.1456						
2	17.416	5.0879	79.0	(0 1 0)	1.2349						
3	21.612	4.1085	65.0	(-1 0 1)	1.5293						
4	21.612	4.1085	65.0	(-1 0 2)	1.5293						
5	22.721	3.9104	85.0	(1-1 0)	1.6068						
6	25.989	3.4258	100.0	(1 0 0)	1.8341						
7	25.989	3.4258	100.0	(-1 0 3)	1.8341						
8	27.707	3.2171	39.0	(1-1 1)	1.9531						
9	32.533	2.7500	17.0	(1 1-3)	2.2848						
10	32.533	2.7500	17.0	(0-2 1)	2.2848						
11	42.374	2.1313	17.0	(1 0-5)	2.9480						
12	44.242	2.0456	8.0	(2 0-4)	3.0716						
13	46.640	1.9459	11.0	(1 2-2)	3.2290						
14	49.567	1.8376	8.0	(0 3-2)	3.4193						
15	52.934	1.7284	6.0	(2-3 0)	3.6353						

Thursday, May 09, 2013, 1:19 PM • University of Michigan

APPENDIX C

PROTON NUCLEAR MAGNETIC RESONANCE SPECTRA

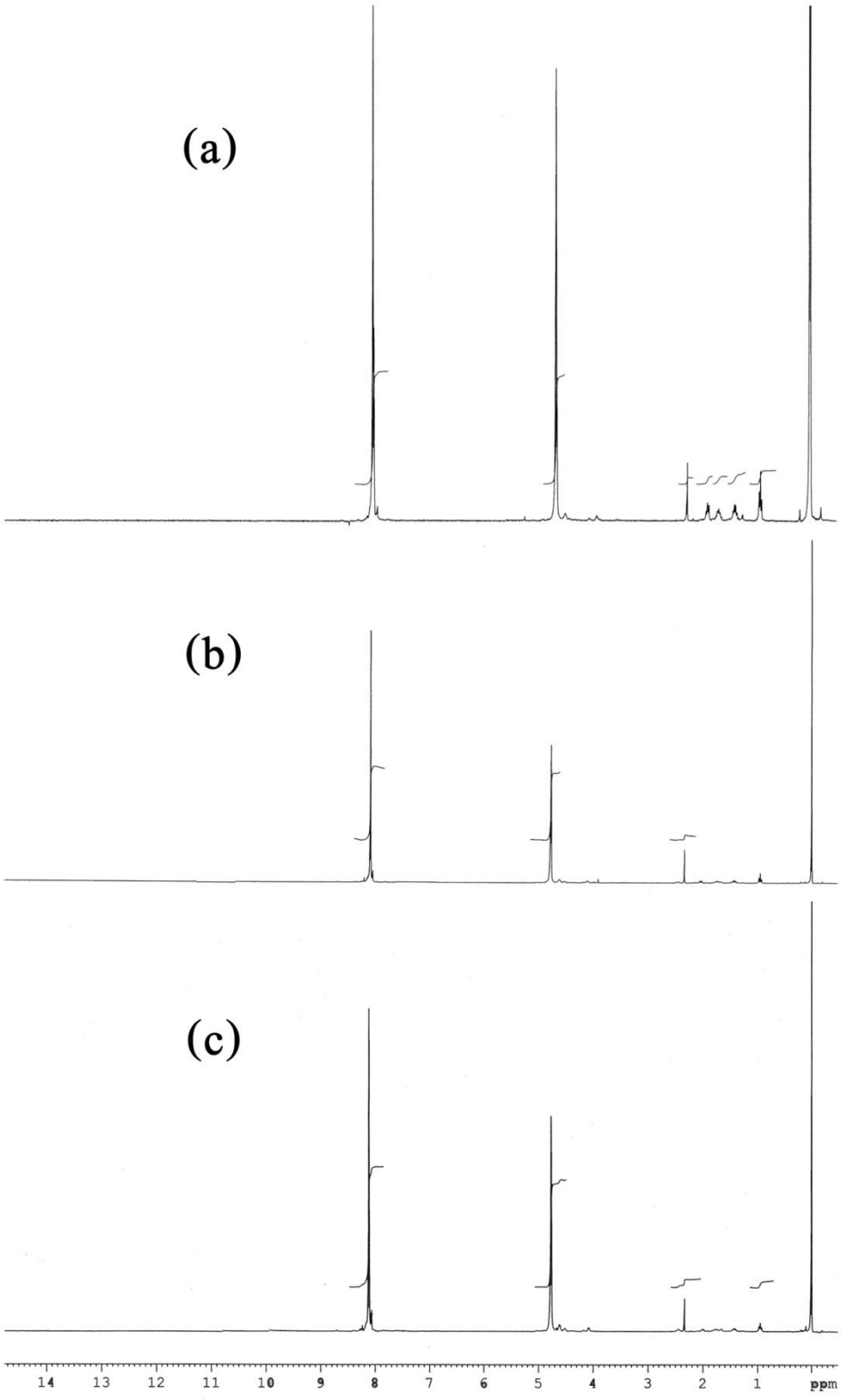

Figure C-1 ^{1}H-NMR spectra of PET homopolymer ring-opening polymerized at 180 °C (a), 200 °C (b) and 230 °C (c) for 8 hr

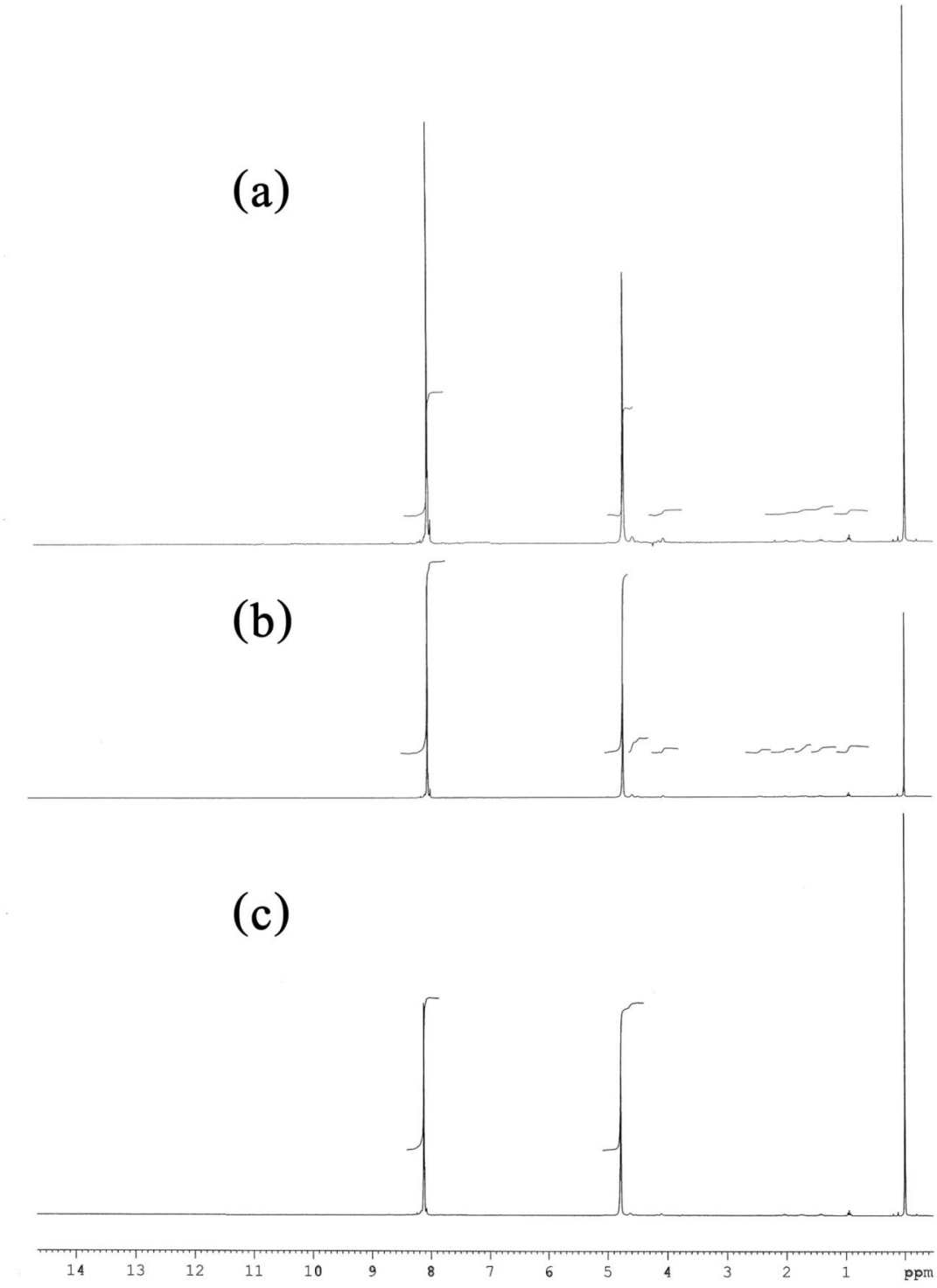

Figure C-2 ^{1}H-NMR spectra of PET homopolymer ring-opening polymerized at 200 °C (a), 230 °C (b) and 250 °C (c) for 24 hr

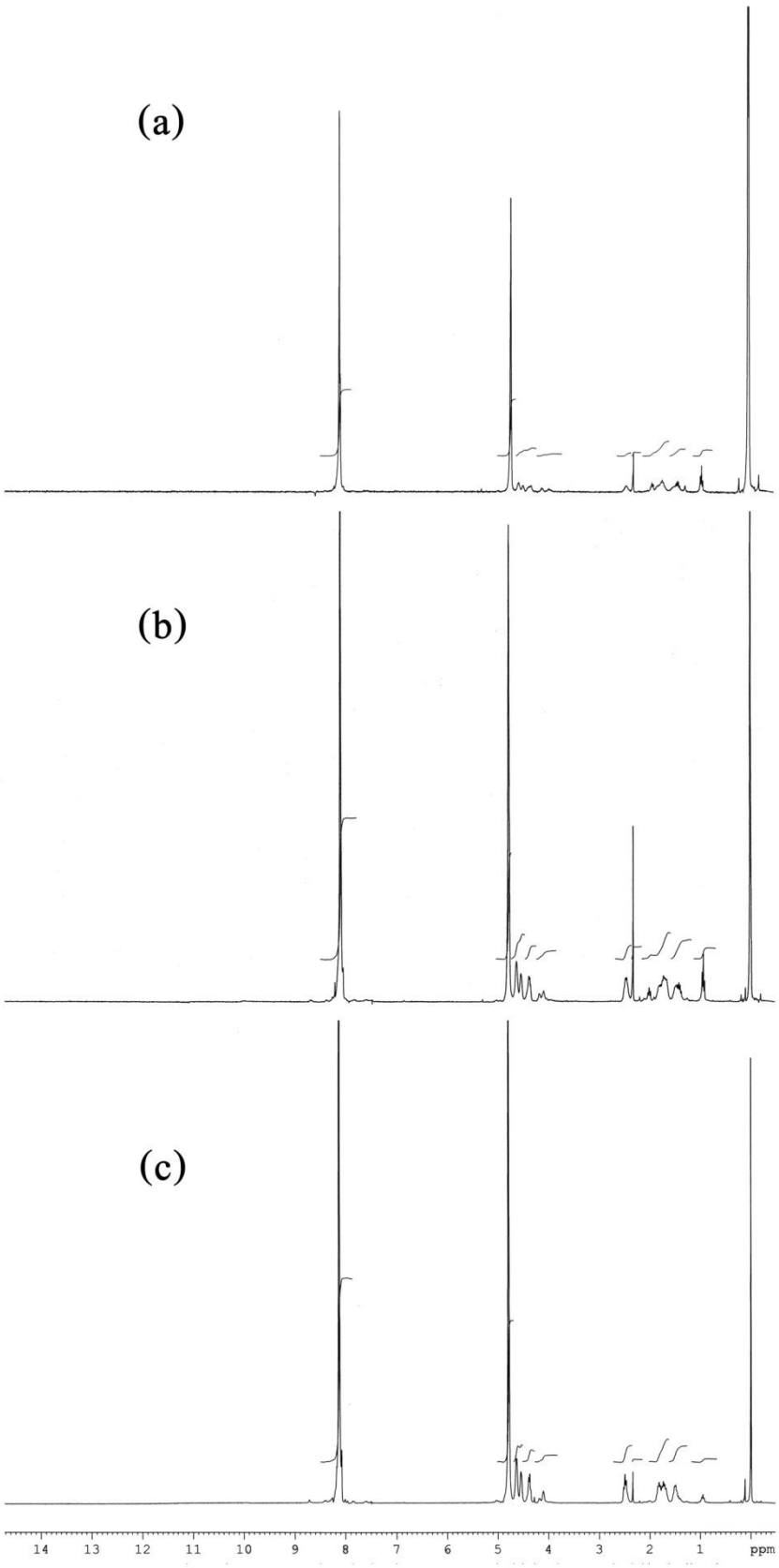

Figure C-3 ^{1}H-NMR spectra of copolymer with 90 %mol ET content ring-opening polymerized at 180 °C (a), 200 °C (b) and 230 °C (c) for 8 hr

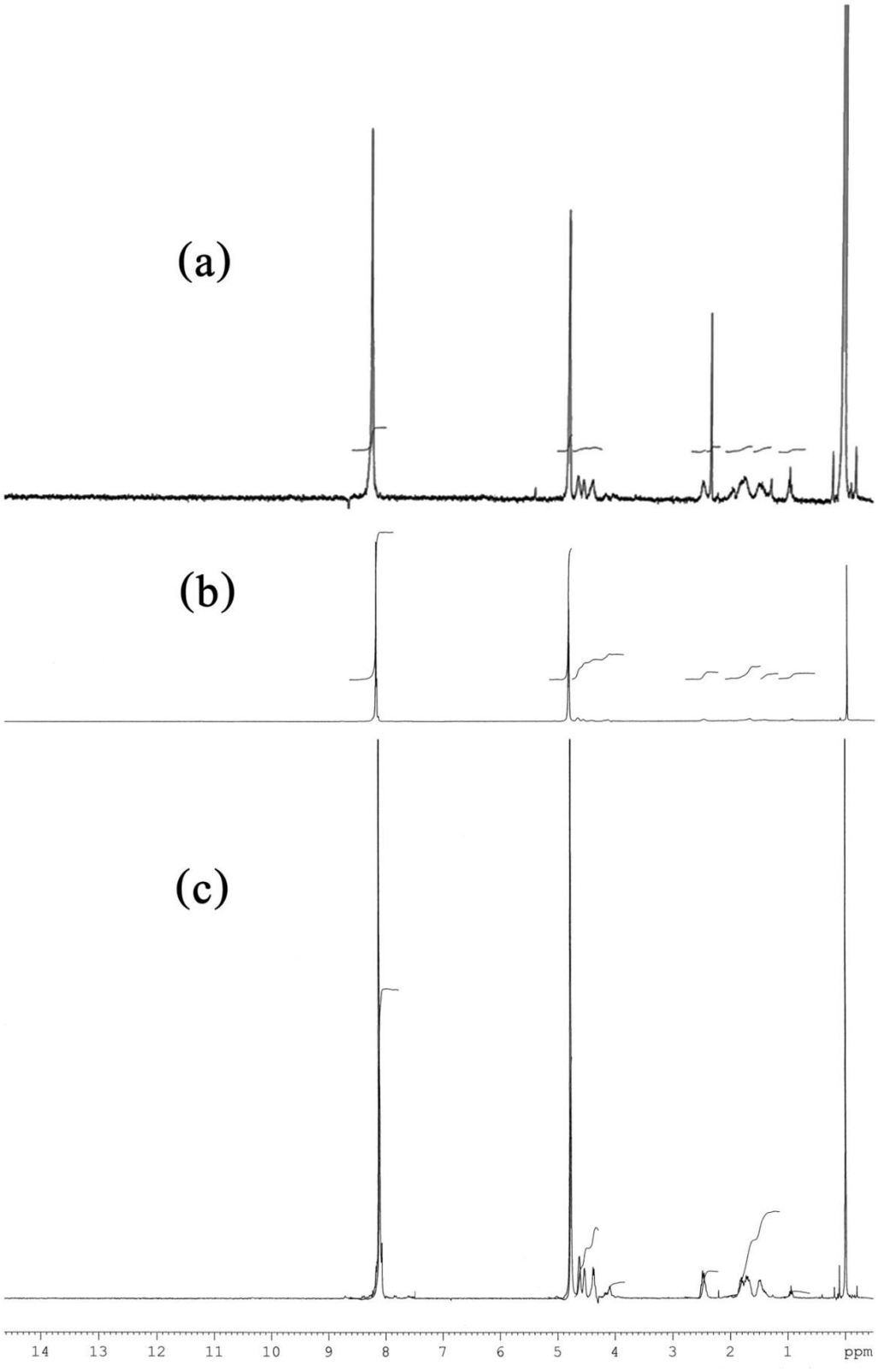

Figure C-4 ^{1}H-NMR spectra of copolymer with 90 %mol ET content ring-opening polymerized at 180 °C (a), 200 °C (b) and 230 °C (c) for 24 hr

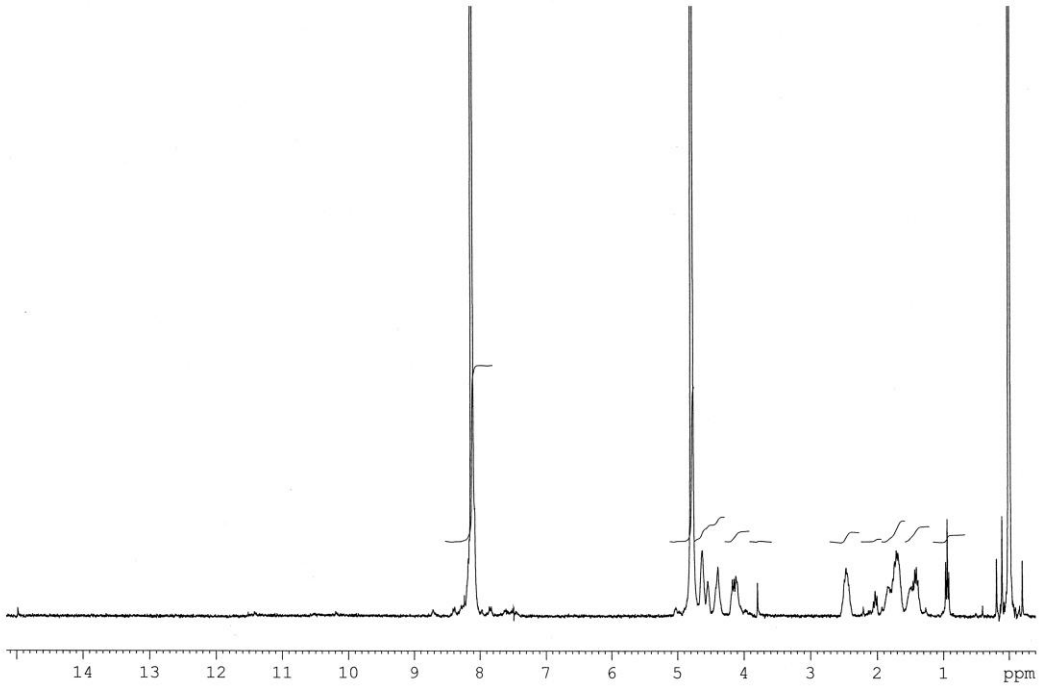

Figure C-5 ^{1}H-NMR spectrum of copolymer with 90 %mol ET content ring-opening polymerized at 250 °C for 24 hr

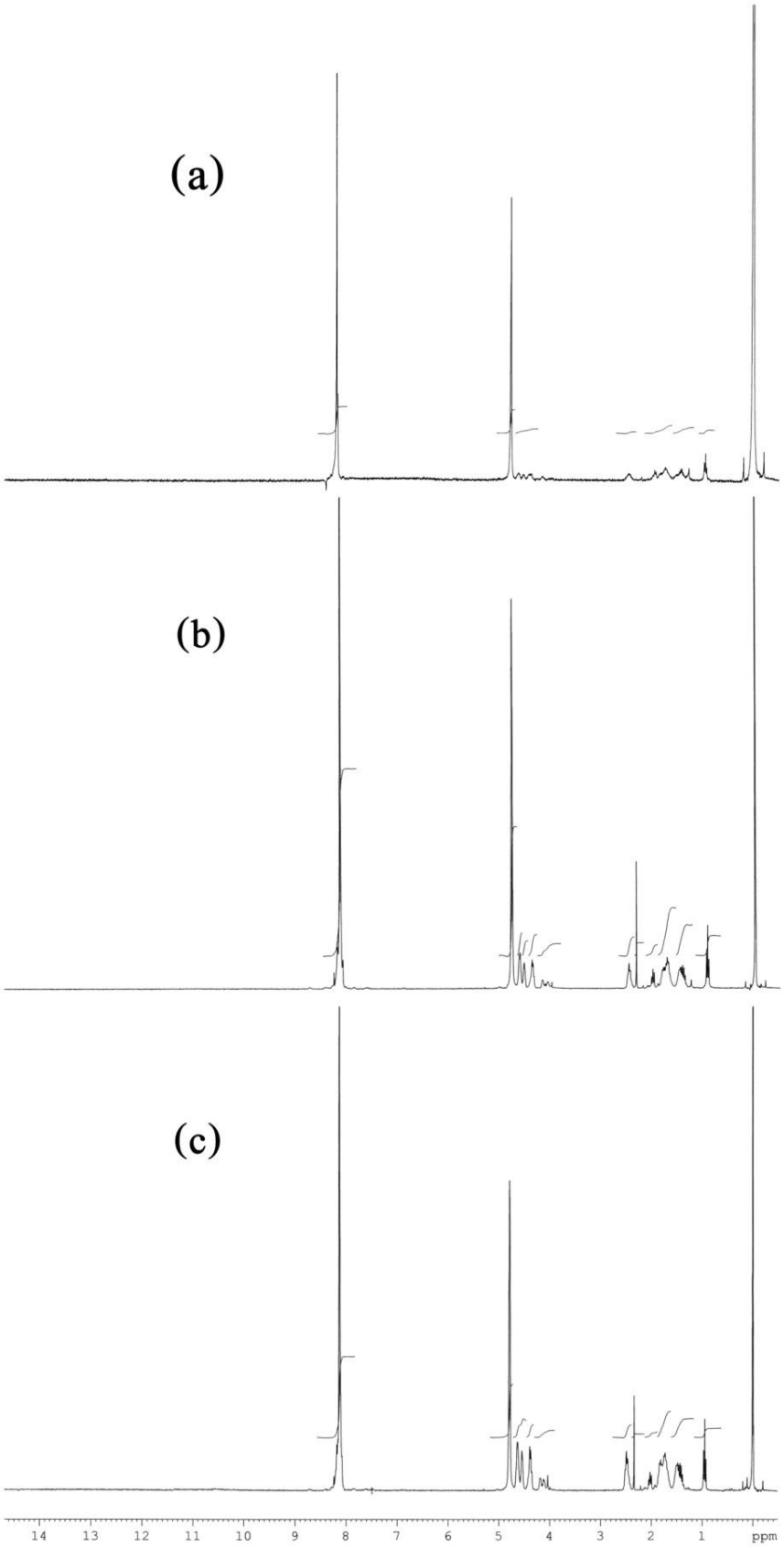

Figure C-6 ^{1}H-NMR spectra of copolymer with 80 %mol% ET content ring-opening polymerized at 180 °C (a), 200 °C (b) and 230 °C (c) for 8 hr

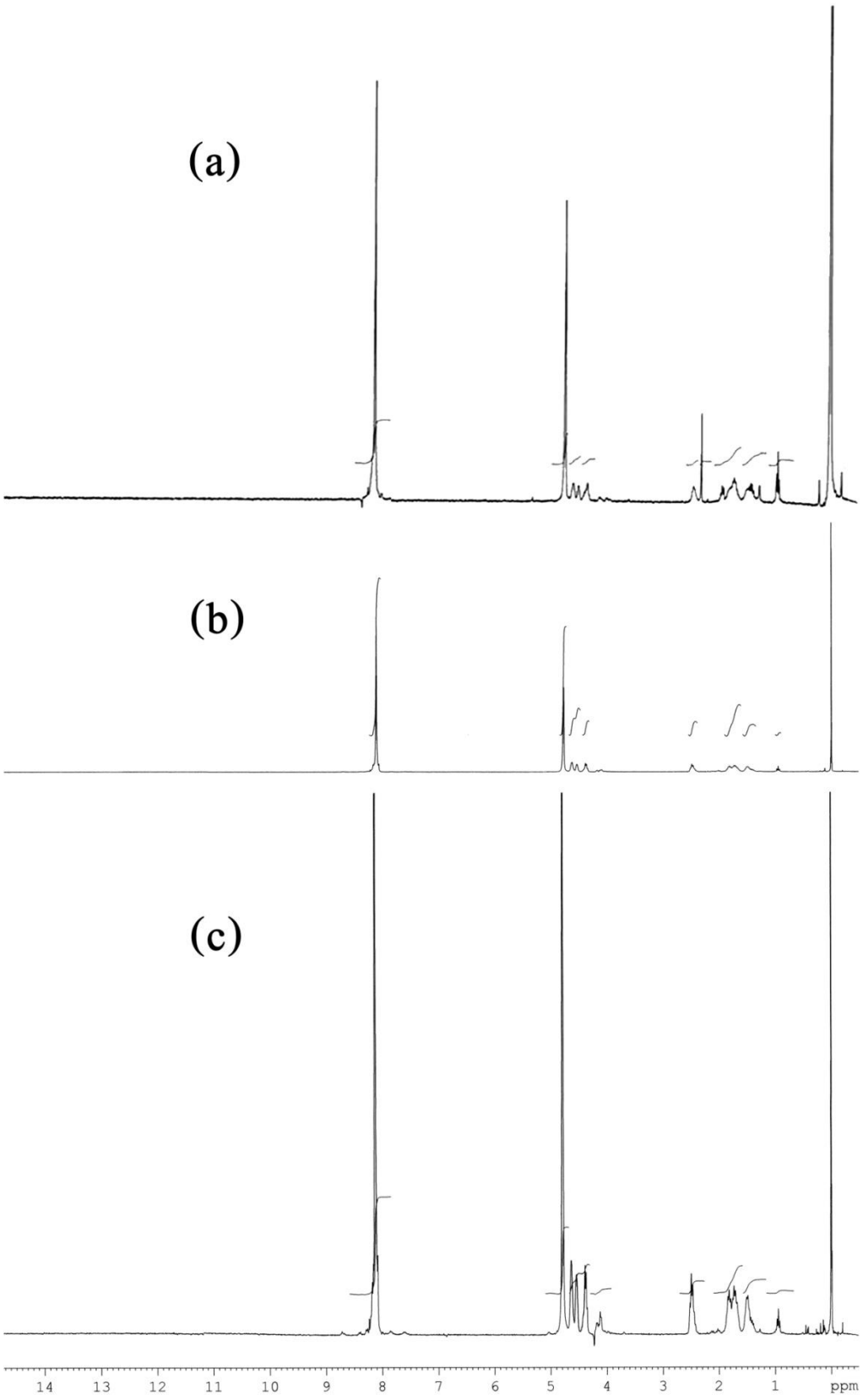

Figure C-7 ^{1}H-NMR spectra of copolymer with 80 %mol ET content ring-opening polymerized at 180 °C (a), 200 °C (b) and 230 °C (c) for 24 hr

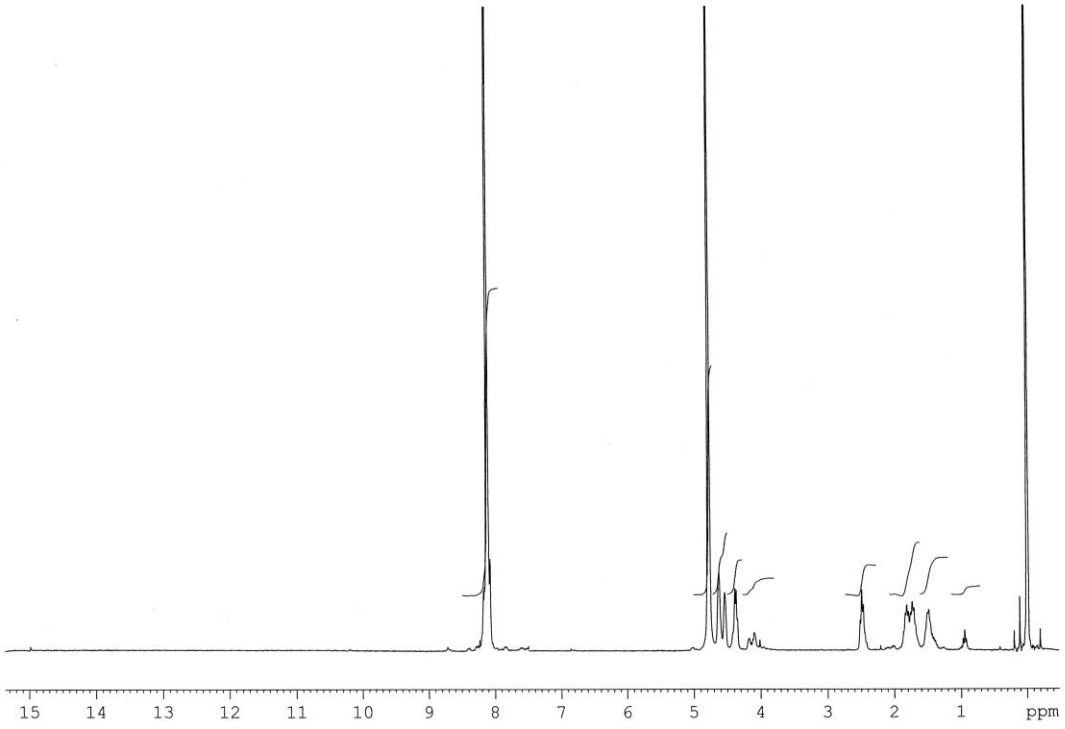

Figure C-8 ^{1}H-NMR spectrum of copolymer with 80 %mol ET content ring-opening polymerized at 250 °C for 24 hr

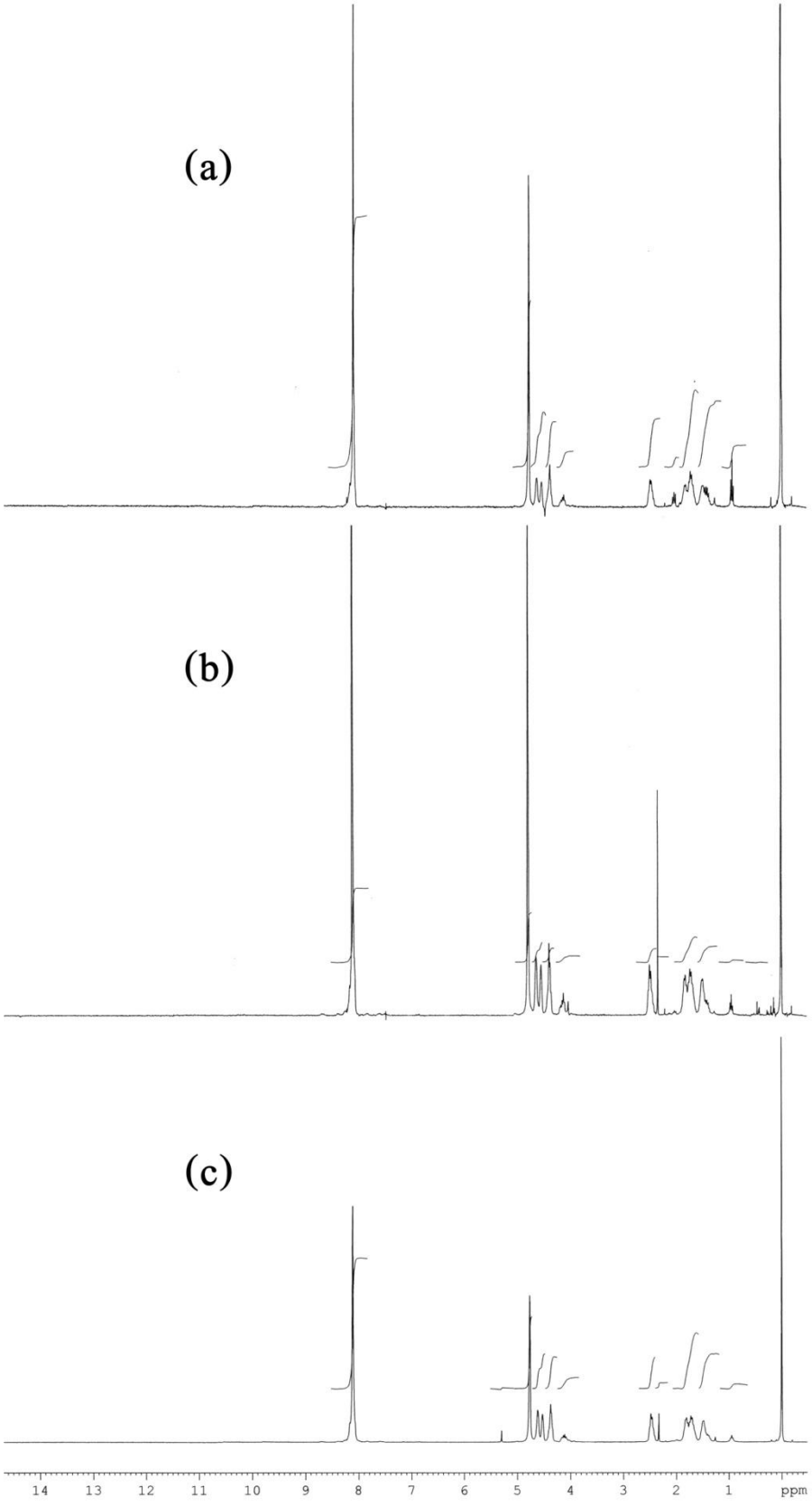

Figure C-9 ^{1}H-NMR spectra of copolymer with 70 %mol ET content ring-opening polymerized at 180 °C (a), 200 °C (b), and 230 °C (c) for 8 hr

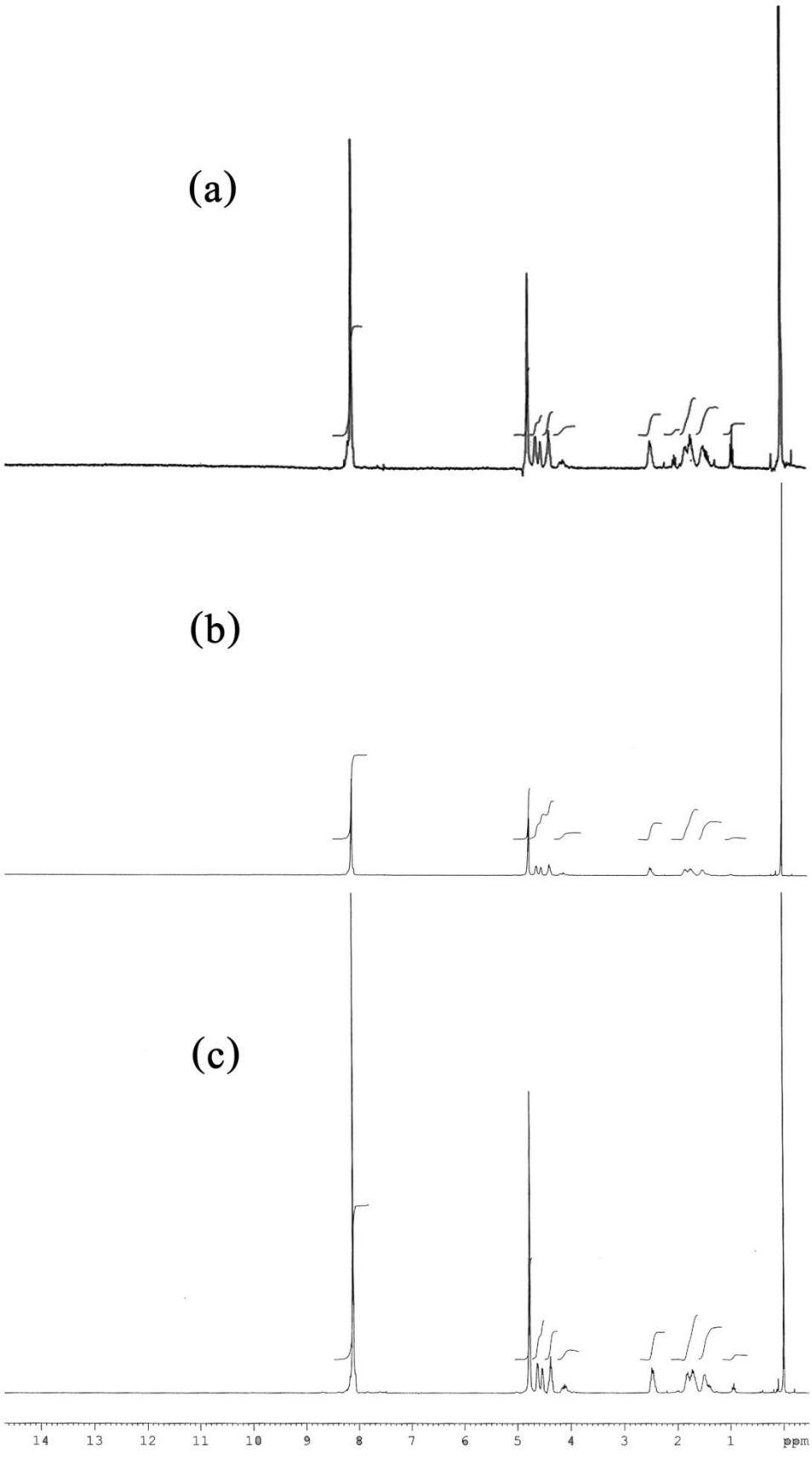

Figure C-10 ^{1}H-NMR spectra of copolymer with 70 %mol ET content ring-opening polymerized at 180 °C (a), 200 °C (b), and 230 °C (c) for 24 hr

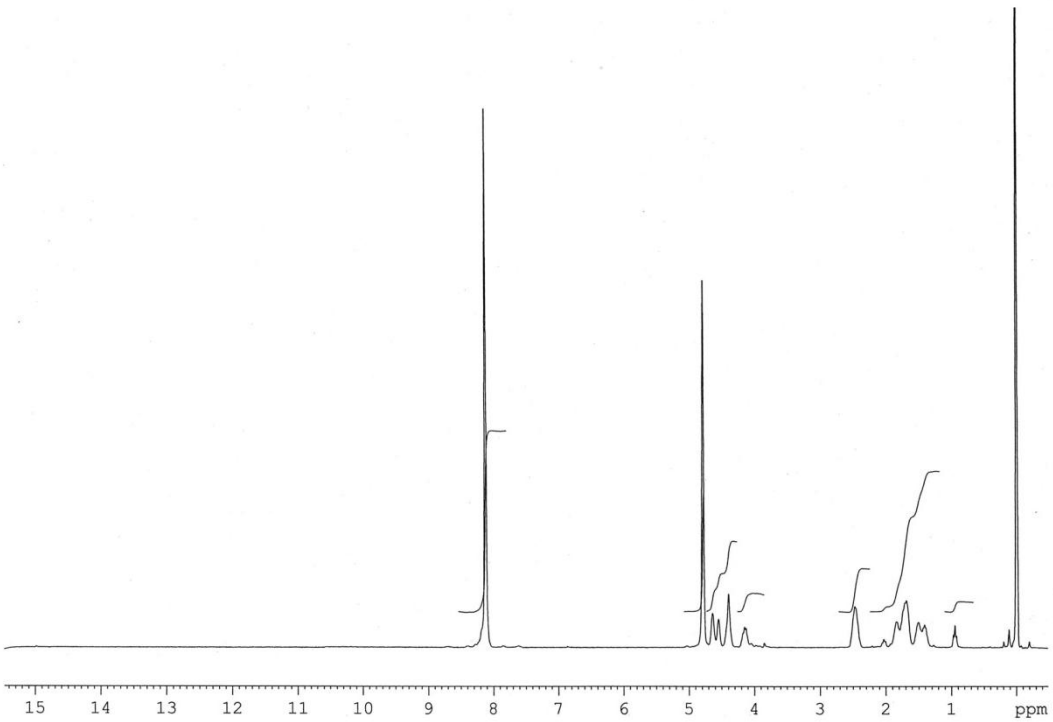

Figure C-11 ^{1}H-NMR spectrum of copolymer with 70 %mol ET content ring-opening polymerized at 250 °C for 24 hr

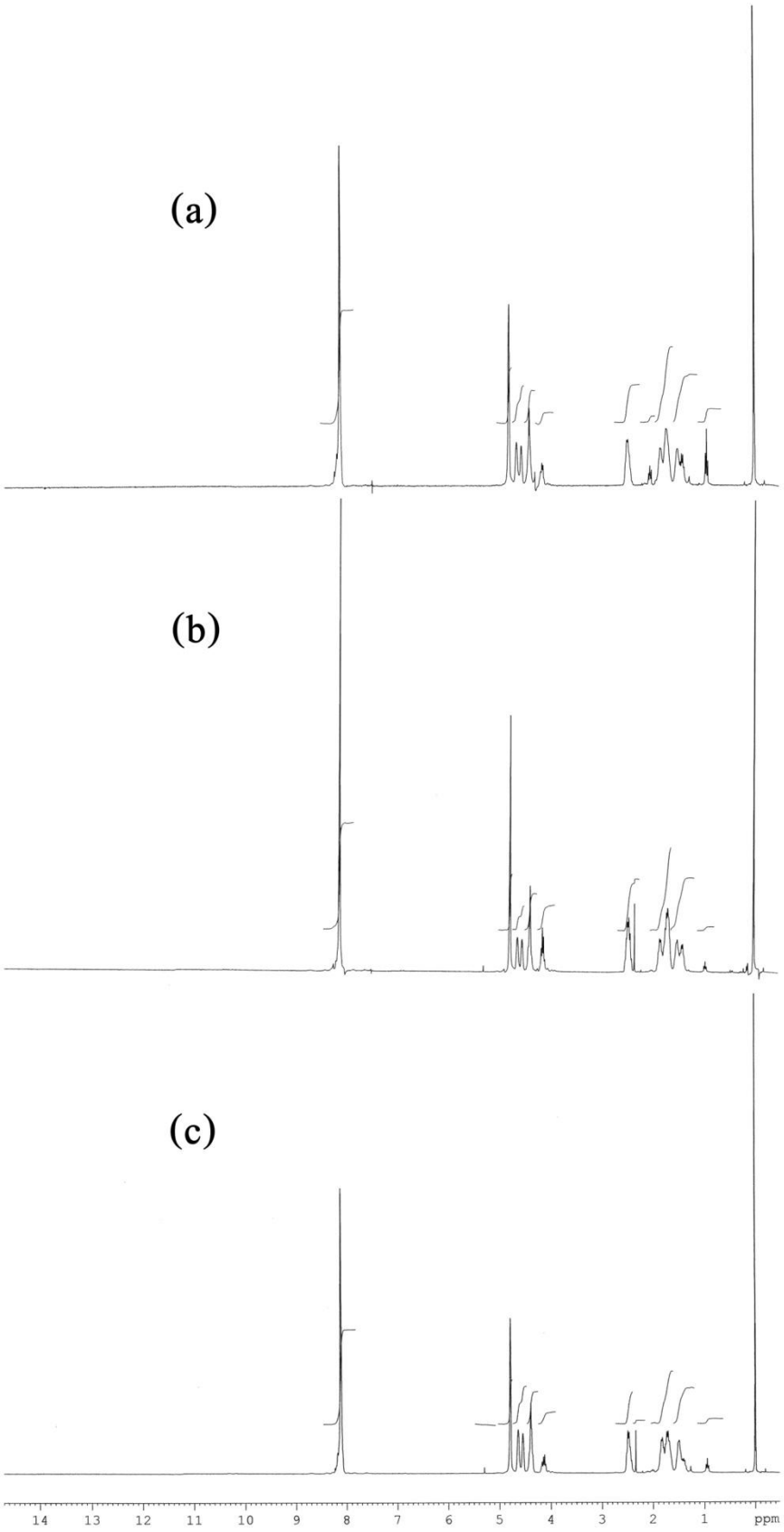

Figure C-12 ^{1}H-NMR spectra of copolymer with 60 %mol ET content ring-opening polymerized at 180 °C (a), 200 °C (b), and 230 °C (c) for 8 hr

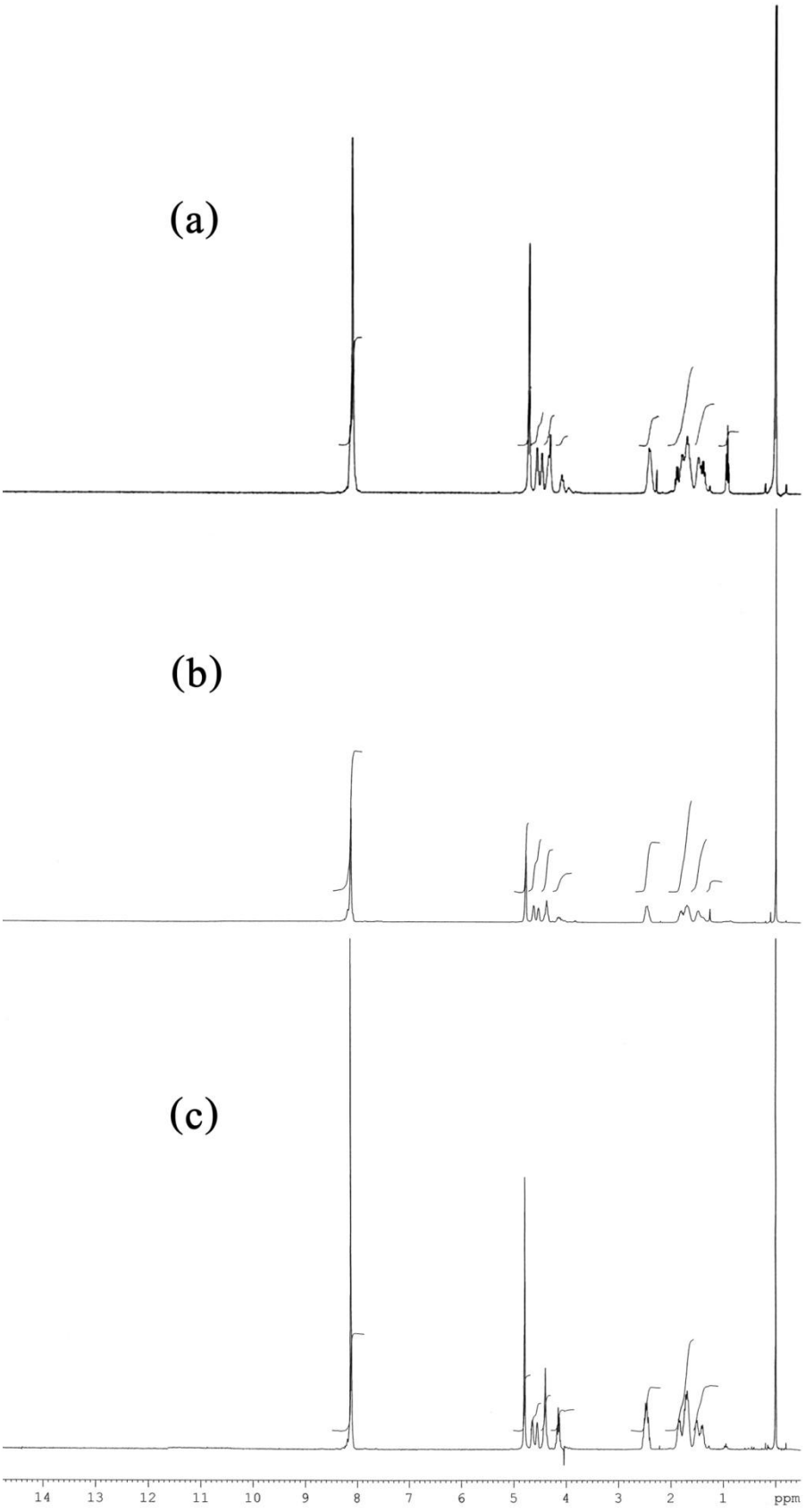

Figure C-13 ^{1}H-NMR spectra of copolymer with 60 %mol ET content ring-opening polymerized at 180 °C (a), 200 °C (b), and 230 °C (c) for 24 hr

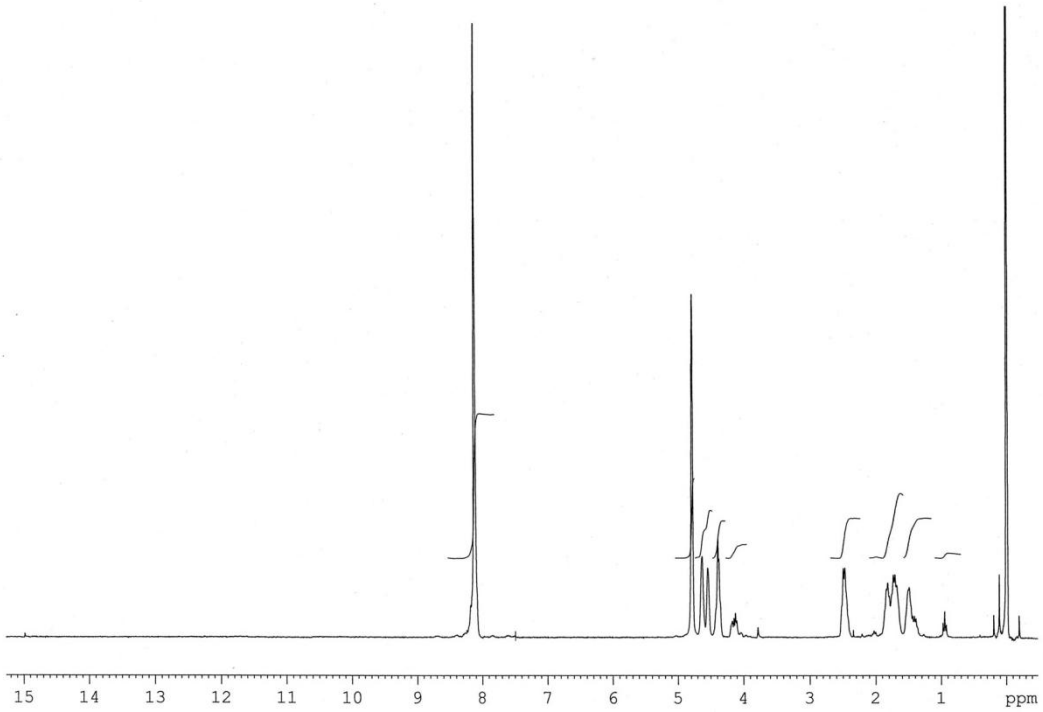

Figure C-14 ^{1}H-NMR spectrum of copolymer with 60 %mol ET content ring-opening polymerized at 250 °C for 24 hr

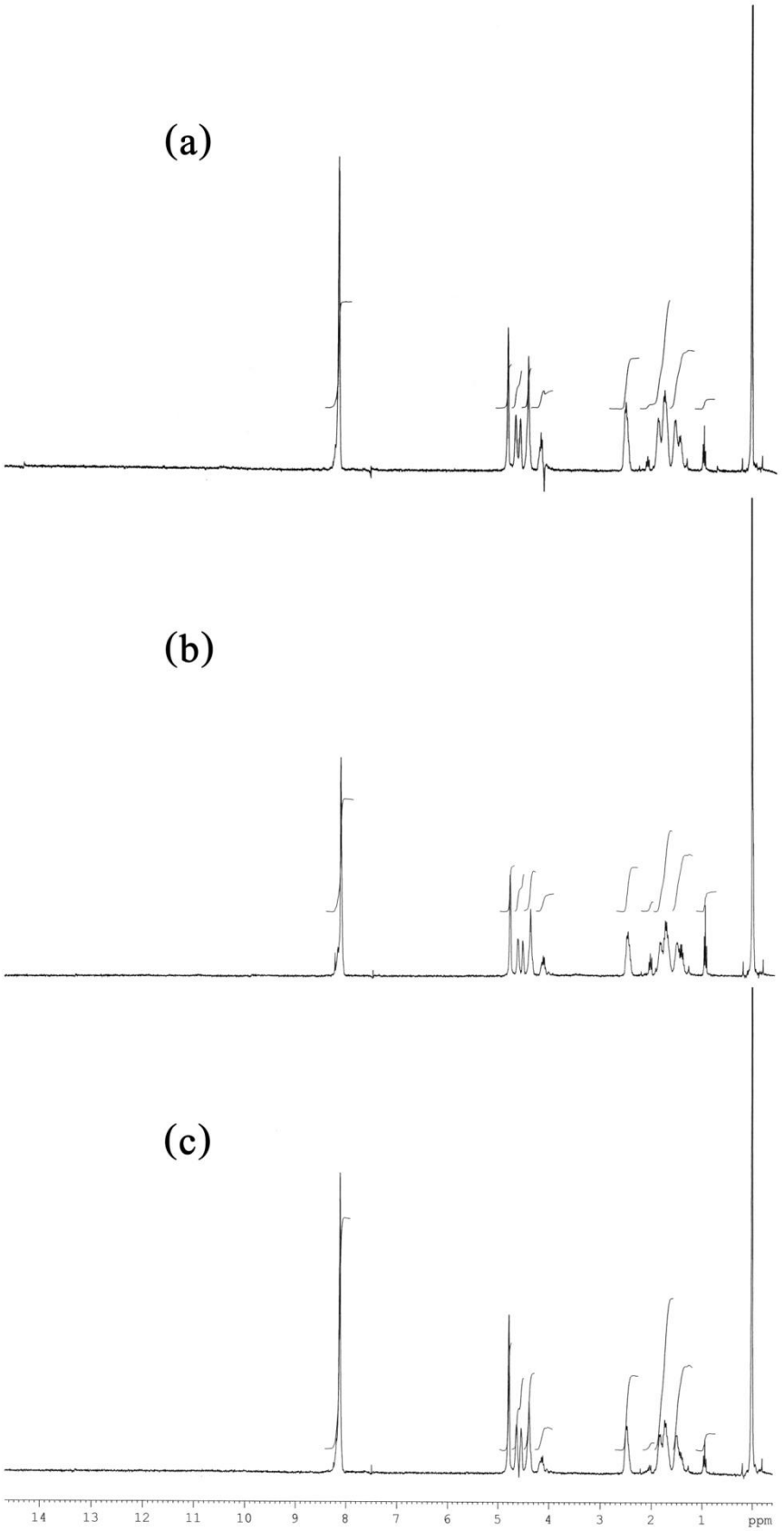

Figure C-15 ^{1}H-NMR spectra of copolymer with 50 %mol ET content ring-opening polymerized at 180 °C (a), 200 °C (b) for 8 hr and at 200 °C (c) for 24 hr

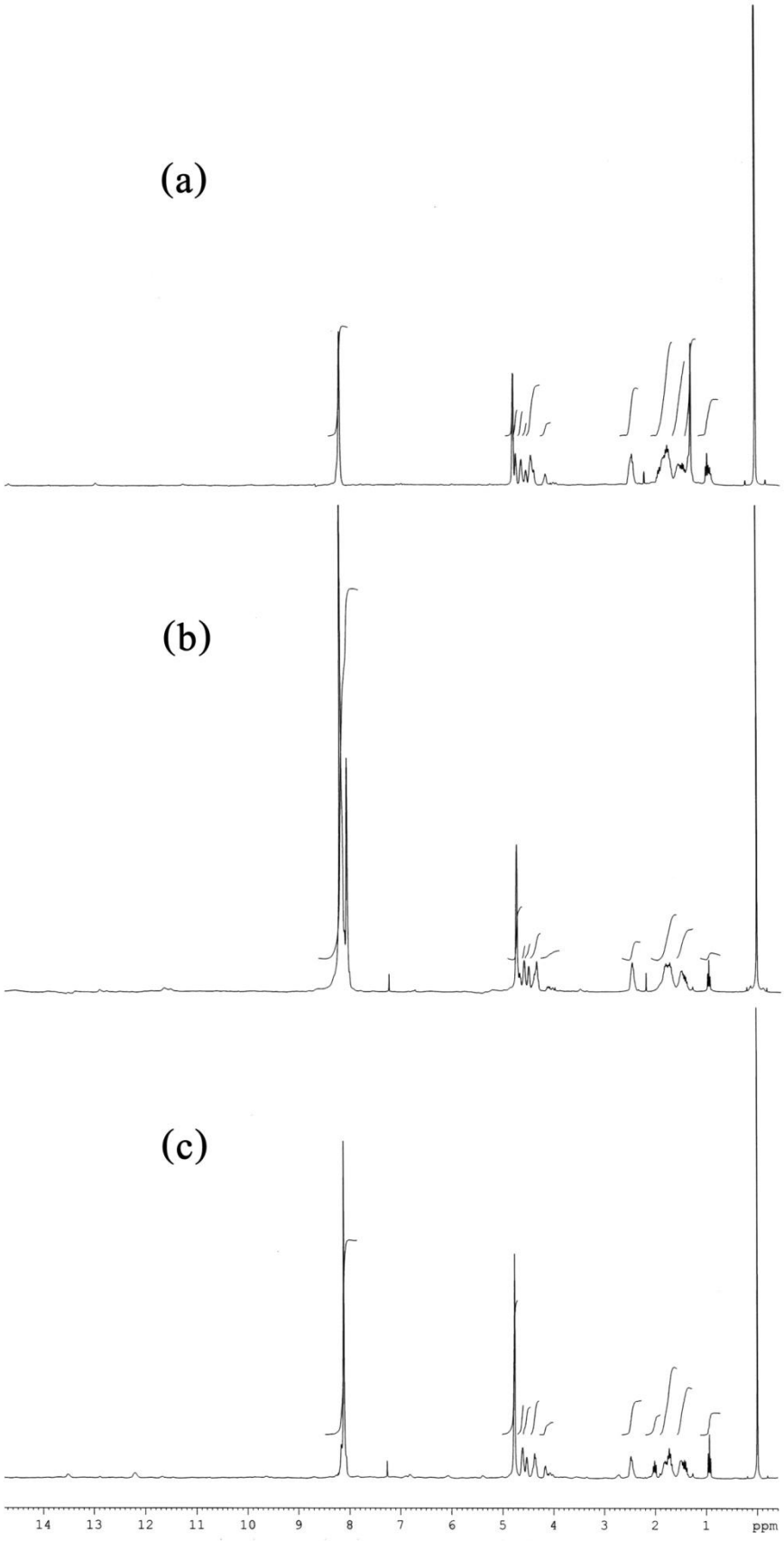

Figure C-16 ^{1}H-NMR spectra of PET-*co*-PCL copolymers with 60 (a), 70 (b) and 80 (c) %mol ET content in the composite with 50 %wt CS which ring-opening polymerized at 180 °C for 24 hr

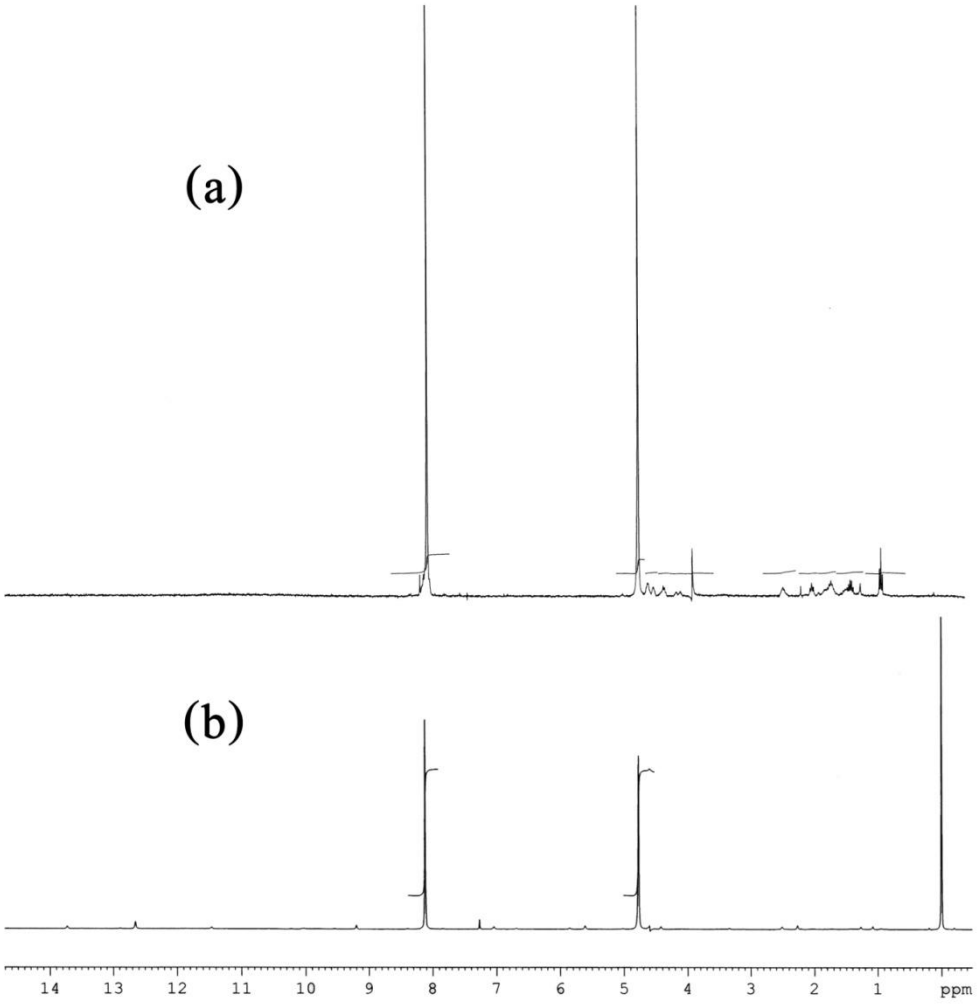

Figure C-17 ^{1}H-NMR spectra of PET-*co*-PCL copolymers with 90 (a) and 100 (b) %mol ET content in the composites with 50 %wt CS which ring-opening polymerized at 180 °C for 24 hr

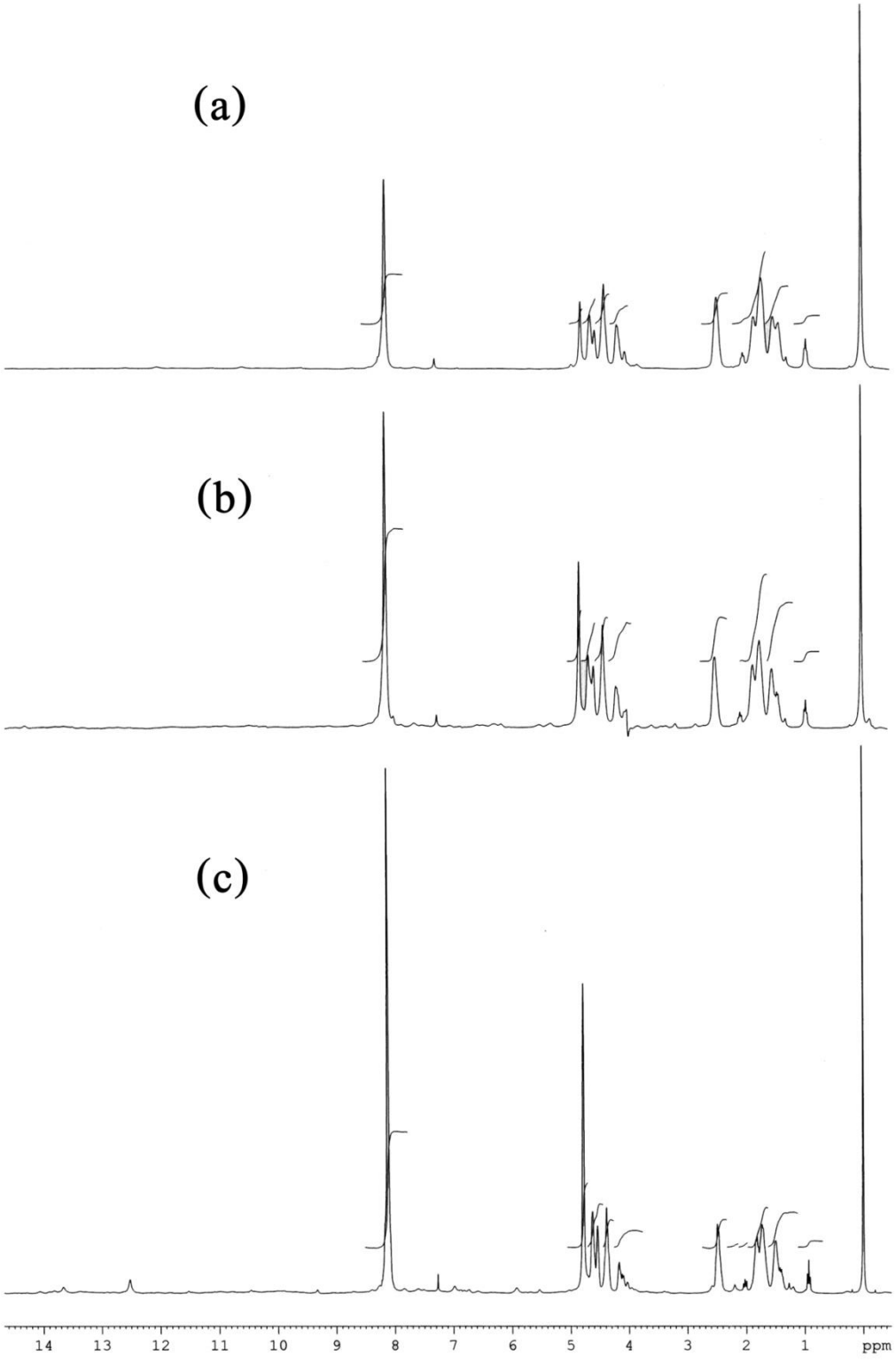

Figure C-18 ^{1}H-NMR spectra of PET-*co*-PCL copolymers with 50 (a), 60 (b) and 70 (c) %mol ET content in the composites with 50 %wt CS which ring-opening polymerized at 200 °C for 24 hr

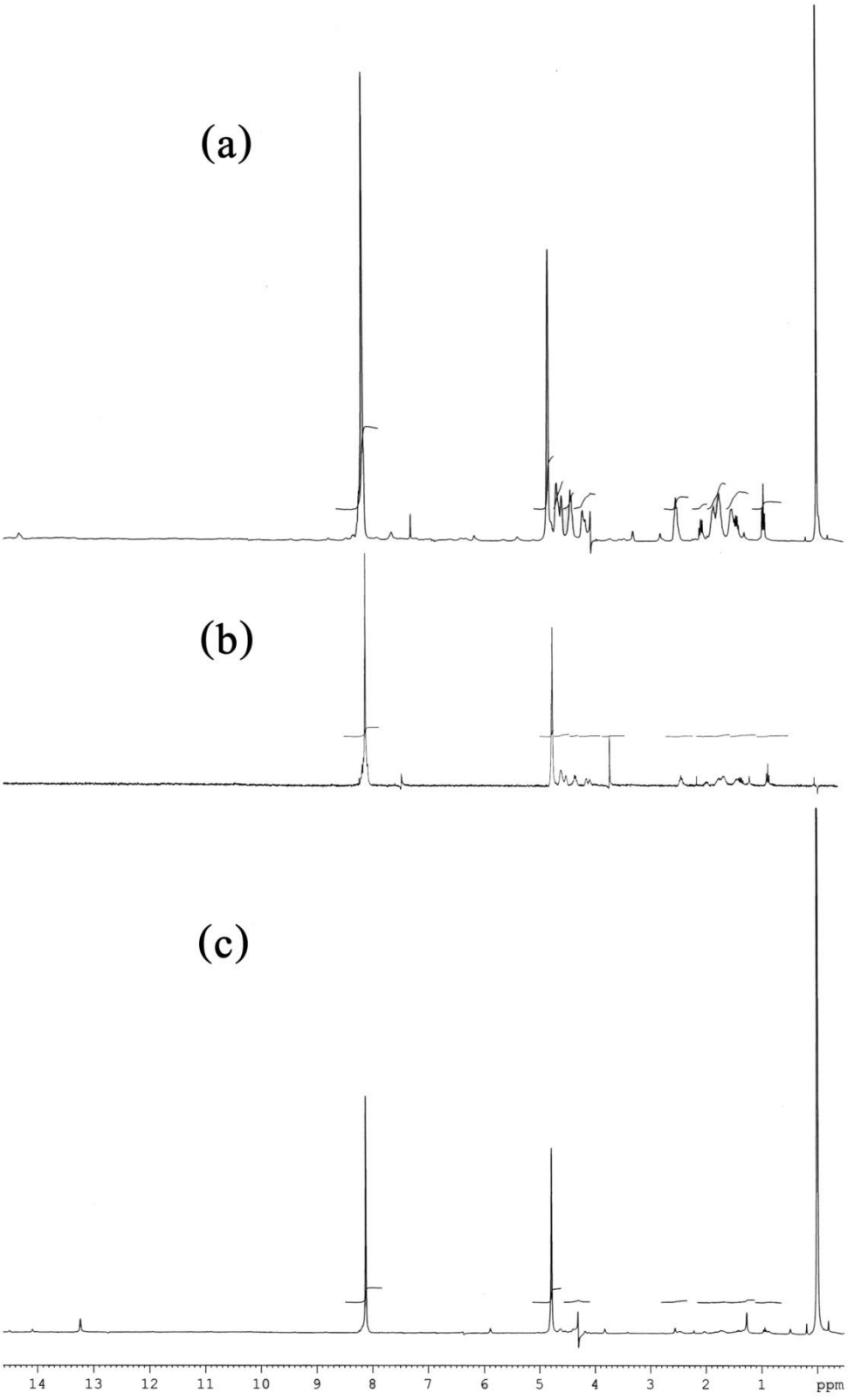

Figure C-19 ^{1}H-NMR spectra of PET-*co*-PCL copolymers with 80 (a), 90 (b) and 100 (c) %mol ET content in the composite with 50 %wt CS which ring-opening polymerized at 200 °C for 24 hr

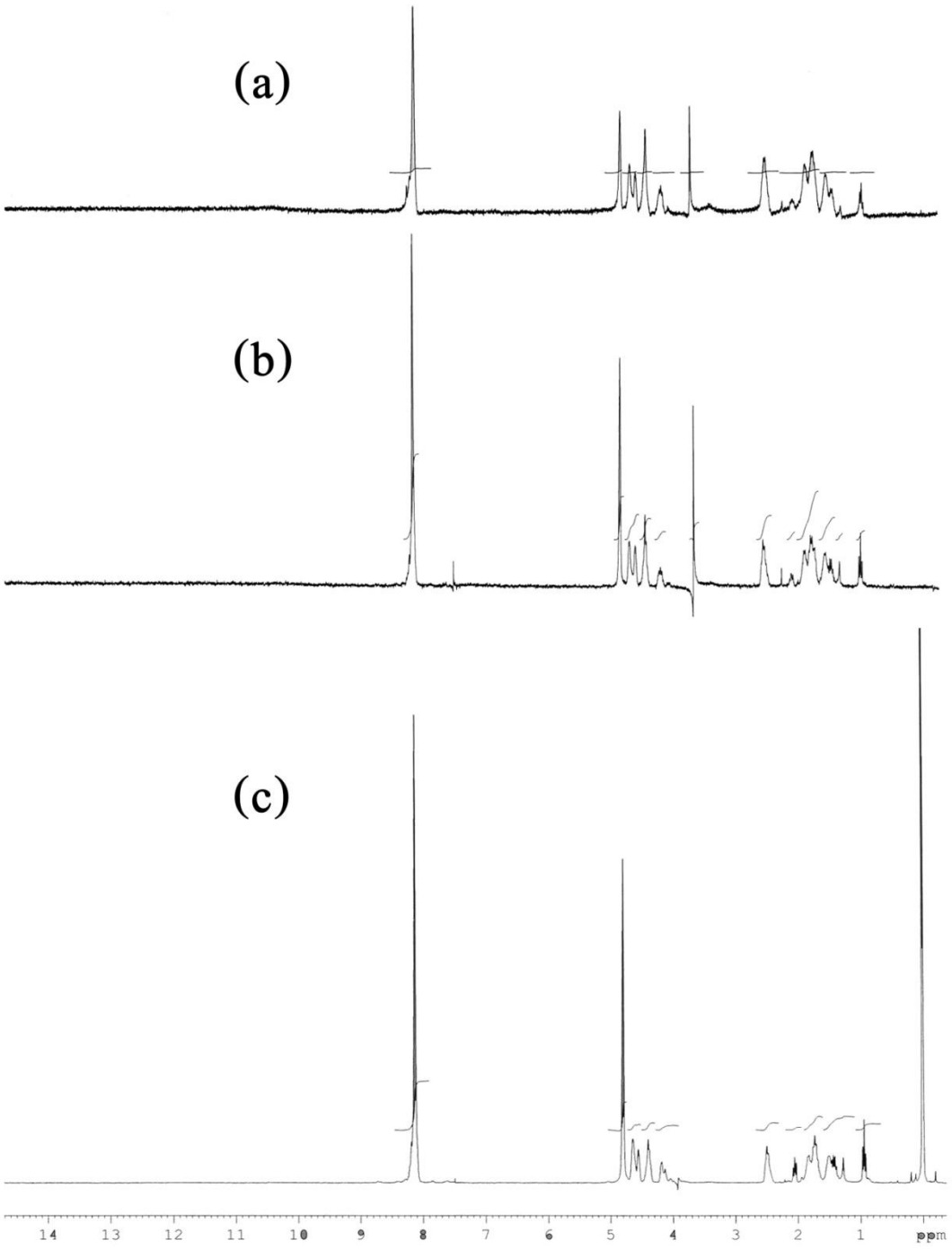

Figure C-20 ^{1}H-NMR spectra of PET-*co*-PCL copolymers with 50 (a), 60 (b) and 70 (c) %mol ET content in the composites with 60 %wt CS which ring-opening polymerized at 180 °C for 24 hr

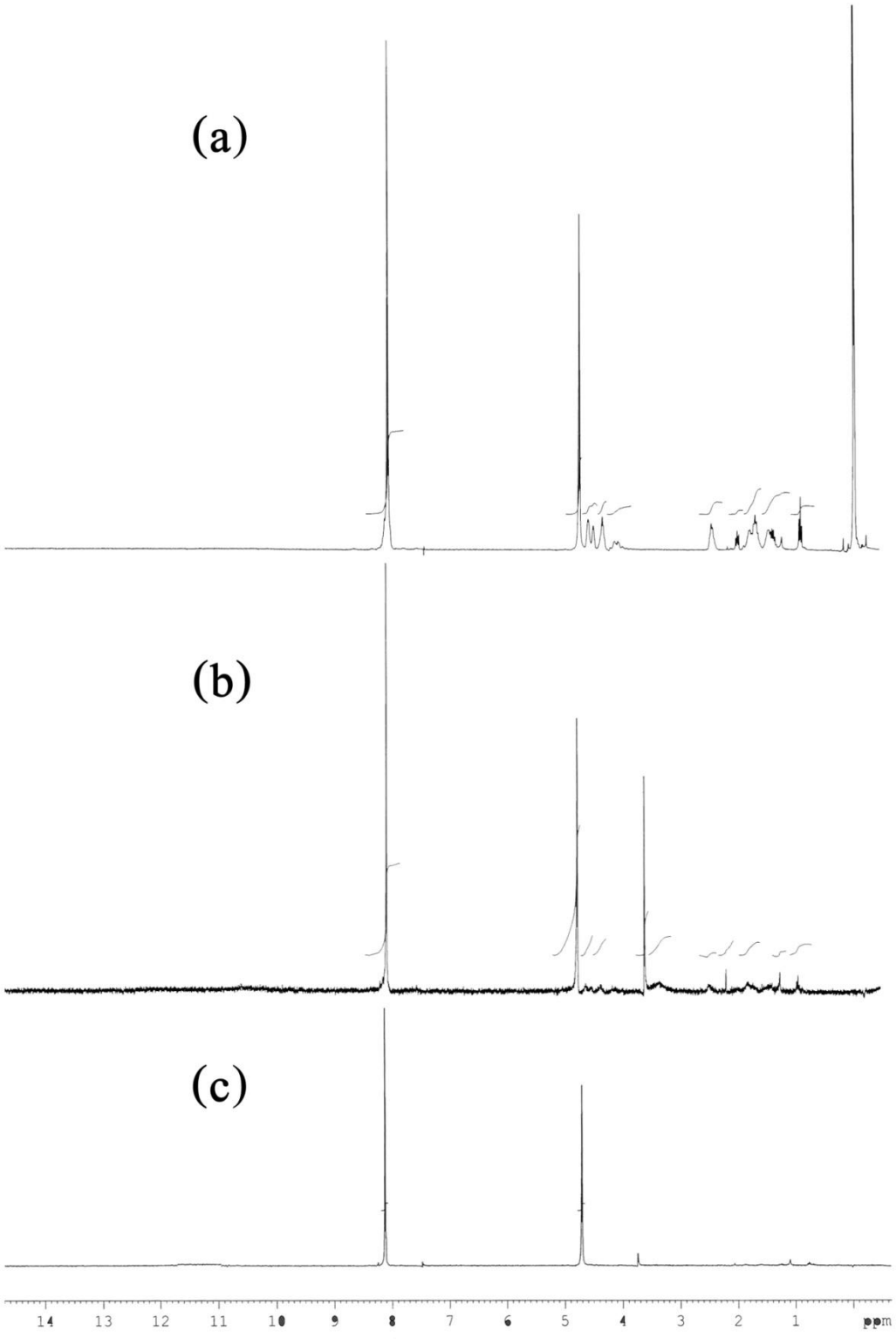

Figure C-21 ^{1}H-NMR spectra of PET-*co*-PCL copolymers with 80 (a), 90 (b) and 100 (c) %mol ET content in the composites with 60 %wt CS which ring-opening polymerized at 180 °C for 24 hr

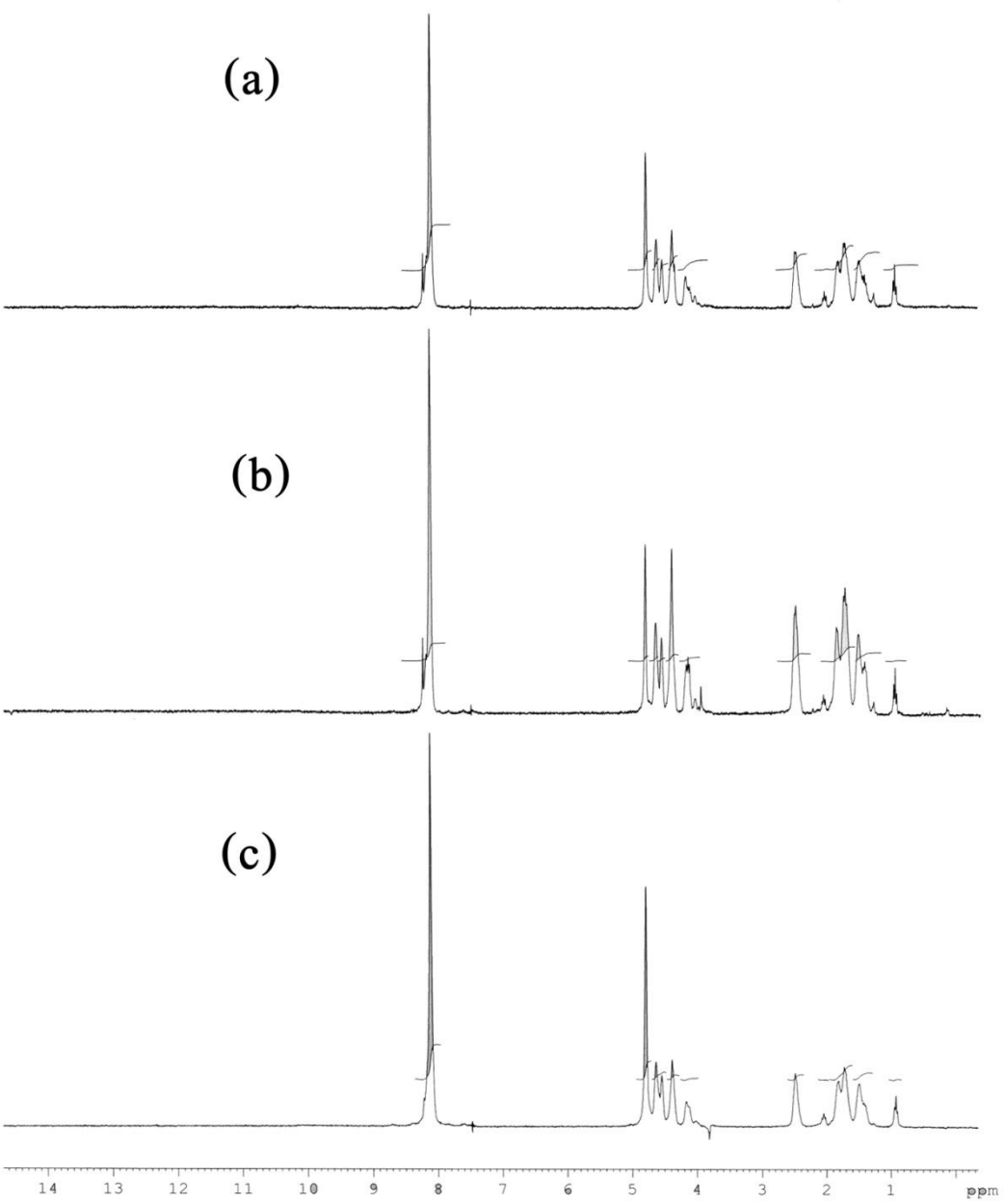

Figure C-22 ^{1}H-NMR spectra of PET-*co*-PCL copolymers with 50 (a), 60 (b) and 70 (c) %mol ET content in the composites with 60 %wt CS which ring-opening polymerized at 200 °C for 24 hr

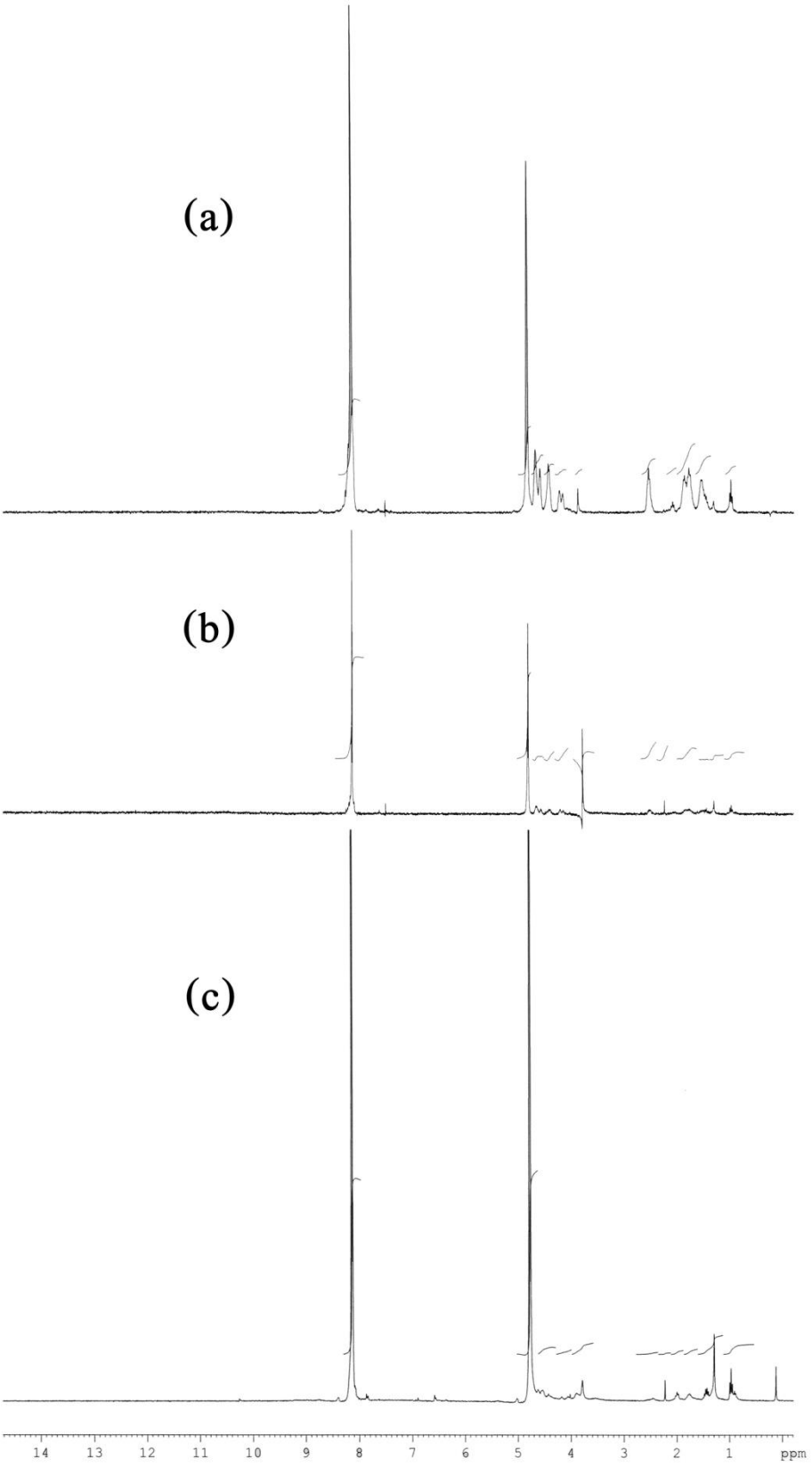

Figure C-23 ^{1}H-NMR spectra of PET-*co*-PCL copolymers with 80 (a), 90 (b) and 100 (c) %mol ET content in the composites with 60 %wt CS which ring-opening polymerized at 200 °C for 24 hr

Table C-1 Chemical shift integration of calcium silicate/poly(ethylene terephthalate-co-caprolactone) composites (CS/PET-co-PCL)

Sample	Chemical shift integration (%mol)			
	HO-ET1 δ 4.8 ppm	CO-ETCL2 δ 4.6 ppm	CO-ETCL1 δ 4.4 ppm	HO-CL4 δ 4.2 ppm
S50-E9C1-180-24	81.3	6.3	6.3	6.3
S50-E8C2-180-24	47.3	20.6	23.5	8.5
S50-E7C3-180-24	35.7	19.2	34.6	10.4
S50-E6C4-180-24	34.9	14.9	39.8	10.5
S50-E5C5-180-24	8.5	18.2	48.3	25.1
S50-E9C1-200-24	55.6	14.8	14.8	14.8
S50-E8C2-200-24	37.1	19.6	23.1	20.3
S50-E7C3-200-24	34.0	22.6	27.7	15.7
S50-E6C4-200-24	20.4	15.3	34.2	30.2
S50-E5C5-200-24	11.2	18.6	43.5	26.7
S60-E9C1-180-24	70.9	11.0	18.2	0.0
S60-E8C2-180-24	54.0	7.6	23.2	15.2
S60-E7C3-180-24	51.3	8.4	25.2	15.1
S60-E6C4-180-24	35.7	21.4	28.6	14.3
S60-E5C5-180-24	19.0	23.8	38.1	19.0
S60-E9C1-200-24	69.2	0.3	12.7	17.8
S60-E8C2-200-24	49.5	19.6	20.6	10.3
S60-E7C3-200-24	54.8	20.5	19.2	5.5
S60-E6C4-200-24	15.8	20.8	43.3	20.0
S60-E5C5-200-24	22.8	21.5	32.9	22.8

Table C-2 Probabilities, sequence length and molecular weight of copolymers in CS/PET-co-PCL composites

Sample	Probabilities of all dyad sequences				L_T	L_C	M_T	M_C
	P_{TT}	P_{TC}	P_{CC}	P_{CT}				
S50-E9C1-180-24	0.93	0.07	0.80	0.20	14.5	5.0	2784.0	570.0
S50-E8C2-180-24	0.68	0.32	0.09	0.91	3.1	1.1	597.9	124.7
S50-E7C3-180-24	0.90	0.10	0.00	1.00	9.6	0.8	1843.6	95.4
S50-E6C4-180-24	0.36	0.64	0.26	0.74	1.6	1.2	298.3	153.4
S50-E5C5-180-24	0.10	0.90	0.29	0.71	1.1	1.4	213.6	161.4
S50-E9C1-200-24	0.76	0.24	0.00	1.00	4.3	1.0	816.0	114.0
S50-E8C2-200-24	0.62	0.38	0.00	1.00	2.7	0.8	509.9	89.7
S50-E7C3-200-24	0.59	0.41	0.13	0.87	2.4	1.2	464.1	130.9
S50-E6C4-200-24	0.53	0.47	0.27	0.73	2.1	1.4	410.0	155.4
S50-E5C5-200-24	0.14	0.86	0.31	0.69	1.2	1.5	223.5	165.7
S60-E9C1-180-24	0.71	0.29	0.00	1.00	3.4	0.1	654.8	15.6
S60-E8C2-180-24	0.81	0.19	0.31	0.69	5.1	1.5	985.0	165.2
S60-E7C3-180-24	0.81	0.19	0.33	0.67	5.4	1.5	1027.2	171.0
S60-E6C4-180-24	0.65	0.35	0.42	0.58	2.9	1.7	548.6	195.4
S60-E5C5-180-24	0.28	0.72	0.35	0.65	1.4	1.5	265.9	175.4
S60-E9C1-200-24	0.92	0.08	0.76	0.24	12.4	4.3	2370.7	485.0
S60-E8C2-200-24	0.74	0.26	0.39	0.61	3.8	1.6	728.6	187.1
S60-E7C3-200-24	0.81	0.19	0.28	0.72	5.2	1.4	993.1	157.2
S60-E6C4-200-24	0.31	0.69	0.20	0.80	1.5	1.3	279.3	142.1
S60-E5C5-200-24	0.48	0.52	0.26	0.74	1.9	1.4	366.1	153.8

APPENDIX D

DIFFERENTIAL SCANNING CALORIMETER

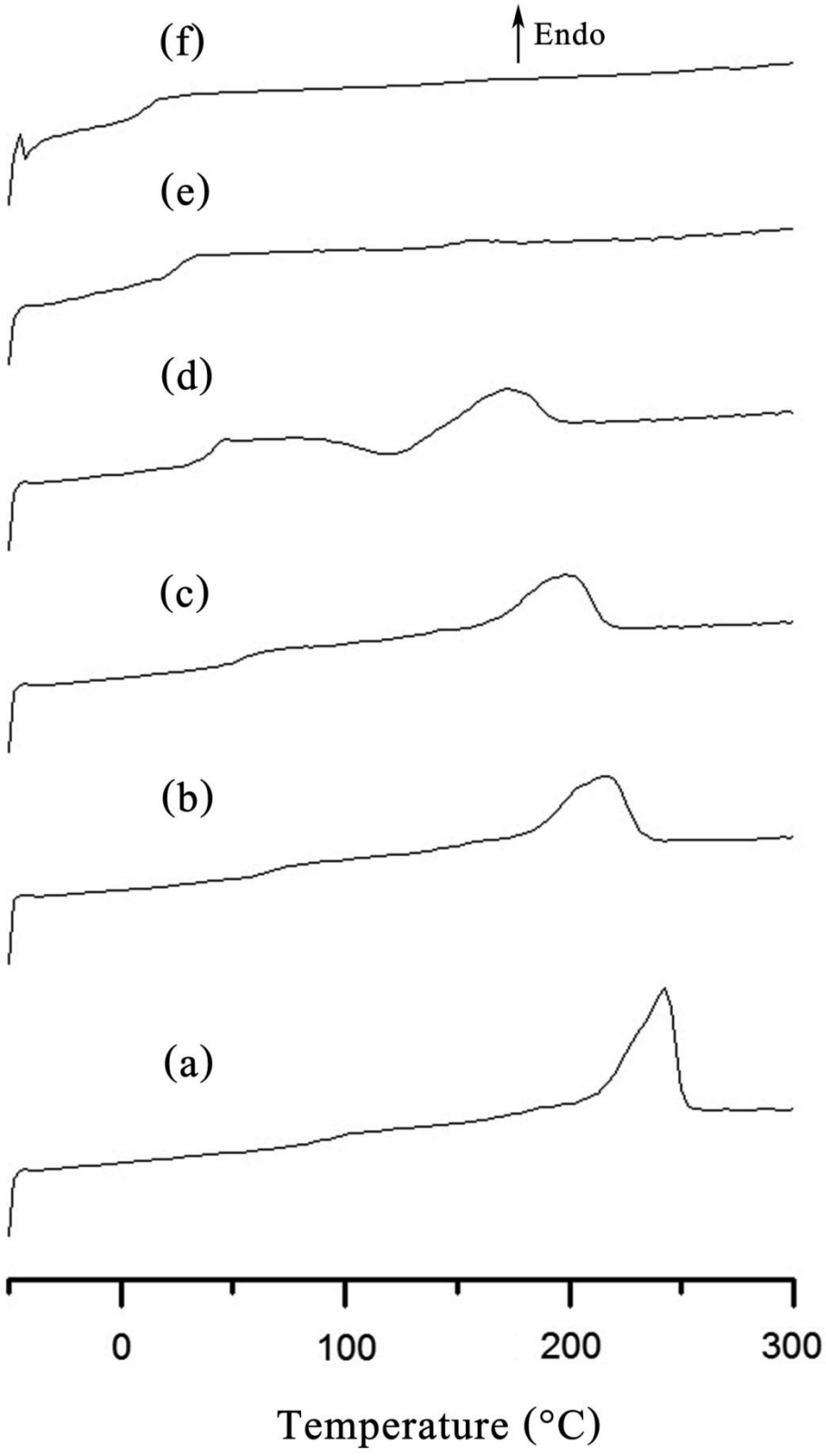

Figure D-1 Second heating DSC thermograms of PET-*co*-PCL copolymers (E10C0-180-8 (a), E9C1-180-8 (b), E8C2-180-8 (c), E7C3-180-8 (d), E6C4-180-8 (e) and E5C5-180-8 (f))

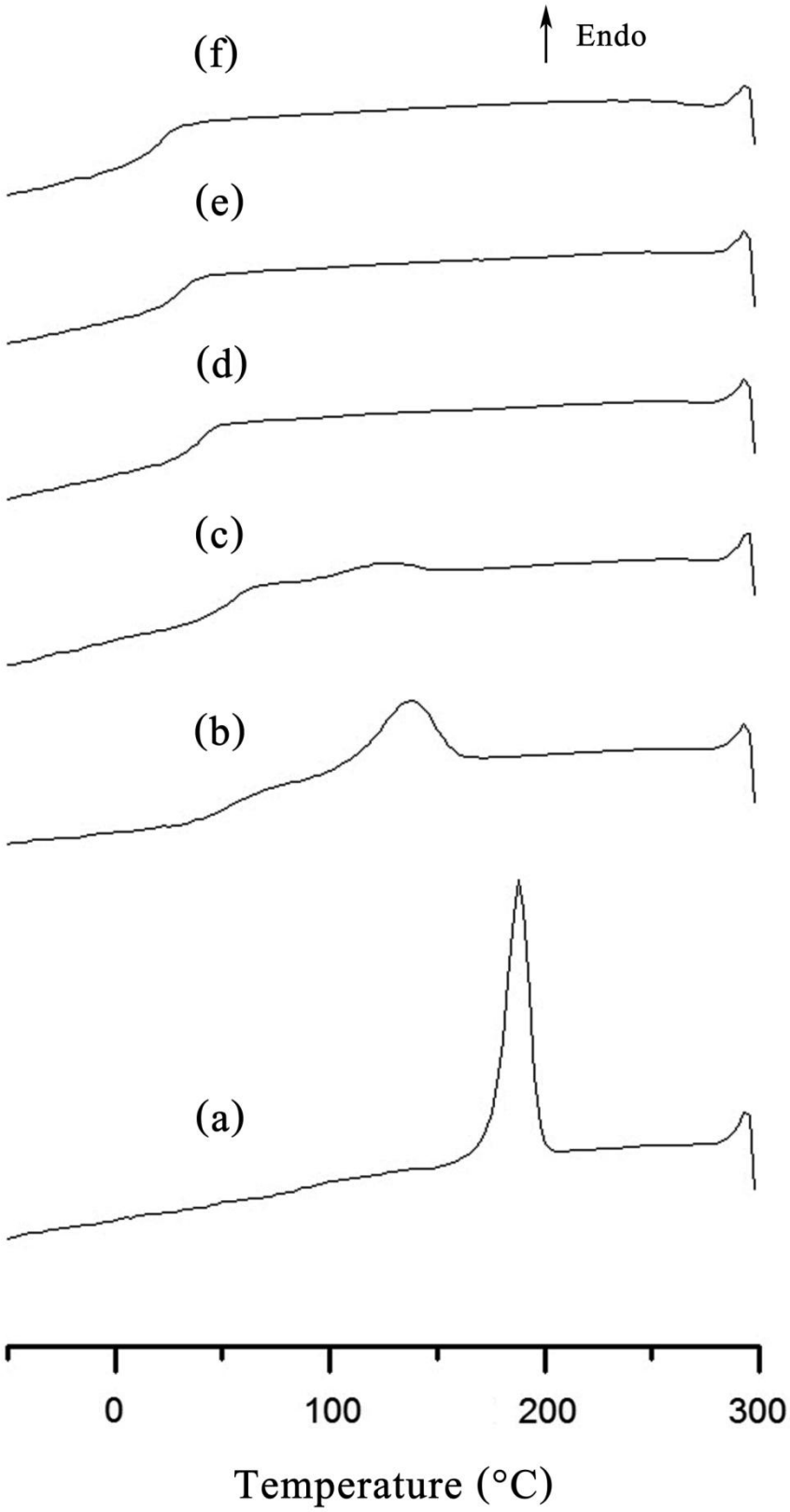

Figure D-2 Second heating DSC thermograms of PET-*co*-PCL copolymers (E10C0-180-24 (a), E9C1-180-24 (b), E8C2-180-24 (c), E7C3-180-24 (d), E6C4-180-24 (e) and E5C5-180-24 (f))

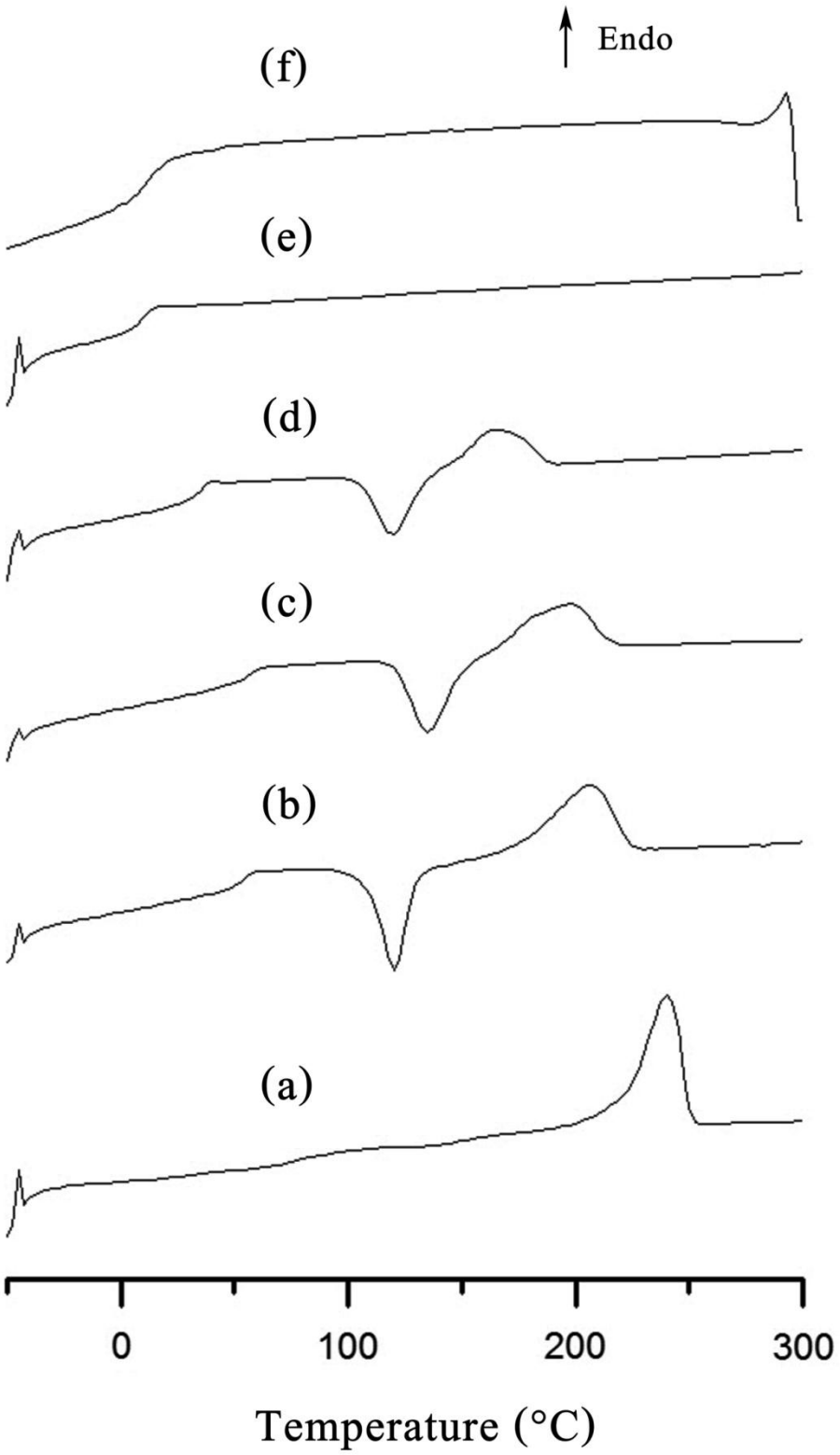

Figure D-3 Second heating DSC thermograms of PET-*co*-PCL copolymers (E10C0-200-8 (a), E9C1-200-8 (b), E8C2-200-8 (c), E7C3-200-8 (d), E6C4-200-8 (e) and E5C5-200-8 (f))

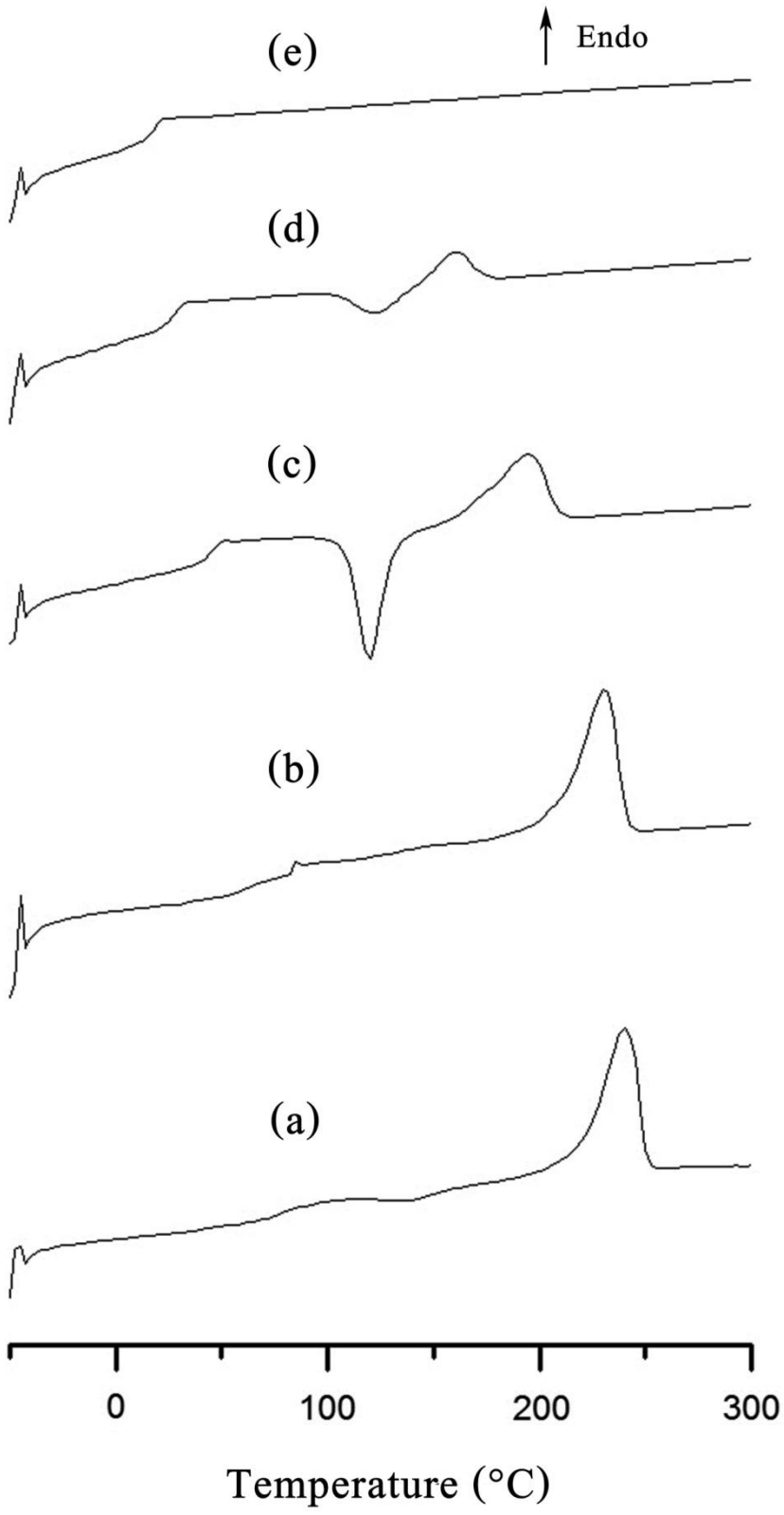

Figure D-4 Second heating DSC thermograms of PET-*co*-PCL copolymers (E10C0-230-8 (a), E9C1-230-8 (b), E8C2-230-8 (c), E7C3-230-8 (d) and E6C4-230-8 (e))

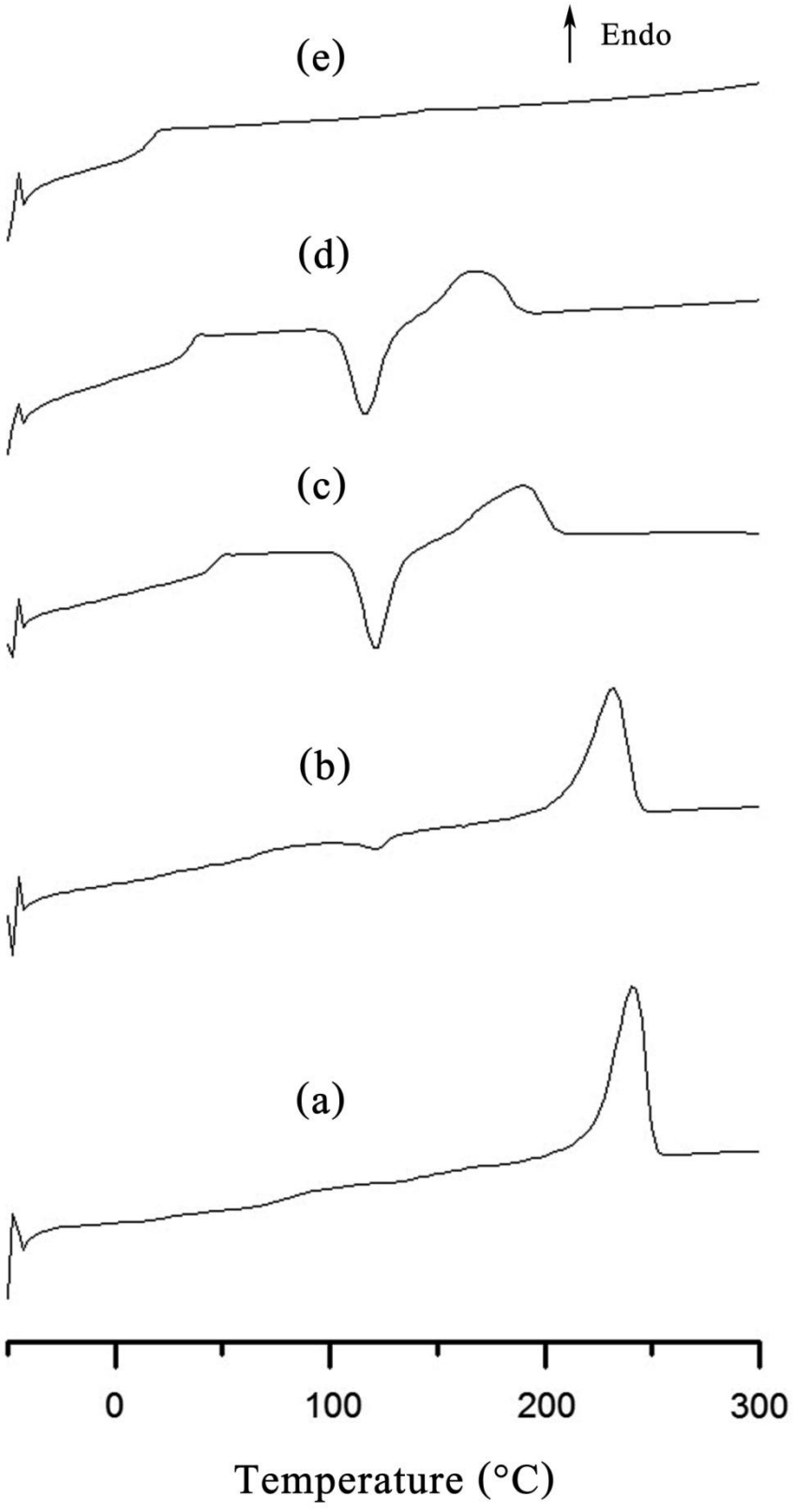

Figure D-5 Second heating DSC thermograms of PET-*co*-PCL copolymers (E10C0-230-24 (a), E9C1-230-24 (b), E8C2-230-24 (c), E7C3-230-24 (d) and E6C4-230-24 (e))

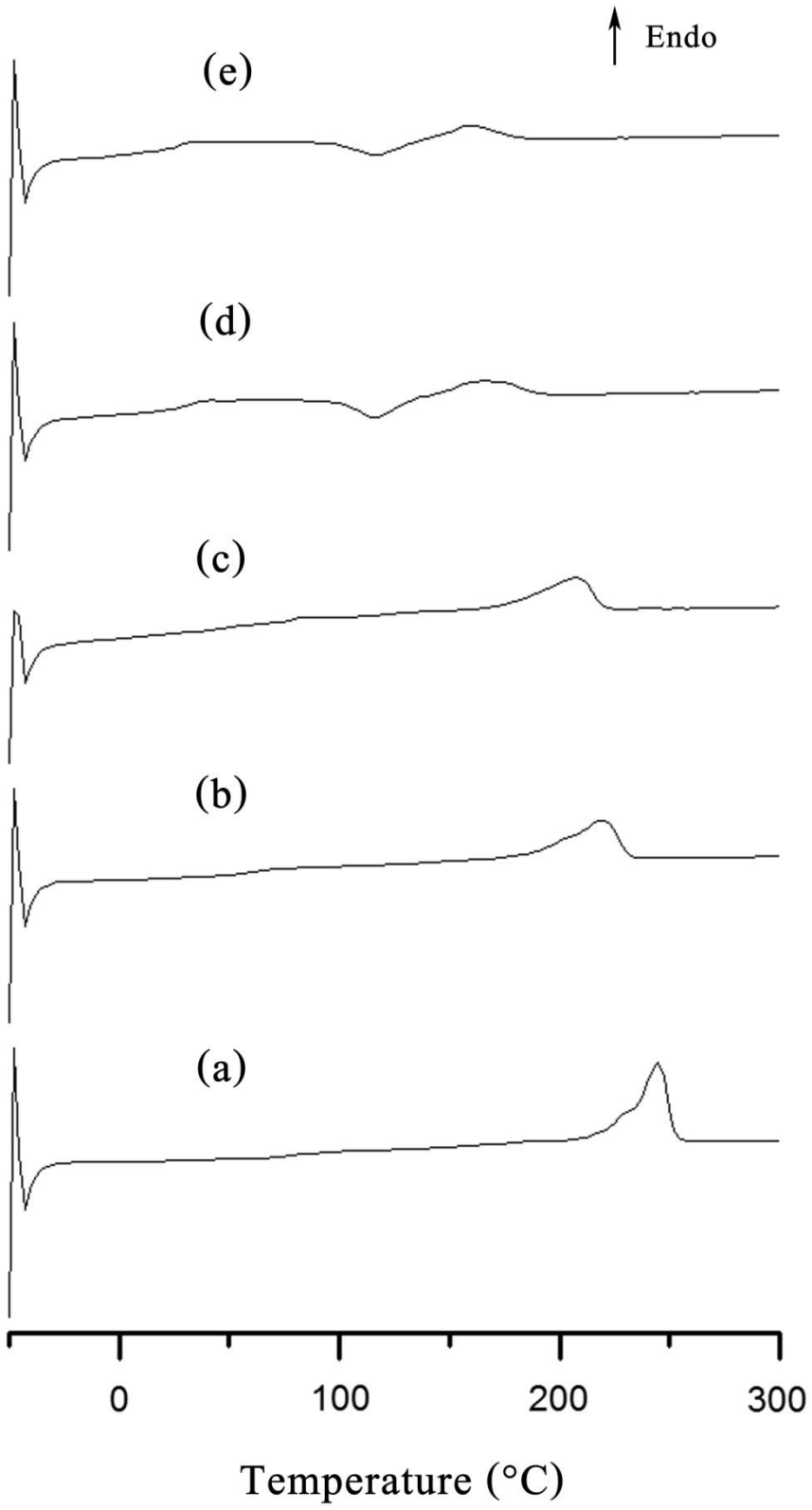

Figure D-6 Second heating DSC thermograms of PET-*co*-PCL copolymers (E10C0-250-24 (a), E9C1-250-24 (b), E8C2-250-24 (c), E7C3-250-24 (d) and E6C4-250-24 (e))

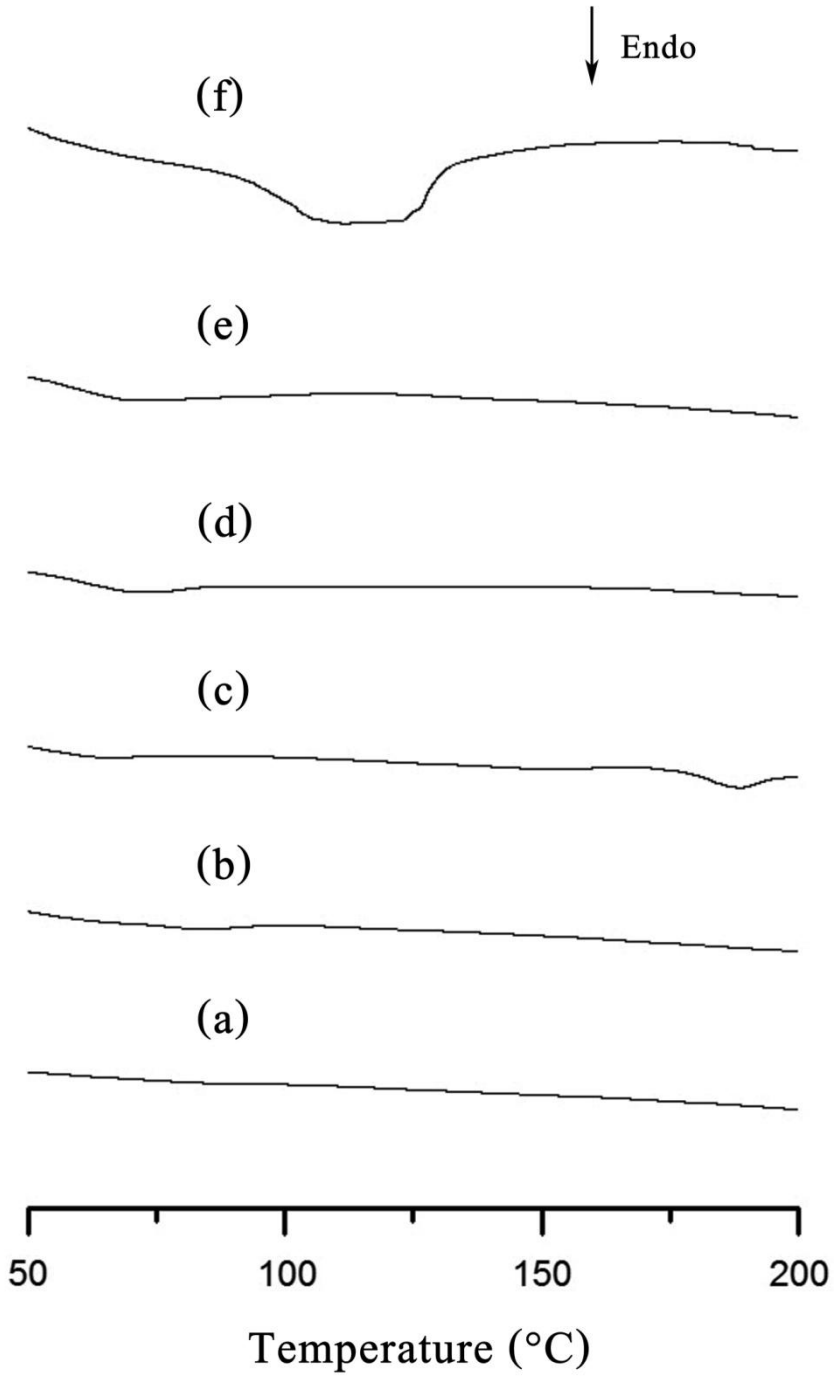

Figure D-7 DSC thermograms of S50-E10C0-200-24 (a), S50-E9C1-200-24 (b), S50-E8C2-200-24 (c), S50-E7C3-200-24 (d), S50-E6C4-200-24 (e) and S50-E5C5-200-24 (f) composites before annealing (1st heating)

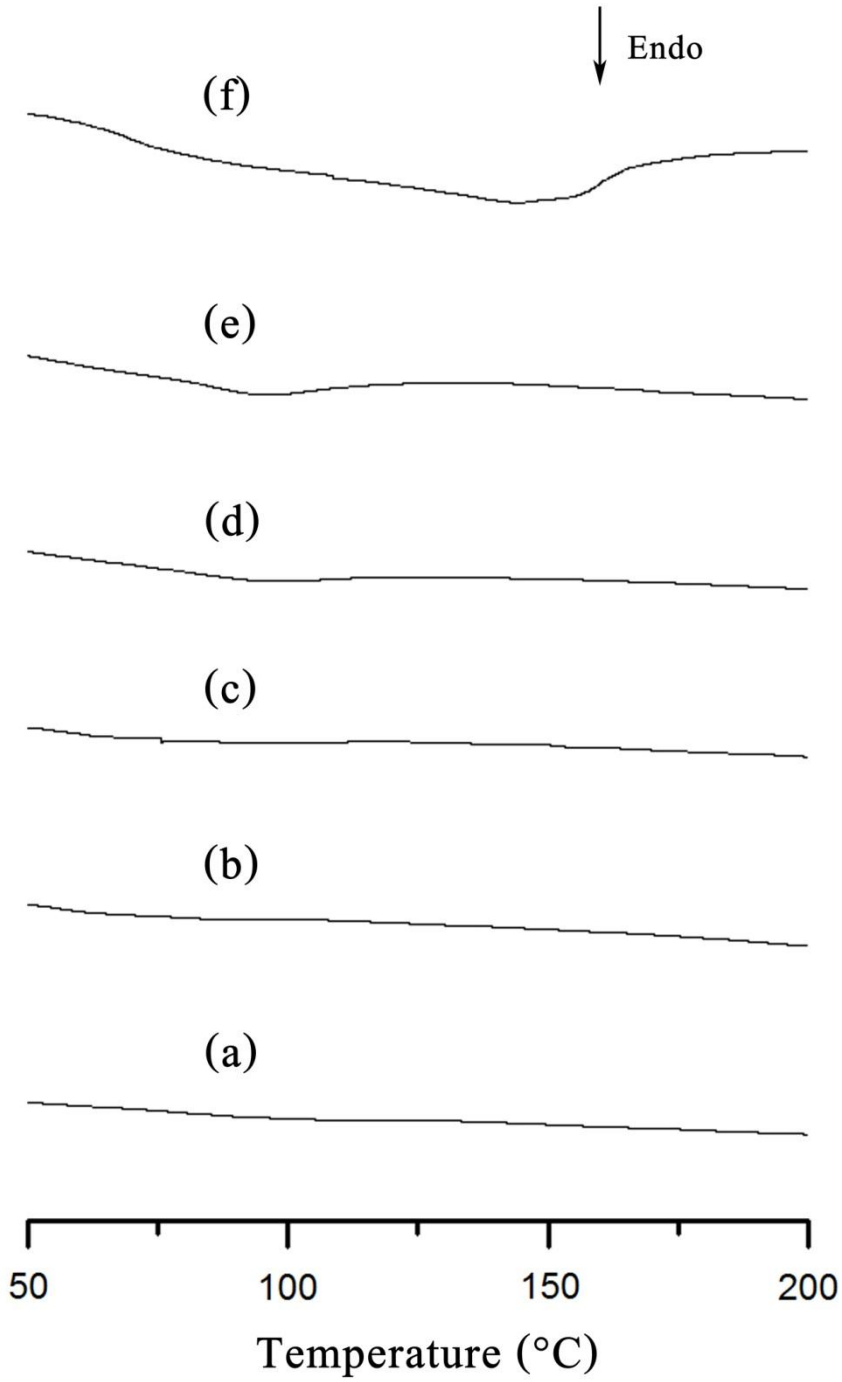

Figure D-8 DSC thermograms of S60-E10C0-180-24 (a), S60-E9C1-180-24 (b), S60-E8C2-180-24 (c), S60-E7C3-180-24 (d), S60-E6C4-180-24 (e) and S60-E5C5-180-24 (f) composites before annealing (1st heating)

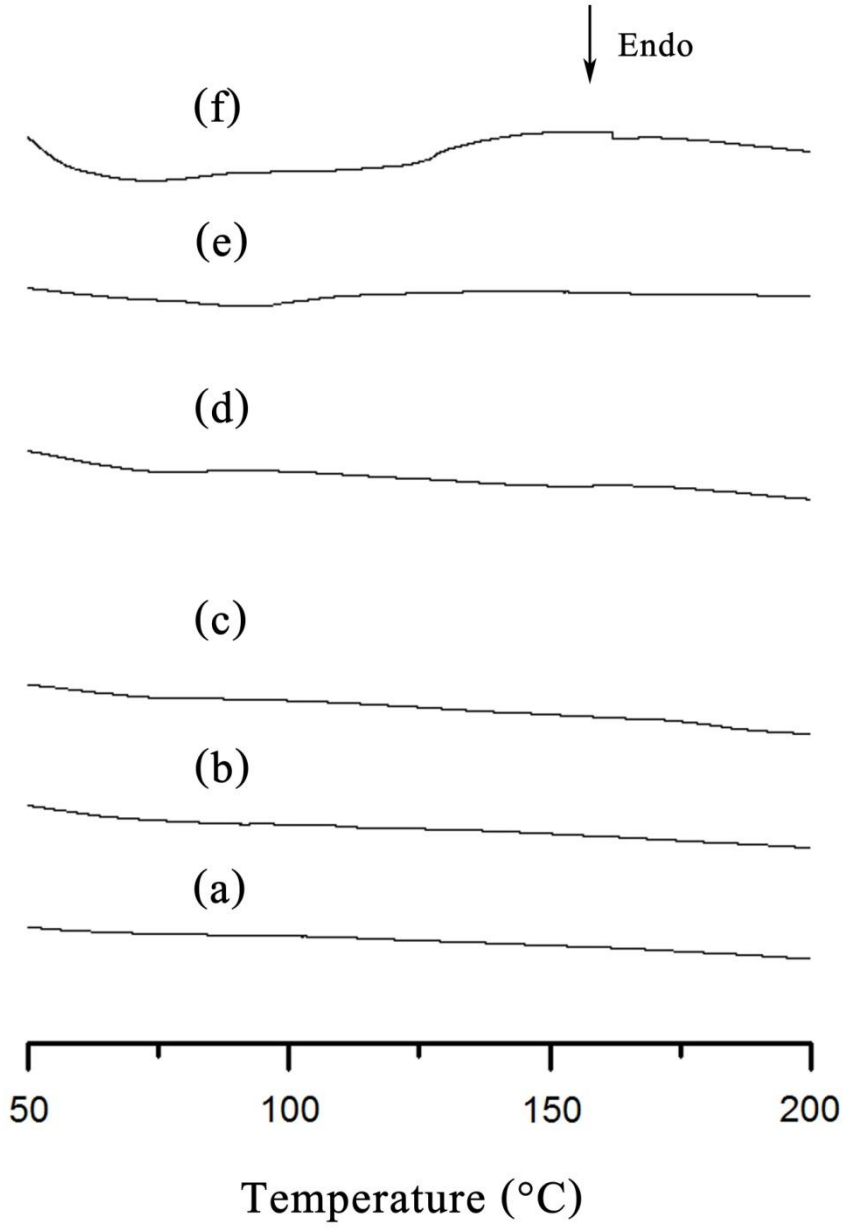

Figure D-9 DSC thermograms of S60-E10C0-200-24 (a), S60-E9C1-200-24 (b), S60-E8C2-200-24 (c), S60-E7C3-200-24 (d), S60-E6C4-200-24 (e) and S60-E5C5-200-24 (f) composites before annealing (1st heating)

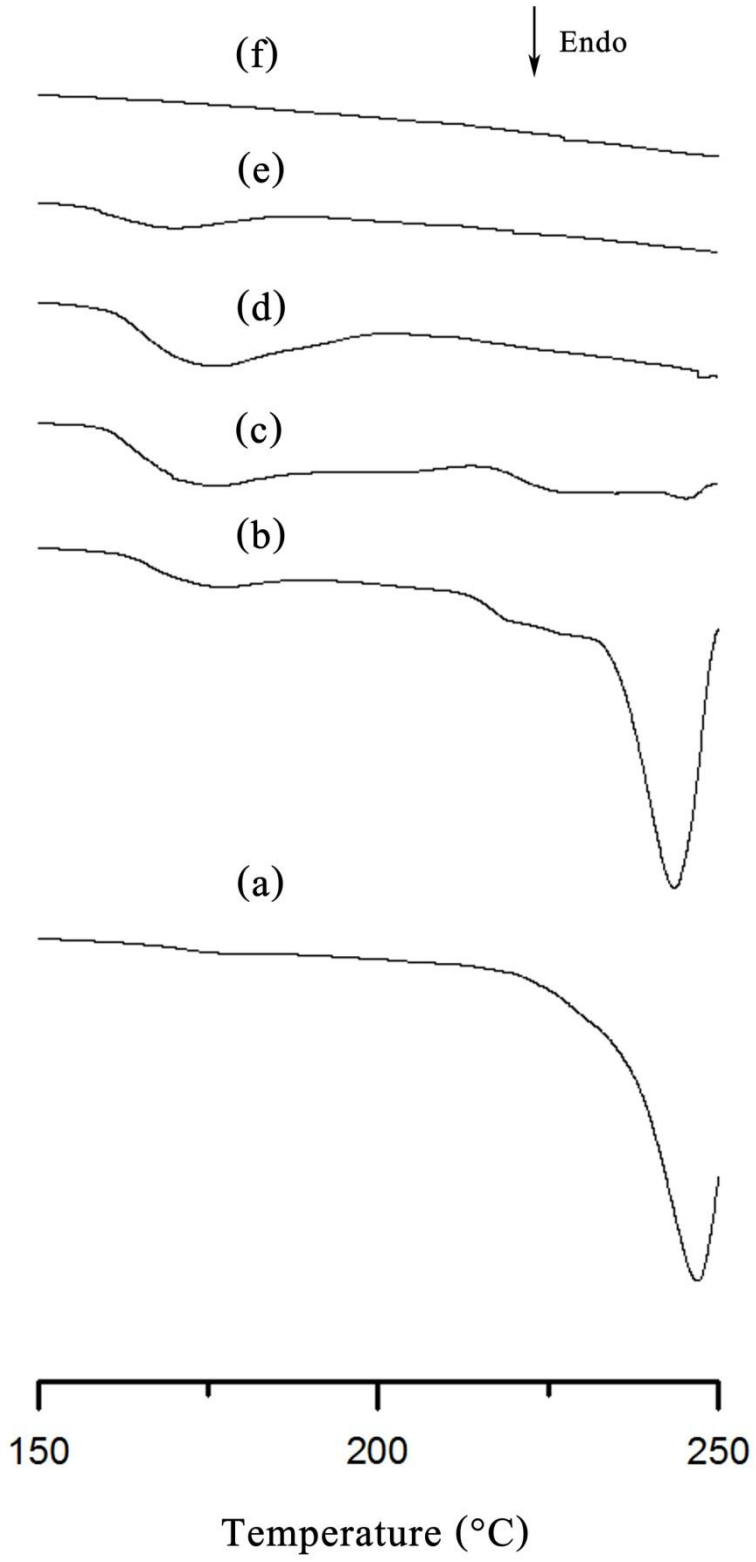

Figure D-10 DSC thermograms of S50-E10C0-200-24 (a), S50-E9C1-200-24 (b), S50-E8C2-200-24 (c), S50-E7C3-200-24 (d), S50-E6C4-200-24 (e) and S50-E5C5-200-24 (f) composites after annealing (1st heating)

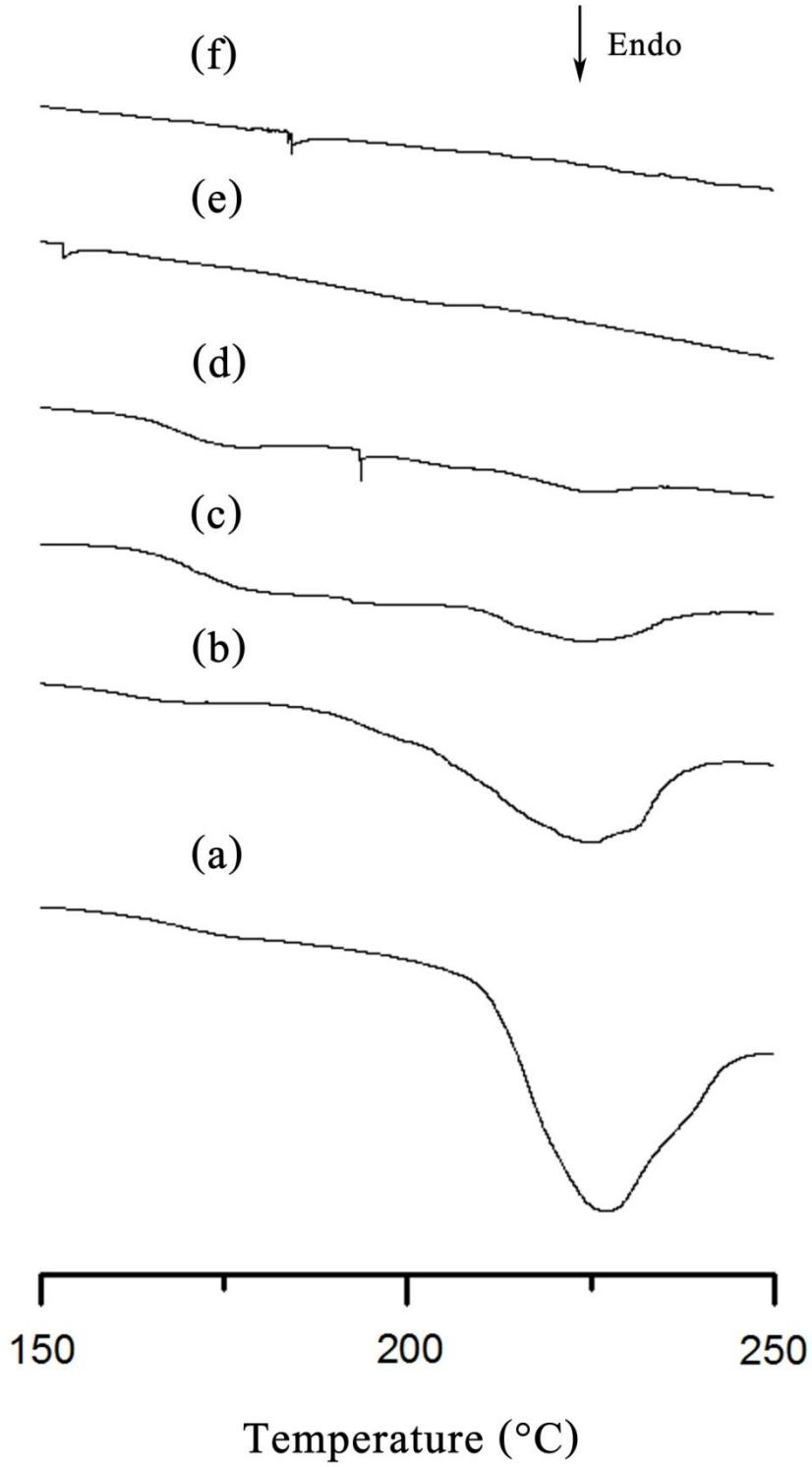

Figure D-11 DSC thermograms of S60-E10C0-180-24 (a), S60-E9C1-180-24 (b), S60-E8C2-180-24 (c), S60-E7C3-180-24 (d), S60-E6C4-180-24 (e) and S60-E5C5-180-24 (f) composites after annealing (1st heating)

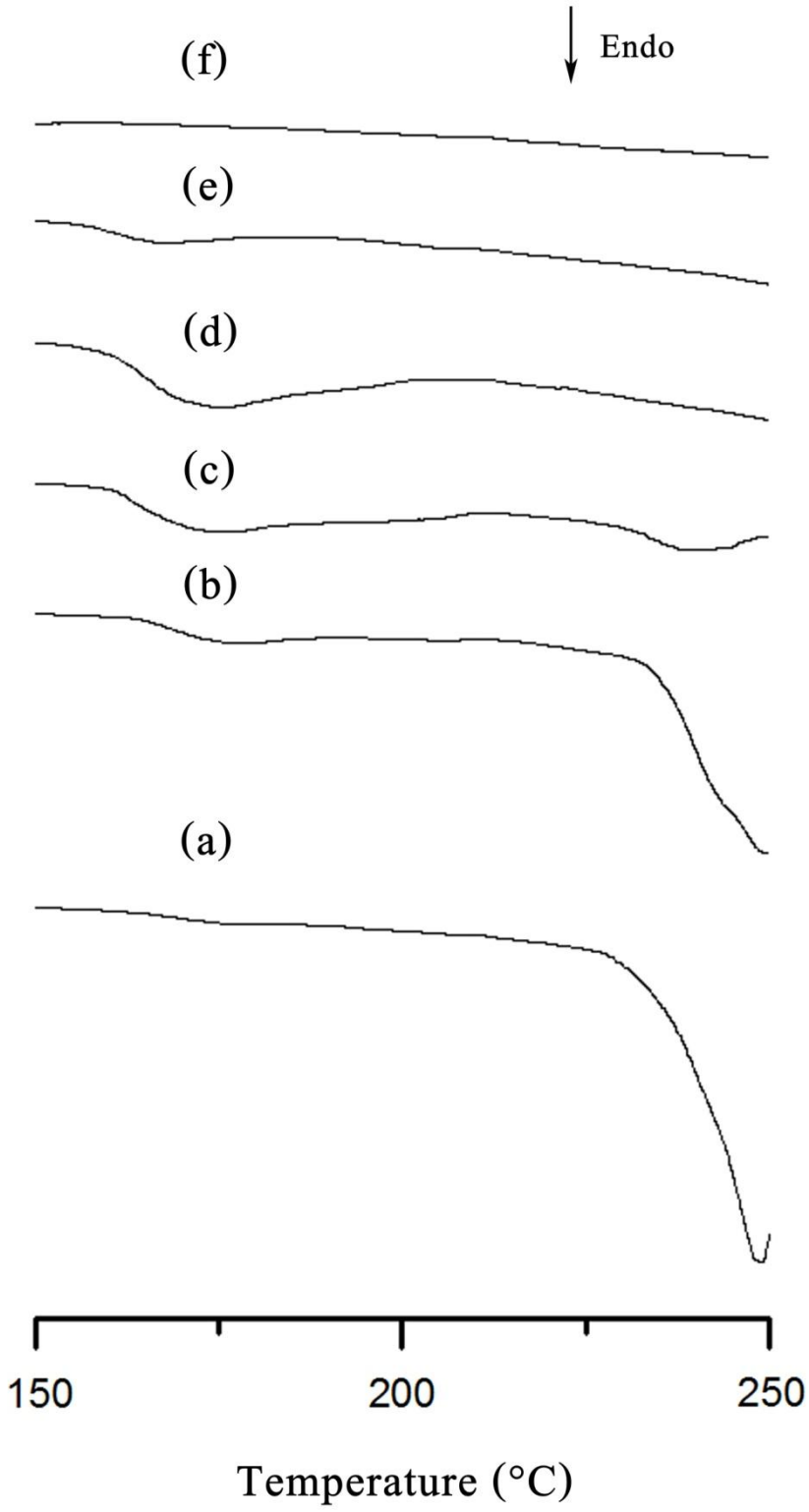

Figure D-12 DSC thermograms of S60-E10C0-200-24 (a), S60-E9C1-200-24 (b), S60-E8C2-200-24 (c), S60-E7C3-200-24 (d), S60-E6C4-200-24 (e) and S60-E5C5-200-24 (f) composites after annealing (1st heating)

Table D-1 Thermal properties of CS/PET-*co*-PCL composites before and after annealing

Sample	Before annealing							After annealing						
	T_g (°C)	First heating		Second heating		T_c (°C)	ΔH_c (J/g)	T_g (°C)	First heating		Second heating		T_c (°C)	ΔH_c (J/g)
		T_m (°C)	ΔH_m (J/g)	T_m (°C)	ΔH_m (J/g)				T_m (°C)	ΔH_m (J/g)	T_m (°C)	ΔH_m (J/g)		
S60-E10C0-180-24	83.4	217.5	34.7	241.3	26.7	187.1	38.4	78.9	226.0	35.3	240.4	34.3	189.7	55.9
S60-E9C1-180-24	70.2	225.0	28.6	232.9	21.6	174.9	28.2	71.7	167.4 224.5	0.7 22.3	226.1	25.2	173.6	35.0
S60-E8C2-180-24	68.1	221.5	11.7	223.3	10.5	152.3	18.3	63.9	178.2 223.5	1.2 4.9	215.2	16.3	152.5	14.0
S60-E7C3-180-24	60.2	n/a	n/a	206.9	4.7	124.8	5.8	60.7	175.7 224.6	1.7 1.3	205.8	9.9	132.5	6.6
S60-E6C4-180-24	47.8	n/a	n/a	n/a	n/a	n/a	n/a	44.0	n/a	n/a	n/a	n/a	n/a	n/a
S60-E5C5-180-24	38.4	n/a	n/a	n/a	n/a	n/a	n/a	39.3	n/a	n/a	n/a	n/a	n/a	n/a

Table D-1 (cont.)

Sample	Before annealing							After annealing						
	T_g (°C)	First heating		Second heating		T_c (°C)	ΔH_c (J/g)	T_g (°C)	First heating		Second heating		T_c (°C)	ΔH_c (J/g)
		T_m (°C)	ΔH_m (J/g)	T_m (°C)	ΔH_m (J/g)				T_m (°C)	ΔH_m (J/g)	T_m (°C)	ΔH_m (J/g)		
S50-E10C0-200-24	82.6	246.2	46.9	244.7	36.0	194.4	47.8	87.8	235.7	38.9	246.6	36.4	195.2	47.4
S50-E9C1-200-24	73.3	243.2	30.2	228.1	23.4	172.2	28.3	75.8	175.3 243.5	4.2 38.7	227.5	27.0	177.5	44.4
S50-E8C2-200-24	67.6	186.7 232.5	3.5 3.9	206.1	10.2	153.3	14.4	70.0	177.5 223.1	9.3 5.6	216.4	24.4	160.2	21.7
S50-E7C3-200-24	56.6	n/a	n/a	203.1	2.6	134.6	9.5	64.1	175.2	11.8	206.2	11.6	138.3	12.9
S50-E6C4-200-24	52.2	n/a	n/a	n/a	n/a	n/a	n/a	34.7	169.5	3.3	n/a	n/a	n/a	n/a
S50-E5C5-200-24	19.5	n/a	n/a	n/a	n/a	n/a	n/a	25.7	n/a	n/a	n/a	n/a	n/a	n/a

Table D-1 (cont.)

Sample	Before annealing							After annealing						
	T_g (°C)	First heating		Second heating		T_c (°C)	ΔH_c (J/g)	T_g (°C)	First heating		Second heating		T_c (°C)	ΔH_c (J/g)
		T_m (°C)	ΔH_m (J/g)	T_m (°C)	ΔH_m (J/g)				T_m (°C)	ΔH_m (J/g)	T_m (°C)	ΔH_m (J/g)		
S50-E10C0-180-24	82.4	233.5	35.1	242.3	39.3	190.6	50.4	84.8	230.2	34.2	242.4	39.8	203.8	54.1
S50-E9C1-180-24	78.5	224.3	27.8	231.9	25.0	180.5	30.3	79.8	177.0 227.2	1.2 23.9	233.5	25.5	176.8	36.5
S50-E8C2-180-24	63.8	223.1	19.2	206.9	23.9	147.8	18.1	61.6	176.9 222.4	6.5 20.7	207.7	27.6	151.4	27.5
S50-E7C3-180-24	56.0	219.1	1.7	206.1	6.0	132.0	5.8	51.9	175.0 220.9	8.0 4.3	203.5	7.8	139.2	10.5
S50-E6C4-180-24	41.2	215.2	2.1	192.0	1.5	141.4	4.7	41.6	167.6	6.2	190.6	2.3	139.1	9.2
S50-E5C5-180-24	37.7	n/a	n/a	n/a	n/a	n/a	n/a	31.5	n/a	n/a	n/a	n/a	n/a	n/a

APPENDIX E

SCANNING ELECTRON MICROSCOPE

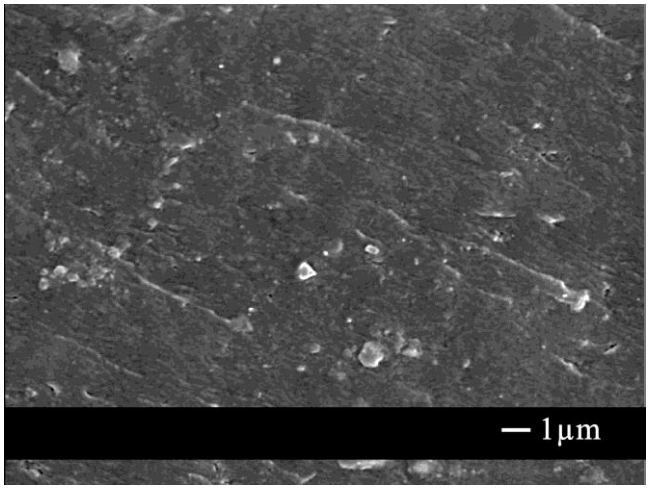

Figure E-1 SEM micrographs of the neat copolymer with 70:30 PET:PCL molar ratio ROP at 180 °C for 24 hr

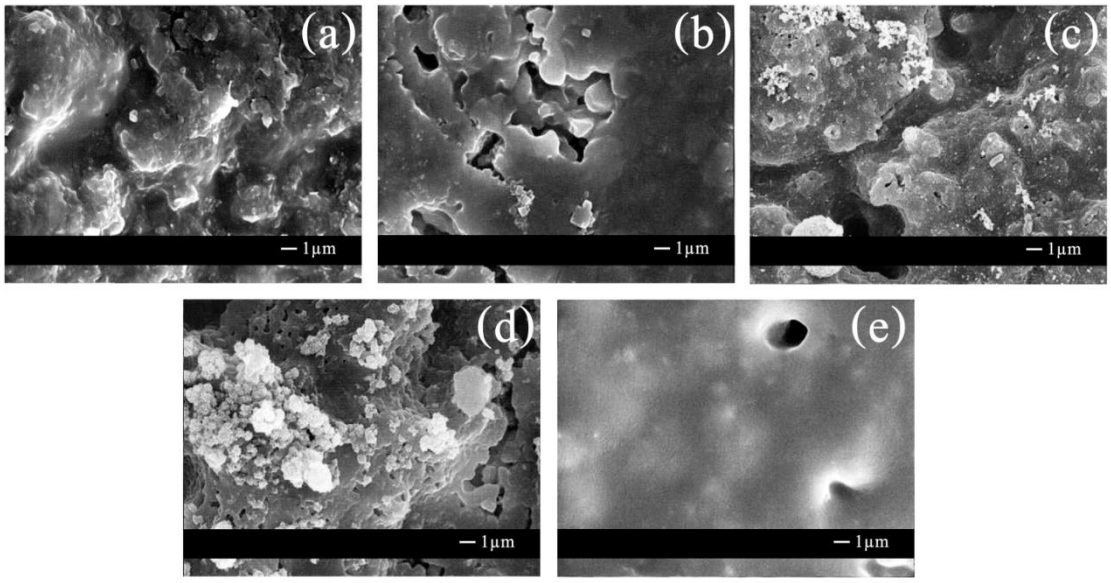

Figure E-2 SEM micrographs of S50-E5C5-180-24 composite before (a) and after soaking in SBF for 7 days (b), 14 days (c), 21 days (d) and 28 days (e)

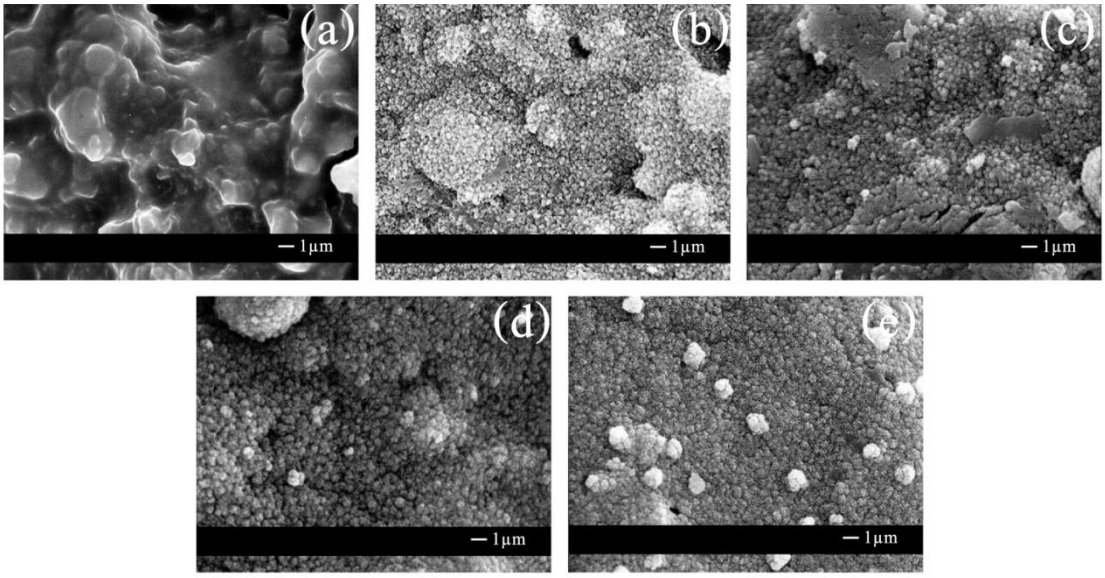

Figure E-3 SEM micrographs of S50-E6C4-180-24 composite before (a) and after soaking in SBF for 7 days (b), 14 days (c), 21 days (d) and 28 days (e)

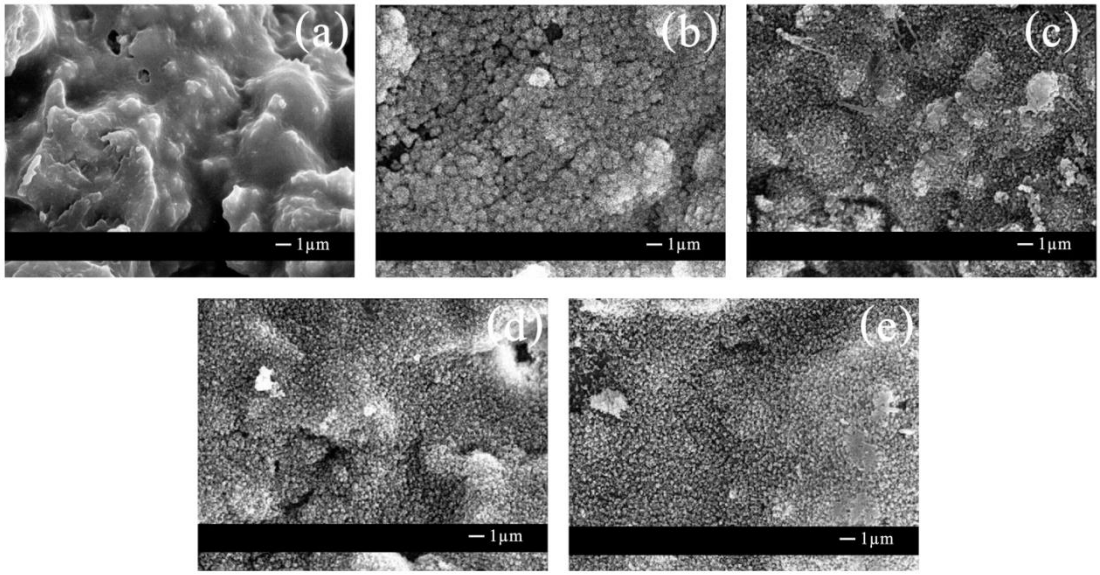

Figure E-4 SEM micrographs of S50-E7C3-180-24 composite before (a) and after soaking in SBF for 7 days (b), 14 days (c), 21 days (d) and 28 days (e)

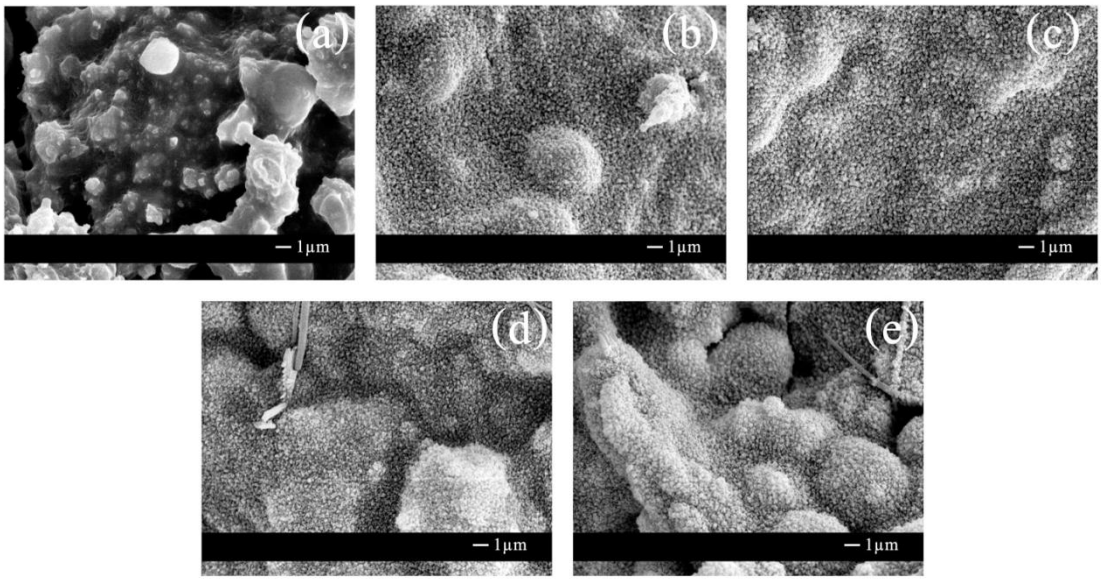

Figure E-5 SEM micrographs of S50-E8C2-180-24 composite before (a) and after soaking in SBF for 7 days (b), 14 days (c), 21 days (d) and 28 days (e)

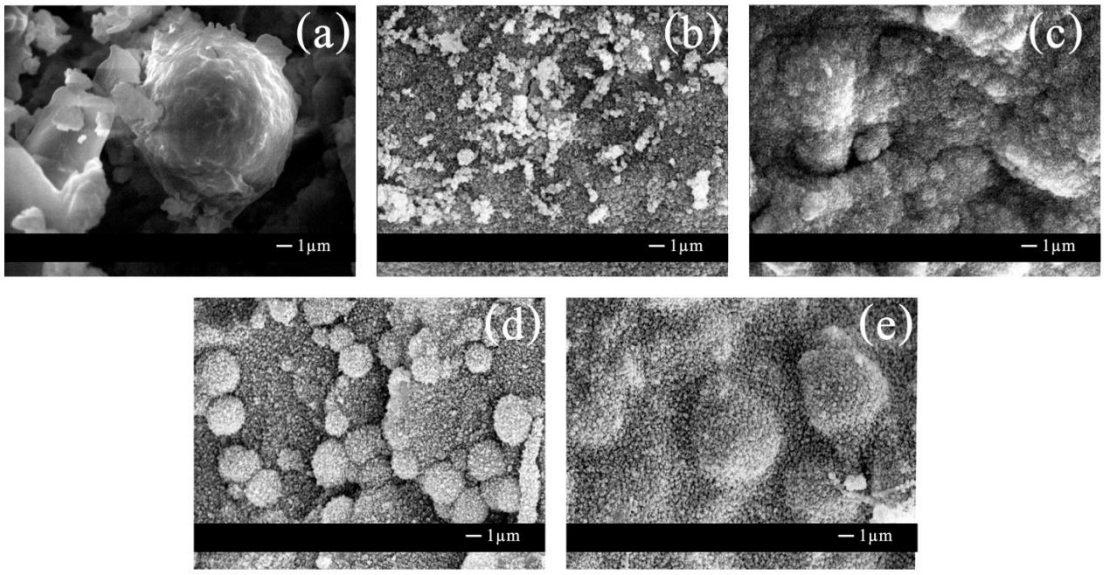

Figure E-6 SEM micrographs of S50-E9C1-180-24 composite before (a) and after soaking in SBF for 7 days (b), 14 days (c), 21 days (d) and 28 days (e)

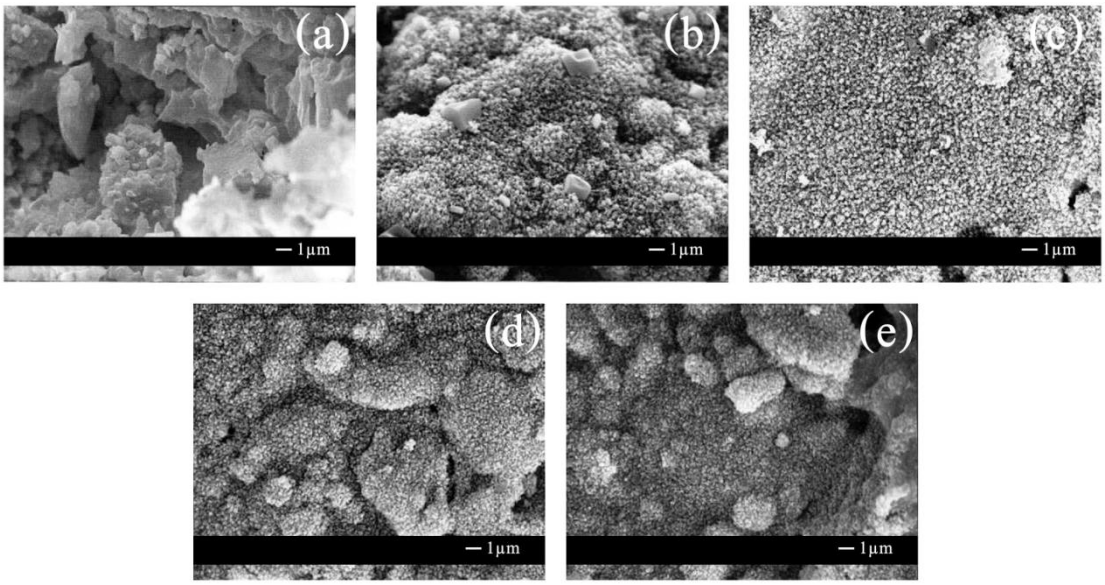

Figure E-7 SEM micrographs of S50-E10C0-180-24 composite before (a) and after soaking in SBF for 7 days (b), 14 days (c), 21 days (d) and 28 days (e)

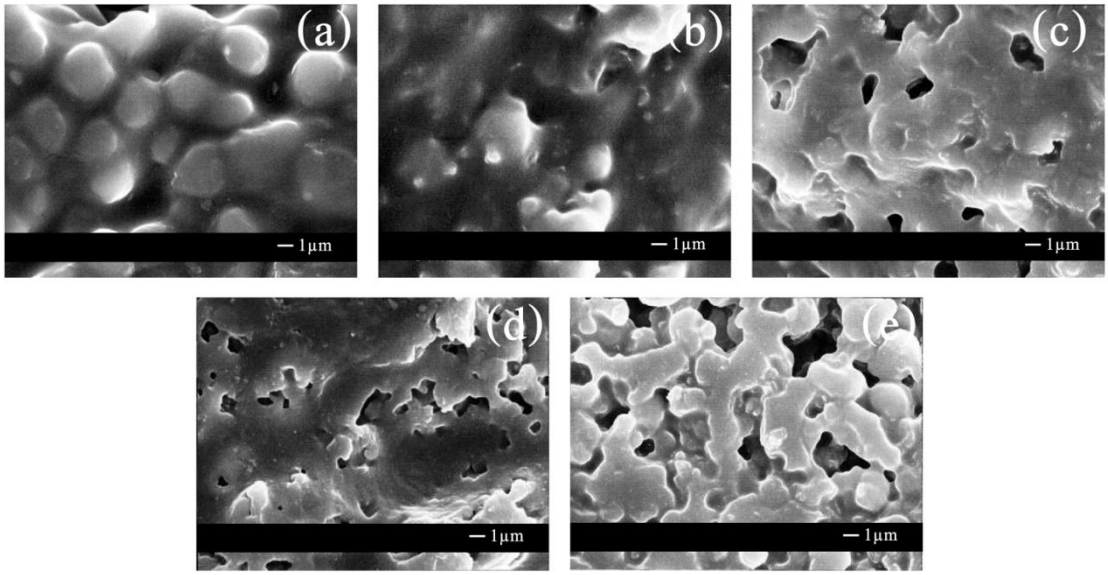

Figure E-8 SEM micrographs of S50-E5C5-200-24 composite before (a) and after soaking in SBF for 7 days (b), 14 days (c), 21 days (d) and 28 days (e)

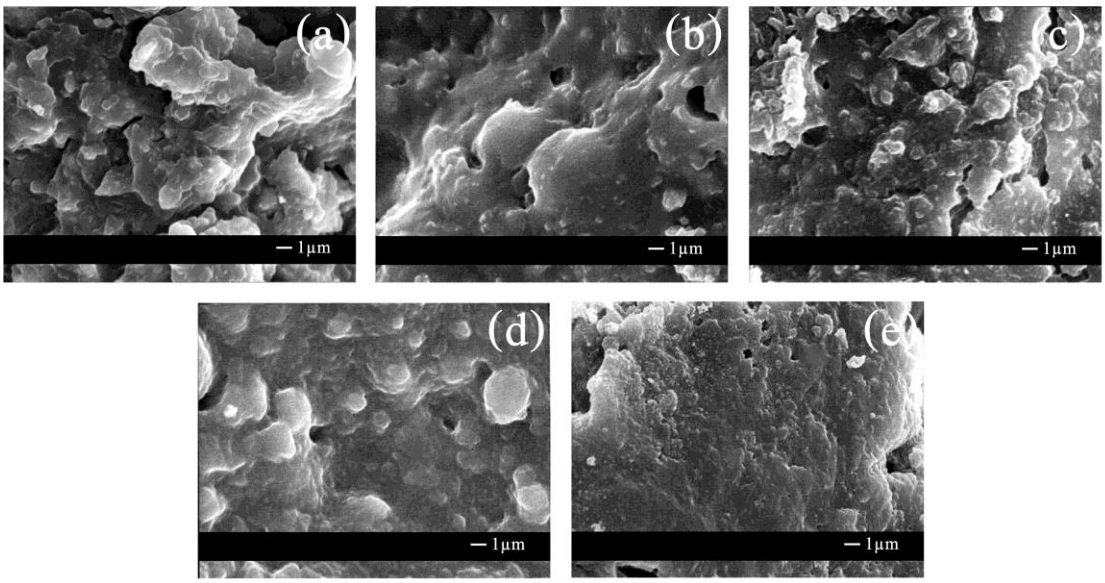

Figure E-9 SEM micrographs of S50-E6C4-200-24 composites before (a) and after soaking in SBF for 7 days (b), 14 days (c), 21 days (d) and 28 days (e)

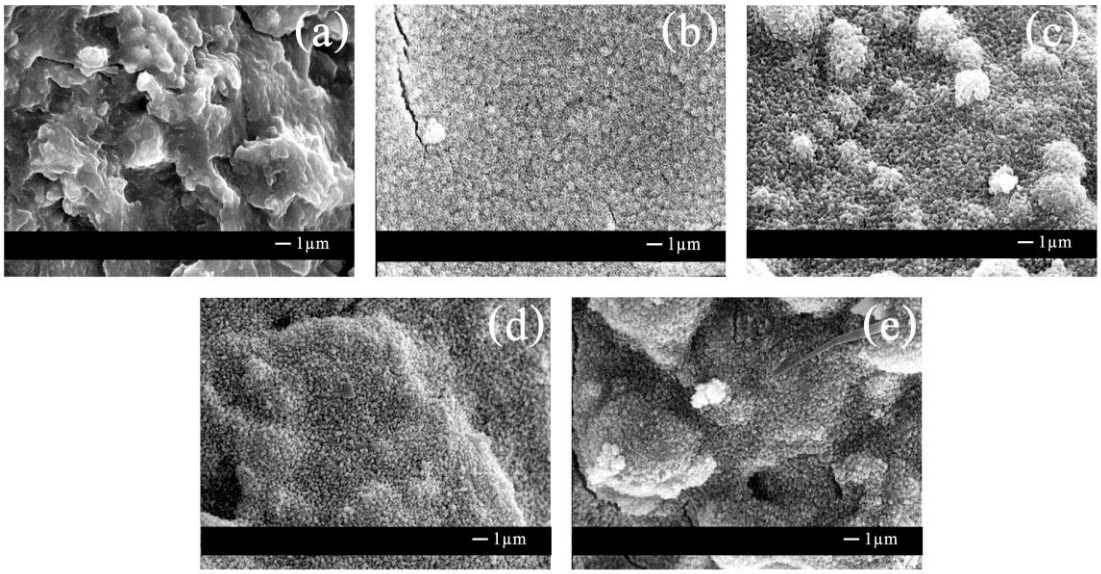

Figure E-10 SEM micrographs of S50-E7C3-200-24 composites before (a) and after soaking in SBF for 7 days (b), 14 days (c), 21 days (d) and 28 days (e)

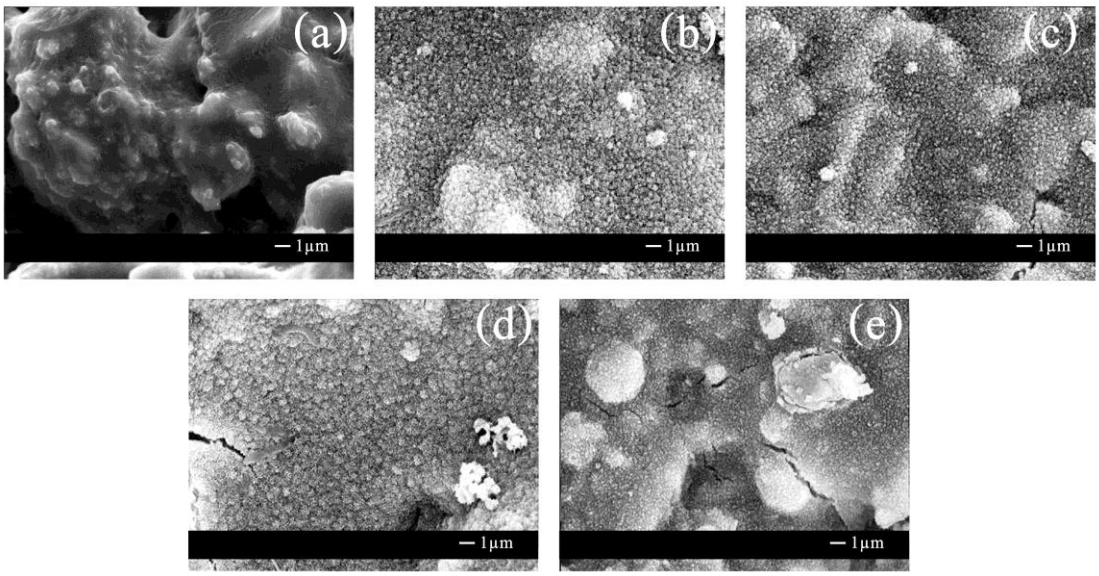

Figure E-11 SEM micrographs of S50-E8C2-200-24 composites before (a) and after soaking in SBF for 7 days (b), 14 days (c), 21 days (d) and 28 days (e)

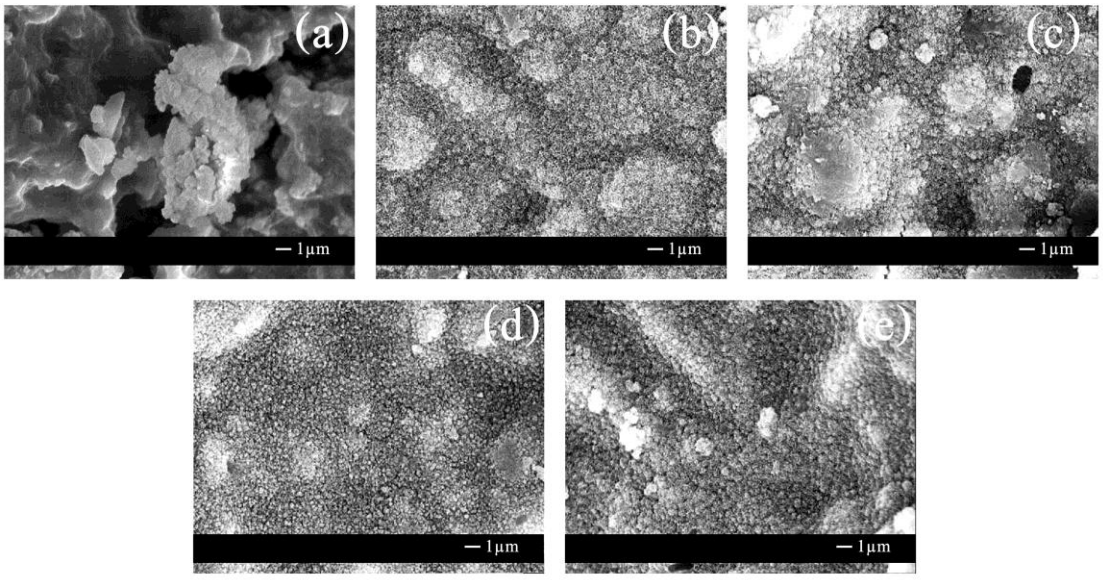

Figure E-12 SEM micrographs of S50-E9C1-200-24 composites before (a) and after soaking in SBF for 7 days (b), 14 days (c), 21 days (d) and 28 days (e)

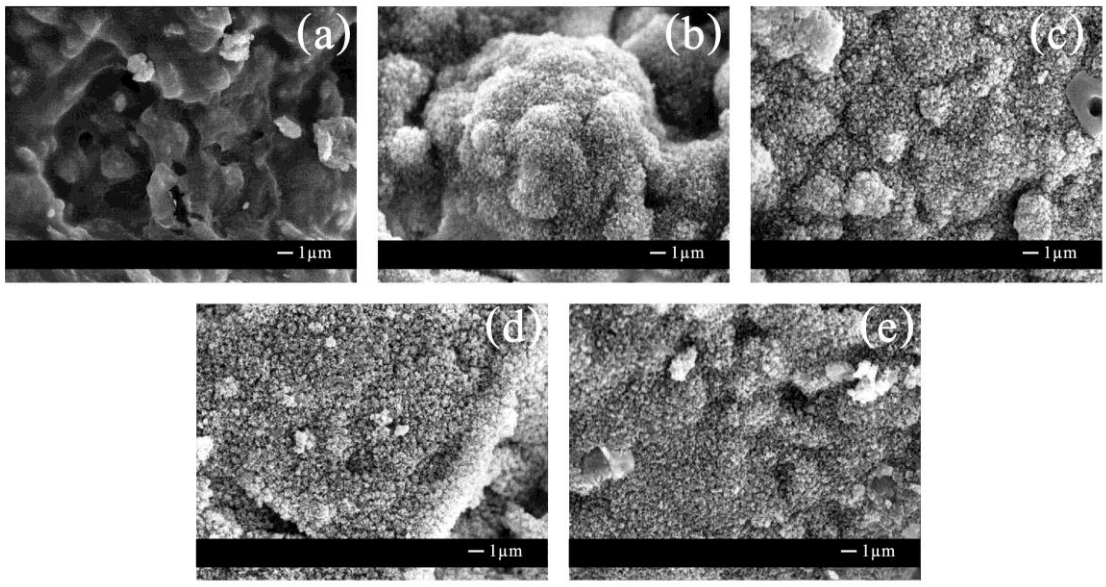

Figure E-13 SEM micrographs of S50-E10C0-200-24 composites before (a) and after soaking in SBF for 7 days (b), 14 days (c), 21 days (d) and 28 days (e)

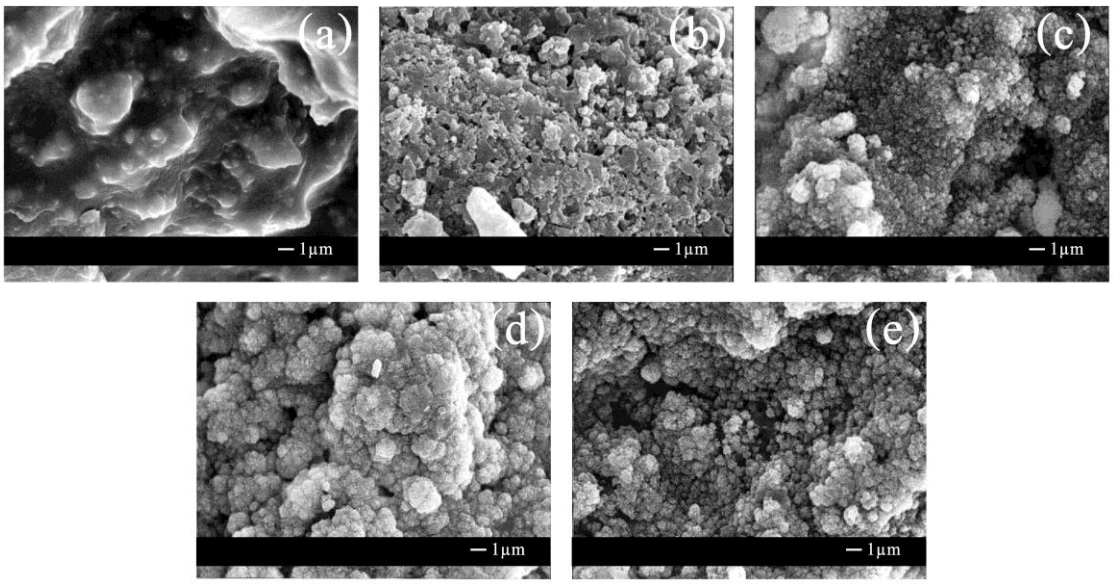

Figure E-14 SEM micrographs of S60-E5C5-180-24 composites before (a) and after soaking in SBF for 7 days (b), 14 days (c), 21 days (d) and 28 days (e)

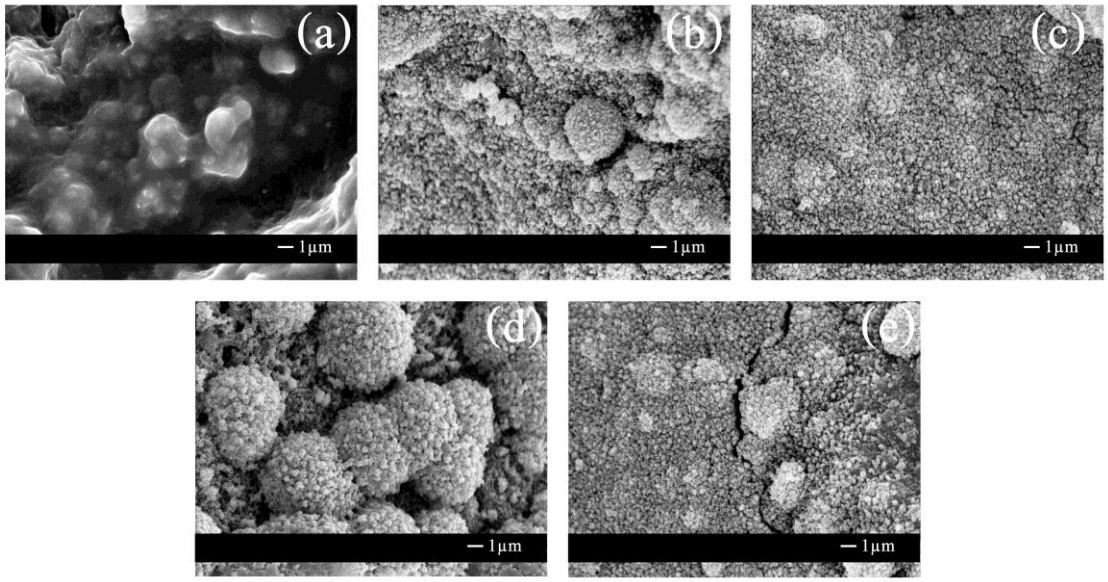

Figure E-15 SEM micrographs of S60-E6C4-180-24 composites before (a) and after soaking in SBF for 7 days (b), 14 days (c), 21 days (d) and 28 days (e)

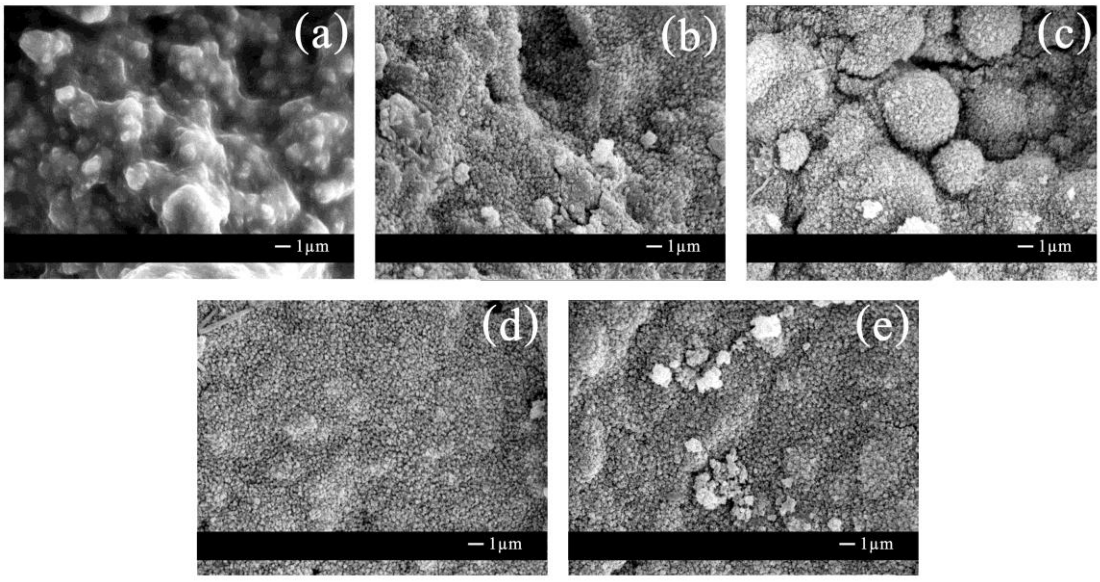

Figure E-16 SEM micrographs of S60-E7C3-180-24 composites before (a) and after soaking in SBF for 7 days (b), 14 days (c), 21 days (d) and 28 days (e)

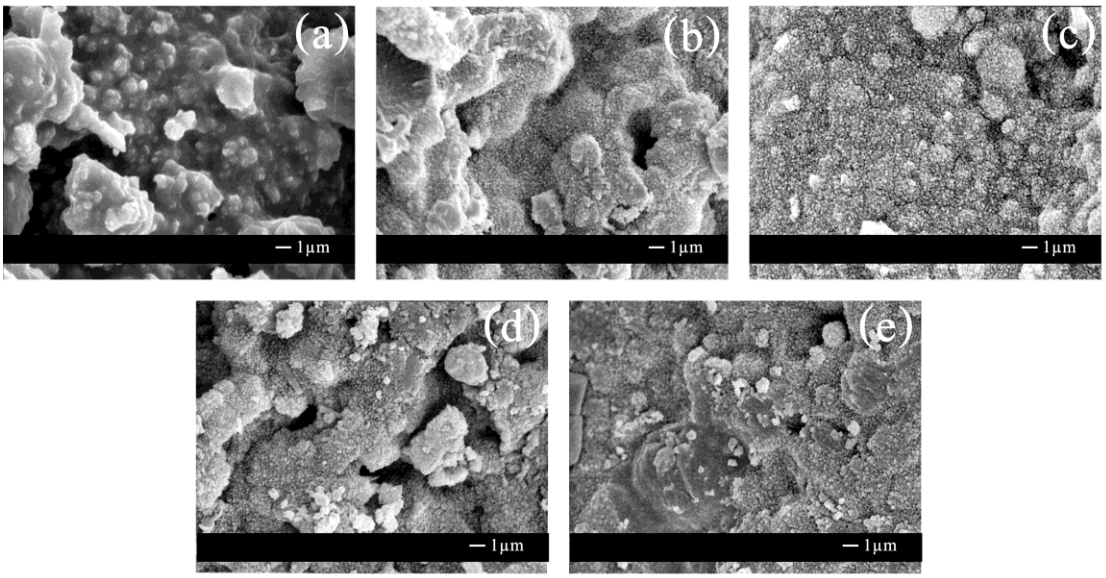

Figure E-17 SEM micrographs of S60-E8C2-180-24 composites before (a) and after soaking in SBF for 7 days (b), 14 days (c), 21 days (d) and 28 days (e)

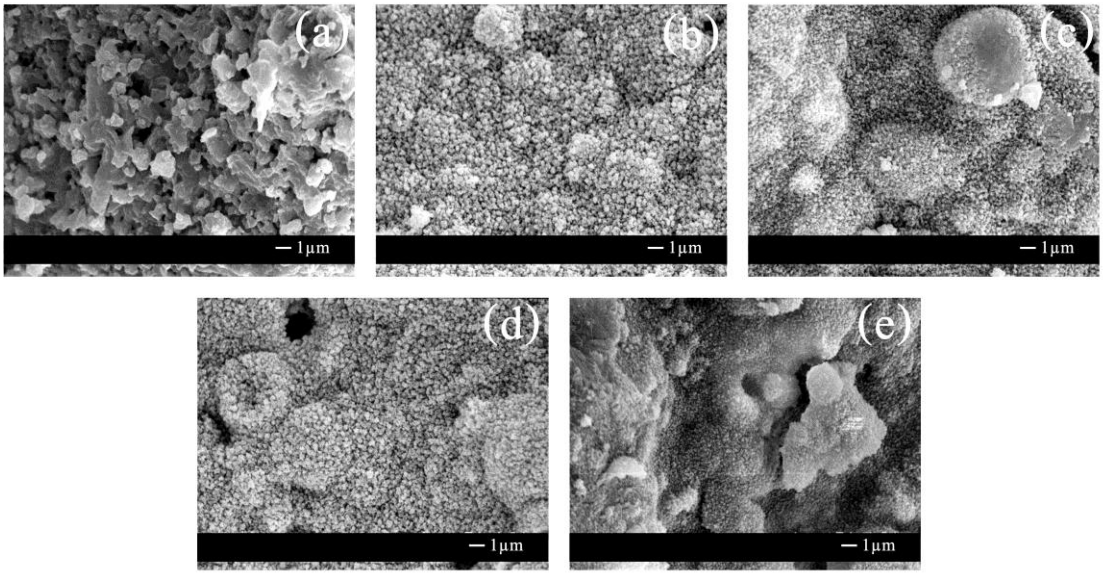

Figure E-18 SEM micrographs of S60-E9C1-180-24 composites before (a) and after soaking in SBF for 7 days (b), 14 days (c), 21 days (d) and 28 days (e)

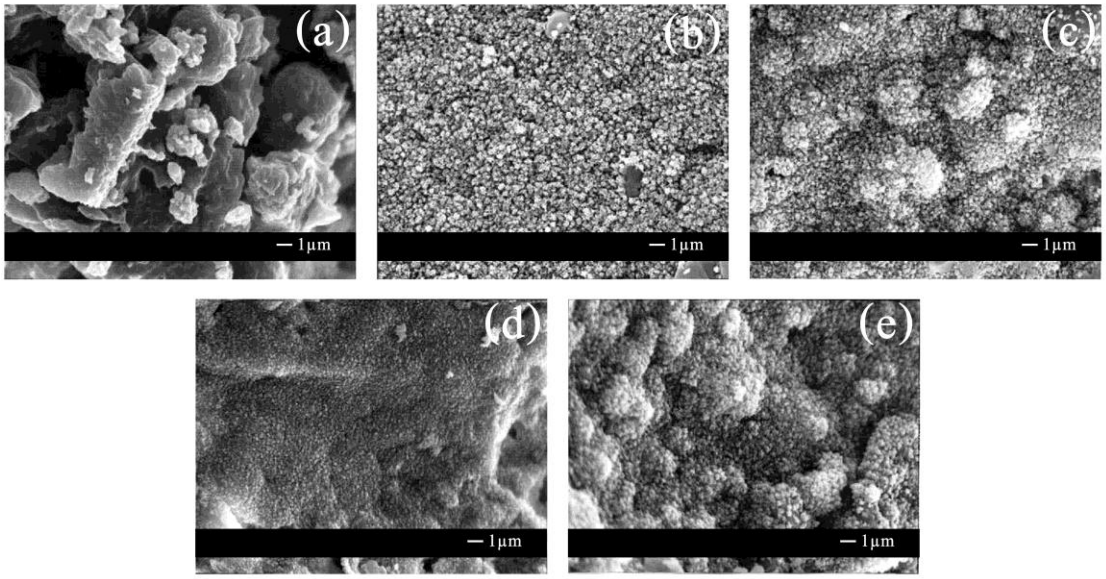

Figure E-19 SEM micrographs of S60-E10C0-180-24 composites before (a) and after soaking in SBF for 7 days (b), 14 days (c), 21 days (d) and 28 days (e)

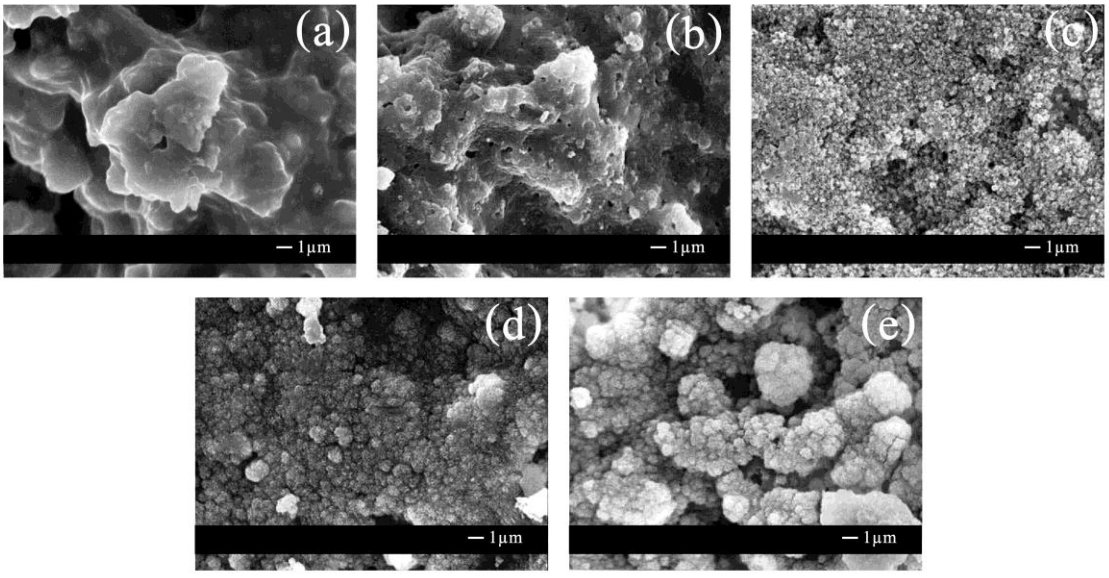

Figure E-20 SEM micrographs of S60-E5C5-200-24 composites before (a) and after soaking in SBF for 7 days (b), 14 days (c), 21 days (d) and 28 days (e)

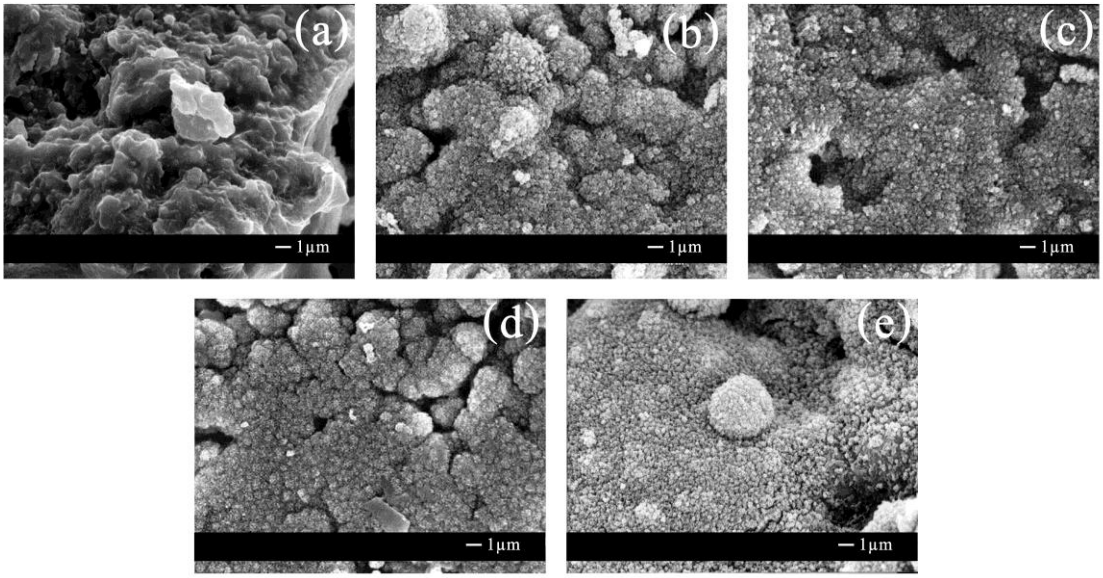

Figure E-21 SEM micrographs of S60-E6C4-200-24 composites before (a) and after soaking in SBF for 7 days (b), 14 days (c), 21 days (d) and 28 days (e)

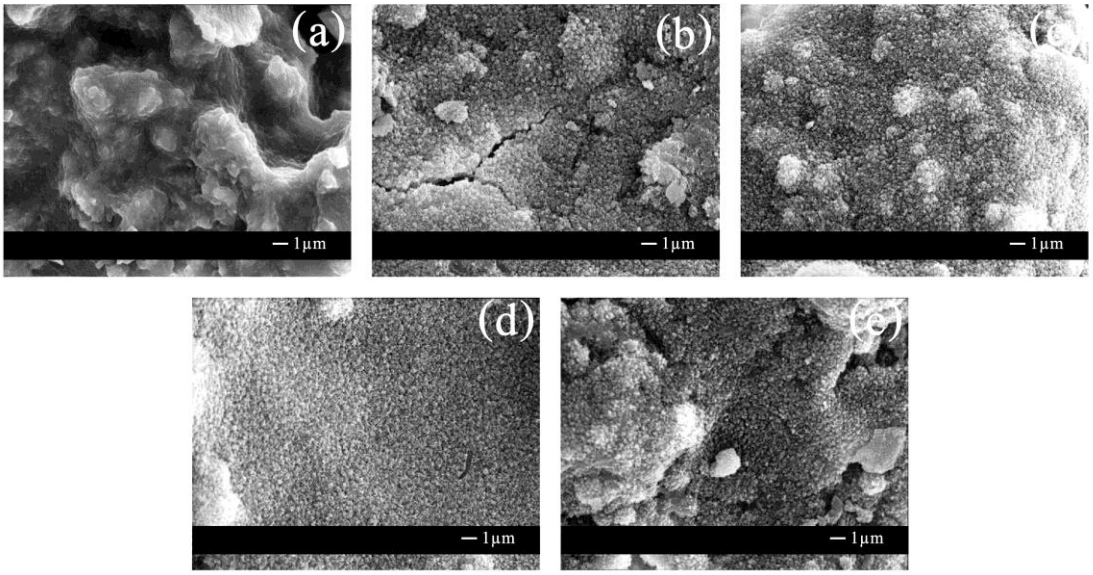

Figure E-22 SEM micrographs of S60-E7C3-200-24 composites before (a) and after soaking in SBF for 7 days (b), 14 days (c), 21 days (d) and 28 days (e)

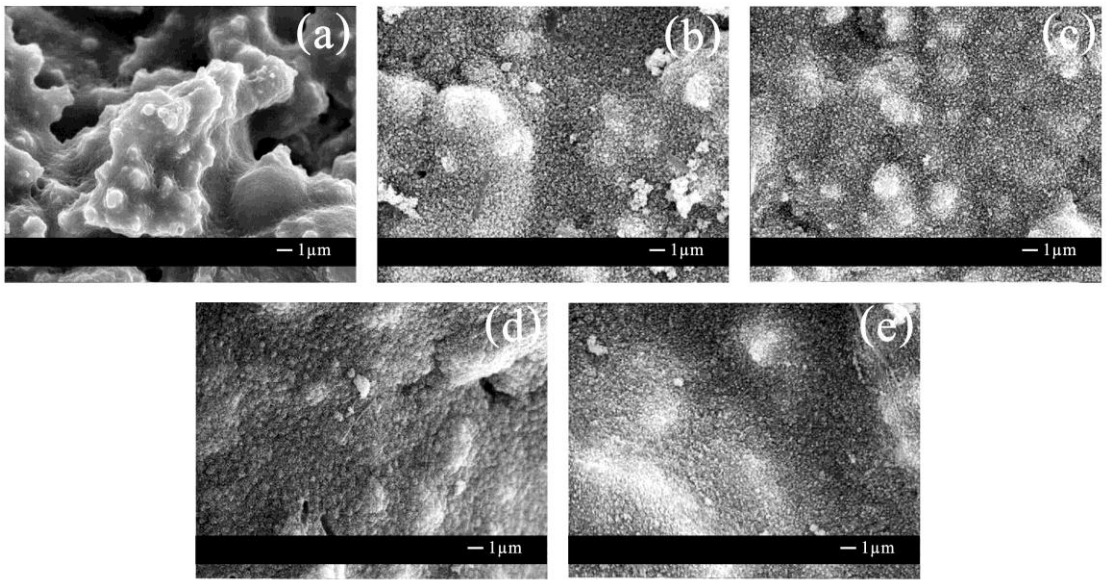

Figure E-23 SEM micrographs of S60-E8C2-200-24 composites before (a) and after soaking in SBF for 7 days (b), 14 days (c), 21 days (d) and 28 days (e)

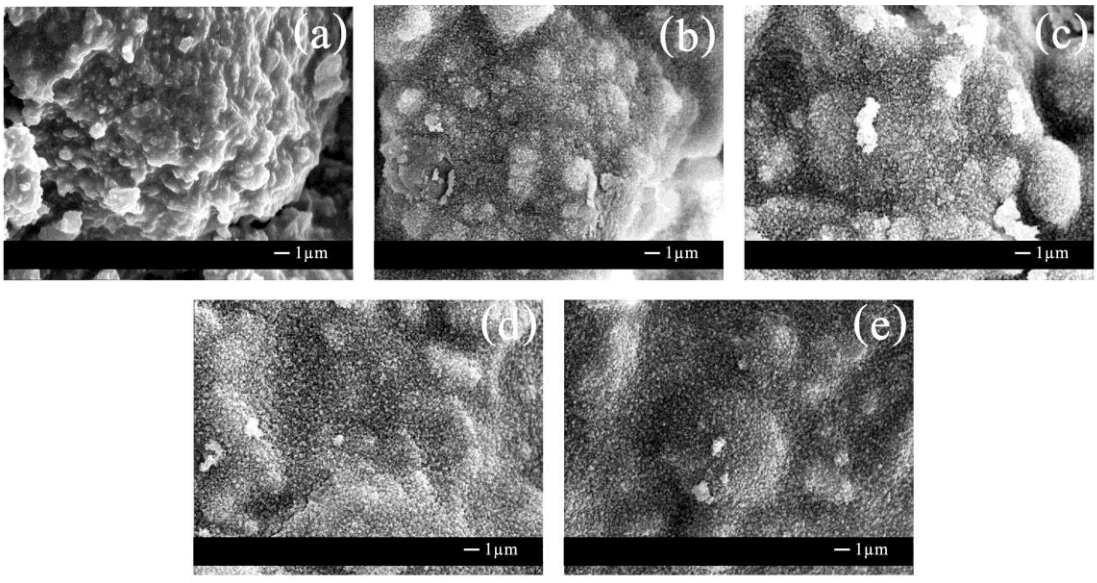

Figure E-24 SEM micrographs of S60-E9C1-200-24 composites before (a) and after soaking in SBF for 7 days (b), 14 days (c), 21 days (d) and 28 days (e)

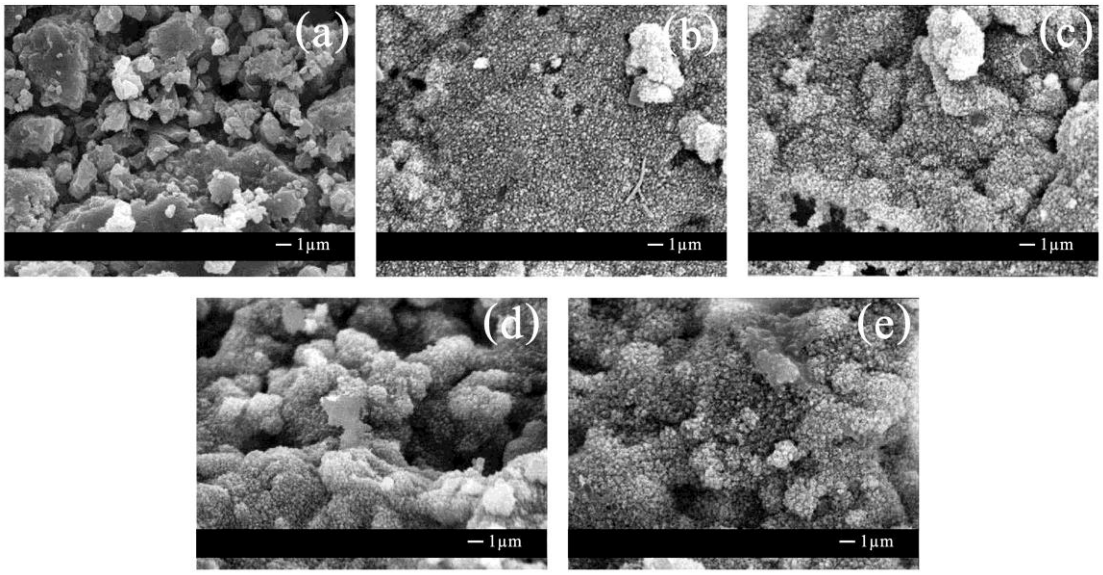

Figure E-25 SEM micrographs of S60-E10C0-200-24 composites before (a) and after soaking in SBF for 7 days (b), 14 days (c), 21 days (d) and 28 days (e)

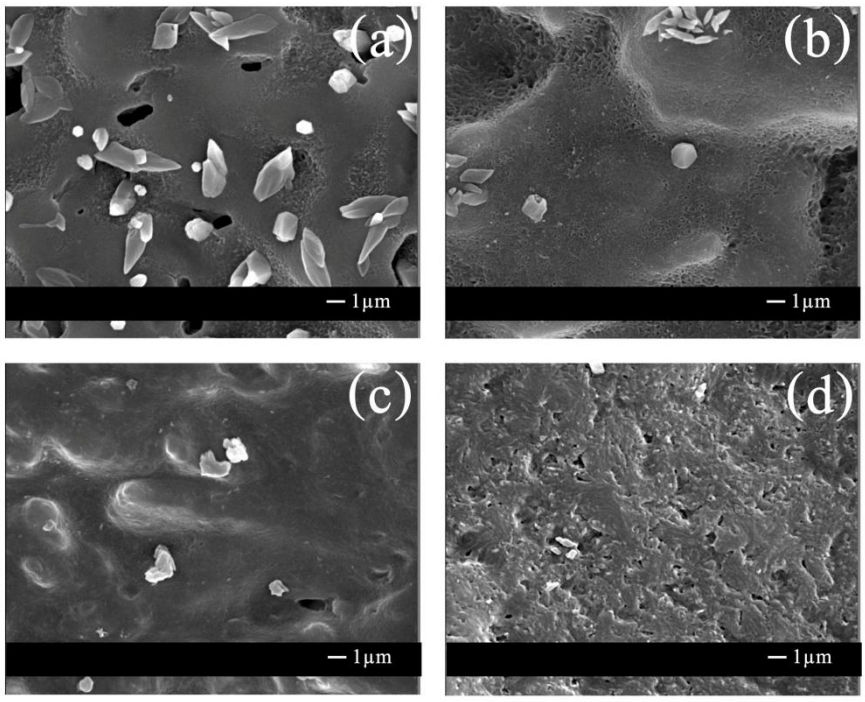

Figure E-26 SEM micrograph of E7C3-180-24 (a), E8C2-180-24 (b), E10C0-180-24 (c) and E8C2-200-24 (d) copolymers after soaking in 5 %v/v H_2O_2 solution for 28 days

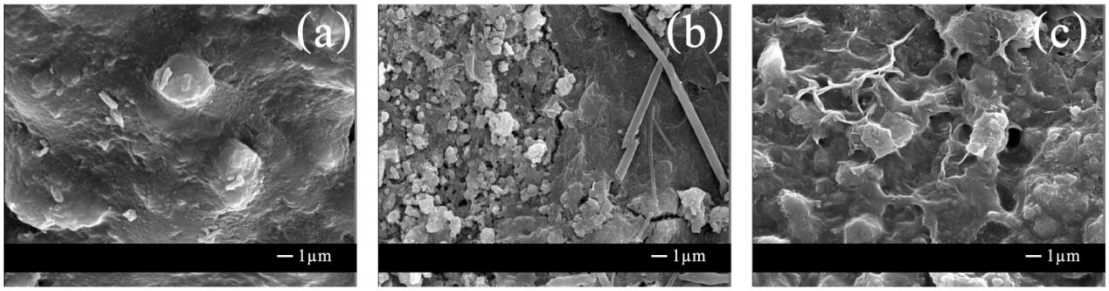

Figure E-27 SEM micrograph of S50-E7C3-180-24 (a), S50-E8C2-180-24 (b) and S50-E10C0-180-24 (c) composites after soaking in 5 %v/v H_2O_2 solution for 28 days

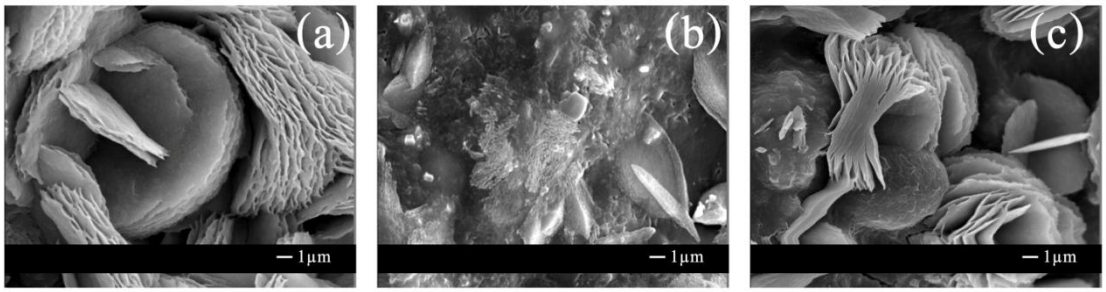

Figure E-28 SEM micrograph of S50-E7C3-200-24 (a), S50-E8C2-200-24 (b) and S50-E9C1-200-24 (c) composites after soaking in 5 %v/v H_2O_2 solution for 28 days

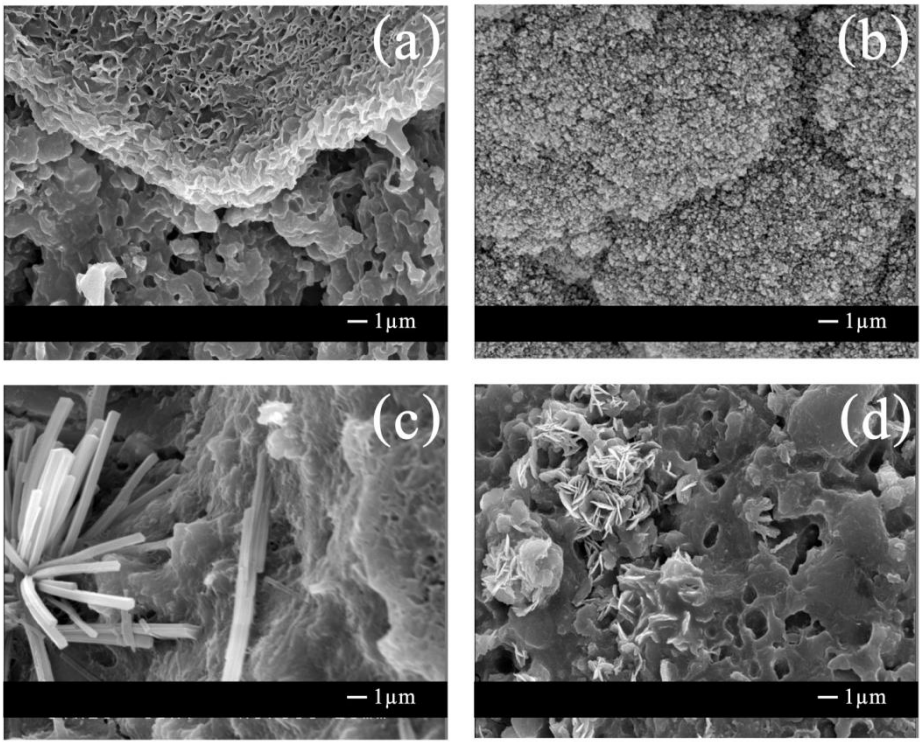

Figure E-29 SEM micrograph of S60-E5C5-180-24 (a), S60-E6C4-180-24 (b), S60-E7C3-180-24 (c) and S60-E10C0-180-24 (d) composites after soaking in 5 %v/v H_2O_2 solution for 28 days

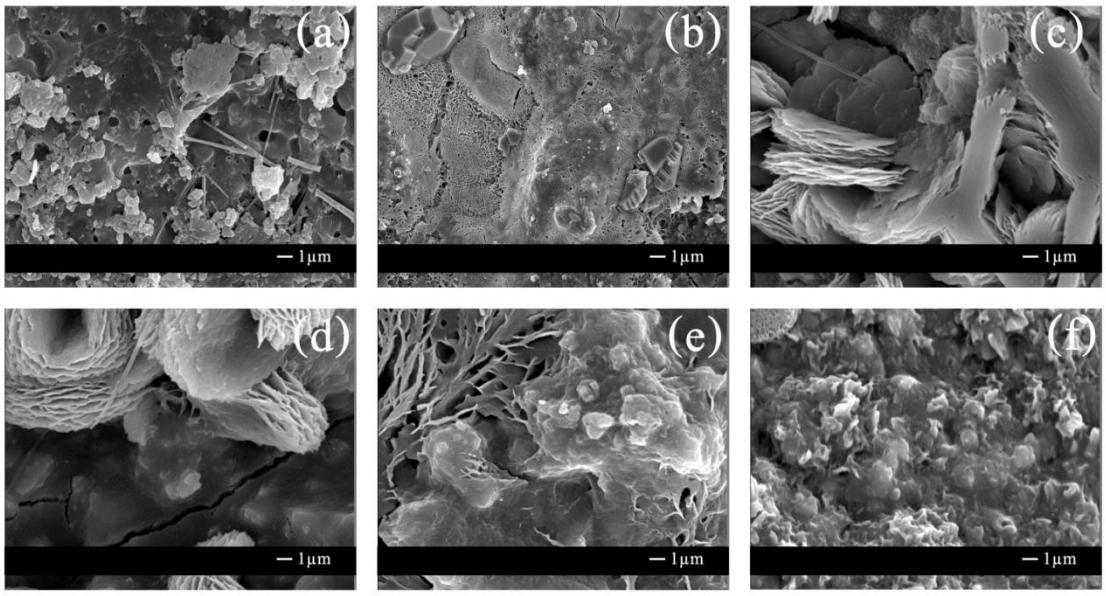

Figure E-30 SEM micrograph of S60-E5C5-200-24 (a), S60-E6C4-200-24 (b), S60-E7C3-200-24 (c), S60-E8C2-200-24 (d), S60-E9C1-200-24 (e) and S60-E10C0-200-24 (f) composites after soaking in 5 %v/v H_2O_2 solution for 28 days

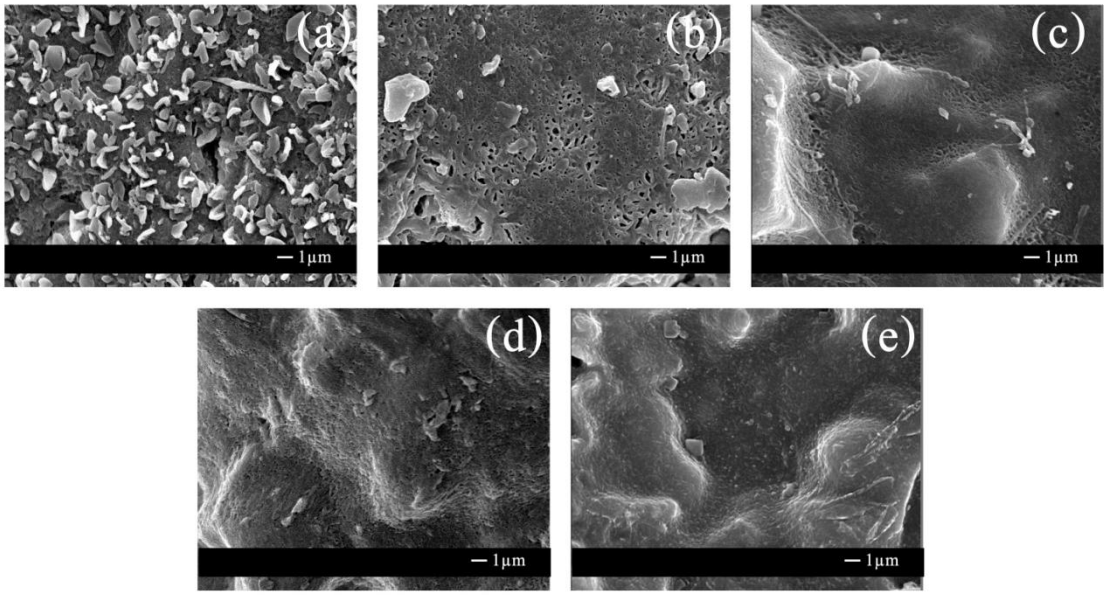

Figure E-31 SEM micrograph of E6C4-180-24 (a), E7C3-180-24 (b), E8C2-180-24 (c), E9C1-180-24 (d) and E10C0-200-24 (e) copolymers after soaking in PBS solution for 28 days

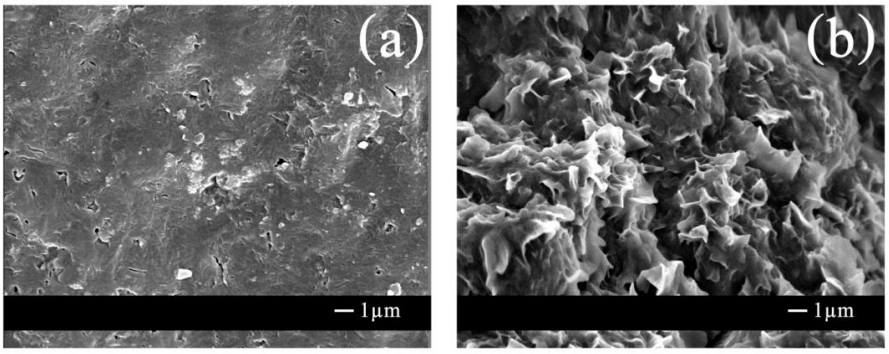

Figure E-32 SEM micrograph of E8C2-200-24 (a) and E10C0-200-24 (b) copolymers after soaking in PBS solution for 28 days

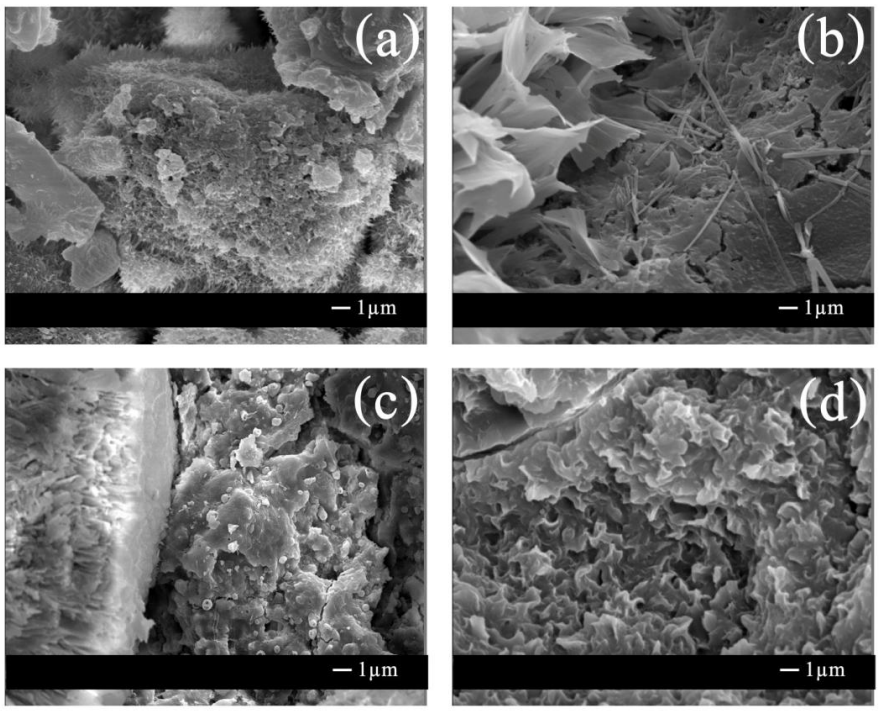

Figure E-33 SEM micrograph of S50-E10C0-180-24 (a), S50-E7C3-200-24 (b), S50-E8C2-200-24 (c) and S50-E10C0-200-24 (d) composites after soaking in PBS solution for 28 days

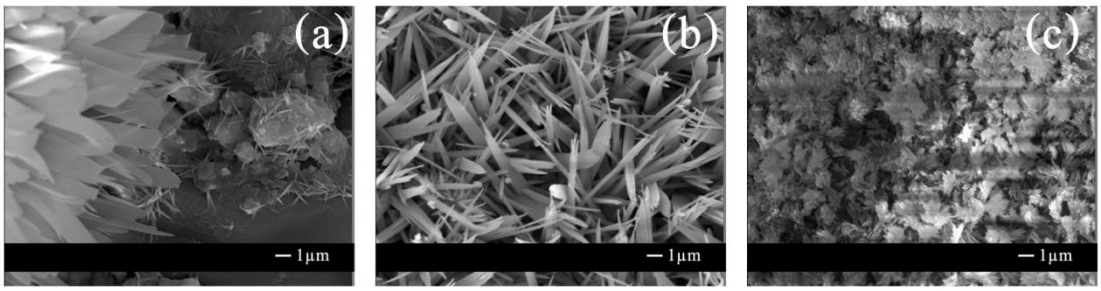

Figure E-34 SEM micrograph of S60-E7C3-180-24 (a), S60-E8C2-200-24 (b) and S60-E10C0-200-24 (c) composites after soaking in PBS solution for 28 days

APPENDIX F

MECHANICAL PROPERTIES

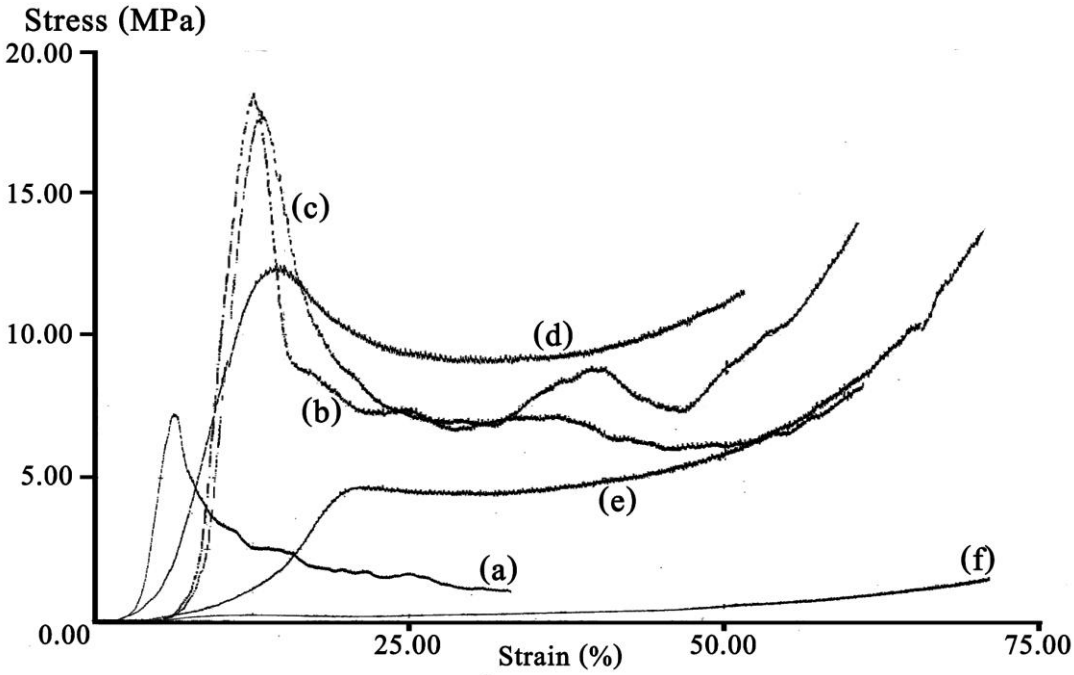

Figure F-1 Stress-strain curve of CS/PET-*co*-PCL composites with 50 %wt CS containing 100:0 (a), 90:10 (b), 80:20 (c), 70:30 (d), 60:40 (e), 50:50 (f) of C-OET:CL molar ratios at 180 °C ROP temperature for 24 hr

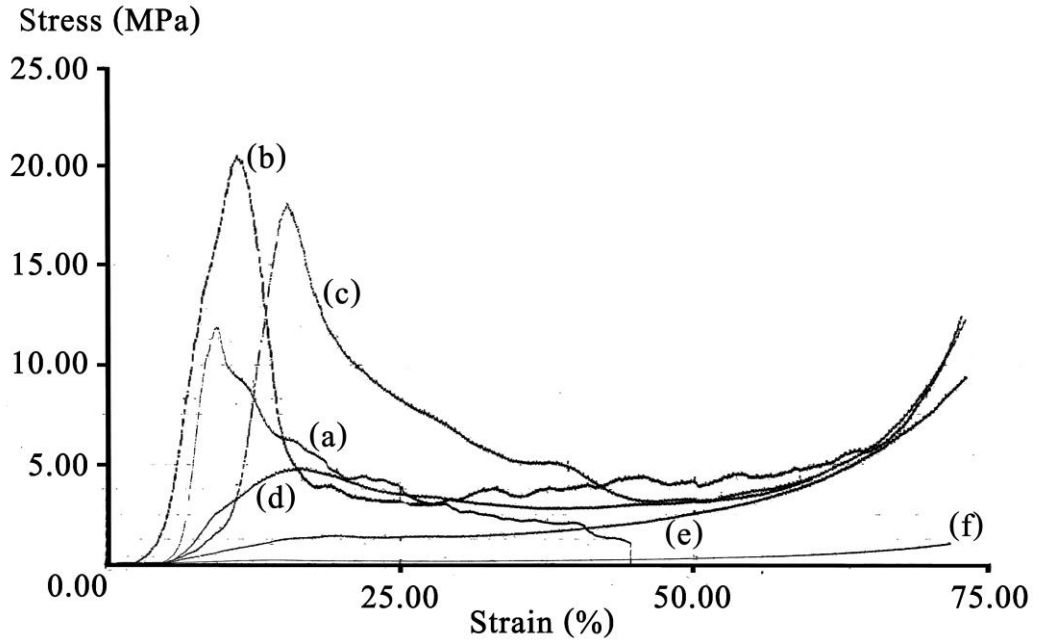

Figure F-2 Stress-strain curve of CS/PET-*co*-PCL composites with 50 %wt CS containing 100:0 (a), 90:10 (b), 80:20 (c), 70:30 (d), 60:40 (e), 50:50 (f) of C-OET:CL molar ratios at 200 °C ROP temperature for 24 hr

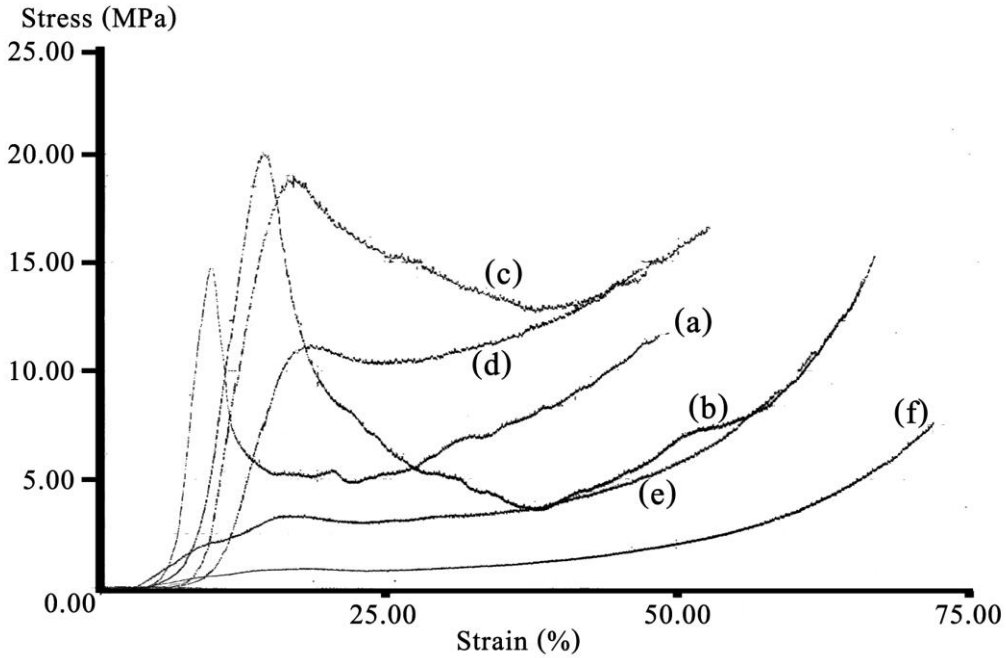

Figure F-3 Stress-strain curve of CS/PET-*co*-PCL composites with 60 %wt CS containing 100:0 (a), 90:10 (b), 80:20 (c), 70:30 (d), 60:40 (e), 50:50 (f) of C-OET:CL molar ratios at 200 °C ROP temperature for 24 hr

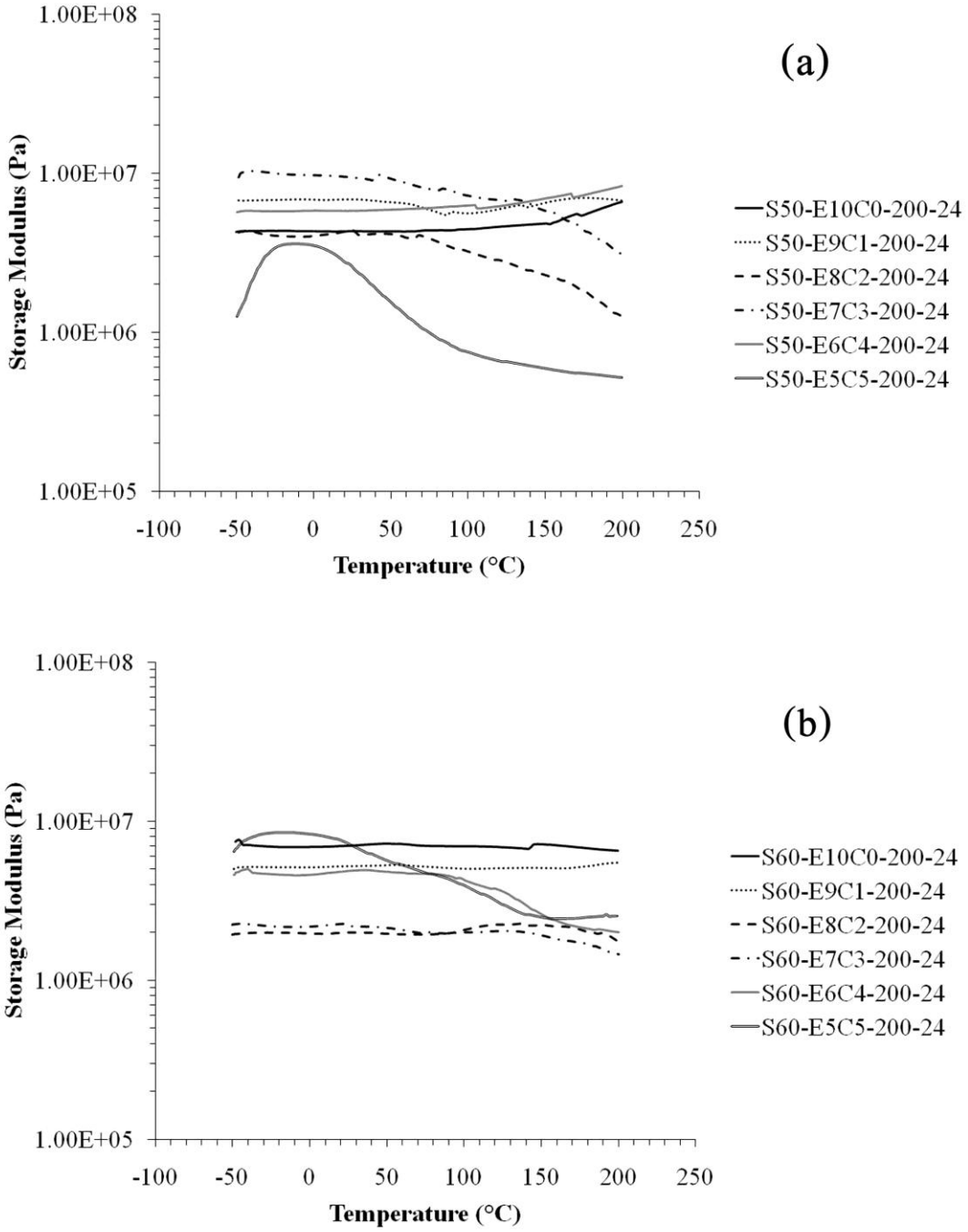

Figure F-4 Storage moduli (E') of CS/PET-*co*-PCL composites containing 50 %wt copolymers (a) and 40 %wt copolymers (b) (ROP temperature as 200 °C for 24 hr)

APPENDIX G

X-RAY DIFFRACTION

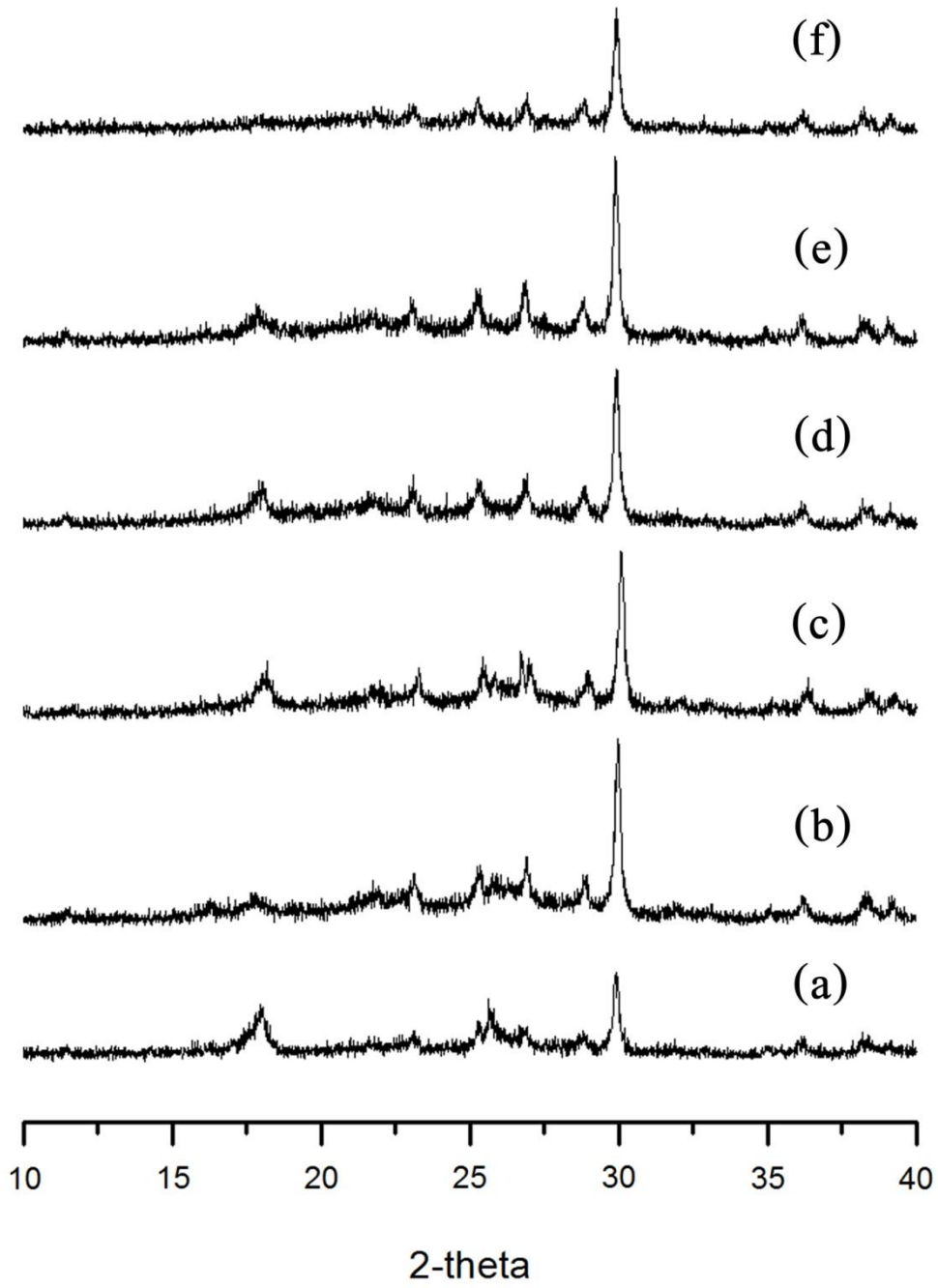

Figure G-1 XRD patterns of (a) S50-E10C0-200-24, (b) S50-E9C1-200-24, (c) S50-E8C2-200-24, (d) S50-E7C3-200-24, (e) S50-E6C4-200-24 and (f) S50-E5C5-200-24 composites before annealing

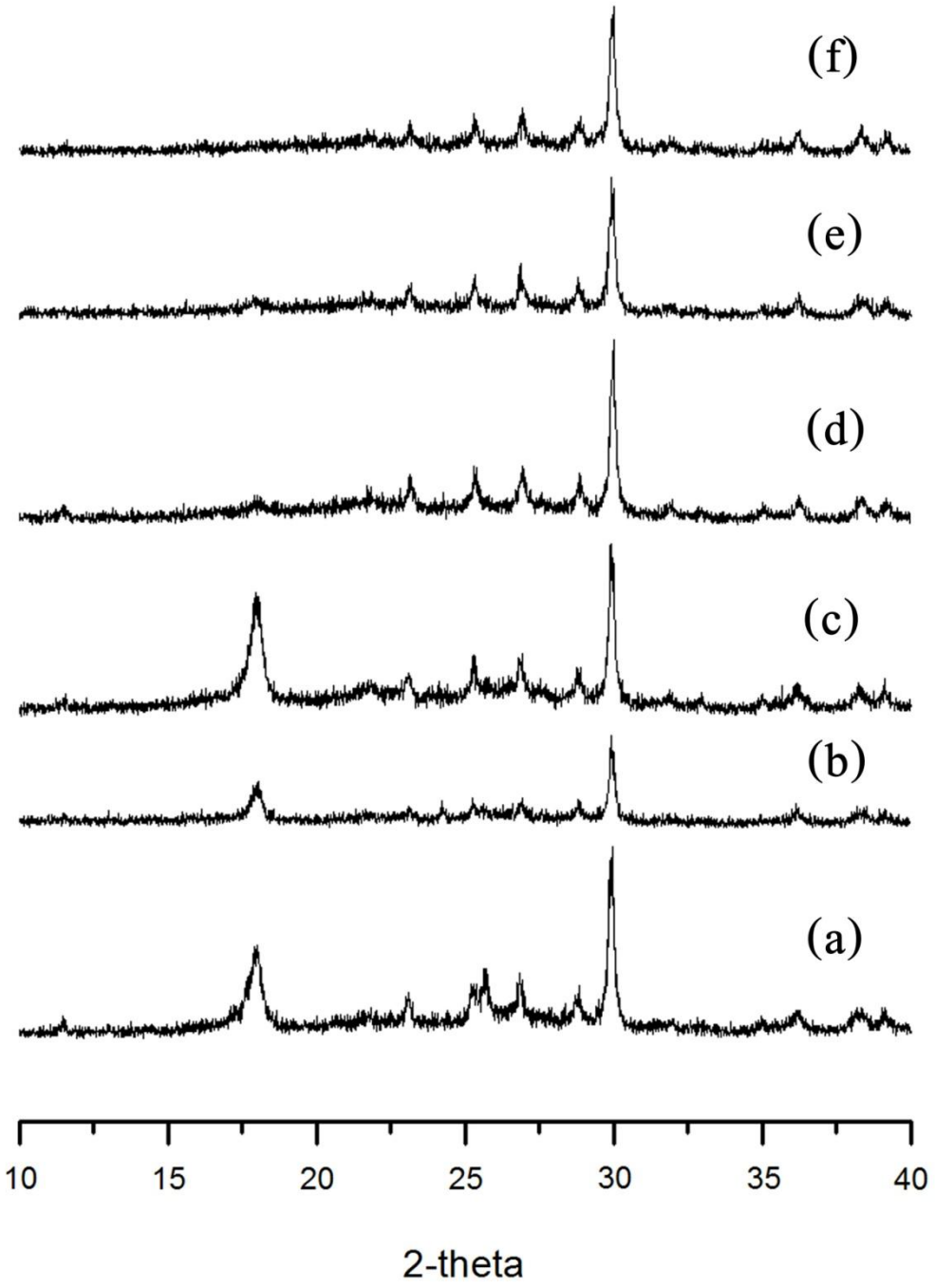

Figure G-2 XRD patterns of (a) S60-E10C0-180-24, (b) S60-E9C1-180-24, (c) S60-E8C2-180-24, (d) S60-E7C3-180-24, (e) S60-E6C4-180-24 and (f) S60-E5C5-180-24 composites before annealing

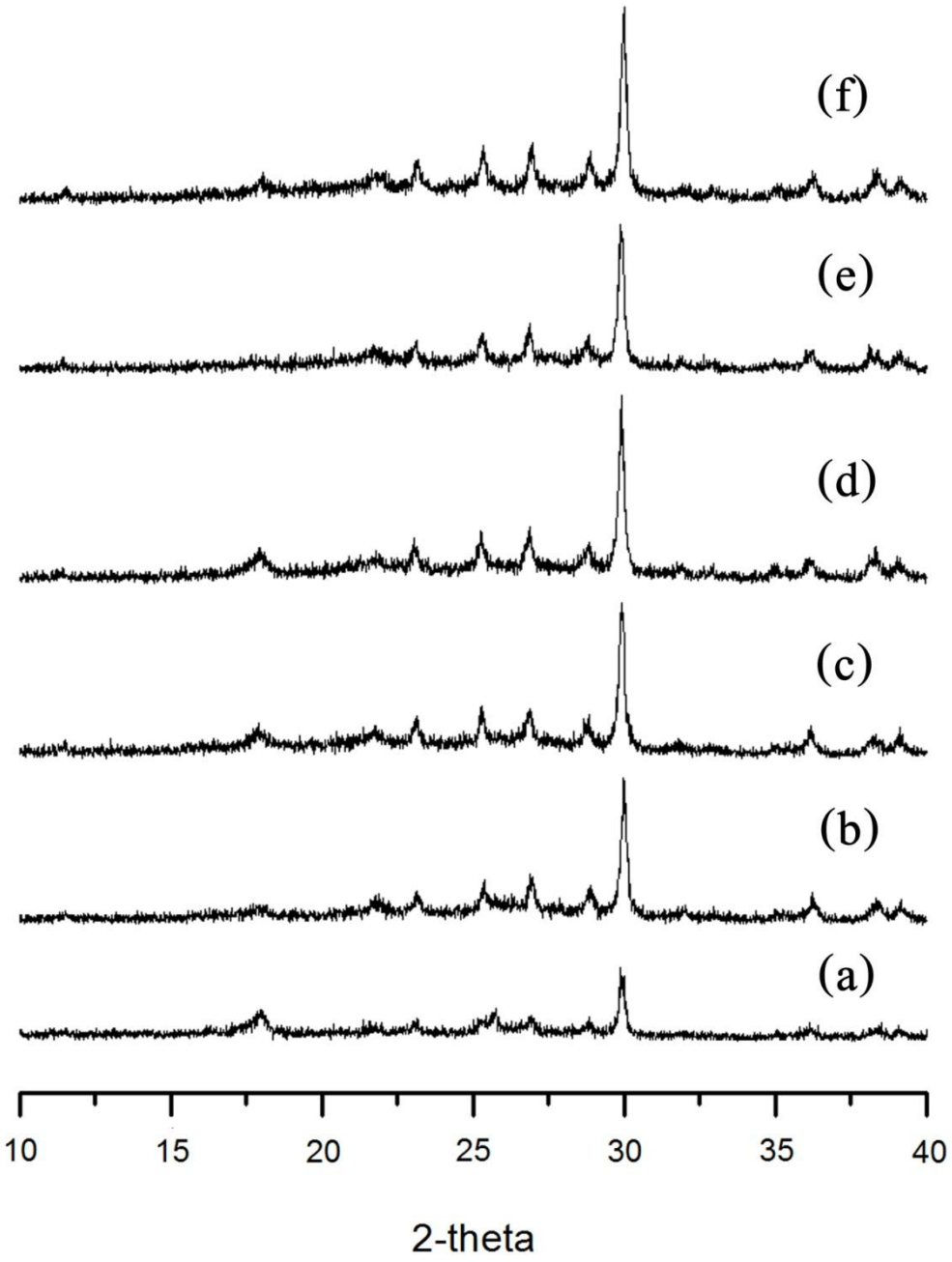

Figure G-3 XRD patterns of (a) S60-E10C0-200-24, (b) S60-E9C1-200-24, (c) S60-E8C2-200-24, (d) S60-E7C3-200-24, (e) S60-E6C4-200-24 and (f) S60-E5C5-200-24 composites before annealing

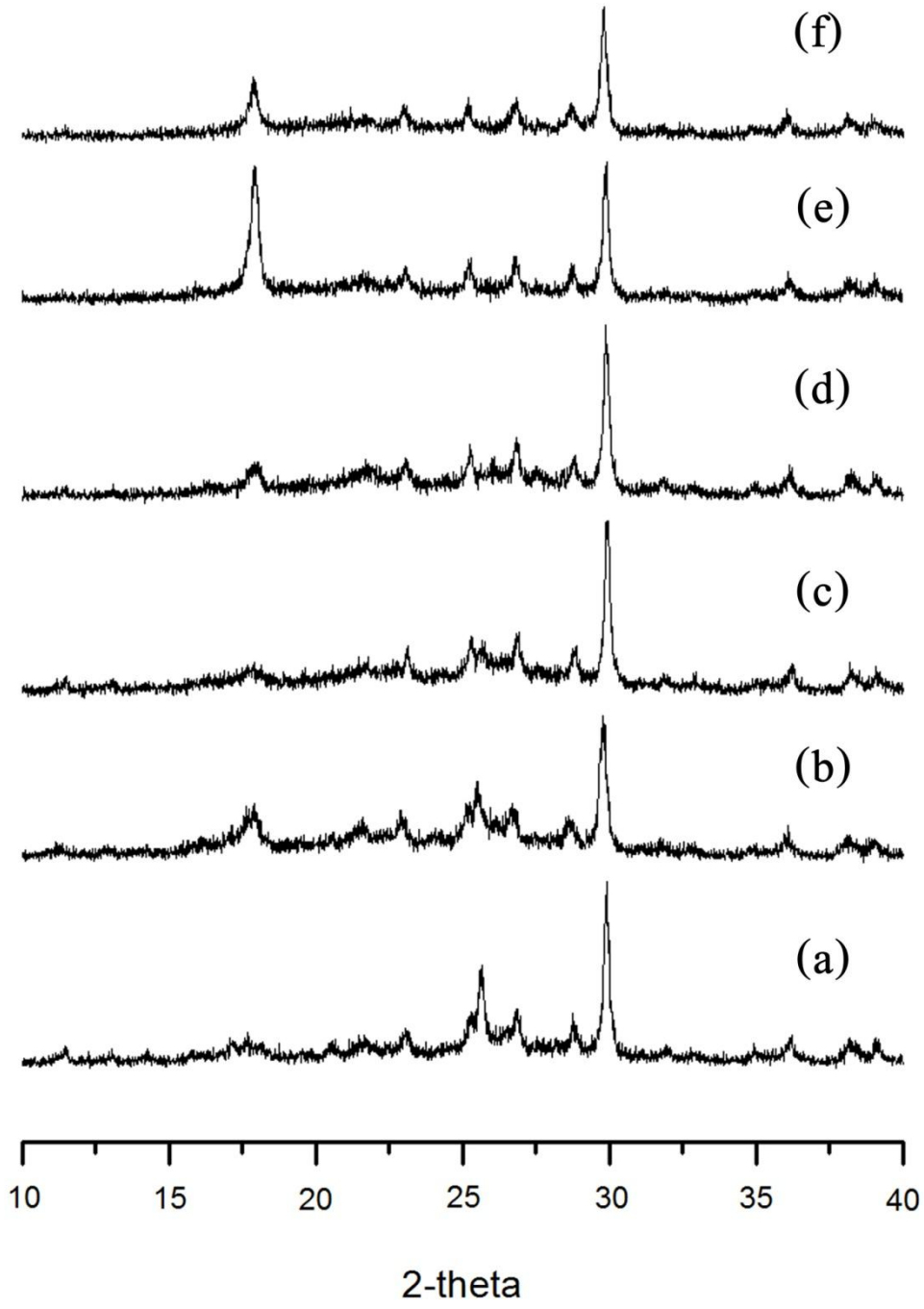

Figure G-4 XRD patterns of (a) S50-E10C0-180-24, (b) S50-E9C1-180-24, (c) S50-E8C2-180-24, (d) S50-E7C3-180-24, (e) S50-E6C4-180-24 and (f) S50-E5C5-180-24 composites after annealing

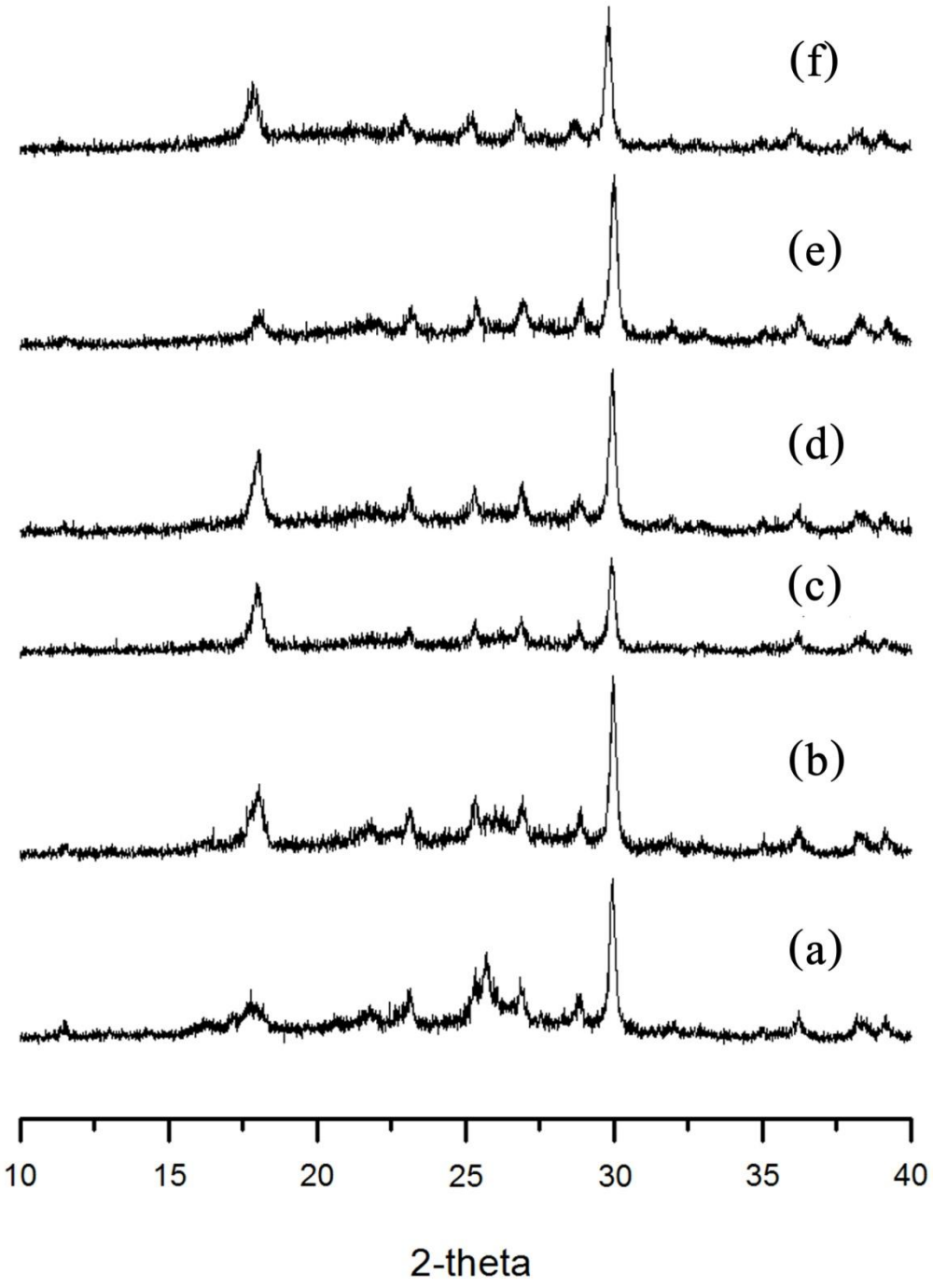

Figure G-5 XRD patterns of (a) S50-E10C0-200-24, (b) S50-E9C1-200-24, (c) S50-E8C2-200-24, (d) S50-E7C3-200-24, (e) S50-E6C4-200-24 and (f) S50-E5C5-200-24 composites after annealing

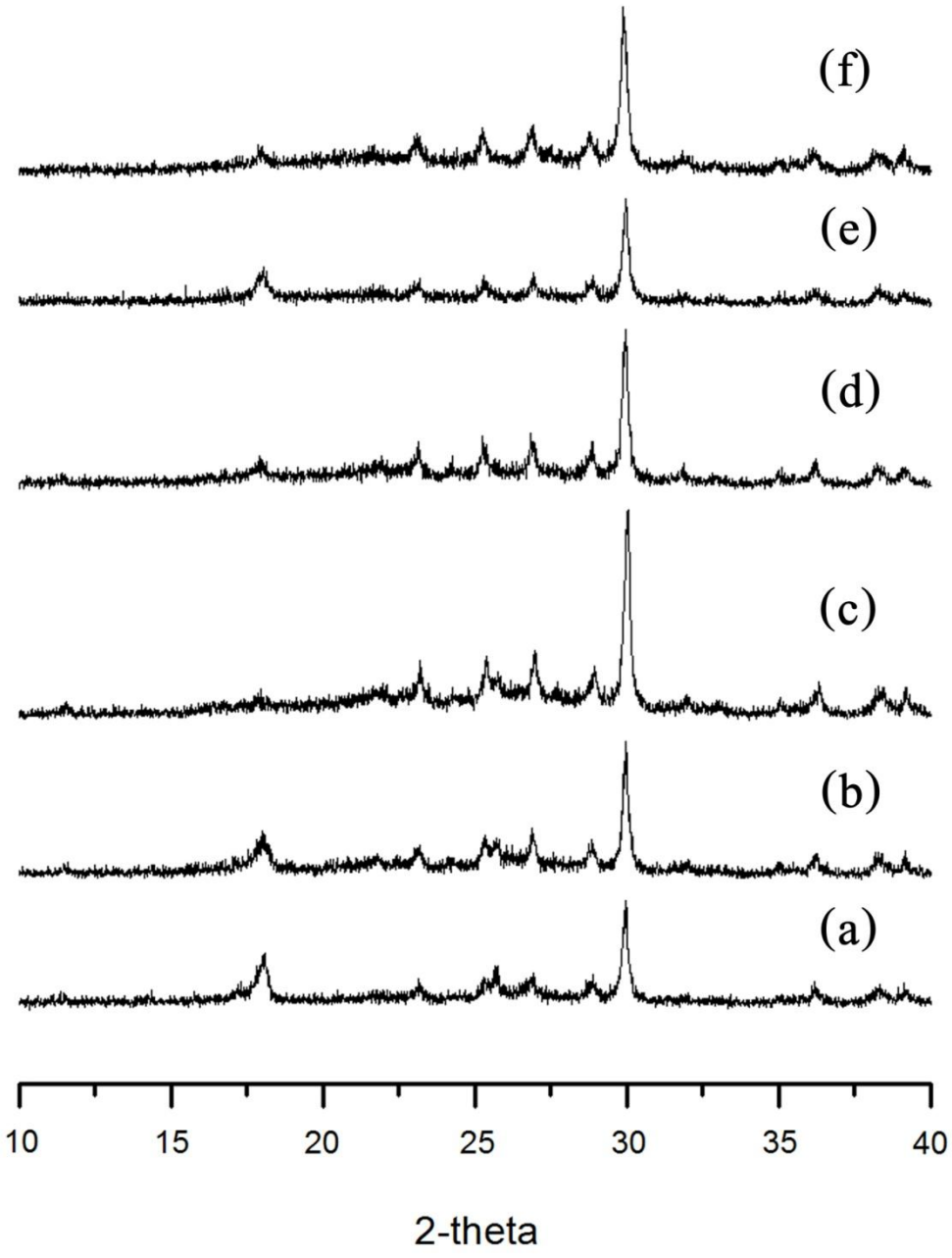

Figure G-6 XRD patterns of (a) S60-E10C0-180-24, (b) S60-E9C1-180-24, (c) S60-E8C2-180-24, (d) S60-E7C3-180-24, (e) S60-E6C4-180-24 and (f) S60-E5C5-180-24 composites after annealing

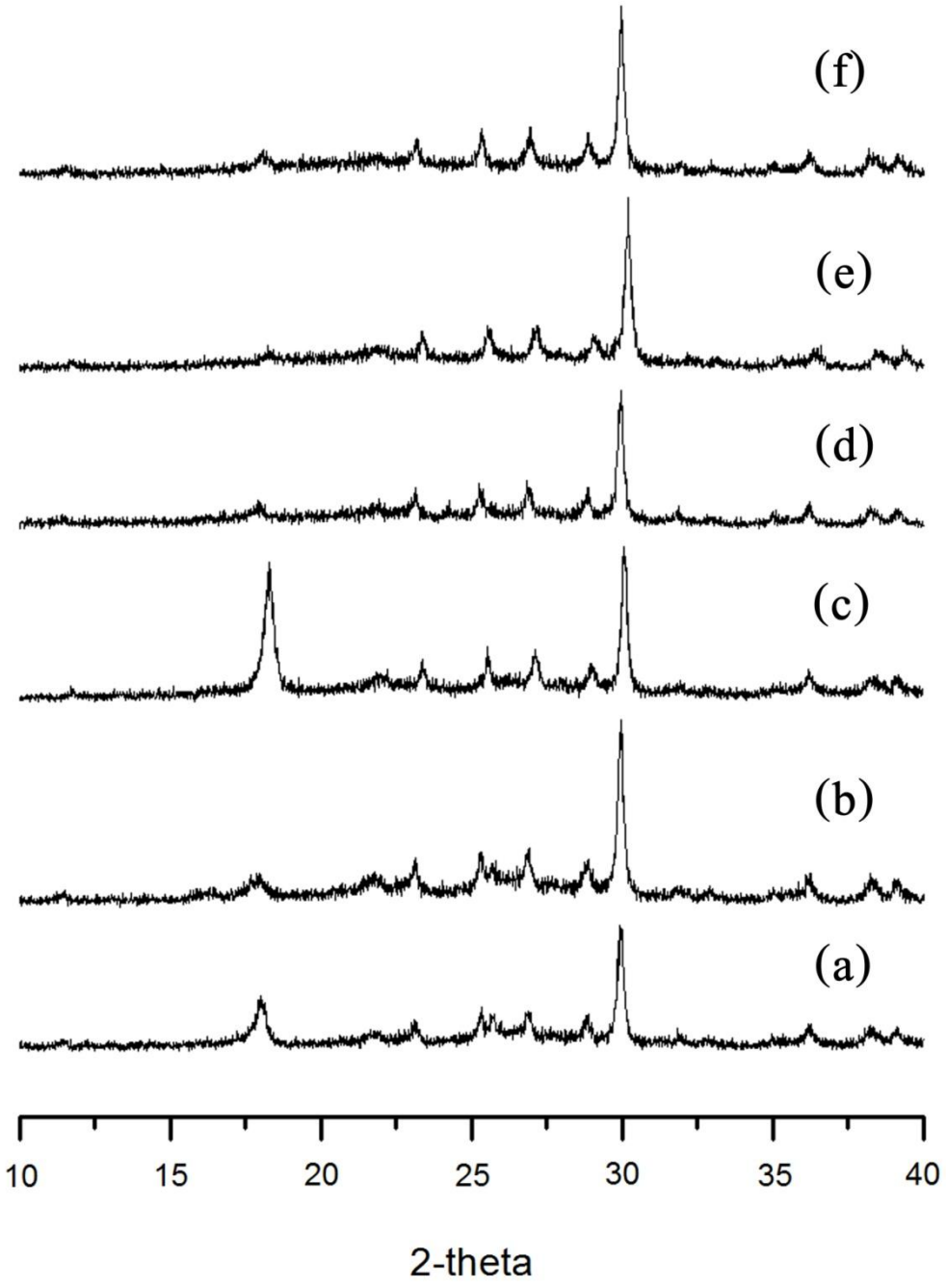

Figure G-7 XRD patterns of (a) S60-E10C0-200-24, (b) S60-E9C1-200-24, (c) S60-E8C2-200-24, (d) S60-E7C3-200-24, (e) S60-E6C4-200-24 and (f) S60-E5C5-200-24 composites after annealing

Table G-1 Crystalline size of CS and PET calculated from 2θ = 29.9 and 25.5°, respectively in composites after annealing

Sample	ACS of CS (nm)	ACS of PET (nm)
S60-E10C0-200-24	35.88±1.66	35.67±0.33
S60-E9C1-200-24	36.98±1.06	41.02±12.27
S60-E8C2-200-24	37.83±0.36	n/a
S60-E7C3-200-24	34.94±0.73	n/a
S60-E6C4-200-24	33.00±1.03	n/a
S60-E5C5-200-24	35.93±2.55	n/a
S60-E10C0-180-24	35.45±0.21	28.35±0.62
S60-E9C1-180-24	36.99±1.29	31.74±3.13
S60-E8C2-180-24	35.24±4.02	32.56±1.01
S60-E7C3-180-24	37.49±1.33	n/a
S60-E6C4-180-24	36.23±0.22	n/a
S60-E5C5-180-24	33.79±3.90	n/a
S50-E10C0-200-24	35.99±0.34	30.90±2.39
S50-E9C1-200-24	36.07±0.00	46.63±8.88
S50-E8C2-200-24	36.72±2.43	n/a
S50-E7C3-200-24	34.80±1.15	n/a
S50-E6C4-200-24	32.29±1.44	n/a
S50-E5C5-200-24	32.22±1.51	n/a
S50-E10C0-180-24	39.16±1.54	33.19±5.11
S50-E9C1-180-24	33.44±2.58	32.35±4.06
S50-E8C2-180-24	41.12±1.96	43.21±8.85
S50-E7C3-180-24	38.34±2.96	n/a
S50-E6C4-180-24	39.51±1.81	n/a
S50-E5C5-180-24	39.00±1.77	n/a

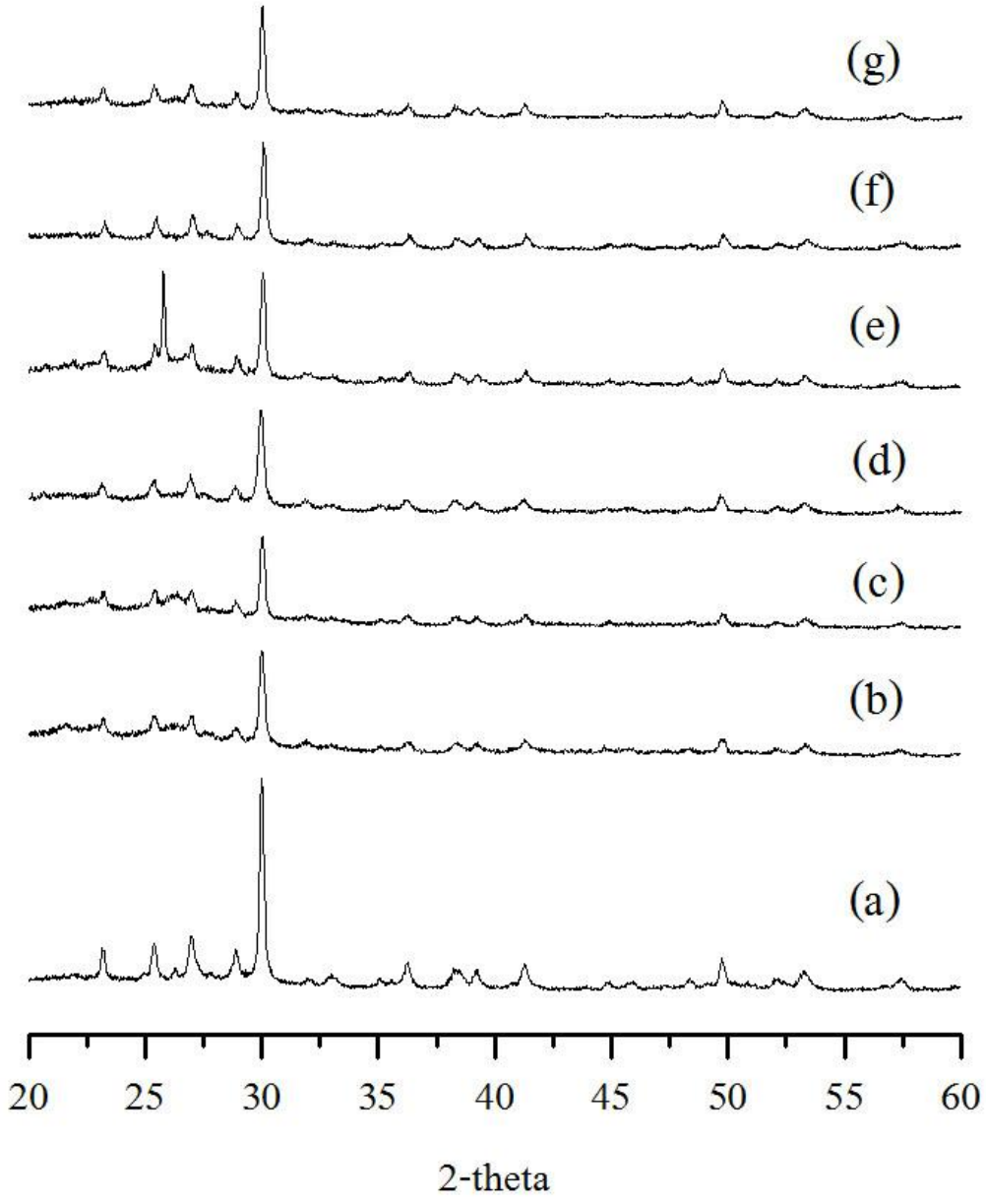

Figure G-8 XRD patterns of (a) CS, S50-E8C2-180-24 before (b) and after (c) 28-day SBF soaking, S60-E8C2-180-24 before (d) and after (e) 28-day SBF soaking, S60-E8C2-200-24 before (f) and after (g) 28-day SBF soaking

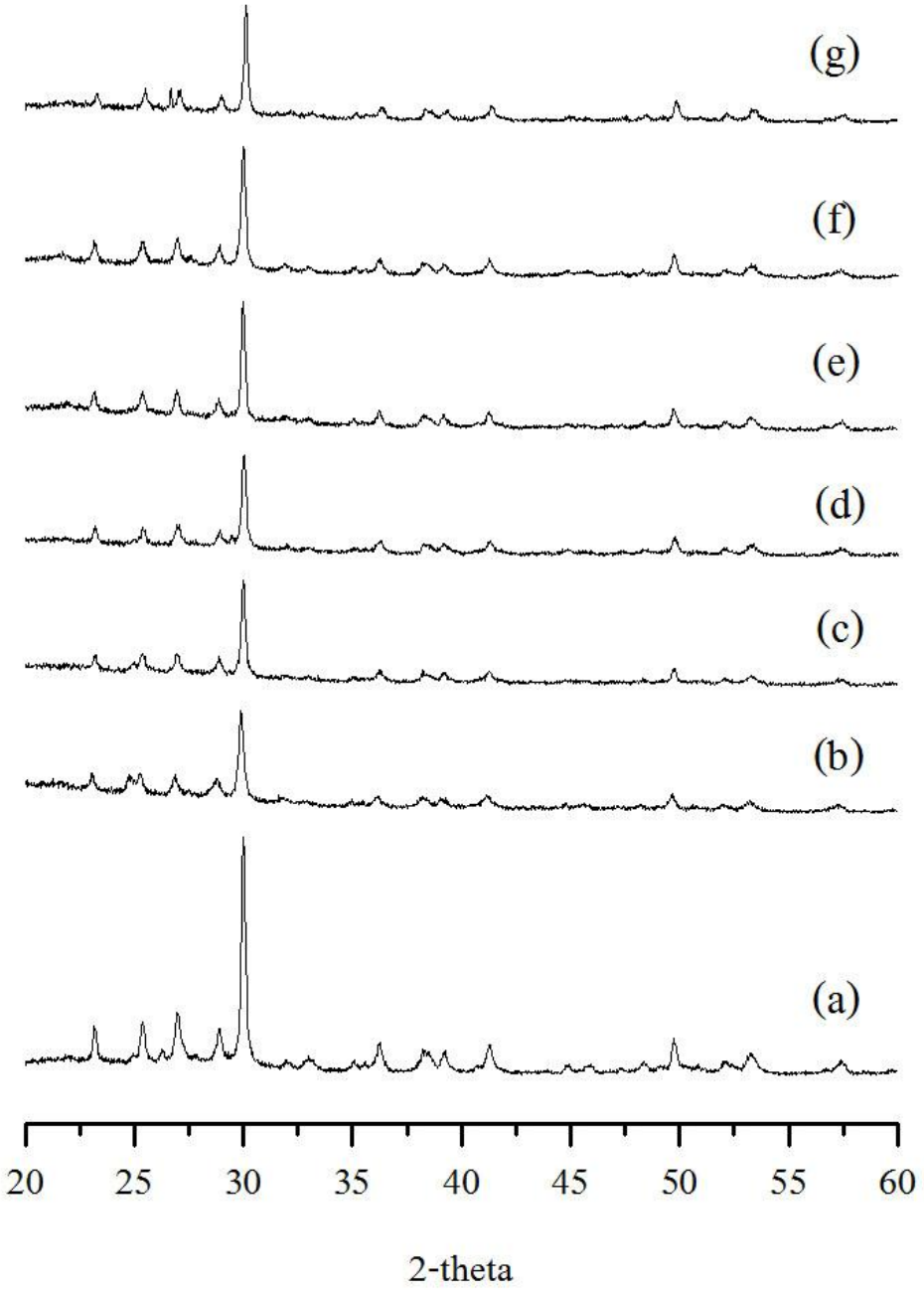

Figure G-9 XRD patterns of (a) CS, S50-E5C5-200-24 before (b) and after (c) 28-day SBF soaking, S60-E5C5-180-24 before (d) and after (e) 28-day SBF soaking, S60-E5C5-200-24 before (f) and after (g) 28-day SBF soaking